Final Report

Prepared for:

National Institute for Coastal and Marine Management/RIKZ

Large-scale sandpits

Hydrodynamic and morphological modelling of large-scale sandpits

M.D. Klein

M.Sc. Thesis

June 1999

WL | delft hydraulics

CLIENT: National Institute for Coastal and Marine Management/RIKZ

TITLE: Large-scale sandpits
Hydrodynamic and morphological modelling of large-scale sandpits

ABSTRACT:

Large-scale, marine sand mining in front of the Dutch coast might be necessary in the near future in order to meet the needs of sand for regular engineering works and/or for a possible second Maasvlakte or a national airport on an artificial island.

In order to make a socio-economically and environmentally sound decision with respect to location and magnitude of sandpits, one has to know the hydrodynamic and morphological consequences of such large-scale mining areas in advance. This study takes place in the research-program Coast*2000, coordinated by the National Institute for Coastal and Marine Management/RIKZ.

This study is performed with the Delft3D modelling software. Numerical models of sandpits in all sorts of variants have been used to study the hydrodynamic and morphological behaviour of sandpits. The emphasis in the hydrodynamic part of this study is on the influence of Coriolis and on the orientation of the sandpit with respect to the main current direction.

The morphological computations is performed over a period of 1000 years, which is necessary because of the time scale of such bottom disturbances. Aspects of the morphological simulations are the propagation of the sandpits, the developments of the slopes and the resemblance in behaviour between sandpits and tidal sand banks.

REFERENCES:

VER.	ORIGINATOR	DATE	REMARKS	REVIEW	APPROVED BY
1	M.D. Klein	1999-07-06		M.J.F. Stive	A. Roelfzema 7/6/99

PROJECT IDENTIFICATION:	z2615							
KEYWORDS:	Large-scale sandpits, hydrodynamic and morphological modelling							
CONTENTS:	TEXT PAGES	88	TABLES	16	FIGURES	62	APPENDICES	2
STATUS:	☐ PRELIMINARY		☐ DRAFT		☒ FINAL			

Preface

This study into the behaviour of large-scale sandpits serves as my M.Sc. thesis in order to finish the study Civil Engineering at Delft University of Technology.

I am grateful for the opportunities that were offered to me to execute this study at WL|Delft Hydraulics. There I did not only learn a lot about the topic of this study itself but also about coastal morphology in general. I can honestly say that by means of the things I have heard, seen and learned, that the field of coastal morphology has fascinated me.

I would like to thank a number of persons. First of all I would like to thank drs. Sander Hoogewoning from the National Institute for Coastal and Marine Management (RIKZ) for the possibility to perform my thesis on such a relevant, topical and practical subject. I also would like to thank him for his advice and his enthusiasm about the results. Furthermore I would like thank dr.ir. Dano Roelvink (WL|Delft Hydraulics and Delft University of Technology) for his heaps of advice and his assistance to overcome a lot of resistance of the computer and its software. I would also like to thank dr.ir. J. van de Graaff (Delft University of Technology), who, with his sharp and to-the-point remarks, made me think more about the input of the model and the results of it. The last member of the graduating-committee is prof.dr.ir. M.J.F. Stive (WL|Delft Hydraulics and Delft University of Technology), whom I would like to thank for his remarks and advice concerning the finishing-touch of several parts of this study. And of course there are many others, e.g. my temporary colleagues and my fellow graduate students, who will not be mentioned by name, but who are certainly not thanked less.

Contents

Appendices

List of Figures

*) These figures are included in the text

Summary

This study is performed in order to gain insight in the hydrodynamic and morphological behaviour of large-scale sandpits. These pits might be needed in the near future for the supply of sand for several purposes, like beach nourishment and civil works. Besides the yearly returning amounts of sand, large amounts might be needed in the near future for the construction of the second Maasvlakte or a national airport on an artificial island in the North Sea. The major part of sand supply used to be extracted from waters like rivers, lakes and the Dutch Waddenzee. Increased insight in the consequences of mining activities in these waters has led to a shift of sand extraction from these areas to marine sand extraction in front of the Dutch coast. To be able to predict the effects of these (large-scale) sandpits in advance this study, among others, is performed.

The study into the behaviour of these large-scale sandpits is performed with the Delft3D software of WL|Delft Hydraulics. Numerical computations of sandpits in many configurations are executed.

This study can be divided in two major parts. The first part consists of the study of the water movement in and around sandpits. The study of the water movement is performed with increasing complexity. It runs from stationary boundary conditions without the influence of Coriolis to simulations with tidal boundary conditions including the influence of Coriolis. This study is a continuation of a study performed earlier, viz. Labeur (1998).

The stationary current pattern without the influence of Coriolis is extensively described and several phenomena like the maximum and minimum current velocity and the adjustment length of the current in the sandpit are determined. These aspects are approached with theoretical considerations and the numerical results are compared with these theoretical values. The length-width ratio is an important parameter for the current velocities in the sandpit.

Qualitative aspects of the stationary current pattern in which the influence of Coriolis is implemented are described in Chapter 6. The most important result is that the Coriolis force causes an asymmetric inflow at the upstream limit of the sandpit, disturbing the complete picture of the current pattern as it is observed in case without Coriolis. Another important aspect is whether the Coriolis force and the advection of the current work in the same direction or not.

The results of the computations of the current pattern in case of tidal boundary conditions are the tide-averaged current patterns around the sandpits. Again these patterns are described extensively, as a function of the dimensions of the pit. The influence of Coriolis on the tide-averaged current pattern is only minor in case of rotated sandpits. The only significant difference is that outside the sandpit larger velocities occur when Coriolis is implemented. The parallel sandpits -i.e. sandpits with their longitudinal axis parallel to the

tidal axis- show however a current pattern that differs significantly from the situation without Coriolis. Besides the orientation of the pit, also the length of the pit influences the tide-averaged current pattern.

The second part of the study concerns the morphological behaviour of sandpits. It focuses on three aspects, viz. the development of the slope of the sandpit, the propagation of the sandpit and the resemblance between the morphological behaviour of sandpits and the behaviour of tidal banks.

The influence of a number of input variables has to be checked before the final morphological simulations could be performed. This tuning process is based upon the model of a reference trench as well as a 10×10 km^2 sandpit. The result is a well-tuned model. A morphological development of a reference trench is compared with the results of a previous study into the behaviour of trenches, like shipping channels and harbour entrances. The main difference between this study and the previous study, which used a well-calibrated model, is the applied modelling software. This study makes use of Delft3D that resolves the depth-averaged shallow water equations. The previous study made use of SUTRENCH that resolves the width-averaged advection-diffusion equation. The qualitative resemblance between the results of the two studies is fairly good. There is about a factor two between the transport rates, which can also be considered as a rather well result.

The major part of the morphological study, however, consists of simulations of the morphological development of a number of sandpits and a number of variants. These variants consist of a computation with a simplified tidal motion, depth-variants and a variant with a large residual current velocity. Besides these, also the influence of the boundary conditions on the morphological development is studied. In the vicinity of the sandpits the autonomous bottom developments range from -1.0 to +0.5 m, which means 1 mm/year. There are areas with large bottom changes ranging from -7 to +3.5 m, but these areas are very small and in the outermost corners of the modelling area, away from the sandpit.

From the computations it appears that the length-width ratio of the sandpit has only a minor influence on the morphological consequences. Only the 22 m deep, 10×5 km^2 showed qualitatively differences. The magnitude of the area, enclosed by the 22.5 m depth isoline, increases maximal 50% in x- as well as y-direction.

The resemblance in behaviour between sandpits and tidal banks is present in the parallel and positively -i.e. sandpits of which the longitudinal axis is rotated anti-clockwise with respect to the tidal axis- orientated sandpits. The observed features of these pits correspond with previous analytical approaches of the behaviour of deepening of a horizontal bottom.

The quantitative results still have to be used with care. The long simulation time and the influence of the boundary conditions leads to some inaccuracies. The qualitative results however are rather reliable and can very well be used in practice and can serve as a good basis for further study.

1 Introduction

Civil engineering works, building of houses and the agricultural sector in the Netherlands yearly demand 72 million m^3 sand. A part of that amount -7 million m^3/year- is used for beach nourishment, in order to maintain the coastline of the Dutch coast. This sand used to be gained from rivers, lakes and the Dutch Waddenzee.

Increased insight in the morphological and environmental consequences of extraction of sand in these areas has led, also under pressure of nature protection organizations, to restricted sand mining activities in these areas. The Dutch Waddenzee is in a dynamic equilibrium with its outer delta. Sand mining disturbs that equilibrium, since mining in the Waddenzee is compensated by the supply of sand out of the outer delta and vice versa. Furthermore, the bottoms of the shallower lakes are part of important and vulnerable ecosystems. Many waterfowls and fishes depend on the rich dinner table, which the bottom is. As a result of the restricted sand mining in the above mentioned waters alternatives have been sought and found in mining in the North Sea. Subsequently sand mining in the North Sea has increased. Sea sand mining is only allowed at depths of at least 20 m or 20 km offshore in case the isoline of 20 m depth lies further than 20 km offshore. Sand mining is allowed over a maximum depth of 2 m. An exception to these prescriptions are the shipping channels (Euromaas-channel and the IJ-channel). There mining landward of the 20 m depth isoline is allowed to a maximum depth of 5 m.

Besides the yearly amount of sand needed for construction activities on the mainland and maintenance of the shore, large projects are being planned. Despite the small size of the country, Holland accommodates two major mainports of Europe, the port of Rotterdam and Schiphol airport. Both mainports are growing, or at least have the potential to grow if only there is sufficient land available. Artificial islands in the North Sea or extension of the existing shore might provide that land. Hundreds of millions cubic meters of sand are needed for the construction of that artificial land.

Due to its large scale it is important to be able to predict the impact of such sandpits on constructions and activities offshore and on the Dutch coast itself. Many functions are concerned with the Dutch coast, e.g. fishery, transport, pipelines, protection against high waters and nowadays also large-scale sand mining. The interests of some functions collide with others. It is the task of the government to consider these interests and to make a socially sound policy. Therefore understanding of the hydrodynamic and morphological behaviour of sandpits is indispensable.

Within the research-program Coast*2000, coordinated by the National Institute for Coastal and Marine Management/RIKZ (part of Rijkswaterstaat), several studies of the morphological behaviour of the Dutch Coast are performed. This master thesis takes place within that framework. Results of this thesis will be used by RIKZ to advice the "Directorate North Sea" of Rijkswaterstaat with respect to large-scale mining.

Sandpits can be seen as just mining areas but also as a guidance for the current. Sandpits can be used to e.g. deviate a current away from a construction, for example the second Maasvlakte in order to prevent serious erosion caused by contraction of the current around the tip of the Maasvlakte.

The objectives of this study are to gain insight in the influence of Coriolis and obliquity of the sandpit on the stationary and tide-averaged current patterns in and around several sandpits, varying in length, width and orientation. With this obtained knowledge of the flow phenomena, the morphological computations are set-up and performed. Gaining insight in the morphological behaviour of sandpits is the second, major objective of this study.

Chapter 2 defines the problem statement and the objectives of this study. Chapter 3 discusses the physical background of (sandpits in) the North Sea and the principles and assumptions on which the modelling software and the input are based. Chapter 4 treats the modelling software. Chapter 5 discusses features of the stationary current pattern without the influence of Coriolis, and Chapter 6 discusses the stationary current pattern around a number of pits including the influence of Coriolis. In Chapter 7 tidal boundary conditions are applied, with and without Coriolis. These chapters lead to Chapter 8 in which the morphological computations of a number of sandpits are performed. Chapter 9 finally summarizes the results of this study and gives the recommendations for further study.

2 Problem definition

2.1 Objective of this study

The objective of this study is to gain deeper understanding of the water motion in and around large-scale, marine sand extraction pits. This knowledge of the water motion is the basis for the understanding of the morphological development of such mining areas, which is the second, major objective of this study. This knowledge is required in order to be able to predict the influence of large-scale sandpits on the coast or constructions in sea. One has to know how large the area is that is influenced by the sandpit, how fast a sandpit can propagate and whether it will sedimentate or not. Of special interests are the development of the pit, the total area which is morphologically influenced, the propagation of the pit, sedimentation and erosion areas and the resemblance with the morphological behaviour of tidal sand banks.

Studies into the hydraulic behaviour of large-scale sandpits have already been performed, e.g. Labeur (1998) and Ribberink (1989). The difference between these studies and this study is the special attention to the influence of the Coriolis force and the influence of obliquity of the sandpits on the water motions in and around sandpits. Knowledge on the long term morphological behaviour of sand mining areas is limited. Walstra et al. (1998) focuses on the morphological behaviour over 50 years of the Euromaas-channel and pits with comparable characteristics. In Walstra et al. (1997) the morphological behaviour over 50 years of sandpits -needed for a possible second Maasvlakte- was calculated. In the second part of this study the qualitative behaviour of sandpits with varying dimensions is analysed, on a more structurated basis for much longer time scale (1000 years) than performed before.

2.2 Set-up of the study

To study the hydrodynamic and morphological aspects of large-scale sandpits numerical models are used. The currents in and around many pits varying in length, width, depth and orientation are to be calculated. This study is divided in two major parts, viz. the hydrodynamic and the morphological part.

The hydrodynamic study is gradually built up in complexity. The most simple hydraulic conditions, stationary boundary conditions without the influence of Coriolis, are discussed in Chapter 5. Maximum and minimum current velocities in the sandpit, the order of magnitude of the influenced area around the sandpit, the adjustment length and the velocities and the discharges on the edges of the sandpit are studied.

The second series of numerical calculations are performed with stationary boundary conditions, including the Coriolis force (Chapter 6). Both the current pattern around sandpits with a channel axis parallel to the x-axis and oblique sandpits are considered. The

stationary current pattern is described and compared with the stationary current pattern without the influence of Coriolis. Besides this qualitative description, the current patterns, both with and without Coriolis, are quantitatively described by means of the minimum and maximum current velocities that are present in and around the sandpit.

The third series (Chapter 7) consist of simulations with tidal boundary conditions, first without the influence of Coriolis and later with the Coriolis force. In this way the particular aspects of obliquity, Coriolis and harmonic boundary conditions can be discerned and the feature of the current pattern can be explained.

With these three series the current pattern around sandpits and particular features of that current are known and can be explained. The insight in these particular aspects is needed because in case of the morphological calculations these intermediate steps are not taken, but only morphological calculations with tidal boundary conditions including the influence of Coriolis are made.

The study of the morphological development of sandpits is performed over a very long time span. The magnitude of the areas and the morphological time scale (see Hulscher, 1996) is so large that long simulation times are needed. It is interesting to know whether the sandpit propagates and, if it does, how fast and with which characteristics. Other aspects of the morphological study are the development of the slope and the resemblance between the morphological development of a sandpit and the development of a trench, like shipping channels in front of the Dutch coast. The last aspect of the morphological modelling is whether the behaviour of the sandpit is analogous to the behaviour of tidal sand banks.

The study of Walstra (1998) consists of 2DV computations of a shipping channel with a well-calibrated model. The results of that study are used to compare the morphological results of this study. In this study a 2DH computation of the same shipping channel as used in Walstra (1998) with the hydraulic conditions that are used in the present study, is performed. This offers the possibility to compare the magnitude of the sediment transports of the well-calibrated Walstra study with the sediment transports obtained in this study.

2.3 Reading guide

This report contains much information, which is not always interesting for everybody. Therefor these reading guide is written. Chapter 5 is some kind of a summary of previous studies, that were already performed on the stationary water motion in and around sandpits. Chapters 6 and 7 add new knowledge to the already obtained results. In these chapters the influence of Coriolis and obliquity of the sandpit on the (stationary and tidal) water motion are studied. This combination has not yet been studied in previous studies.

For those who are interested in the morphological development of sandpits, Chapters 5, 6 and 7 are meant as an introduction and one is referred to Chapter 8, though some morphological effects are explained with the knowledge obtained in the previous chapters.

3 Physical background and modelling principles

3.1 Introduction

This chapter describes the physical background and the modelling principles that are deployed in this study. On the one hand the conditions occurring in the North Sea are taken as a starting-point for getting input data. On the other hand many simplifications are made to be able to distinguish purely the influence of the sandpits on the current and the morphology.

Section 3.2 discusses the hydraulic and morphological conditions as they occur in the North Sea. On basis of these conditions some input variables are deduced. These conditions lead also to the assumptions and simplifications that are used in this study and which are treated in Section 3.4. Section 3.3 discusses the governing equations on which the modelling software is based.

3.2 Hydraulic and morphological conditions of the North Sea

Large-scale sandpits are meant to supply sand for construction activities near the Dutch coast, onshore as well as offshore. The most logical location for sandpits is therefore the North Sea in front of the Dutch coast. A large part of the input data is deduced from the conditions as they are present in the North Sea in front of the Dutch coast. The latitude of the Dutch coast is about 50° North, so when the Coriolis force has to be implemented, the latitude of the modelling area is set to 50° North.

As mentioned in the introduction to this study, the current demands made upon large-scale sandpits are such that sandpits are situated in water deeper than 20 m. In fact, this still water depth is applied in the models. In case of stationary boundary conditions a water level of 0 m is imposed on the downstream boundary of the modelling area. Since the uniform bottom level is set at -20 m, a water depth of 20 m is present at the downstream boundary. In case of tidal boundary conditions, the sinusoidal water level variation is imposed with respect to this zero water level. The bottom of the North Sea consists of sand. The d_{50} of the grains in front of the Dutch coast varies roughly between 0.15 and 0.25 mm.

The bathymetry of the Dutch coast, like many other coasts, is rather dynamic. Besides autonomous developments which find their origin in the interaction of tidal currents, wind- and wave-induced currents, changes of the mean water level etc., consequences of human interference in the coastal system are noticeable. The major part of these interactions and measures are present in the breaker zone. Sandpits however are to be mined in deeper water outside the breaker zone, in which the tidal motion is the dominant factor, determining the hydraulic conditions. Another interesting topic of resent research, e.g. Hulscher (1996), is the presence, the orientation, the propagation and sometimes the growth of large, rhythmic

bottom patterns, designated as tidal banks or sand waves, which are also found outside the breaker zone. An interesting aspect of this study is whether sandpits can present the same characteristics as tidal banks. This is one of the aspects of Chapter 8.

In the North Sea a diurnal tide dominates. The North Sea itself is too small to generate a tide, but the tidal wave of the Atlantic Ocean enters the North Sea, increases in amplitude and propagates in an anti-clockwise motion through the North Sea. That's why the flood direction in front of the Dutch coast is northwards.

The dominant wind direction in Holland is south-west. Winds from north-west, however, represent the most severe weather conditions. Due to the long fetch, the set-up of the water level can be larger and also the opportunity for growth of waves, by means of wind-wave interaction, is larger. These aspects play a role in the breaker zone, where wave-induced currents are of importance. This study deals with sandpits in deep water, thus outside the breaker zone. The parameters, describing the propagation and breaking of waves, are therefore hardly of importance in this study.

3.3 Governing equations

The equations which describe the three-dimensional water motion are based on the principles of conservation of mass and momentum. That set of equations is called the Saint-Venant equations. The principle of conservation of a quantity means that what comes in must come out or must be stored.

The modelling software is based on the depth-averaged shallow water equations, which can be deduced from the Saint-Venant equations. Equations (3.1), (3.2) and (3.3) resemble the depth-averaged shallow water equations and Equation (3.4) represents the general sediment transport equation. Appendix A treats the complete Bijker sediment transport formula. Equation (3.5) presents the equation for the bottom changes.

$$\frac{\partial u}{\partial t}+u\frac{\partial u}{\partial x}+v\frac{\partial u}{\partial y}+g\frac{\partial \eta}{\partial x}-fv+\frac{gu|U|}{C^2(d+\eta)}-\frac{F_x}{\rho_w(d+\eta)}-\upsilon\left(\frac{\partial^2 u}{\partial x^2}+\frac{\partial^2 u}{\partial y^2}\right)=0 \quad (3.1)$$

$$\frac{\partial v}{\partial t}+u\frac{\partial v}{\partial x}+v\frac{\partial v}{\partial y}+g\frac{\partial \eta}{\partial y}+fu+\frac{gv|U|}{C^2(d+\eta)}-\frac{F_y}{\rho_w(d+\eta)}-\upsilon\left(\frac{\partial^2 v}{\partial x^2}+\frac{\partial^2 v}{\partial y^2}\right)=0 \quad (3.2)$$

$$\frac{\partial \eta}{\partial t}+\frac{\partial (d+\eta)u}{\partial x}+\frac{\partial (d+\eta)v}{\partial y}=0 \quad (3.3)$$

$$S=S_b+S_s \quad (3.4)$$

$$(1-\varepsilon)\frac{\partial z_b}{\partial t}+\frac{\partial S_x}{\partial x}+\frac{\partial S_y}{\partial y}=0 \tag{3.5}$$

with

$$S_b = bd_{50}\frac{q}{C}\sqrt{g}\cdot e^{(A_r)}(1-\varepsilon)$$

$$S_s = 1.83S_b\left(I_1 \ln(\frac{33.0h}{r_c})+I_2\right)$$

in which:

u	=	current velocity in x-direction	[m/s]
v	=	current velocity in y-direction	[m/s]
g	=	gravity acceleration	[m/s^2]
η	=	elevation of the water surface, with respect to the zero level	[m]
f	=	Coriolis parameter	[s^{-1}]
|U|	=	absolute current velocity, defined as $\|U\| = \sqrt{u^2+v^2}$	[m/s]
C	=	Chézy friction coefficient	[m^{½}/s]
d	=	water depth	[m]
F_x	=	source terms for external stresses	[N/m^2]
ρ_w	=	density of water	[kg/m^3]
υ	=	kinematic viscosity	[m^2/s]
S_b	=	bottom sediment transport	[m^3/s/m]
S_s	=	suspended sediment transport	[m^3/s/m]
ε	=	porosity of the sediment	[-]
z_b	=	the vertical coordinate of the bed level	[m]
$S_{x,y}$	=	depth-integrated bed and suspended sediment in x- and y-direction, respectively	[m^3/s/m]

Equations (3.1) and (3.2) represent the momentum equation in x- and y-direction, respectively. In Equation (3.3) the conservation of (the water) mass is expressed. Equation (3.4) is also a based on the conservation principle, not on the conservation of water but on the conservation of sediment. To complete this set of equations, a formula for the sediment transport rate S is necessary, which relates the current velocity and the sediment transport. In this study the sediment transport formula of Bijker is applied. One is referred to the manual of Delft3D-MOR and Appendix A for the exact definition of this formula.

These differential equations are translated by the modelling software into difference equations, since differential equations are continuous functions and computers can only handle discrete functions. Figure 3.1 shows the computational grid of Delft3D-FLOW. This is a so-called staggered grid, which means that the water levels and the current velocities are determined in different grid points.

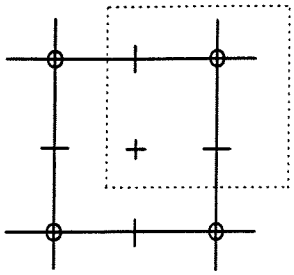

Figure 3.1: The computational grid of Delft3D-FLOW

3.4 Assumptions and simplifications

Numerical models are used because the equations describing the motion of water are too complicated to resolve them analytically. Some theoretical approaches though are used, mainly to deduce the boundary conditions and to describe features of the stationary current pattern. Reality on its turn is much more complicated than the models nowadays can represent. This section, therefore will describe the simplifications that are used in this study. These simplifications follow from the governing equations and from additional assumptions, in order to study purely the effect of sandpits. Also some assumptions concerning physical parameters are made in order to gain input data for the Delft3D software. Appendix B summarizes the physical input parameters as they are used in this study.

2DH
Since the horizontal scale of the flow phenomena around sandpits is much larger than the vertical one, the application of a depth-averaged model is justified.

Turbulence
Since use is made of a depth-averaged model, turbulence is not included in this study, because an essential feature of turbulence is its three-dimensional character. Also the magnitude of the modelling area and the grid cells exclude turbulence. The total process of turbulence runs from eddies with a magnitude of the order of the water depth to energy dissipation due to the molecular viscosity. Large eddies, with a length scale of a number of grid cells, might be resolved in this study but small eddies and dissipation on molecular scale can not be resolved. The eddies that can not be resolved, are included in the bottom friction, which serves as a closing term.

Another aspect that might induce turbulence, in the form of mixing layers, is flow separation due to a too steep slope of the sandpit. Flow separation approximately occurs on slopes steeper than 1:8. The maximum slope of the banks of the sandpit that is employed in this study is 1:25. Because in reality no flow separation will occur, there is also no need to take this aspect into account.

Uniformity
Input parameters concerning friction, Coriolis and viscosity are assumed to be uniformly distributed over the entire modelling area.

Flat bottom
Though sandpits are supposed to be mined in front of the Dutch coast, the sandpits in this study are not implemented in a model with the bathymetry of the Dutch coast, but in a model with a flat bottom. This study aims at gaining insight in the influence and behaviour of sandpits only. Therefore a flat sea bottom has been implemented. No effects of a sloping bottom level are taken into account.

Tidal motion
As far as the hydrodynamic study is concerned, the tidal boundary condition is schematized to one harmonic component, viz. diurnal tide component with two ebb periods and two flood periods every 24^h48^m. The phase difference between the upstream and downstream boundaries is approximated with the propagation celerity of shallow water waves. It is tried to keep the water motion as simple as possible by assuming that the velocity and the water level reach their maximum in the same place and at the same time. Although these conditions do occur in the North Sea, also phase differences between peak velocity and the water level have been observed. The influence of the phase differences on the residual current pattern is studied and discussed in Chapter 7. The current velocity amplitude is assumed to be 0.5 m/s. This is a value that is rather common in the North Sea. Subsequently, the stationary current velocity is also assumed to be 0.5 m/s.

In order to obtain more realistic morphological results, the tidal movement is in the morphological part of the study schematized with the M0, M2 and M4 component. In Chapter 8 is described how these boundary conditions are deduced from model output.

Waves
Wind waves have been implemented in the model to stir up sediment from the sea bottom. Because of the large depth of the sea in which sandpits are to be constructed the parameters influencing the breaking of waves and refraction need not to be specified. Wave parameters like H_s and T_p are assumed to be uniform and constant. The significant wave height is set at 1.5 m and T_p is 6 s.

4 The Delft3D software

4.1 Introduction

The Delft3D software of WL|Delft Hydraulics was the basic modelling software in this study. This software package consists of Delft3D-MOR and several pre- and postprocessing tools. This chapter will describe the general set-up of a model with Delft3D and the additional tools that are used.

The Delft3D-MOR shell contains a number of modules, viz. Delft3D-FLOW, Delft3D-WAVE, Delft3D-TRAN and Delft3D-BOTT. Delft3D-FLOW can be used independently, without other modules and without the shell. This module calculates only the motion of water, based on the shallow water equations. This single part of the Delft3D software is used for the calculations which are discussed in Chapters 5, 6 and 7. The morphological simulations of Chapter 8 are performed with all modules.

Section 4.2 states the direction definitions, as they are applied in this study. Sections 4.3 to 4.7 discuss the particular modules, their most important input parameters, the formulas they are based on and the way they are used within the shell. Section 4.8 treats the post-processing programs that are applied. For more detailed information on these modules one is referred to the manuals of these modules.

4.2 Direction definitions

The following (direction) definitions are used, see Figure 4.1.

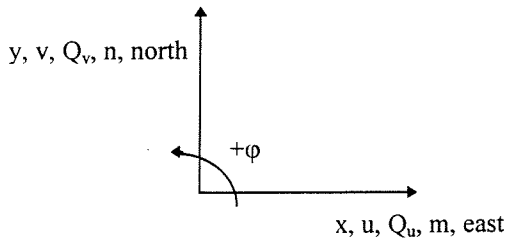

Figure 4.1: Direction definitions

The main current direction is the x-direction, since the boundary conditions are imposed at the lines x=0 and the opposite model boundary at x=120, 100 and 50 km, respectively dependent on the magnitude of the modelling area. Furthermore, the positive y-direction is also referred to as the north, the positive x-direction as the east. These directions should be considered independently of possible orientations of sandpits in front of the Dutch coast.

4.3 Delft3D-MOR

The Delft3D-MOR module is the shell for the morphological computations. In that module the execution sequence of the particular modules and the computation time of these modules are defined. The sequence of the modules can be translated into a process tree. Figure 4.2 shows the process tree as it is deployed in the morphological computations of the sandpits, described in Sections 8.5, 8.6 and 8.7.

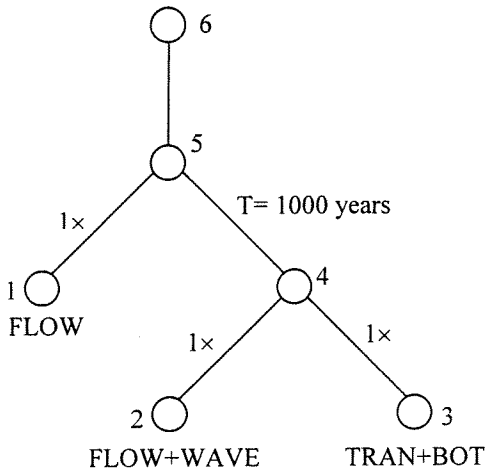

Figure 4.2: The Delft3D-MOR process tree

First only the water motion (node 1) is calculated in order to reach a dynamic equilibrium, in which disturbances, caused by differences in initial and boundary conditions and the 'real' situation, are diminished. Five tidal periods are sufficient to reach such an equilibrium. Next (node 2), the water motion including the interaction with waves during one tidal period is calculated, which is the basis of sediment transport and morphological computation (node 3). Sediment transports are calculated and with these values the morphological changes within one morphological time step are calculated. This morphological time step can be defined by the user or can be automatically determined by the computer, see Section 4.6. On basis of that new bottom the sediment transports can be calculated again, if one decides to perform more than one sediment transport and bottom change computation per flow computation. This loop can be repeated a number of times. E.g. in one of the simulations of Section 8.2 the controller of node 3 is defined such that node 3 is executed 5 times. After that, node 2 is executed again: a new water motion is computed. This process is continued until the defined total simulation time (i.e. the time defined in controller IV, in this study 1000 years) is reached.

4.4 Delft3D-FLOW module

This section describes the input that is necessary for a successful flow simulation. One should notice that not all possible input parameters of the Delft3D software are discussed here. Only the relevant parameters are mentioned. As mentioned before, the flow module can be executed independently. This option is used in Chapters 5, 6 and 7.

4.4.1 Computational grid

With the Rgfgrid module of the Delft3D software computational grids can be created. Four square computation grids are used for the computations of the water motion and the morphology. These grids with their dimensions are:

- 120×120 km^2 with grid cells of 500×500 m^2 for 100 km long sandpits
- 100×100 km^2 with grid cells of 500×500 m^2 for sandpits between 20 and 60 km
- 75×75 km^2 with grid cells of 250×250 m^2 for the morphological computations
- 50×50 km^2 with grid cells of 250×250 m^2 for sandpits 20 km and smaller

These magnitudes of the model grid combined with the implemented sandpits leave at least 10 km model area at both sides of the sandpit. In the morphological study also a reference model of a trench is used, which is implemented in a 4×0.5 km^2 grid with 25×25 m^2 grid cells.

Another consideration concerning the choice of the space step, besides the amount of grid cells, is the wavelength of the tidal wave. One wave should contain a number of grid cells. A tidal wave with a period of 12^h24^m in a water depth of 20 m results in a wavelength of about 625 km. Of course this condition is amply fulfiled in this model.

In fact the time and space steps are iteratively determined, because they are very closely related and determine the magnitude of the model, the total computation time and the accuracy of the results.

Finally, a latitude has to be prescribed in order to account for Coriolis. When no influence of Coriolis is desired, one assumes the modelling area to be situated on the equator. In reality, the Coriolis force depends also on the latitude. The magnitude of the models in this study might demand a non-uniform Coriolis force. In order to be able to implement a non-uniform force, one has to use spherical coordinates. For simplicity reasons, this option has not been used and the Coriolis parameter is assumed to be uniform in the modelling area.

4.4.2 Bottom profile

The bottom files are made in the Quickin5 module. The bottom files are based on the current demands, which are made upon large-scale marine sand mining. The undisturbed sea bottom level was assumed to be at 20 m below the water surface.

The depth of the sandpits is one of the variables in the simulations, viz. 2, 5, 8 and 10 m below the undisturbed sea bottom level. The bottom level difference between the

undisturbed sea bottom and the bottom of the sandpit is 'spread' over one grid cell. The result is a minimum slope of 1:250 and a maximum slope of 10:250. For several reasons the choice has been made not to refine the grid locally in order to be able to create in all depth-variants the same slope. The number of grid cells is already large, without refining the grid. The expected influence of the slope on the results was not significant. Lastly, a small cell size is needed in order to be able to create exactly the same slope in all calculations. Small cell dimensions require also small time steps. Because of the large amount of grid cells and a maximum simulation time of 75 hours, a small time step and even a larger number of cells is undesirable.

4.4.3 Time parameters

Numerical simulations with stationary boundary conditions are performed over a period of 48 hours. That period is long enough for the model to adapt itself to the boundary conditions and to reach a stationary situation. The time span in case of harmonic boundary conditions is 75 hours. In this period the water motion is able to adapt itself to the boundary conditions and a complete tidal period of 12^h24^m is available for data generation and postprocessing.

The time step, which is used in numerical calculations depends on the grid cell dimensions and the propagation celerity of a shallow water wave. The required time step can be determined with the CFL-condition. A so-called Courant number is defined as in Equation (4.1).

$$CFL = \frac{c \cdot \Delta t}{\Delta x} \tag{4.1}$$

in which:

c = the propagation celerity of a disturbance in shallow water, defined as $\sqrt{gh}$ [m/s]

In numerical calculation schemes that are not unconditionally stable, the demand for stability is CFL<1. This condition means that information, e.g. a disturbance of the water level, is not allowed to travel faster in the numerical model ($\Delta x/\Delta t$) than in reality (c).

Delft3D-FLOW however, does have a numerical scheme that is unconditionally numerically stable. In that case another CFL-condition is valid, viz. CFL<20. This is a condition concerning the accuracy of the calculations. In case of the 250×250 m^2 grid cells in first instance a time step of 3 minutes is chosen. Later, when the results proved to be the same for a time step of 4 minutes, the latter time step is used. These numbers result in a maximum Courant number of

$$\frac{\Delta t \cdot \sqrt{gh}}{\Delta x} = \frac{240 \cdot \sqrt{9.81 \cdot 30}}{250} = 16.5$$

and in a minimum Courant number of

$$\frac{\Delta t \cdot \sqrt{gh}}{\Delta x} = \frac{240 \cdot \sqrt{9.81 \cdot 30}}{500} = 8.2$$

These values of the Courant number are sufficiently small, regarding accuracy demands.

Like the space step, also the time step should be chosen sufficiently small, in order to obtain a large enough resolution concerning the tidal period. The time step of 4 minutes fulfils that criterion.

Other time parameters have to be given in the preparation of the output file. A time step for the history files is one of them. That time step needs to be a multiple of the computation time step. Also begin and end time and time steps for the communication and map files are needed.

4.4.4 Initial and boundary conditions

The initial condition of the model is imposed as a water level. The more the initial water level differs from the water level, belonging to the boundary conditions, the more time is needed before the model is adapted to the boundary conditions. In all simulations the initial water level has been set at 0 m, which means a water depth of 20 m at the downstream boundary of the modelling area.

On at least two opposite boundaries of the model area boundary conditions have to be imposed. These conditions might be a water level, a current velocity and/or a discharge.

A combination of two water level boundary conditions, designated as h-h boundaries, do fixate the water levels but, in principle, every current velocity can occur at every water depth. The current velocities are however determined by water level differences between the two boundaries of the modelling area, but strange numerical aspects are not excluded.

Two current velocity boundary conditions (u-u boundaries) do not fixate the water level. Several simulations with the same boundary conditions might result in the same number of different water levels. The water level around which the tidal motion oscillates is defined in the initial condition. The influence of the initial condition is only present in the first time step(s). When there is a difference between the product u(t)h(t) calculated at both boundaries, a net discharge is present. This lead to slowly filling or emptying of the modelling area. However, the magnitude of the area is so large and these residual discharges are generally so small that a significant change of the zero water level needs much more time than in these simulations is available.

The combination of a current velocity upstream and a water level downstream (u-h boundaries) is the best insurance for a successful simulation. With that combination both the amount of water entering the modelling area and the accompanying water level are determined in advance. This set of conditions is used in Chapters 5 and 6.

The remaining two boundaries are specified as closed boundaries over which water can be attracted or discharged. Every chapter or section will discuss the boundary conditions that are applied in that chapter. The stationary boundary conditions including Coriolis are discussed in Section 6.2. The tidal boundary conditions with and without Coriolis are treated in Sections 7.4.1 and 7.2.1, respectively. The applied boundary conditions in the morphological computations are discussed in Section 8.3.

An important input parameter for the stationary boundary conditions is the so-called α-factor. With stationary boundary conditions water level disturbances can be reflected into the modelling area again, instead of leaving the modelling area. This factor is defined in order to create weakly reflective boundaries.

4.4.5 Remaining input

Physical parameters
The modelling software offers the possibility to change the physical parameters like the gravity acceleration, water density, salinity, temperature, etc. All these values are set at the default value, see Appendix B. Also the roughness has not been changed. The Chézy coefficient in x- as well as in y-direction is assumed to be 65 $m^{1/2}/s$.

Numerical parameters
The most important numerical parameter that has to be specified is the time step. See Section 4.3.3 for the discussion of the time parameters that have been used.

Processes
The Delft3D software offers the possibility to implement certain physical processes in the model. These processes are salinity, temperature, constituents, wind, waves and secondary flow.

Observation points
In order to obtain history results, one can prescribe observation points for which certain quantities (like water levels and current velocities) can be stored.

4.5 Delft3D-WAVE module

In this study waves are implemented in order to stir up the sediment from the bottom of the sea. Waves are supposed to be uniform and regular approaching only from one direction. Since the waves do not break in this model, no artificial wave-induced currents are caused.

In this model a separate computational grid for waves has to be created. But by choosing the right boundary conditions for the waves, this grid can have the same dimensions as the computational grid of the flow. This boundary condition implies that waves on the lateral boundaries have the same properties as the waves at the upstream boundary. The grid cells however can be much larger since breaking and refraction are not of importance. No detailed wave data has to be obtained, only the influence of the wave on the velocity near the bottom.

The wave module offers the possibility to account for refraction, wind growth, bottom dissipation, surf dissipation, white-capping and current dissipation. In order to reach a uniform wave field friction coefficients for the bottom dissipation have been set at zero (no bottom dissipation of wave energy). Despite that, a small gradient of the significant wave height can be observed, probably due to a non-uniform water depth.

Other parameters, that have to be defined, are: significant wave height, peak period, width of the energy density spectrum. It has been striven not to influence the tidal currents by the waves. Appendix B summarizes the most important input parameters, as they are used in this study.

4.6 Delft3D-TRAN module

Three types of sediment transport can be implemented, viz. total transport, silt transport and bottom and suspended sediment. The total transport module assumes that the suspended sediment distribution in the vertical is the equilibrium concentration distribution, contrary to the third module in which the suspended sediment is calculated on basis of the bottom transport. The total sediment transport option should be used when the characteristic length scale of the model is longer than the adjustment length of the sediment transport. As the current velocities, the sediment concentration distribution needs some length to adapt itself to the hydraulic conditions. When the grid sizes are larger than this length this aspect of the sediment transport need not to be taken into account. Section 8.2 discusses the influence of the transport mode on the morphological results. Also in that section a choice is made for the transport mode that will be applied in the remainder of the study. The silt option is used for very fine sediment in which cohesion plays a role. This option is not used in this study.

An appropriate transport formula is chosen in order to calculate the bottom transport and to calculate either the corresponding suspended transport or the equilibrium concentration profile of the sediment transport.

In this study the Bijker transport formula is implemented to calculate the sediment transport S'. This calculated sediment transport can be corrected for different physical as well as numerical effects. One of these aspects is the effect of the bottom slope on the sediment transport rate. The slope influences the critical shear stress and the direction of the transport.

In this study two of these corrections are used, viz. α_s and α_n. The magnitude of the sediment transport S now becomes $\alpha_s\alpha_n S'$. The coefficient α_s resembles the effect of the bed level gradient on the sediment transport. This coefficient is calculated according to Equation (4.2).

$$\alpha_s = 1 + \alpha_{bd}\frac{\partial z_b}{\partial s} \tag{4.2}$$

in which α_{bd} [m^2] has to be specified in the input file. In the input file and in the figures of Chapter 8 α_{bd} is designated as ALFABD.

Factor α_n represents the correction of the sediment transport gradients. This coefficient is also determined with Equation 4.2 but with α_{nn} in stead of α_{bd}. The user has to define the method with which α_{nn} is calculated. In the input file NSTAB represents those options. Many options are possible but only two options are used in this study, viz. option 5 and 6. Option 5 reads:

$$\alpha_{nn} = \frac{\overline{S}(\frac{\alpha_{sta} \cdot b_e}{\overline{h}})^2 \cdot \Delta t}{2(1-\varepsilon_{por})} \tag{4.3}$$

in which:

$\overline{S}$	=	tide-averaged sediment transport	[m^3]
$\overline{h}$	=	tide-averaged water depth	[m]
α_{sta}	=	user-defined stability coefficient	[$m^{½}s^{-½}$]
b_e	=	velocity power of the sediment transport	[-]
Δt	=	morphological time step	[min]
ε_{por}	=	porosity of the sediment	[-]

According to option 6, coefficient α_{nn} is calculated as follows:

$$\alpha_{nn} = \frac{\alpha_{sta} b_e \cdot \Delta l}{2\overline{h}} \tag{4.4}$$

in which:

Δl	=	local grid cell length	[m]

The choice of NSTAB is related to the method of determining the morphological time step. When a constant time step is applied, NSTAB should be 5. If the time step is automatically determined, then NSTAB is 6 is the best option. One should notice that NSTAB does not correspond to a physical property.

The morphological time step can be defined by the user but can also be determined by the computer. The computer calculates the optimal time step on basis of the bed sediment transport. One should notice that when the suspended sediment contributes a considerable amount of sediment, the optimal time step calculated only on basis of the bed load might lead to instabilities.

The boundary conditions of the sediment transport are chosen such that the equilibrium sediment concentrations are imposed.

4.7 Delft3D-BOTT module

The bottom change module mainly consists of parameters that describe if, when and how data is stored.

As it is described in the sections above, the user can freely choose for each module the simulation time, the sequence of execution and the number of times they are executed. In order to interpret the results of the morphological computations correctly one has to know the procedure that is employed in order to deal with simulations that consists of more than one bottom computation per flow computation. When for example 5 bottom calculations (and thus also 5 sediment transport calculations) are performed per flow computation, use is made of the so-called continuity step. After the calculation of the velocity field sediment transport rates and subsequently bottom changes are calculated. For the next (sediment transport and bottom changes) calculations one assumes the discharges in the grid cells to be constant. On basis of this discharge, the new water depth and a relation between water depth, discharge and sediment transport the new sediment transport rates and the belonging bottom changes are calculated. This is repeated until a new flow computation is started. Section 8.2 discusses the influence of the number of sediment transport and bottom changes computations per flow computation.

The numerical calculation scheme of the morphological module is not unconditionally stable. One should be careful choosing the morphological time step, when one decides not to use the option to let the computer determine the time step.

4.8 Postprocessing programs

The Delft3D software is equipped with a General Postprocessing Program (GPP). The data that are stored during the numerical computation can easily be visualized with GPP. Several additional tools are available for e.g. averaging or subtracting of data sets.

Another tool with which data can be selected and be converted to e.g. Excel files is Viewer Select (VS). With VS cross-sections and longitudinal sections can easily be obtained.

The data used in the postprocessing is read from the communication and map files that are generated by the Delft3D software.

5 Stationary water motion

5.1 Introduction

This chapter deals with the numerical calculations of the 2DH water movement, which are caused by stationary boundary conditions without the influence of Coriolis. The purpose of this chapter is to gain insight in the features of the stationary current pattern in and around sandpits.

As will become clear in the remainder of this chapter, the current in and around sandpits depends on the length, width and depth of the sandpit. To gain insight in that dependence, a large number of simulations are performed, see Table 5.1. The depth varies between 2 and 10 m, the length between 2 and 100 km and the width is 5 or 10 km. Furthermore some simulations are performed for oblique sandpits, rotated over +45° and -45° with respect to the main flow direction.

Table 5.1: The executed simulations and the corresponding volumes of the pit [$*10^6$ m^3]

Length [km]	w=5 km d=22 m	w=10 km d=22 m	w=5 km d=25 m	w=10 km d=25 m	w=5 km d=28 m	w=10 km d=28 m	w=5 km d=30 m	w=10 km d=30 m
2					80			
3					120			
4	40				160			
5		100	125	250	200	400	250	500
6	60				240			
7					280			
8	80				320			
9					360			
10	100	200	250	500	400	800	500	1000
11					440			
12	120				480			
13					520			
14	140				560			
15		300	375	750	600	1200	750	1500
16	160				640			
17					680			
18	180				720			
19					760			
20	200	400	500	1000	800	1600	1000	2000
40	400	800	1000	2000	1600	3200	2000	4000
60	600	1200	1500	3000	2400	4800	3000	6000
100	1000	2000	2500	5000	4000	8000	5000	10000

Table 5.1 shows all simulations that have been executed with stationary boundary conditions. The numbers indicate the amount of sand that such a pit will supply. One combination of depth and width have been simulated extensively, viz. the sandpits with a

depth of 28 m and a width of 5 km. The 22 m deep and 5 km wide sandpits have been simulated less extensively than the former combination, but still rather many lengths were examined. Because of the laborious work, the other combinations were simulated 'only' in case of 7 length variations. Since it is expected that the trend of the results is similar for all simulations, the omission of these lengths will not essentially influence the results. Because the omitted lengths are the shorter lengths, the shape of the graphs of Figures 5.9, 5.10 and 5.11 are the same as they would have been when more (shorter) sandpits would have been considered. Besides these simulations also a number of rotated sandpits, of which only the +45° rotated, 30 m deep 40×5 km^2 sandpit is discussed, are simulated. Table 6.2 shows, however, the minimum and maximum current velocities of all these rotated pits and of a number of the parallel pits.

Section 5.2 discusses the applied boundary conditions. Section 5.3 describes the general feature of the stationary current pattern in and around parallel as well as rotated sandpits. On basis of the observed features, Section 5.4 discusses a theoretical approach of some aspects of that stationary pattern. These approaches are applied to the parallel pit only. Section 5.5 discusses the magnitude and shape of the area, which is influenced by the sandpit. The comparison between the theory of Section 5.4 and the simulations are made in Sections 5.6, 5.7 and 5.8. In these sections the minimum and maximum current velocity in the center longitudinal section of the sandpit are discussed. Also the length, the current needs to adjust itself to the hydraulic conditions in the sandpit is discussed. Section 5.9 deals with the velocities on the edges of the sandpit and with the discharges into and out of the sandpit. Section 5.10 summarizes the results of this chapter.

5.2 Boundary conditions

Two boundary conditions are imposed. At the upstream boundary a current velocity of 0.5 m/s is imposed. At the downstream boundary the water level is set at 0 m. This means a water depth of 20 m at the downstream border of the modelling area. The water surface slope adapts itself according the Chézy formula (5.1). This formula is based on a current in which the bottom shear stress is in equilibrium with the pressure gradient of the water.

$$u = C\sqrt{hi} \tag{5.1}$$

in which:

i = slope of the water surface [m/m]

In all simulations the Chézy friction coefficient is set at 65 $m^{1/2}/s$. Together with a downstream water depth of 20 m this results in an average water slope of $3*10^{-6}$. Since the bottom of the sea has been simplified to a horizontal one, the water slope causes a non-uniform water depth, also in the undisturbed areas. The water depth at the downstream boundary has a fixated value, viz. 20 m. The maximum water depth is $20+3*10^{-6}\times120{,}000$ = 20.36 m. This means an imposed discharge of 10.18 m^3/s per unit of width. The same amount of water has to leave the area through a smaller cross-section causing a larger velocity than 0.5 m/s. The velocity of 0.5 m/s at the upstream boundary increases to 0.509 m/s, which is only an increase of 1.8%. In many aspects of this chapter this difference is negligible. When the difference can not be neglected (e.g. when the adjustment length is

determined) the values of the velocities are adapted according to a linear distribution of this difference over the total length of the modelling area.

5.3 Stationary current pattern

Figure 5.1 shows the general picture of the current velocities in the steady state in and around a parallel and a +45° rotated 40×5 km^2, 30 m deep sandpit. In this picture the velocity components u and v are plotted. Because of the relatively small v-velocities, the plot of the u-velocities represents also the plot of the current magnitude; the differences are only very small. Figure 5.2 shows the stationary current velocities in the center longitudinal section of the parallel sandpit.

In and around both pits one can distinguish alternating acceleration and deceleration of the current. These areas in case of the parallel pit are:

- Increasing velocity at upstream side of the sandpit
- Significant deceleration of the current just entering the sandpit
- Deceleration areas besides the sandpit
- Increasing velocity in the sandpit
- Deceleration of the current in the downstream part of the sandpit
- Increased current velocity outside the downstream part of the pit

A number of these areas can also be discerned in Figure 5.2. The observed features in the above mentioned areas can be explained as follows. Water particles approaching the sandpit experience the effect of the reduced resistance further downstream, in the sandpit. This reduction is due to the increased water depth in the sandpit. The influence of such a disturbance is noticeable upstream, when the current velocity is sufficiently small. The so-called Froude number is defined as the ratio of the current velocity u and the propagation celerity of disturbances in shallow water $\sqrt{gh}$. When this ratio is smaller than 1 ($u < \sqrt{gh}$), (water level) disturbances can propagate in the upstream direction. In case of tidal currents, this condition is amply met (0.5 m/s vs. 14 m/s). So, water particles approaching the sandpit will accelerate. This acceleration in front of the sandpit is accompanied by a lower water level, resulting in a water level gradient, in both the x- and the y-direction. The gradient in y-direction adds water from aside to the main current entering the sandpit. Figure 5.3 demonstrates this. In this figure the differences between the water levels just north of a 40×5 km^2 sandpit and the water levels in a longitudinal section in the undisturbed area and the discharges in y-direction are plotted. A positive water level difference (water level in the undisturbed area is larger than near the sandpit) means a discharge in negative y-direction, thus a discharge into the sandpit.

In the sandpit itself the cross-section is larger than in front of the sandpit. One can state that the discharges just in front of the sandpit and just in the sandpit are equal; no extra water has been attracted yet from aside. This assumption of constant discharge and the simple formula Q=uA explain the fact that there is a significant deceleration of the current in the first part of the sandpit.

There is also a water level difference between the water level in the pit and its surroundings, see Figure 5.3. In the upstream part of the sandpit the water levels of the pit's surroundings are higher than the water level in the pit, resulting in the inflow of water into the sandpit: the flow adapts itself to the hydraulic conditions in the sandpit. The current velocity is increasing, in the beginning rather fast, slowly more downstream and not at all somewhat downstream of the middle of the sandpit, reaching a maximum value. Whether this maximum is the equilibrium current velocity depends on the length, width and depth of the sandpit. More downstream the water level in the pit becomes higher than in the surrounding areas, resulting in a lateral outflow of discharge. In Section 5.9 these discharges are discussed.

Approaching the downstream end of the sandpit, the currents in the pit decelerate again. The water in the sandpit partly discharges over the limits parallel to the x-axis, but mainly discharges over the downstream edge, see also Table 5.6 and Figure 5.12. Outside the sandpit, conservation of mass again results in an accelerating velocity. Due to viscosity this plume spreads out, so that far downstream there is no influence of the sandpit anymore.

The +45° rotated sandpit shows two major differences, compared to the parallel pit:

- The current velocities in the sandpit are not as large as in case of the parallel pit
- Hardly any deceleration of the current occurs along the lateral limits of the sandpit

The current through the rotated sandpit is directed more cross-wise, contrary to the current the parallel pit, that is directed in longitudinal direction of the sandpit. The northern lateral limit can be regarded as the upstream limit of the sandpit; hardly any lateral inflow of extra water occurs. Thus one can hardly speak about an increased discharge in case the sandpit is rotated.

The current velocity along the lateral limits of the rotated sandpit is determined by three aspects:

- Advection of velocities in the downstream direction
- Deceleration of the current because of the decreased discharge; this decrease of discharge is mainly caused by the fact that water is added to the main current that enters the pit over the upstream short edge of the pit
- In case of the northern edge, acceleration of the current due to the reduced resistance in the sandpit
- In case of the southern limit, acceleration due to the reduced cross-section

Along the northern border the influence of the accelerating effects (advection of high velocities from upstream and reduction of the resistance in the sandpit) decreases and the influence of the decelerating effect increases, finally leading to the observed deceleration area near the downstream end of the northern limit.

Along the southern lateral limit, the influence of the advection of lower velocities is already soon diminished, leading to the observed acceleration of the current along a large part of the southern edge.

5.4 Theoretical approach

In this section the minimum and the maximum current velocity in the sandpit and the adjustment length of that current are approached in a theoretical manner. With the help of an analytical approach of current phenomena one is able to draw some conclusions in advance about the behaviour of the current in sandpits. Later, when large-scale sandpits are actually designed, it might be helpful to have theoretical tools, with which a (rough) design can be made. When discussing the results of the simulations in Sections 5.6, 5.7 and 5.8, the theoretical values are compared with the numerically calculated ones.

5.4.1 Absolute minimum current velocity

After entering the sandpit, the current decelerates significantly, due to the increased cross-section. When one assumes that the discharge just in front of the sandpit is equal to the discharge just in the sandpit -a situation that will occur in an infinitely wide sandpit- the absolute minimum current velocity follows from the principle of conservation of mass. No extra discharge at all is attracted into the sandpit. In coherence with the principle of conservation of mass, the minimum current velocity can be described according to Equation (5.2).

$$\frac{u_{pit}}{u_{out}} = \frac{h_0}{h_{pit}} \tag{5.2}$$

in which:

u_{pit} =	minimum velocity just in the sandpit	[m/s]
u_{out} =	the current velocity just in front of the sandpit	[m/s]
h_{pit} =	the water depth in the sandpit	[m]
h_0 =	still water depth = 20	[m]

5.4.2 Absolute maximum current velocity

After the deceleration in the beginning of the sandpit, the current adapts itself slowly to the hydraulic conditions in the sandpit, reaching a maximum velocity. Whether this maximum current velocity is also the equilibrium current velocity, that belongs to the hydraulic conditions, depends on the length of the sandpit. An equilibrium velocity is reached when the sandpit is long enough to attract a sufficient amount of water over the pit's limits parallel to the main current. The equilibrium current velocity can be described with an adapted form of the Chézy formula, Equation (5.3).

$$\frac{u_{\max}}{u_0} = \sqrt{\frac{h_{pit}}{h_0}} \tag{5.3}$$

in which:

u_{max}=	the maximum current velocity in the sandpit	[m/s]
u_0 =	0.5	[m/s]

Equation (5.3) is derived assuming that the Chézy coefficient as well as the slope of the water surface inside and outside the pit are equal. The fact that these slopes are equal points to the assumption that an equilibrium in the pit is reached when the sandpit has attracted as much water as it needs. This situation is designated as the 'far-field' approach, that occurs when the width of the sandpit is much smaller than the length, see e.g. Ribberink (1989). This is contrary to the assumptions of the previous section, in which the pit should be infinitely wide. The velocities calculated with Equation (5.3) can be regarded as the absolute maximum current velocity that can occur in the sandpit.

In principle three situations with respect to the maximum current velocities exist. These situations are presented in Figure 5.4 and described beneath.

I. The maximum current velocity is smaller than the undisturbed current velocity as defined in the boundary conditions ($u_{max}<u_0$)
II. The maximum current velocity is larger than the undisturbed current velocity and smaller than the equilibrium current velocity. ($u_0<u_{max}<u_e$)
III. The maximum current velocity is the equilibrium current velocity ($u_{max}=u_e$)

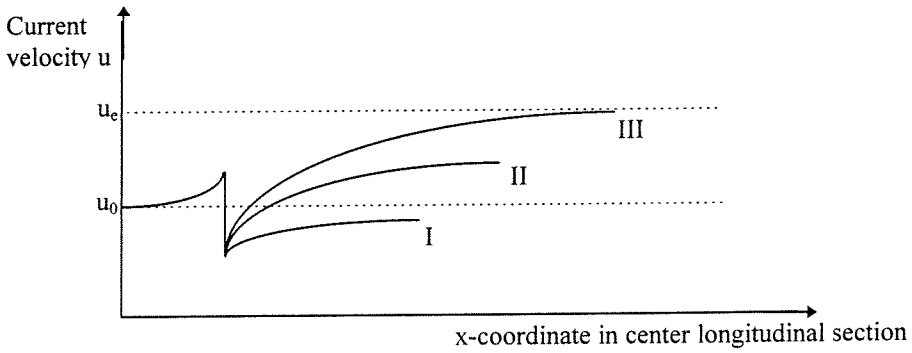

Figure 5.4: Three options for the maximum current velocity

In Section 5.6 the results of the computations regarding the magnitude of the maximum current velocity and the range of that velocity, according to Figure 5.4, are discussed.

5.4.3 Adjustment length

The adjustment of the current in the sandpit to the local hydraulic conditions needs a certain length and time. The adaptation time in these computations is not of interest, because of the stationary boundary conditions. A measure for the actual adjustment length is the adjustment length scale λ_w. This does not mean that where the x'-coordinate is equal to the adjustment length scale the current has reached its maximum velocity, let alone the equilibrium velocity. From the theory appears that this length scale can be expressed as the ratio between the friction term and the convective inertia term of the depth-averaged shallow water equations. This yields for λ_w:

$$\lambda_w = \frac{C^2 \cdot h}{2g} \tag{5.4}$$

This parameter originates from Equation (5.5), see De Vriend (1996) and Ribberink (1986). Figure 5.5 shows the definition of the variables and constants of Equation (5.5). With Equation (5.5) and the current velocities in the center longitudinal section of a 100×5 km^2 sandpit, in which the maximum current velocity is assumed to be the equilibrium current velocity, the adjustment length scale λ_w can be determined on basis of the computations and can be compared with the theoretical value calculated with Equation (5.4).

$$\frac{u(x')^2 - u_e^2}{u_0^2 - u_e^2} = e^{-\frac{x'}{\lambda_w}} \tag{5.5}$$

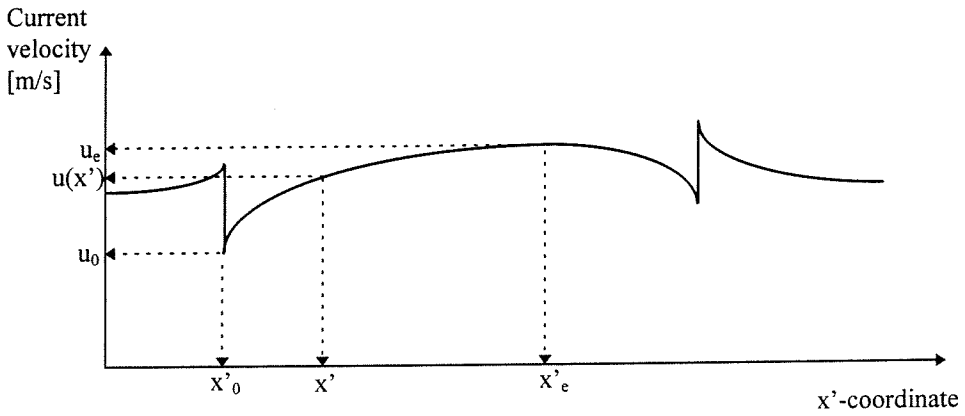

Figure 5.5: Definitions of parameters in Equation (5.5)

Equation (5.5) implies that the relative velocity difference between the velocity at beginning of the pit u_0 and a velocity u(x') somewhere in the accelerating part of the pit and the equilibrium current velocity u_e decreases according to a negative exponential function.

Velocity u_e as well as u_0 are known. Also the velocity u(x') is known in every grid cell. With a choice for x', expressed in a multiple of the adjustment length and resulting in a relative velocity difference, velocity u(x') can be calculated. By counting the grid cells, in which the current velocity is smaller than the calculated value of u(x'), starting at the beginning of the sandpit, the adjustment length scale (or a multiple of it, dependent on the choice of x') is known with an accuracy of 500 m.

For example, one chooses x' as three time the adjustment length scale. It means that the relative velocity difference has decreased to 5% (e^{-3}). With u_e and u_0 known, velocity u(x') can be calculated and the adjustment length can be determined.

The discussion of the theoretical and the numerical results concerning the adjustment length scale are discussed in Section 5.8.

5.5 Area of influence

In this section some conclusions about the magnitude of the area, that is influenced by the sandpit, are drawn. The extent to which the current pattern in and around the sandpit is changed with respect to the undisturbed situation might be of importance for shipping's interests. One has to bear in mind that these current velocities are depth-averaged values. The current velocities near the bottom are in general smaller than at the surface.

Figure 5.6 shows the plots of the current pattern magnitudes around four, 30 m deep pits. The contour classes of the plots have been chosen such that the areas in which the current velocity differs at least 3% and 5% from the undisturbed current velocity of 0.5 m/s are drawn.

The length in y-direction of the area, in which the velocity has decreased more than 5% is about two-third of the length of the sandpit. This holds, however, only for lengths smaller than about 20 km.

Twenty kilometer long sandpits are already long enough to spread the inflow of water along the sandpit. That appears from the limited length in y-direction of the influenced area. Longer sandpits show a different shape of the influenced area. Dependent on the width and depth of the sandpit, the area of influence tends to split in two, with a part at the beginning and a part at the end of the pit. The less water is attracted to the sandpit, the more this effect occurs.

The length of the area in front of the pit in which larger velocities occur are as long as the width of the sandpit. The high velocity area at the downstream end of the sandpit is somewhat longer than the width of the sandpit.

5.6 Minimum velocity in the center longitudinal section

Table 5.2 shows the results of Equation (5.2) and the numerical computations. One should notice that the water depth has been assumed to be the undisturbed water depth. Both water depths are in reality somewhat smaller due to the acceleration of the current in front of the pit and due to the much lower level of the bottom of the pit.

Table 5.2: Theoretically and numerically determined minimum velocities in a 100×5 km² pit

depth	theoretical ratio u_{pit}/u_{out}	calculated ratio of u_{pit}/u_{out}	relative difference
30	0.667	0.750	12.4 %
28	0.714	0.787	10.2 %
25	0.800	0.855	6.9%
22	0.909	0.936	3.0%

One can see that there is a rather large difference between the theory and the computations. This difference increases with increasing depth of the pit. The general picture is that the

computations overestimate the current velocity in the sandpit with respect to the theoretical values. Two reasons explain these differences.

The first reason is the fact that the discharge in front of the pit is not equal to the discharge just in the pit. Already in the first grid cell of the sandpit extra water has been added from aside to the current in the pit. Even the maximum lateral discharge occurs in the first grid cell. This also explains the differences between the depth variants. The larger the depth the larger the lateral discharges into the sandpit.

The second reason is that the discharge in front of the sandpit is already larger than the discharges in case of an infinitely wide one.

To sketch this, Figure 5.7 shows the current velocities in the center longitudinal section in case of a 'infinitely' wide sandpit and a 5×5 km^2 sandpit both of 30 m deep. One can clearly see the influence of the extra discharge that is added to the sandpit; significantly larger velocities occur. One can also see that the minimum current velocity in the infinitely wide sandpit obeys rather well to Equation (5.2). With u_{out} = 0.5 m/s and h_0/h_{pit} = 0.667 the minimum current velocity should result in 0.33 m/s. This is indeed the minimum velocity according to Figure 5.7.

5.7 Maximum velocity in the center longitudinal section

This section will discuss the results of the simulations as far as the maximum current velocity in the sandpit is concerned. When in this section is spoken about the (maximum) current velocity, the (maximum) current velocity in the center longitudinal section of the sandpit is meant. Two aspects are of importance in this section.

- The magnitude of the maximum current velocity
- The maximum current velocity with respect to u_e and u_0

Before discussing the maximum current velocities in the center longitudinal section, one should notice that the maximum current velocity in a cross-section of the sandpit does not always occur in the center of the pit. Figure 5.8 shows the u-velocity distribution in three cross-sections, viz. in the upstream part, in the middle and in the downstream part of the sandpit. One can see that the velocities in the center cross-section are rather uniformly distributed. The other two cross-sections show a larger current velocity at the sides of the pit. These larger velocities in the upstream part are the results of attraction of discharge from aside and contraction of the current in front of the sandpit. At the downstream end this distribution is caused by the outflow of water in a plume, where the opposite of contraction happens.

Figures 5.9, 5.10 and 5.11 present the results of the computations concerning the relative maximum current velocity in the center longitudinal section of the sandpit. The maximum relative current velocity is determined by dividing the difference between u_0 (=0.5 m/s) and the actual velocity by u_0. These plots show the maximum current velocity plotted against the length, the length-width ratio and the length-depth ratio of the sandpits, respectively. In Figure 5.9 the maximum current velocity in the center longitudinal section of the sandpit is

plotted as a function of the length of the sandpit. Especially the lines, which resemble the 22 m and 25 m deep sandpits, show that the current velocity tends to a maximum. The current velocity hardly increases in sandpits that are 5 km wide and longer than about 60 km. The velocity in a 100 km long 30 m deep sandpit still has not reached the equilibrium velocity. The relative maximum current velocities in the 10 km wide pits lag these velocities in the 5 km wide ones. The wider pits need more length to reach an equilibrium state. Clearly can be seen that in case of the 22 m deep sandpit the velocity in the wide pit almost equals the velocity in the narrow one. When the sandpits would be longer, these velocities are expected to become the same. This is according to the Chézy formula, in which the width has no influence. A wide pit can only be seen as one-dimensional when also the length is larger. Though not completely visible in the figure, this independence is also expected for the deeper sandpits. One can state that in case of very long sandpits the width does not influence the maximum current velocity. One should notice that an equilibrium current occurs in sandpits with lengths that are beyond the present practice.

Figure 5.9 as well as Figures 5.10 and 5.11 show the importance of the depth regarding the maximum current velocities. The numerically calculated current velocities as well as the values according to Equation (5.3) are presented in Table 5.3. The numerically calculated maximum velocity in the 100 km long and 5 km wide pit is assumed to be the equilibrium current velocity.

Both water depths in Equation (5.3) are determined assuming that the water level is horizontal, with a water depth of 20 m, while actually a sloping water level is present, resulting in a maximum water level difference of 0.36 m. Both values of the water depth could be corrected with e.g. 0.18 m. This is however not done, because also the magnitude of the correction is uncertain and the difference between the corrected and not-corrected current velocities are only minimal.

Table 5.3: Comparison of the maximum current velocity in 100×5 km^2 sandpits

Depth of the sandpit [m]	Theoretically deduced relative equilibrium velocity	Theoretically deduced absolute equilibrium velocity [m/s]	Simulated relative equilibrium velocity	Simulated absolute equilibrium velocity [m/s]
22	1.049	0.525	1.054	0.527
25	1.118	0.559	1.110	0.555
28	1.183	0.592	1.162	0.581
30	1.225	0.612	1.194	0.597

One can see that the numerically calculated values of the maximum current velocity differ more from the theoretically deduced values as the depth increases. This phenomenon is explained in Section 5.8, where the adjustment length of the current is discussed. The velocity in a 22 m deep pit has increased with 5.4% with respect to the undisturbed situation (0.5 m/s). The deeper the sandpit the larger the increase of the current velocity in the sandpit. The velocity increases from 11.0% and 16.2% in 25 and 28 m deep sandpits respectively, to 19.4% in 30 m deep sandpits.

In case of 22 and 25 m deep sandpits the theoretical and the computed maximum current velocities differ less than 1%, which is a negligible difference. The differences in case of the deeper two pits are 2% and 3%. Also the velocities in these two depth variants can be sufficiently accurately described with the Chézy formula. The difference between the theory and the model results however, increases as the depth increases. In the considered range of depths this difference is not very large, but might become too big to use the Chézy formula as a simple tool for estimating the maximum velocity, when depths of e.g. 40 or 45 m are applied. It does however give an upper limit for that velocity.

An other remarkable phenomenon can be seen in Figure 5.10. All lines intersect in the point where the length-depth ratio is about 3 and the relative current velocity amounts to 1.025. One can state that the lines also intersect the x-axis at (roughly) the same place, where the length-depth ratio is about 2.5-3.0. This means that transition of the current from deceleration to acceleration, in comparison with the undisturbed velocity, is independent of the depth and depends on the critical value for the length-width ratio.

5.8 Adjustment length

This section discusses the length the current needs to adjust itself to the new hydraulic conditions in the sandpit. Figure 5.9 shows that a sandpit of about 60 km is a minimum requirement to reach an equilibrium current (in case of a 5 km wide sandpit). Therefore the adjustment length is determined on the basis of the data obtained with calculations of 100 km long and 5 km wide sandpits. The current velocities in the center longitudinal section are used. Since the length is sufficiently long to have an uniform velocity distribution in the cross-section of the pit, the velocities in the center longitudinal section are a rightful choice.

The adjustment lengths of the current according to Equations (5.4) and (5.5) are summarized in Table 5.4. As one can see from Figure 5.2 there is a large part of the sandpit with a very small change in velocity. The adjustment length scale is therefore very sensitive for the value of u(x'). Even a difference of 0.001 m/s can cause an adjustment length scale that differs a factor 2. In order to account for this sensitivity, the adaptation length is determined for both 0.99*u(x') and 1.01*u(x'), designated as $u(x')^-$ and $u(x')^+$. Also the choice of the x'-coordinate influences the adjustment length scale. That is the reason why the adjustment length scale has been calculated for three values of x'-coordinate, viz. $x=\lambda_w$, $x=2\lambda_w$ and $x=3\lambda_w$, designated as $\lambda_{36.8\%}$, $\lambda_{13.5\%}$ and $\lambda_{5\%}$, respectively.

Table 5.4: Numerically calculated and theoretical determined adjustment length scales

Depth	λ_{theory} [m]	Velocity u(x')	$\lambda_{36.8\%}$ [m]	$\lambda_{13.5\%}$ [m]	$\lambda_{5\%}$ [m]
22	4738	$U(x')^+$	12000	not adjusted	not adjusted
		$U(x')^-$	5000	6000	8000
25	5375	$U(x')^+$	9000	16000	not adjusted
		$U(x')^-$	6500	7000	6800
28	6030	$U(x')^+$	10000	13000	not adjusted
		$U(x')^-$	7500	8000	8200
30	6460	$U(x')^+$	10000	12750	not adjusted
		$U(x')^-$	8000	8750	9000

The influence of the choice of x'-coordinate is clear in case of $u(x')^+$. With increasing x'-coordinate the adjustment length increases. This aspect is less pronounced in the deeper sandpits. The adjustment length, that is based on $u(x')^+$ clearly does not match the negative exponential function, shown in Equation (5.4).

The adjustment length calculated with $u(x')^-$ shows some influence of the choice of the x'-coordinate. One can state that the adjustment length based on $u(x')^-$ matches the negative exponential function rather well, independent of the depth of the pit.

When the adjustment lengths calculated on the basis of $u(x')^-$ are assumed to be the true adjustment lengths that follow from the numerically calculations, these adjustment lengths match rather well with the theory. The deeper the pit the larger the difference between theory and the numerical calculations. The relative difference is about 30% in all depth variants. Despite the differences between theory and the numerical results, the influence of the depth on the adaptation length is clear. The deeper the pit the larger the adjustment length scale.

One of the reasons for the increasing difference with increasing depth might be the fact that more water is attracted to the sandpit when the depth is larger. More water adds more kinetic energy to the current in the sandpit. Equation (5.4) is deduced for situations in which the discharge is constant. The current through sandpits has not the same feature as the flow conditions for which Equation (5.4) was deduced.

The theoretical value is deduced from situations, in which the discharge does not change. An equilibrium state is reached when the amount of energy gained by the pressure gradient equals the energy losses due to friction. As mentioned before, the discharge in sandpits increases. Besides the energy gained by the pressure gradient, energy increases because extra water with a certain amount of kinetic energy is added. It can be expected that the current needs more time and space to adapt itself to the hydraulic condition in the sandpit.

5.9 Velocities and discharges at the edges of the sandpit

In order to obtain a complete picture of the water movement in and around sandpits, the discharges and the velocities on the edges are discussed. Only the current velocities on the edges, which are perpendicular to the main current, are treated. Table 5.5 presents the current velocities in the center grid cell of the upstream and downstream edge (u_c) as well as the width-averaged velocities on these edges (u_a) of the 100 km long sandpit.

The velocity u_c in the center grid cell is a bit larger than the averaged velocity u_a. It means that the velocity distribution along the upstream and downstream edges is not uniform. The difference between u_c and u_a increases with increasing depth and decreasing width. Besides that, the difference is larger at the downstream boundary. Also the velocities themselves are larger at the downstream edge than at the upstream one. It means, as mentioned before, that water from aside is attracted. In case of stationary boundary conditions, the discharges into the sandpit reach a stationary state.

Table 5.5: Current velocities on the upstream and downstream edges of the 100 km long sandpit

Dimensions of the sandpit	u_c upstream [m/s]	u_a upstream [m/s]	u_c downstream [m/s]	u_a downstream [m/s]
w=5 km, d=22 m	0.519	0.516	0.547	0.541
d=25 m	0.543	0.538	0.599	0.589
d=28 m	0.564	0.557	0.646	0.634
d=30 m	0.577	0.568	0.674	0.661
w=10 km, d=22 m	0.519	0.517	0.546	0.543
d=25 m	0.541	0.538	0.595	0.591
d=28 m	0.560	0.556	0.637	0.632
d=30 m	0.570	0.567	0.662	0.657

The discharges into and out of the 100×5 and 100×10 km^2 and 30 m deep sandpit are presented in Figure 5.12 and Table 5.6.

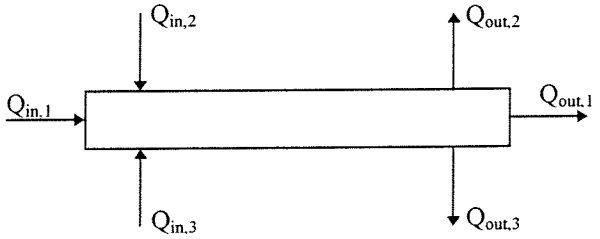

Figure 5.12: Resultant discharges into and out of the sandpit

Table 5.6: Discharge distribution around the 100 km long and 30 m deep sandpit

Resultant discharge	Discharges in 100×5 km^2 pit[$*10^3$ m^3/s]	Discharges in 100×10 km^2 pit [$*10^3$ m^3/s]
$Q_{in,1}$	55.5	110.0
$Q_{in,2}$	11.2	22.4
$Q_{in,3}$	9.53	23.0
$Q_{out,1}$	62.5	123.0
$Q_{out,2}$	6.86	14.5
$Q_{out,3}$	6.86	14.6

These discharges are taken from the grid cells, in which the depth is 20 m, bordering the bank of pit. The mass balance of water entering and leaving the pit is in both situations fulfiled, although small round off errors are present.

There is an asymmetry in the inflow from aside, because $Q_{in,2}$ and $Q_{in,3}$ are not equal. This might be explained by the influence of the numerical scheme.

One can see that the discharges Q_1 are almost proportional to the width of the sandpit. Although not represented in the table, this proportionality is independent of the depth of the

sandpit. Despite the contraction of the current in front of the sandpit, proportionality occurs rather well.

The discharges $Q_{in,2}$ and $Q_{in,3}$ that enter the pit from aside are not proportional to the width of the pit. When the width doubles these discharges more than double. These discharges depend on the water level gradient perpendicular to the pit's axis. This water level gradient on its turn depends apparently on the width of the sandpit.

5.10 Conclusions

The results of this chapter show that the general features of the current pattern in and around the sandpit consist of a number of acceleration and deceleration areas, which are caused by an increased or decreased cross-section and an increased or decreased discharge. Obliquity of the sandpit is hardly of influence on this pattern.

The maximum current velocity in the center longitudinal section of the sandpit can be well described with the formula of Chézy. The length-width ratio of the sandpit appears to be an important parameter for this maximum current velocity. A ratio of three is a critical value for the maximum current velocity. Sandpits with a ratio larger than three have a maximum current velocity that is larger than the undisturbed current velocity, imposed by the boundary conditions. The equilibrium current velocity is reached only in a 5 km wide and 22 m deep sandpit, with a minimum length of about 60 km.

The adjustment length scales determined with Equation (5.5) and the model results are not always equal to the theoretical values of Equation (5.4). Firstly, the adjustment length proved to be very sensitive to the method with which the adjustment length is determined. Secondly, the conditions that occur in the sandpit (attraction of water) do not correspond to the assumptions on which Equation 5.4 is based.

Another interesting feature of the current in and around sandpits is the fact that the discharges that are attracted from aside to the sandpit are more than proportional to the width.

6 Stationary water motion including Coriolis

6.1 Introduction

This chapter deals with the description of the current pattern in and around the sandpits, obtained by numerical calculations in which stationary boundary conditions are imposed including the influence of Coriolis. The dimensions of the sandpits have been chosen such that the influence of the width and the length on the qualitative picture of the stationary current pattern can be studied. The most important aspect of this chapter is the influence of Coriolis together with obliquity of the sandpit on the stationary current pattern. The depth of all pits have been set at 30 m, because the effects that will occur will be most pronounced in the deepest pit.

The Coriolis force is actually an artificial force. It has to be implemented in numerical models in order to take into account the effect of the gradient of the rotation speed of the earth in the latitude direction.

Table 6.1 shows the simulations that are performed with stationary boundary conditions including Coriolis. The numbers indicate the volumes of the pit in millions m^3. The 40×5 km^2 and 30 m deep sandpit is taken as the standard case. The other simulations are performed in order to study several aspects of the pits dimensions on the stationary current pattern. Only the simulations that give relevant (additional) information are presented in the plots. The direction of the angle of rotation is defined in Figure 4.1.

Table 6.1: Executed simulations with stationary boundary conditions including Coriolis

orientation → dimensions ↓	+45° rotated	+22.5° rotated	parallel	-22.5° rotated	-45° rotated
40×5 km^2	2000	2000	2000	2000	2000
40×10 km^2	4000		4000		4000
20×5 km^2	1000		1000		1000
10×5 km^2	500		500		500
10×10 km^2	1000		1000		

These numerical calculations are the second step in obtaining knowledge of the current pattern in and around large-scale sandpits. Section 6.2 discusses the boundary conditions that are imposed. Section 6.3 describes the stationary current pattern including Coriolis around several pits, varying in orientation. Section 6.4 discusses the sensitivities of the results for the dimensions of the pit. Section 6.5 summarizes the maximum current velocities as they occur somewhere in or near the sandpit. Not only the values of the stationary current including the Coriolis force but also the maximum velocities as they were present in the results of Chapter 5 are included. Section 6.6 finally summarizes the conclusions of this chapter.

6.2 Boundary conditions

The numerical calculations in this chapter are performed with a current velocity boundary condition at the upstream and a water level boundary condition at the downstream border of the modelling area. When Coriolis is included in a numerical model with these boundary conditions, the influence of the Coriolis force is more pronounced present than it would be in reality. With the main current in positive x-direction, the Coriolis force causes a water level slope in y-direction, with increasing water level in negative y-direction. Everywhere in the modelling area the water level adapts itself according to the Coriolis force, except at the downstream boundary, where a (horizontal) water level is imposed. This causes a strong gradient of the water level in the x-direction, which on its turn causes a current that in reality does not exist. The downstream boundary condition should be corrected. When a water level at the downstream boundary is imposed with the same slope as would be caused by the Coriolis force, then there is no artificial water level gradient and thus no artificial currents.

In practice, the water level slope that is caused by the Coriolis force and that has to be imposed follows from two terms of the differential equation for the conservation of momentum of the depth-integrated shallow water equation, Equation (3.2). These two terms are shown in Expression (6.1).

$$g\frac{\partial \eta}{\partial y} = -fu \tag{6.1}$$

in which:

f	=	Coriolis parameter = $2\omega\sin\varphi$	[s^{-1}]
u	=	0.5	[m/s]

and:

ω	=	the rotation celerity of the earth = $7.27*10^{-5}$	[rad/s]
φ	=	geographical position (latitude) of the modelling area = 50° north	

The first term in Equation (6.1) represents the force (per unit of mass) due to the water level gradient in y-direction. The second term represents the contribution of the Coriolis force to the total amount of momentum. Although the u-current is not uniform, the value of 0.5 m/s is used to calculate the correction of the downstream water slope.

The water slope that has to be imposed is $5.68*10^{-6}$ and, with a modelling area of 100×100 km^2, a water level difference of 0.568 m between the northern and southern boundary of the modelling area has to be imposed. This adjustment is equally spread over the downstream boundary, resulting in a water level of -0.284 m in the north and +0.284 m in the south of the downstream boundary, see Figure 6.1.

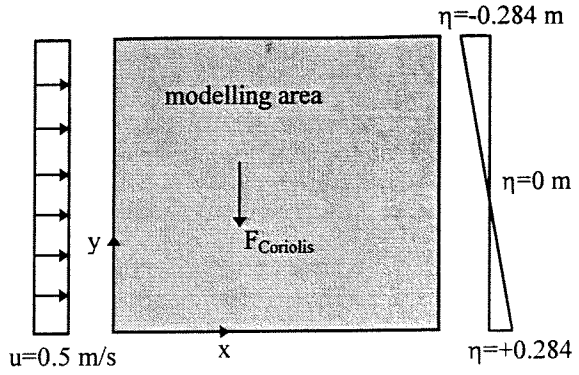

Figure 6.1: Stationary boundary including Coriolis

After correcting the boundary conditions the result is an uniform velocity field (if a sloping bottom is implemented, which is not the case in these simulations) and a sloping water level in the direction perpendicular to the main current. Of course in case of the 50×50 km^2 grid the corrections are halved.

6.3 Stationary current pattern

This section discusses the current pattern around parallel and rotated sandpits induced by stationary conditions including the influence of Coriolis. One should keep in mind that the Coriolis force is proportional with the current velocity. It means that when the current velocity increases the Coriolis force increases and subsequently the deflection of the current to the right increases. Figures 6.2 to 6.6 present the stationary current patterns. The upper left plot shows the current velocity in x-direction, velocity u. Like in Chapter 5, the plot of the u-velocity is also representative for the current magnitudes. The lower left plot shows the v-component of these plots. The upper right plot shows the vector plots of the current magnitudes and the lower right plot shows the current magnitude in cross-section AA", as it is defined in the upper left plot.

Another aspect one should keep in mind when analyzing the results is the correction of the downstream boundary condition. The correction of the downstream boundary condition is based upon a current velocity of 0.5 m/s, though the current velocity on that border is in general somewhat larger and not uniformly because of the influence of the outflow out of the sandpit.

The Coriolis force asserts its influence as follows. In general, a water level gradient in y-direction will be present due to the Coriolis force. That's the reason why the water level boundary condition could not be a horizontal one. This water level gradient is about equal to the gradient that would develop in case of an undisturbed bottom. The current velocities in and around the sandpit deviate from the undisturbed current velocities, so that the water level gradient and the Coriolis force are not in equilibrium anymore. When the current velocity is larger than (about) 0.5 m/s the Coriolis force is larger than the force induced by the water level gradient, and results in an additional v-velocity in negative y-direction. The opposite happens when the current velocity is smaller than 0.5 m/s.

6.3.1 +45° rotated sandpit

Figure 6.2 shows the results of the simulations that is performed in case of a 40 km long and 5 km wide sandpit that is +45° rotated. When analyzing the results, one should compare Figure 6.2 with the plots of Figure 5.1. The following differences with the current pattern without Coriolis can be discerned:

- The area of increased velocities is shifted somewhat to the south
- South of the sandpit, current velocities with a rather large v-component in northward direction are present
- A clear deceleration area north of the sandpit
- Relatively high current velocities along the southern lateral limit of the sandpit, as can be seen from the plot of velocities in cross-section AA"
- The jet-like outflow at the downstream end of the pit is orientated to the left, in the opposite direction of the Coriolis force

The larger velocities in front of the downstream end of the sandpit cause a larger Coriolis force on that body of water. The result is that that area with relatively high velocities is situated more to the south. This rather small effect has significant consequences. The deceleration area at the south of the sandpit in the current pattern without Coriolis can not be observed anymore. The slightly shifted inflow area causes advection of relatively high velocities, south of the sandpit. Since these velocities have a rather large v-component, in the direction of the pit, water that tends to flow out of the pit over the southern lateral limit of the pit is hindered, resulting in the concentration of the current, which on its turn leads to the observed high velocities along that edge.

Because the inflow at the head of the sandpit is shifted to the south, the deceleration area along the northern limit can develop.

A combination of phenomena causes the northwards orientated outflow plume. In first instance one would expect that the Coriolis force directs that plume to the south. Especially the plot of the current velocities in y-direction show that this does not occur. Water entering at the head of the pit, tends to follow the line of least resistance, which is the direction of the longitudinal axis. Water entering the pit over the northern lateral edge forces this current, due to inertia, more to the southern lateral limit. The Coriolis force enhances this forcing. The current at the south of the pit hinders the outflow over the southern limit, resulting in the concentration of the current. These currents from the south causes that the outflow at the downstream end is forced in the northern direction, in the opposite direction of the Coriolis force. The deflection of this plume is amplified by the fact that the current decelerates in the downstream part of the pit. The current approaching through the sandpit tends to avoid this area. Under influence of the current velocities along the southern limit of the pit and the reduced Coriolis force (with respect to the water level gradient), the current in the sandpit is forced to the north.

6.3.2 +22.5° rotated sandpit

The current pattern around this pit is presented in Figure 6.3. Some remarkable differences with the +45° variant can be discerned:

- Higher velocities in cross-section AA"
- Even stronger deflection to the north of the jet-like outflow, with respect to the longitudinal axis
- The current pattern as a whole is more concentrated in the sandpit itself, since the orientation of the pit is more in direct line with the main current

The explanations of these observed phenomena are analogous to the ones mentioned in Section 6.3.1. Some effects are amplified by the fact that this pit is orientated more parallel to the main current.

6.3.3 Parallel sandpit

Figure 6.4 shows the water motion in a sandpit with the longitudinal axis in the direction of the main current. This figure should be compared with Figure 5.1. The stationary current pattern has the following characteristics:

- Also this pit has an asymmetrical inflow at the upstream edge of the pit and a jet-like outflow, with an orientation more or less to the north
- Two deceleration areas can be discerned, with this difference that the southern deceleration area stretches itself not completely along the southern limit
- A rather uniform distribution of the current velocities in cross-section AA", though the velocities in the south are somewhat higher
- The plot of the v-velocities show as if water is transported from the area south of the sandpit to the area north of the sandpit

One can see that water is added to the only from the south. Again this has to do with the asymmetric inflow.

6.3.4 -22.5° rotated sandpit

Figure 6.5 shows the stationary current pattern around the -22.5° rotated sandpit. A number of aspects can be discerned, which in most cases differ from the previous orientations:

- Two clear acceleration and deceleration areas can be discerned, like they are observed in the +45° rotated sandpit without the influence of Coriolis
- Significantly smaller velocities, in comparison with the parallel and the positively rotated sandpits, occur in this pit
- The plot with the v-velocities show that water enters the pit from the south and that water discharges out of the pit over the northern limit. Also these velocities are smaller than in the previous pits

Contrary to the positively rotated sandpits, the Coriolis force and the inertia in negatively orientated sandpits work in opposite directions. This orientation of the pit also decreases, or even hinders the inflow of water from the north. Thus less water enters the pit, which results in the observed low velocities. One can see that despite these low velocities and despite the opposite directions of the Coriolis force and the inertia, some concentration of the current occurs.

6.3.5 -45° rotated sandpit

The stationary current pattern under influence of the Coriolis force around the -45° rotated sandpit is presented in Figure 6.6. Some characteristics of the flow pattern are summarized below:

- The magnitude of the velocities are even smaller than in case of the -22.5° rotated sandpit
- Water flows constantly out of the sandpit over the northern limit

Again the deceleration of the current near the downstream end causes the water approaching through the sandpit to deflect and avoid that area. Inflow of water from the south pushes the water in the observed direction. The flow partly discharges over this edge but the flow is mainly bent away from that edge and discharges over the long edge of the pit. This is concluded from the plot with the velocities in y-direction, Figure 6.6. In this picture can be seen that the direction of the current velocity in y-direction changes two times in the downstream part of the sandpit. The large part with the negative direction is the part where the current tries to follow the longitudinal axis of the pit. The other, small part with the negative direction is the part in which water is discharged over the small downstream edge. The part with the positive direction is represents the north-east orientated high-velocity plume.

6.3.6 Conclusions

The stationary current pattern is determined by two major phenomena and the aspects of acceleration and deceleration of the current velocity. The first important phenomenon is the asymmetric inflow of water into the sandpit at the upstream end caused by the Coriolis force. This asymmetry results in relatively high velocities along the southern lateral limit of the pit.

The second, important aspect is whether the Coriolis force amplifies or compensates the inertia of the current entering the pit. Negatively orientated pits show a counterbalancing between these two phenomena, resulting in relatively low velocities in the pit. The opposite is true for positively orientated pits.

6.4 Sensitivities of the results

This section will discuss the sensitivities of the results for variation of the width and length of the sandpit. Figure 6.7 shows the current patterns around several pits, with varying dimensions.

To study the influence of the width on the current pattern, numerical calculations with +45° rotated 40 km long and 10 km wide sandpits have been executed. The qualitative picture of the current pattern does not change as the width of the sandpit changes. The particular acceleration and deceleration areas are present at the same location as they were found in the 5 km wide variant. A difference however is the magnitude of the extreme velocities that occur in and around the pits, see Table 6.2.

The length has some influence on the current pattern. The shorter the pit, the more the plume at the downstream end is orientated to the south in comparison with the longer pits. A shorter length means also less discharge that enters the pit over the southern edge. The result is that the current is not deflected to the north-east corner of the pit the same extent as the longer pits. Another consequence of the reduced discharge is that only a small area with rather high velocities occur in the pit. Figure 6.7 shows as an example the current pattern around a +45° rotated 10 km long and 5 km wide sandpit. The smaller the pit the smaller the maximum value of the current velocity. The minimum velocity however is slightly larger in case of the shorter sandpits.

The most extreme case to observe the influence of the length (and the width) is a square sandpit. Figure 6.7 shows the current pattern around such a pit. One can clearly distinguish the acceleration and deceleration areas that already were observed in previous pits. Even pits with a pronounced two-dimensional character, like this one, show hardly any difference. One noticeable aspect of the shorter pits is the fact that the velocities in the sandpit itself are rather small.

6.5 Magnitude of the velocities

To give a complete overview of the current patterns around several sandpits, the minimum and maximum current velocities in these variant are summarized in Table 6.2. It is emphasized that the minimum and maximum current velocities do not necessarily occur in the center longitudinal section of the sandpit. The plots of the stationary current patterns indicate where these maximum and minimum velocities occur. The ranges of the contour classes are chosen such that effects that are described in the previous sections are also visible in the plots. Besides this, it is also tried to give an indication of the maximum and minimum velocities. This combination is however not always feasible. Therefore Table 6.2 is added, in order to present the maximum and the minimum current velocities to complete the plots of this and the previous chapter.

The largest maximum velocities occur in the positively rotated sandpits and the smallest minimum velocities occur the negatively rotated sandpits. The extreme velocities in the parallel pit are moderate. The range of the velocities is in case of the implementation of Coriolis larger than the computations without Coriolis.

Table 6.2: Minimum and maximum current velocities with stationary boundary conditions [m/s]

Pit dimensions [km^2]	Pit orientation	U_{min}		U_{max}	
		No Coriolis	Including Coriolis	No Coriolis	Including Coriolis
40×5	+45°	0.368	0.357	0.619	0.661
	+22.5°	0.409	0.428	0.648	0.678
	parallel	0.427	0.421	0.662	0.670
	-22.5°	0.407	0.378	0.651	0.614
	-45°	0.368	0.334	0.619	0.578
40×10	+45°		0.322		0.701
	parallel		0.378		0.683
	-45°		0.285		0.605
20×5	+45°		0.318		0.674
	parallel	0.424	0.401	0.649	0.668
	-45°		0.306		0.604
10×10	+45°		0.280		0.662
	parallel		0.352		0.619
10×5	+45°	0.406	0.310	0.634	0.651
	parallel		0.393		0.632
	-45°		0.311		0.616

6.6 Conclusions

This chapter showed that the Coriolis force has a significant influence on the stationary current pattern. The asymmetrical inflow at the upstream short limit of the sandpit causes concentration of the current along the lateral edge towards which the Coriolis force works, resulting finally in an outflow that is orientated in opposite direction of the Coriolis force.

Another important aspect is whether the Coriolis force and the inertia of the current work in the same direction or opposite directions. In positively orientated sandpits, where these two terms of the depth-averaged shallow water equations amplify each other, relatively high velocities are found in the sandpit. Also parallel sandpits show relatively high velocities. In negatively rotated sandpits, in which the direction of these forces are opposite to each other, significantly smaller current velocities occur. The results also indicate that the 22.5° rotated sandpits show larger current velocities than both the 45° rotated sandpits and the parallel sandpit.

In general, one can state that the stationary current patterns including the influence of Coriolis show the most extreme current velocities, compared to the minimum and maximum current velocities that occur in the patterns without the influence of Coriolis.

7 Tidal water motion

7.1 Introduction

This chapter will deal with the numerical calculations, which are performed with symmetrical tidal boundary conditions. These boundary conditions are more realistic than the stationary boundary conditions, which were used in Chapters 5 and 6. In first instance the influence of Coriolis is neglected.

Table 7.1 shows the simulations that are performed with tidal boundary conditions with and without the influence of Coriolis. Because the pits that are rotated 22.5° showed no qualitatively different behaviour than the 45° rotated ones, these variants are omitted in this chapter, although their maximum tide-averaged current velocities are presented in Table 7.3. It all concerns, like in the previous chapter, 30 m deep sandpits. Again the numbers indicate the volumes of the pit in million m^3.

Table 7.1: Executed simulations with tidal boundary conditions with and without Coriolis

Orientation → Dimension↓	+45° rotated	parallel	-45° rotated
40×5 km^2	2000	2000	2000
40×10 km^2	4000	4000	4000
20×5 km^2	1000	1000	1000
10×5 km^2	500	500	500
10×10 km^2	1000	1000	

Section 7.2 discusses the input of the model, as far as it differs from the input mentioned in Chapter 4. These differences are mainly present in the boundary conditions. Section 7.3 discusses the results of the numerical simulations with tidal boundary conditions without the influence of Coriolis. In Section 7.4 the tide-averaged current pattern, caused by tidal boundary conditions and Coriolis, in and around sandpits is presented. The tide-averaged current pattern, with and without Coriolis, around a square 10×10 km^2 sandpit is dealt with separately in Section 7.5. Section 7.6 gives some attention to the maximum tide-averaged current velocities as they occur with and without Coriolis. Section 7.7 finally summarizes the conclusions of this chapter.

7.2 Model input

This section describes the input of the model as far as it differs from the input mentioned in Chapter 4.

7.2.1 Boundary conditions

In principle, the combination of a current velocity and a water level boundary condition is the best insurance for a successful numerical calculation. In case of a tidal water motion, without the influence of Coriolis, the former combination of boundary conditions can be applied. The choice of the boundary conditions, amplitude as well as phase difference, are of importance for the tide-averaged current pattern.

First of all one should discern the particular aspects of each combination of tidal boundary conditions. Therefore four simulation are performed; one pair (Figure 7.1) with u-h boundary conditions without the influence of Coriolis, but in which the effect of a phase shift between the peaks of the water level and the current velocity is studied. A second pair of computations (Figure 7.2) is performed with u-u boundary conditions in order to study the influence of Coriolis on the tide-averaged current pattern.

The combination of a current velocity and a water level imposes a symmetric current velocity signal at one boundary and a symmetric water level signal at the other. It means that the modelling software calculates a water level at the western boundary and a current velocity at the eastern boundary. Due to friction the western water level amplitude and the eastern current velocity amplitude are both larger than the values that are imposed with the boundary conditions. Since the influence of the friction is larger during ebb than during tide, the result is an asymmetric tidal motion. Altogether this results in a tide-averaged velocity of zero at the western boundary and a eastwards directed tide-averaged velocity at the eastern boundary. Thus, there is a gradient in the tide-averaged current.

This effect is essentially different from residual currents (or discharges) as they are observed along the Dutch coast. The direction of the residual currents are also in the flood direction but its origin is totally different. The product u(t)h(t) during the flood period is larger than during the ebb period, which means that a net discharge is present in the direction of the tide.

Figure 7.1 shows the tide-averaged current patterns, resulting from computations with u-h boundary conditions. The upper plot shows the pattern when the velocities and the water levels are in phase with each other. The lower plot shows the current pattern when there is one hour phase difference between the velocities and the water levels. One can see that the tide-averaged current velocity at the western boundary is indeed zero. One can also see that the phase difference results in a larger gradient of the tide-averaged current pattern. It also has a clear influence on the tide-averaged current pattern in and around the pit. The general effect of a phase shift is that larger velocities occur; even in the direction opposite to the tide-averaged current the current velocities are larger than in the case when no phase shift is imposed.

A combination of two symmetrical current velocity boundary conditions shows a somewhat different pattern. Figure 7.2 shows two plots with tide-averaged current patterns. Both plots are obtained from calculations with two current velocity boundary conditions, between which the phase difference amounts to the time the tidal wave needs to reach the other side of the modelling area. The upper plot shows the current pattern without Coriolis, the lower area the current pattern including the influence of Coriolis. The current pattern without the influence of Coriolis shows that the tide-averaged current velocities at the boundaries are zero, but in the middle of the modelling area, where the tidal wave is being influenced by friction, a small tide-averaged velocity is present.

The Coriolis force disturbs the whole pattern. Besides the influence it has on the current in and around the pit, it also significantly influences the current pattern at the boundaries. Although the arrows are not really visible, the contour map tells that the tide-averaged velocities are rather large. This pattern is, however, the most favourable, when Coriolis is implemented. Other combinations, e.g. two water level boundaries or two velocity boundaries with a phase difference, results in even more disturbed patterns at the boundaries. These results lead to the decision to use u-h boundary conditions when Coriolis is omitted and u-u boundary conditions when Coriolis is included.

Preliminary simulation runs proved that the sandpit has no influence on the amplitude of the vertical tidal motion on the boundaries. The calculated amplitudes in case of computation with a sandpit are equal to the amplitudes in case of computations without a sandpit. This holds for all variants of the magnitude of the current velocities.

The boundary conditions that are imposed in this hydrodynamic part of the study consist of only one component, viz. the M2 component with a period of 12^h24^m. Because of the length of the modelling area there is a phase difference between the two borders of the modelling area. With a tidal wave celerity of $\sqrt{gh}$ =14.0 m/s and a length of the modelling area of 100 km the tidal wave needs 1.98 hours to travel from one side to the other. This means a phase difference of 57.57° (360° stands for one tidal period).

Simple wave approach

The magnitude of the velocity and the water level amplitude can be deduced from the simplified equation for conservation of mass, viz. the simple wave equation, see Equation (7.1). One can see that friction in this approximation is neglected.

$$\frac{\partial \eta}{\partial t} + \frac{\partial q_x}{\partial x} = 0 \qquad (7.1)$$

in which:

q_x = specific discharge in x-direction [m^3/ms]

When the general solution for η is assumed as $\eta = \hat{\eta}\cos(\omega t - kx)$ and the general solution for q as $q = \hat{q}\cos(\omega t - kx)$ Equation (7.1) can, after some manipulation, be reworked into:

$$\omega\hat{\eta} - k\hat{q} = 0 \qquad (7.2)$$

in which:

ω	=	period of the tidal wave	[rad/s]
k	=	wave number defined as $2\pi/L$	[m^{-1}]

and:

L	=	the tidal wavelength	[m]

With $\frac{\omega}{k} \approx \sqrt{gh}$ this results in Equation (7.3), which describes the amplitude of the tidal wave as a function of the amplitude of the discharge or the current velocity.

$$\hat{\eta} = \frac{\hat{q}}{\sqrt{gh}} \approx \frac{\hat{u}}{\sqrt{g/h}} \tag{7.3}$$

In order to be consistent with Chapters 5 and 6 the velocity amplitude is set at 0.5 m/s (5000 m^3/s per grid cell) resulting in a water level amplitude of 0.714 m.

The simple wave approach, however, proves to be too simple. The phase differences between the two boundaries are not according to the expectations. Also the amplitudes of the sine boundary conditions showed too much difference between one border and the other. Either the water levels or the current velocities are resembled properly but not both in the same time. Since the current velocity is the most important variable in this study, one could chose the boundary conditions such that these are resembled well. This could be done by imposing two discharge boundary conditions. The water levels can however not be unambiguously determined. Every simulation with the same boundary conditions can result in different amplitudes around a different zero level. Continuity is guaranteed, but the differences in water levels are such that realistic results are not always obtained. Therefore the choice was made to use an other, more complicated method to determine the boundary conditions.

'Simple wave approach' including friction

This method consists of an analytical solution for the simplified governing equations, see Equations (7.4) and (7.5). Contrary to the simple wave approach friction is considered in this method.

$$\frac{\partial h}{\partial x} + \frac{1}{gA_s}\frac{\partial Q}{\partial t} + \frac{1}{C^2 A_s^2 R} Q|Q| = 0 \tag{7.4}$$

$$B\frac{\partial h}{\partial t} + \frac{\partial Q}{\partial x} = 0 \tag{7.5}$$

in which:

A_s	=	the wet cross-section, i.e. the water depth times the width	[m^2]
R	=	the hydraulic radius	[m]
Q	=	discharge	[m^3/s]

These equations are originally deduced for long waves in rivers, which explains the one-dimensional character of the equations. For application in two-dimensional cases these equations are rewritten such that they are valid per unit width. In order to reach that, the width B is assumed to be 1 m and the surfaces are divided by the unit width, resulting in the depth.

After some mathematical operations, the relation between the water levels and the discharges on the upstream and downstream borders are given by Equations (7.6) and (7.7).

$$h(L) = L_v h(0) + M_v Q(0) \tag{7.6}$$

$$Q(L) = N_v h(0) + L_v Q(0) \tag{7.7}$$

in which:

$L_v = \cosh(rL)$

$M_v = -\frac{r}{B\omega i}\sinh(rL)$

$N_v = -\frac{B\omega i}{r}\sinh(rL)$

$r = p + iq$

$p = \pm\omega\sqrt{mB}\sqrt{1/2}\sqrt{-1+\sqrt{1+\left(\frac{k}{\omega m}\right)^2}}$

$q = \pm\omega\sqrt{mB}\sqrt{1/2}\sqrt{+1+\sqrt{1+\left(\frac{k}{\omega m}\right)^2}}$

$k = \frac{8}{3\pi}\left(\frac{1}{C^2 A_s^2 R}\right)\hat{Q}$

$m = \frac{1}{gA_s}$

In these equations 'L' stands for the length of the modelling area and '0' for the western boundary of the modelling area. With the principle of conservation of mass ($Q(0) = Q(x) = 10$ m^2/s) and Equation (7.7) the water level amplitude at the upstream boundary can be determined. The upstream amplitude of the water level variation is according to this approximation 0.808 m. With Equation (7.6) this results in a downstream amplitude of the water level of 0.558 m. This value for the downstream water level differs considerably with the value of 0.714 m that was found with the simple wave approximation. The friction apparently has a significant influence on the results. This is not very surprising because of the large length of the modelling area.

The amplitude of the downstream water level boundary condition is indeed set at 0.558 m and the amplitude of the upstream current velocity boundary condition at 0.5 m/s. There are

still some differences in amplitudes between the boundaries, but these are inevitable and small enough to be acceptable.

7.2.2 Output

The most important output of these calculations is the tide-averaged current velocity field. Current velocities are stored every 24 minutes during one tidal period. That period is defined as the period between two upward or two downward crossings of the x-axis. This means that the time-averaged velocity pattern is determined with 31 values of the current velocity. To study purely the effect of the sandpit the effect of the boundary conditions is corrected. A tide-averaged current pattern above an undisturbed, flat sea bed (without a sandpit) is subtracted from the tide-averaged current patterns above a sea bed including sandpits.

7.2.3 Roughness

In tidal simulations it is more common to use the Manning friction coefficient instead of the Chézy coefficient. The relation between the two-dimensional Manning and the two-dimensional Chézy coefficient is shown in Equation (7.8).

$$n = \frac{\sqrt[6]{h}}{C} \tag{7.8}$$

in which:
n = Manning friction coefficient [$m^{1/3}s$]

With Equation (7.8) the Chézy coefficient of 65 $m^{1/2}/s$ is translated to a Manning coefficient of 0.025 $m^{1/3}s$.

7.3 Tidal motion without Coriolis

A number of simulations are performed to study the residual current pattern in and around sandpits. Since no Coriolis is implemented, the current patterns of the negatively rotated sandpits are the same as the patterns of the positively rotated ones. Therefore only the positively rotated pits are considered.

One should notice that, with tidal boundaries, downstream does not necessarily mean eastwards. When in this and the next chapter is spoken about the downstream or upstream direction, the direction should be seen with respect to the orientation of the current. For example, during the ebb period the downstream direction is westwards.

Figures 7.3 and 7.4 show the tide-averaged current pattern, corrected for the influence of the boundary conditions, around the whole sandpit (upper left plot) and details of the pattern around the two ends of the sandpit (upper right and lower left plots). The lower right plot shows the tide-averaged current velocities in cross-section AA". A positive value of this velocity means that the u-component of that velocity is directed in the positive x-direction. For the magnitude of the velocities one should look at the colour plots and not to

the vectors, which indicate the direction of the current. The length of the vectors are chosen such that they are long enough. This means that in every plot a different unit length of the vectors is used. Since the legend of the plots is based upon one plot, the vector in the legend does not represent all plots.

An important aspect, which appears in Sections 7.3.2 and 7.3.5 is the adjustment of the current in time.

7.3.1 +45° rotated 40×5 km^2 sandpit

In Figure 7.3 the tide-averaged current pattern of the +45° 40×5 km^2 sandpit is plotted. The current pattern shows the following major features:

- Two large circulation areas in the sandpit
- Just outside the sandpit, along the two lateral edges, the current velocity is in opposite direction to the direction of the current just in the sandpit
- The previous two features are confirmed by the current velocities in cross-section AA", from which one can see that the direction of the current changes six times
- In two corners an outwards orientated tide-averaged current velocity is present, viz. the most northern and the most southern corners of the sandpit
- A rather disorderly pattern in the two ends of the sandpit is present, though something like an eddy can be distinguished

It can be observed that the current tends to flow parallel to the pit's axis already at the upstream lateral edge of the pit. This is in contradistinction with the flow pattern under stationary boundary conditions, where the current tends to flow along the downstream lateral edge of the pit. The reason for this is the decelerating effect of the change of the tide. This can be seen as follows. The stationary current pattern is an equilibrium pattern. In the process of reaching this equilibrium the water entering the pit is under influence of the constant input of momentum of water with a velocity of 0.5 m/s. This momentum pushes the current to the other side until an equilibrium is reached. Harmonic boundary conditions, however, can be seen as a succession of a number of stationary conditions. Water is set going, enters the pit and under influence of the increasing current velocity stowed in the direction of the other side. But when a velocity of 0.5 m/s is reached, the velocity decreases again, decreasing also the input of momentum. Water does not reach the other side anymore, but will flow more along the downstream edge of the sandpit. The average pattern over one half of the tidal period is a current that flows along the upstream edge of the sandpit, contrary to the stationary pattern. During the other half of the tidal period the same process at the other side of the pit occurs in the opposite direction. The result is the residual current pattern shown in Figure 7.3.

The direction of the current velocity along the lateral limits, just outside the sandpit, are caused by the outflow of water out of the sandpit. The outflow velocities are apparently larger than the velocities during the other half of the tide, in which the current is directed into the sandpit.

The fact that the outflow velocities are larger than the inflow velocities, was already found in Chapter 5, and is confirmed by the outwards orientated tide-averaged current velocities at both the most northern and southern corners of the sandpit.

7.3.2 parallel 40×5 km^2 sandpit

The tide-averaged current pattern of the parallel 40×5 km^2 sandpit is presented in Figure 7.4 and shows the following characteristics:

- Generally quite small tide-averaged current velocities, which are rather uniformly distributed over the cross-section of the pit
- Outflow at all four corners of the sandpit
- Large circulation areas between the ends of the pit and the center of the sandpit

The tide-averaged current pattern is determined by the outflow velocities. High velocity 'jets' leave the sandpit under an angle of about 45° at all four corners of the sandpit. One can conclude from this that the inflow of water is more concentrated than the outflow, which spreads more. This was already concluded in Section 6.3 from the current patterns including Coriolis, where was stated that the orientation of the high velocity plume was mainly caused by the deflection of the current in the pit in order to avoid the deceleration area in the downstream end of the pit. Although in this situation no Coriolis force is taken into account, the current in the sandpit avoids the deceleration area anyway. Another way to put it is, that the current is deflected due to an opposite pressure gradient (water level) at the downstream end, due to deceleration of the current. Since Coriolis is omitted, the outflow of the current occurs in all four corners and not just in two of them.

One can distinguish large circulation patterns between the ends of the sandpit and the middle of the sandpit. This can be explained as follows. Chapter 5 showed that the current velocities at the downstream edge are larger than the velocities at the upstream edge. It means that more water is discharged over the downstream edge out of the pit than water discharges into the pit over the upstream end. Water must have entered from aside, in order to fulfil the law of continuity. Water entering the pit from aside partly comes from the water that is discharged over the downstream edge out of the pit, explaining the large circulation patterns around the sandpit. Within this pattern four smaller circulation areas occur at each end of the sandpit. Also these smaller circulation areas can be seen as the consequence of water that is discharged out of the sandpit and, with the turn of the tide, entered the pit again.

Sedimentation and erosion are not only determined by the tide-averaged current velocity pattern, but also by the magnitude of the velocities. In fact, the tide-averaged current velocity pattern says something about the direction of the transports; the current magnitude determines the magnitude of the sediment transport. Therefore, like in Chapter 5, the maximum velocity in the center section of this parallel sandpit is determined. The current needs a certain length and time to adapt itself to the hydraulic conditions in the sandpit. In case of stationary boundary conditions the simulation time is chosen such that an equilibrium state is reached, thus time is not the restricting factor concerning the maximum current velocity in the sandpit. The length on the contrary was of influence. With tidal

boundary conditions the adjustment of the current to the changed hydraulic conditions, is now either limited by time (in relatively long sandpits) or by the length of the sandpits, in case of short sandpits. Section 7.3.5 discusses the influence of the length of the sandpit on the tide-averaged current velocities and Section 7.6 summarizes the maximum tide-averaged current velocities, that occur in the simulations of this chapter.

The maximum flood current velocity in the center longitudinal section of this parallel pit amounts to 0.542 m/s and the maximum ebb current velocity is - 0.512 m/s. It can indeed be observed that the ebb current velocity is somewhat smaller than the flood current velocity.

When looking in detail, one can see that the place where the large circulation patterns enter the sandpit is not in the middle of the sandpit. It means that the area, where the ebb velocities are larger than the flood velocities, occupies a larger area of the pit than the area, in which the flood velocities are larger. This seems to be in contradiction with the expectations. The ebb velocities, generally spoken, are smaller than the flood velocities. The smaller water depth during ebb increases the influence of the friction on the current velocities, resulting in smaller velocities. In the sandpit however the velocities are dominated by the reduced cross-section. Both the ebb and the flood currents will decelerate significantly. The relative deceleration of the ebb currents is apparently not as large as the deceleration of the flood currents. After deceleration the current velocity increases due to discharge that is added to the pit. The ebb current in the pit, with a relatively large velocity compared to the flood velocity in the pit (relatively with respect to the undisturbed velocities), might reach earlier (in space) higher velocities, resulting in a larger area, where the ebb velocities are larger than the flood velocities.

7.3.3 Influence of the tidal amplitude

To study the influence of the tidal amplitude on the tide-averaged current pattern calculations with tidal current velocities of 1.0 m/s and 2.0 m/s have been performed, and are presented in the lower left and the upper right plots of Figure 7.5. These plots show that, conform the expectations, the current crosses the pit (to a certain extent) and flows along the downstream lateral edge of the pit. The momentum of the higher velocities is sufficient to stow the current more to the other side of the sandpit.

The plot of the tide-averaged current pattern obtained by computations with a tidal amplitude of 1.0 m/s shows that the currents just inside the pit and just outside are directed in the same direction, contrary to the results of tidal amplitude of 0.5 m/s. One can also see that the outflow out of the sandpit occurs in the two other corners than observed in the standard case.

The plots of the computations with a tidal amplitude of 2.0 m/s show that one large circulation area, partly in the pit and partly outside the pit, has developed.

The plots of Figure 7.5 also confirm the fact that a high velocity does not automatically mean a high tide-averaged current velocity. The magnitude of the highest tide-averaged velocity of the variant with an amplitude of 0.5 m/s is about equal to the one obtained with the variant with an amplitude of 2.0 m/s.

7.3.4 Influence of the width

The tide-averaged current pattern around a parallel 40×10 km^2 sandpit hardly differs from the pattern around a parallel 40×5 km^2 sandpit and is therefore not presented in a figure.

The general picture of the tide-averaged current pattern around a 45° rotated 40×10 km^2 sandpit shows the same features as the narrow variant. The two rotation cells in the sandpit are even more pronounced present. A relatively wide band with small or zero tide-averaged velocities separates these cells. Another small difference between the two width variants can be seen. The current pattern in the outer most parts of the 5 km wide pit shows a disorderly pattern, though something like an eddy can be discerned. This eddy is well developed in the 10 km wide sandpit. In stead of a completely circular eddy, the current tends to discharge out of the sandpit at the corners of the pit.

7.3.5 Influence of the length

In order to determine the influence of the length on the residual current pattern, the current patterns around the parallel 40 km, 20 km, 15 km and 10 km long and 5 km wide sandpits have been studied. Figure 7.6 shows the tide-averaged current pattern around these pits. As far as the 40, and also a bit the 20 km long pits, is concerned, hardly any influence of the length of the pit on the residual current pattern can be seen. Only the magnitude of the residual currents are influenced. Pits of 15 and 10 km long show already a deviant behaviour. The large circulation patterns are in case of the shorter pits more concentrated around the corners of the pit. There are still circulation areas to the middle of the long edges of the sandpit, but these are induced by the concentrated circulation areas around the corner rather than they are a part of these large areas. The shorter pits show a V-like shape of the tide-averaged current pattern near the corners of the sandpit.

It is interesting to look at the maximum current velocity that occurs in the center longitudinal section of the sandpit during the flood period. When these values are compared with the maximum current velocities in the center longitudinal section obtained by simulations with stationary boundary conditions one is able to say whether these maximum velocities are restricted by the length of the sandpit or by length of the tidal period. Table 7.2 presents these velocities.

Table 7.2: Influence of the pit's length on the maximum velocity in the center longitudinal section

	Stationary current [m/s]	Tidal current [m/s]	relative difference
Maximum tide velocity in 40 km long pit [m/s]	0.580	0.542	6.6%
Maximum tide velocity in 20 km long pit [m/s]	0.532	0.519	2.4%
Maximum tide velocity in 15 km long pit [m/s]	0.510	0.401	21.4%
Maximum tide velocity in 10 km long pit [m/s]	0.475	0.392	17.5%

One can see that the (relative) difference between the two maximum current velocities decreases as the length of the pit decreases (40 and 20 km long pits). One would expect that

the maximum current velocity in the center longitudinal section in both variations will become the same. The maximum current velocity is not restricted by time anymore, but the length of the sandpit determines the maximum current velocity. The change in behaviour of the sandpit under tidal boundary conditions can also be seen from Table 7.2. A strong decrease in the maximum current velocity occurs in the 15 km long sandpit. This change in behaviour occurs at a length-width ratio of about four. In Chapter 5 the length-width ratio of three represented the transition from a maximum current velocity smaller than the current velocity boundary condition (0.5 m/s) to a maximum current velocity larger than the 0.5 m/s. In case of tidal boundary conditions the critical value of this parameter is somewhat higher due to the time-lag in the adaptation process, see also Labeur (1998).

The magnitude of the outflow velocities during ebb as well as during flood are apparently not large enough to create large circulation areas around the pit. As is discussed in Chapter 5, the smaller pits do not have the opportunity to attract the discharge that it needs to reach an equilibrium current according to Chézy, resulting in smaller maximum velocities and thus also in smaller outflow velocities. Altogether this leads to local circulation areas around the corner of the sandpit.

7.4 Tidal water motion including Coriolis

In this section the results of the simulations with tidal boundary, in which also the Coriolis force is implemented, are discussed. Since the stationary current patterns around positively and negatively rotated sandpits are not similar, both positively and negatively rotated sandpits have been studied.

In the parallel sandpits of this section, the maximum current velocity is not determined since Coriolis causes an asymmetric flow in the sandpit; the current velocities in the center longitudinal section of the sandpit is not representative anymore for the current in the sandpit.

7.4.1 Boundary conditions

Again the boundary conditions need special attention. Current velocity boundary conditions with an amplitude of 0.5 m/s have been imposed in these calculations, despite the risk that the level of the zero-crossings of the water levels are not at the reference level. This aspect, which might cause artificial phenomena, should be checked after every simulation. By imposing two current velocity boundary conditions continuity is assured. The effect of Coriolis is mainly found in the water levels, which adapt themselves completely to the effects of Coriolis. No artificial gradients in the water level occur, and thus no correction of the boundary conditions has to be used.

7.4.2 +45° rotated 40×5 km^2 sandpit

Figure 7.7 presents the tide-averaged current pattern around a +45° rotated 40×5 km^2 sandpit. The most important difference is the fact that just outside the sandpit the residual velocities in case of Coriolis are three times larger than without Coriolis. This can best be seen in the current velocities in cross-section AA".

The current pattern can be seen as a combination of a circulation pattern around the pit and two smaller circulation patterns in the pit, which rotate in the opposite direction compared with the pattern around the pit. Because the development of the current pattern is limited in time, the influenced area does not stretch as far as the current patterns of the stationary flow.

Like in case of the tidal computations without Coriolis, at two corners the tide-averaged current is directed outwards.

7.4.3 parallel 40×5 km^2 sandpit

Figure 7.8 presents the tide-averaged current pattern around a parallel 40×5 km^2 sandpit. The parallel pit shows significant differences at both ends of the sandpit. Only at two corners of the sandpit a jet-like outflow occurs, in contrast with the tide averaged current in a parallel sandpit without Coriolis. Those two jet-like outflows are completely analogous with the left-orientated high velocity plumes, which are discussed in Section 6.3. When this figure is compared with Figure 7.4 one can see that the current velocities in the center of the sandpit are about equal. The velocities along the lateral edges of the sandpit, however, are much larger when Coriolis is implemented.

In the pit itself one large circulation area can be distinguished. Along the southern edge of the sandpit the direction of the current is equal to the direction of the current in the same pit without the influence of Coriolis. Along the northern border the direction of the tide-averaged current is opposite to the direction of that current as it occurs without the influence of Coriolis.

The current pattern in the ends of the pit shows a disorderly pattern. But when looking at the 10 km wide variant, one can see that near each end two circulation patterns tends to develop. The direction of the residual current is southwards at the western edge and northwards at the eastern edge. These directions are the result of the Coriolis force during inflow and the urge of the flow to avoid the deceleration area, which under influence of the constant inflow from aside and the decreased Coriolis force is pushed in the opposite direction of the Coriolis.

7.4.4 -45° rotated 40×5 km^2 sandpit

Figure 7.9 shows the tide-averaged current pattern around a -45° rotated 40×5 km^2 sandpit. Unlike the current velocities in the sandpit in the simulations with stationary boundary conditions, the magnitude of the tide-averaged current velocities are hardly sensitive for a positive or a negative rotation of the sandpit. The velocities outside the sandpit along the lateral limit are significantly larger, compared to the situation in which Coriolis is ignored.

7.4.5 Influence of the length

In order to study the influence of the length, Figure 7.10 shows the tide-averaged current pattern around a parallel 10×5 km^2 sandpit. The qualitative picture of this variant is hardly different from the longer pit.

There are some differences visible in the velocities in cross-section AA" but these are caused by the fact that this cross-section is taken through some eddies on the edges of the sandpit. Cross-section AA" in case of the 40×5 km^2 sandpit is also taken in the middle but, because of the longer length, this cross-section is taken through a more calm area.

In both pits the outflow at the two corners, which were already mentioned, are visible.

7.5 Results concerning square 10×10 km^2 sandpits

This section discusses the tide-averaged current patterns around the +45° rotated and parallel square 10×10 km^2 sandpit, with and without Coriolis. These patterns are presented in Figure 7.11.

The tide-averaged outflow is in the two other corners than the corners observed in the 40×5 km^2 sandpit. This shift of the flow is well noticeable when the figures of the 40×5 km^2, the 20×5 km^2 and the 10×10 km^2 sandpits are compared with each other.

As in the longer sandpits, one can see that the influence of Coriolis is most pronounced in case of the parallel sandpits. Without the implementation of Coriolis the larger velocities are concentrated around the corners of the pit. The Coriolis force causes a north-south directed tide-averaged current pattern along both limits of the pit perpendicular to the tidal axis. The explanation for this pattern can partly be found in the asymmetric inflow of discharge over the lateral edges of the pit, as described in e.g. Section 6.4.3. The constant input of water from the south during flood (and from the north during ebb) deviates the flow in the pit to the north. In order to 'avoid' the deceleration area at the eastern end of the pit the current orientates itself to the north during tide (and to the south at the western boundary during ebb). Another reason for the north-south direction of the current in these areas is the enhanced deflection of the current to the right under influence of Coriolis in the acceleration areas in front of the sandpit.

The most remarkable effect of the rotation of this square pit is the rather high tide-averaged current velocities, with respect to the other pit configurations. The tide-averaged current velocities are about a factor two or three higher than in case of the 40×5 km^2 variants, see Table 7.3. The influence of Coriolis is, as in the previous cases, hardly of influence on the qualitative picture of the current pattern around rotated sandpits. It has only a relatively small influence on the magnitude of these velocities.

7.6 The magnitude of the (tide-averaged) current velocities

To complete the description of the tide-averaged current pattern around several sandpits, Table 7.3 shows the maximum tide-averaged current velocities that occur in every single pattern.

Table 7.3: Maximum tide-averaged current velocities with and without Coriolis [m/s]

Pit dimension [km^2]	Pit orientation	U_{max}	
		No Coriolis	Including Coriolis
40×5	+45°	0.100	0.090
	+22.5°	0.081	
	parallel	0.035	0.062
	-22.5°	0.081	
	-45°	0.100	0.097
20×5	+45°	0.199	0.185
	parallel	0.059	0.065
	-45°	0.199	0.207
10×5	parallel	0.059	0.066
10×10	+45°	0.186	0.181
	parallel	0.057	0.062

One can see that besides the square pits also the rotated 20×5 km^2 pits show large averaged current velocities. The smallest velocities are present, without exceptions, in the parallel sandpits, in which the magnitude of the velocity is about constant for the sandpits smaller than 20 km. The parallel 40×5 km^2 sandpit shows even a smaller tide-averaged current velocity. Contrary to the results of the stationary current patterns, the 45° rotated sandpits cause larger (tide-averaged) velocities than the 22.5° rotated sandpits.

The emphasis in this chapter is clearly on the tide-averaged current velocities. They are of importance for the sediment transport patterns and do give an indication for the direction of the transport. But there is no relation between the magnitude of the tide-averaged current velocities and the magnitude of the current velocities and thus the sediment transport capacity. A tide-averaged current velocity of 0.1 m/s can occur in a tidal motion with a velocity amplitude of e.g. 0.2 m/s but also in case of a velocity amplitude of 1.0 m/s. The tide-averaged results is the same but the transport rates are completely different, certainly when one considers that the sediment transport is proportional to about the current velocity to the power five.

The large depth of a sandpit might reduce the transport capacity to such an extent that the differences between the current patterns, due to different lengths, are not dominantly present. Another influence that the length of the sandpit has, is the (maximum) current velocity in the sandpit, and thus also the velocities of the water that is discharging out of the pit. So the length of the pit might influence the morphology in two ways. First in the magnitude of the current velocities leaving the pit, and secondly in the pattern of the tide-

averaged current. Both aspects, however have the same origin, viz. the ability of the pit to attract a certain amount of water.

7.7 Conclusions

The results of this chapter show that large, horizontal tide-averaged patterns are present, of which the shape depends on the length, width and orientation of the sandpit.

In Chapter 5 the critical length-width ratio proved to be three. In this chapter, in which tidal boundary conditions are applied, the critical length-width ratio proved to be somewhat larger than three, viz. about four, because also the 20×5 km^2 sandpit already showed a somewhat different behaviour. This agrees with the results of Labeur (1998), which showed a critical length-width ratio between 4 and 5.

When the sandpits are long enough, thus a length-width ratio well above four, time becomes an important factor for the maximum current velocity (in the center longitudinal section of the sandpit). When the length-width ratio is smaller than four, the length of the sandpit mainly determines the maximum current velocity. In principle, one should be able to observe the same maximum current velocity as would be found in case of stationary boundary conditions. That this can not be observed is due to the effect of a different behaviour of the current in a short sandpit in case of a tidal water motion. This different behaviour can be deduced from the relative difference between the maximum current velocity in the stationary and the tidal water motion as presented in Table 7.2.

The influence of Coriolis on the tide-averaged current pattern is twofold. First of all, only two significant outflow regions at the corners remain, one in the north-east and in the south-west corner. Secondly, the circulation patterns are influenced. The current along the lateral limits of the pit have opposite directions, contrary to the pattern without Coriolis.

In case of the rotated sandpits, the tide-averaged current pattern shows two large circulation patterns within the sandpit. When increasing the tidal amplitude to 1 m/s. and thus increasing the influence of advection, the position of the (tide-averged) currents shifts. A further increase to 2.0 m/s shows that one large circulation pattern remains, which extends its influence outside the pit due to the large influence of advection.

8 Morphological calculations

This chapter deals with the morphological computations of large-scale sandpits. The experiences of the previous chapters are taken into account in this chapter. The computations are performed with the modelling software described in Chapter 4.

8.1 Introduction

Comparable study

This chapter discusses the results of the morphological computations of sandpits and relates these results with the results of a previous study, viz. Walstra (1998), performed with SUTRENCH. SUTRENCH resolves the width-averaged (2DV) advection-diffusion equation for suspended sediment transport. With this package morphological changes of cross-sections of a trench due to waves and (tidal) currents can be computed. A morphological computation with Delft3D of a trench as used in Walstra (1998) is executed, in order to relate the magnitude of the changes and the sediment transports. This model functions as a reference model. For the computation of this trench a much smaller modelling area is created (Sections 8.2 and 8.4). In order to obtain more realistic results, and thus to make the two studies comparable, more realistic boundary conditions are imposed in the morphological computations of the sandpits, see Section 8.3.

Tuning of the models

Before obtaining results the two models -of the trench and of the sandpits- had to be tuned and sensitivities of both models for a number of input parameters had to be tested. That testing resulted in the input as it is described in Sections 8.2, 8.4 and 8.5. The right settings of the input parameters are determined on basis of simulations of a 10×10 km^2 sandpit in a 75×75 km^2 computational grid and the model of the reference trench. A modelling area of 50×50 km^2 proved to be too small; the boundaries influenced the results of the computations. In order to be able to study the influence of the size of the grid cells on the results, grid cells of 250×250 m^2 were desirable, anyway. A modelling area of 100×100 km^2 would results in a large number of grid cells. Therefore, it was decided that as an alternative for the 50×50 km^2 grid with 250×250 m^2 grid cells, a computational grid of 75×75 km^2 with 250×250 m^2 grid cells was implemented for the morphological computations of the sandpits. It is emphasized that the models are tuned on basis of the tidal motion with only the M2 component. Section 8.2 describes the tuning of the models.

Morphological aspects

The main focus in this chapter is on three aspects of the morphological development of sandpits. The first aspect is the development of the slopes of the sandpit, or the area that is influenced morphologically by the sandpit. Another interesting aspect is the comparison of the slopes of the sandpits and the slope of the navigation channel to the port of Rotterdam (Maasgeul), which is referred to as the reference trench. Navigation channels can be seen as extremely wide sandpits in which the discharge per unit width remains constant since no extra water is attracted to the sandpit. Therefore it is expected that, since water is added to

the sandpit resulting in an outflow with higher velocities, the slopes of the sandpit will differ from corresponding slopes of a navigation channel under the same conditions.

A second aspect is the migration of the sandpit itself. A rule of thumb for the sediment transport under influence of waves and flow in deep water is 100 $m^3/m/y$, which corresponds to the yearly-averaged sediment transport. This means that a 10 m deep sandpit propagates with a speed of about 10 m/y. The results of Chapter 7 show that there might be pit configurations which behave differently than is expected in first instance.

The third aspect is whether sandpits show the same behaviour as tidal banks. Tidal banks are defined as rhythmic bottom patterns with typical wavelengths of 5-10 km and wave heights up to 10 m. Another characteristic of tidal banks is their orientation. They are found with angles up to 30° between the tidal axis and the wave crests. The two long, lateral edges of the sandpit can be considered as wave crests, see Figure 8.1.

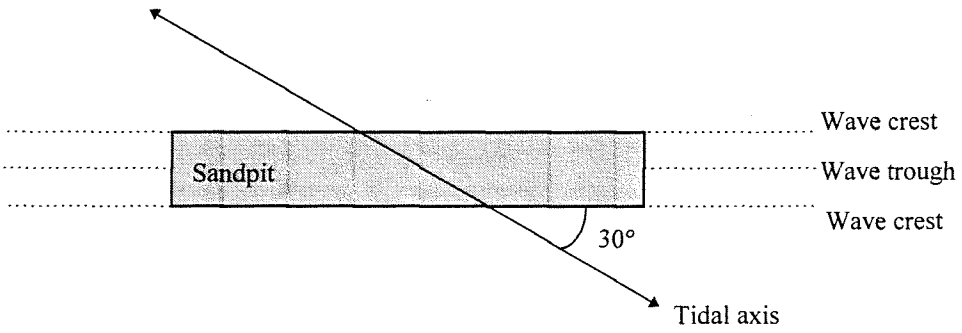

Figure 8.1: A sandpit considered as a tidal bank

Several studies into the behaviour of tidal banks and sand waves have already been performed, e.g. De Vriend (1987), Ribberink (1989), Hulscher (1996) and Németh (1998). The study of De Vriend consisted of an analytical approach of the morphological development of sudden bottom disturbances. Ribberink approached the behaviour of sandpits in an one-dimensional way. He showed analytically that, due to the increase of discharge, the pit might become deeper. Hulscher and Németh studied the behaviour of sandwaves and tidal banks. They showed that, under certain conditions, positively orientated disturbances of the sea bottom can show an increasing amplitude. The latter study concerned also aspects like propagation of these waves and their morphological time scale.

Applied sandpits

For a number of reasons the 30 m deep 25×5 km^2 sandpit was chosen as the longest pit, although in previous chapters a 40×5 km^2 sandpit was the longest one. The first reason is the limitations of the modelling area. The results should be obtained without artificial effects of the boundary conditions as they are observed in the previous chapters, see e.g. Figures 7.1 and 7.2 of Section 7.2. The second reason is the fact that a 25×5 km^2 sandpit does not have an essentially different behaviour than a 40×5 km^2 sandpit. They both have a length-width ratio well above four; a value that corresponds with the transition from local

circulation areas around the corner of the pit to large circulation patterns from the corners to the middle of the pit, as was observed in Chapter 7. The last reason for this change is the practical dimensions of sandpits as they may be used in the future. A 30 m deep, 40×5 km^2 sandpit has a volume that is far beyond the need of several hundreds million m^3 sand for the second Maasvlakte or a national airport on an artificial island. The reason that these large pits are used anyway in the hydrodynamic part of this study is due to the purpose to reach equilibrium currents in the sandpit.

Table 8.1 presents the simulations that are performed in this chapter. The numbers indicate the volumes of sand that such a sandpit would supply. One can see that, even though the largest pits are omitted, the volumes are in some variants still rather large. Since the reference trench is not intended to supply sand, the volume of it is not given.

Table 8.1: The executed simulations and the corresponding volumes of the sandpit [$*10^6$ m^3]

Orientation → Pit dimensions ↓	+45°	0°	-45°
25×5 km^2; d=30 m	1250	1250	1250
25×5 km^2; d=22m	250	250	250
10×10 km^2; d=30 m	1000	1000	
10×5 km^2; d=30 m		500	
10×5 km^2; d=22 m		100	
Reference trench		X	

Simulation time

The morphological computations are performed over a duration of 1000 years. This seems a very long time, but the time scales of such large bottom patterns are so large that one has to simulate such a long time to observe significant bottom changes. One should be very critical about the results of computations which cover such a long period. One of the indications for the assumption that the results are rather reliable is the morphological time step which the modelling software determines during these simulations. The software determines automatically that time step. In these computations morphological time steps up to 20 years are applied. This indicates that the changes are very slow. Because the gradients of the transport in the first years are large, and thus much smaller time steps are used, about 80 bottom calculations are necessary to cover the 1000 years, which is an acceptable number.

Summarizing

Section 8.2 deals with the tuning of some input parameters. Section 8.3 discusses the boundary conditions that are applied in the major part of this chapter. Section 8.4 treats the morphological computations of the reference trench, and the comparison of these results with the Walstra-study. Sections 8.5 and 8.6 discuss the results of the morphological calculations of several sandpits and a number of variations. Section 8.7 indicates the influence of the boundary conditions on the morphological development. Section 8.8 finally summarizes the results of this chapter.

8.2 Tuning of the input parameters

Several parameters in the input file are of importance for the results of the simulations, and therefore have to be tuned. Results of these tuning activities are discussed in this section. The longitudinal sections of the sandpits are used to study the sensitivities of the results for a number of input parameters. These parameters, described in Chapter 4, are:

- Influence of the transport mode and α_{bd}
- The magnitude of the grid cells
- The number of grid cells in the slope of the pit
- Number of bottom calculations per flow computation

Simulations with different values for these parameters are performed. Common sense and a qualitative comparison with the results of the Walstra-study should indicate which value of the parameter is to be applied.

In order to tune the model the 30 m deep, 10×10 km^2 sandpit and the reference trench are used. This sandpit is used because of its small dimensions with respect to the modelling area. Although the influence of the input parameters is treated separately, the parameters are determined in coherence with each other. When not mentioned otherwise, the computations for tuning the model are performed with the following input:

- A flow computation after every sediment transport and bottom level change computation
- Slope of the sandpit of 5:250 m/m
- Only the M2 component of the tide imposed as boundary condition
- In case of the trench:
  - 4×0.5 km^2 computational grid with 25×25 m^2 grid cells
  - u-h boundary conditions
  - No implementation of the Coriolis force
  - Simulation times of 50 years
- In case of the 10×10 km^2 sandpit:
  - 75×75 km^2 grid with 250×250 m^2 grid cells
  - u-u boundary conditions since Coriolis is implemented
  - Simulation times of 1000 years

Preliminary computations proved that the implementation of Coriolis in the model of the reference trench disturbs the results significantly. Areas with large artificial deposition hindered the morphological development of the trench completely. Therefore, Coriolis is not implemented in this model. This also justified by the small size of the modelling area and the one-dimensional character of the current.

The results of this tuning are discussed below and presented in Figures 8.2 to 8.10. One should keep in mind that the direction of the tide current is from the left to the right.

Influence of the transport mode and α_{bd}
As mentioned in Chapter 4, two different transport modules can be implemented. The total transport mode is used when the adaptation length of the sediment concentration profile is

smaller than the characteristic length scale of the studied phenomenon, e.g. the slope of the sandpit or the size of the grid cells. The bed and suspended transport mode is used when the adaptation of the concentration profile is of importance.

Figures 8.2 to 8.6 show the influence of the transport mode on the bottom level of the reference trench after 50 years. Figures 8.2, 8.3 and 8.4 show the morphological changes of the sandpit as a function of the transport mode and the stabilization coefficient α_{bd}. Figures 8.5 and 8.6 compare the influence of α_{bd} per transport mode. One can see that both transport options show wiggles in the bottom level when a value of one is applied for α_{bd}. For higher values of α_{bd} hardly any difference is noticeable between the two transport modes and rather smooth results are obtained.

From Roelvink (1998) it appears that the adaptation length scale of the sediment concentration profile depends on the water depth h, the current velocity u and the settling velocity w_s of the suspended sediment. With a water depth of 20 m and u/w_s=25, the adaptation length amounts to about 100 m, which is smaller than the length of the slope of the sandpit and the grid cell sizes. The small influence, that the adjustment length of the sediment transport in the bed and suspended mode might have on the slope, is easily compensated by the gradient of the bed level. This can be a reason for the fact that there are no differences between the two transport options.

Figure 8.7 shows the influence of α_{bd} on the bottom levels of a 10×10 km^2 sandpit after 1000 years, when the total transport option is applied. Also in this situation wiggles develop in front of the eastern limit of the sandpit in case of α_{bd} is one. A value of 20 for α_{bd} results in a smooth bathymetry, as it is found in the trench with a value of 5 for α_{bd} after 50 years. One should consider whether a value of 20 for α_{bd} is still a realistic value, though the smoothest results are obtained. A high value of α_{bd} tends to smooth or suppress every bottom pattern with a relatively large slope. The result might be that there will never develop bottom patterns even if they might develop in reality.

In order to prevent that this factor suppresses all bottom developments, α_{bd} is set to 5; a rather conservative value.

Influence of the magnitude of the grid cells

Figure 8.8 shows a 10×10 km^2 sandpit in two computational grids with different grid sizes, viz. a grid of 75×75 km^2 with 250×250 m^2 grid cells and a 100×100 km^2 grid with 500×500 m^2 grid cells. One can see that there are significant differences. Although the boundaries of the modelling area are closer to the pit in the small grid, no influence of the boundaries in the pit are noticeable. The two grid variants are, concerning to that aspect, equivalent.

The grid with large cells results in a larger propagation of the pit, compared to the small grid cells. The western slope on its turn is flatter in case of small grid cells. The sedimentation peak in front of the eastern slope of the pit is larger than in case of large grid cells. Because the differences are significant and the smaller cells are assumed to be more accurate, the 75×75 km^2 was introduced as the standard computational grid for the morphological computations.

Influence of the number of grid cells in the slope of the pit

A computation is performed with a slope of 2 m per 250 m. Figure 8.9 compares the result of this simulation with the result of a computation with a slope of 5 m per 250 m. One can see that the number of grid cells in the slope does not influence the magnitude of the eastern slope after 1000 years. Also the most western point of the pit's bottom is in both cases fixated. The length of the slope as well is the same in both situations. The only significant difference is the fact that the sea bottom westwards of the sandpit is smooth in case of the flatter slope. The slope of 5:250 shows some wiggles at the western end of the pit. Another difference is that the erosion of the sea bottom in front of the eastern limit of the pit is larger in case of the 2:250 slope. One can state that this variation in the slope of the sandpit hardly influences the development of the slope itself. Some of the differences are caused by the fact that the flatter slope is also a longer slope and that subsequently the bottom of the pit is somewhat smaller. The results of this comparison does not lead to the decision to change the number of grid cells in the slope, thus to a flatter slope.

Influence of the number of bottom computations per flow computation

The total computation time can be reduced drastically when more sediment transport and bottom change computations per flow computation can be executed. Figure 8.10 shows the results of simulations in which α_{bd} was set to 10 and in which the total transport mode was applied. The two bottoms are obtained with respectively one and five bottom computations per flow calculation. The bottom level just in front of the eastern limit of the sandpit has in both cases the same value. The area of erosion in front of that same side is however rather different. When 5 bottom computations are performed on basis of a constant discharge the erosion is more severe. The shape of the western slope differs also. The lower part of that slope is more or less the same but the upper part shows less erosion in case of 5 bottom computations per flow calculation. It is logical that a simulation with less bottom computations per flow computations is more accurate. Since there is a significant difference between the two results, only one bottom change computation per flow computation is applied in the remainder of this study.

8.3 Boundary conditions

In order to obtain more realistic results it was decided to impose the M0, M2 and M4 components of the tide instead of only the diurnal tide component. Rough information of the tidal motion near Scheveningen was used, viz. 12 combinations of a current velocity (magnitude and direction) and a water level, resulting from numerical calculations. Table 8.2 shows the data derived from Van Rijn et al. (1995). These data are obtained from computations with representative weather condition, viz. wave heights between 1.0 and 1.5 m and a wind direction between 210° and 240° (south-west wind).

First, the current velocity data have to be compiled. The direction of these vectors have all different directions. These vectors are projected on a line that forms the resultant direction of these vectors. Figure 8.11 shows the data points and the resultant direction of the current velocities. When projecting the other data vectors on this line, it is assumed that this line runs through the origin.

Table 8.2: Input data for the tidal analyses

Time [hrs]	1	2	3	4	5	6	7	8	9	10	11	12
u [m/s]	0.00	0.28	0.45	0.37	0.25	0.15	-0.01	-0.15	-0.25	-0.31	-0.29	-0.20
v [m/s]	-0.05	0.26	0.52	0.51	0.40	0.27	0.06	-0.17	-0.35	-0.42	-0.38	-0.28
h [m]	-0.19	0.35	0.95	1.01	0.72	0.38	-0.03	-0.37	-0.42	-0.38	-0.41	-0.38

With help of the least squares method the amplitudes and the phase shifts of the three harmonic components are determined. This method is applied as follows. One assumes that the tidal signal g(t) can be approximated by every individual component as a combination of a sine and a cosine, as in Equation (8.1).

$$g(t) = \sum_n a_n \cos(\omega t) + \sum_n b_n \sin(\omega t) \tag{8.1}$$

When optimizing for every time step the (quadratic) error between g(t) from Table 8.2 and the approximated solution according to Equation (8.1), then also the difference between g(t) and the sum of the harmonic components is minimal. According to this method the amplitudes a_n and b_n can be determined with Equations (8.2) and (8.3).

$$a_n = \frac{\sum g(t) \cdot \cos(\omega t)}{\sum \cos^2(\omega t)} \tag{8.2}$$

$$b_n = \frac{\sum g(t) \cdot \sin(\omega t)}{\sum \sin^2(\omega t)} \tag{8.3}$$

The summons represent the sum of these values for the 12 times on which data is available. The sum of the sine and cosine functions in Equation (8.1) can be written into one component, as in Equation (8.4).

$$A\cos(\omega t - \varphi) \tag{8.4}$$

in which:

$$A = \sqrt{a_n^2 + b_n^2}$$

$$\varphi = \arctan\frac{b_n}{a_n}$$

The amplitudes and the phase shifts which follow from this procedure are presented in Table 8.3 and Table 8.4. These tables are based on the phase shifts which occur at the western boundary of the modelling area. Figure 8.12 shows the comparison of the data of Table 8.2 and the analytically derived tidal motion. First of all one can see that there is a phase shift between these two data sets. These shifts are not disturbing because of the

sinusoidal character of the tidal motion. The current velocities are rather well approached by this analysis. The amplitudes of the water levels however are rather different. The flood water levels are about 0.2 m lower in the approach and the shape of the measured ebb water level curve is hardly represented. This has to do with the limited number of data points and the limited number of tidal components that are taken into account. The calculated water levels do show that the duration of the ebb period is longer than the flood period. Altogether, the results are fairly well suitable to be used as boundary conditions. The artificial morphological consequences of the boundary conditions are discussed in Section 8.7.

Table 8.3: Velocity boundary conditions in case of the reference model of the trench

Tidal component	Amplitude A [m/s]	Rotation celerity ω [°/h]	Phase shift φ [°]
M_0	0.035	0	0
M_2	0.593	29.03	27.63
M_4	0.056	58.06	11.27

Table 8.4: Water level boundary conditions in case of the reference trench

Tidal component	Amplitude A [m]	Rotation celerity ω [°/h]	Phase shift φ [°]
M_0	0.103	0	0
M_2	0.624	29.03	29.93
M_4	0.146	58.06	15.87

8.4 Reference model of a trench

This section will discuss the set-up of a model for numerical, morphological computations of a navigation channel, which forms e.g. the entrance to a harbour. Also the results of these computations are treated in this section. The results of Walstra (1998) are compared with the morphological computations with Delft3D. Additionally, the morphological development of the reference trench under influence of the symmetrical tidal motion is discussed, in order to indicate the importance of the boundary conditions.

The following input has been used to set-up the model for the reference trench:

- 4×0.5 km^2 computational grid with 25×25 m^2 grid cells
- Computational time step of 1 minute
- Width trench = 600 m; depth = 27 m with respect to the still water level
- Slope = 4%; length of the slope = 250 m
- Boundary condition consists of three tidal components, viz. M0, M2 and M4
- No implementation of Coriolis

Figure 8.13 presents the morphological development of the center cross-section of the reference trench obtained in this study. It also shows the trench after 50 years as it is found in the Walstra-study. Figure 8.14 presents the trench of the Walstra-study after 3 and 50 years.

When the Delft3D trench after 100 years is compared with the SUTRENCH results after 50 years, one can distinguish the following differences/resemblances:

- Propagation of the trench measured with the points half-way the slope are equal in both studies
- The slopes in the SUTRENCH results are steeper than the slopes of the Delft3D study
- The bottom levels of the sandpit differ about 1 m

The differences can be explained by the following points, of which the last one might be responsible for all the observed differences.

- Boundary conditions
- Wave conditions
- Grain size distribution (d_{50}= 0.2 mm vs. d_{50}= 0.21 mm)
- Fall velocity (w= 0.02 m/s vs. w= 0.028 m/s)
- Sediment transport equations (Bijker vs. Van Rijn)

In the Delft3D study the western limit of the trench does not influence the eastern boundary. This is concluded from the fact that the bottom of the trench has not changed, where the western slope is not yet present. The opposite is true for the SUTRENCH results; the western slope do influence the eastern slope. Plots of the results of the Walstra-study, concerning a trench that is twice as wide show that the shape of the cross-section is rather similar to the results of the present study. In this case the western slope does not influence the eastern slope; part of the bottom of the sandpit is still undisturbed.

Altogether one can state that the magnitude of the changes and the sediment transport differ about a factor two. Considering the uncertainties in the sediment transport in general, this is an acceptable difference. In the morphological computations in the remainder of this study the same boundary conditions are applied. So one can conclude that also the sediment transports in remainder of this chapter are rather reliable.

Importance of boundary conditions

When the propagation direction of the reference trenches in this section (Figure 8.13) is compared with the propagation direction that was obtained in the tuning process (e.g. Figure 8.3), one can see that the directions of propagation are opposite to each other. That opposite direction can be explained by the boundary conditions and the influence of the waves on the current velocity near the bottom. In a symmetrical tidal motion the influence of the waves during ebb is larger due to the decreased water depth. The result is a tide-averaged sediment transport in the ebb direction. In an asymmetrical tide the larger influence of the waves during is compensated by the larger flood current velocities. This results in a tide-averaged sediment transport in the flood direction, and subsequently in a

propagation of the pit in the same direction. This emphasizes the importance of the boundary conditions.

8.5 Morphological computations of the sandpits

This section discusses the results of the morphological computations of the sandpits, described in Table 8.1. The input of the most important parameters are summarized below.

- 75×75 km^2 computational grid with 90,000 grid cells of 250×250 m^2
- $\alpha_{bd} = 5$
- Automatic time step
- u-u boundary condition, according to Table 8.3
- Coriolis force is implemented

The results of the morphological calculations are presented in the Figures 8.15 to 8.27. Figures 8.15a to 8.27a show the following quantities:

- The upper left plot shows the bottom topography after 1000 years
- The upper right plot presents the bottom changes
- The lower left plot shows the initial tide-averaged sediment transport
- The lower right picture presents the tide-averaged sediment transport after 1000 years

Figures 8.15b,c to 8.27,c show longitudinal section and cross-section through the center of the sandpit. These plots show bottom levels in these sections after 500 and 1000 years and the initial bottoms. The plots after 500 and 1000 years are taken from the initial sections, although the sandpits might have a different position or orientation. In case of the rotated square pit, the cross-section has the same orientation as the cross-section in the positively rotated, rectangular pits.

The isolines of the water depth represent the isolines of 22.5 and 25 m, as far as the 30 deep sandpits are concerned. The plots of the depth-variants, thus the 22 m deep sandpits, show the isoline of 21 m.

The western slopes of the sandpits as they are present after 1000 years are summarized in Table 8.5. The length of the slope is defined as the length between the initial transition from slope to undisturbed bottom to the place where the bottom becomes horizontal again. These values must be considered as a rough indication. Since the pit, which is obtained by the tidal condition with the increased velocity of the M0 component, has propagated more than the length of the pit itself and the orientation is completely different, the length of the slope after 1000 years, determined in the initial longitudinal section, is a quantity without practical value. This pit is therefore not included in Table 8.5. The third column of Table 8.5 presents the dimensions of the rectangular envelope of the 22.5 m depth isoline (or the 21 m deep isoline in case of the depth variants) of the sandpit after 1000 years. Like the length of the western slope, this quantity gives an indication of the maximum width and length of the sandpit after 1000 years, or the area that is influenced by the sandpit.

Table 8.5: The eastern slopes of the longitudinal section after 1000 years

Dimension and orientation of the sandpit	Length of the eastern slope after 1000 years [km]	Dimension of the envelope of the pit after 1000 years [km^2]
+45° rotated 25×5 km^2; d=30 m	15	33×10
parallel 25×5 km^2; d=30 m	8	32×7
-45° rotated 25×5 km^2; d=30m	4	25×8
parallel 10×5 km^2; d=30 m	14	16×6
+45° rotated 25×5 km^2; d=22 m	17	34×8
parallel 25×5 km^2; d=22 m	9	31×6
-45° rotated 25×5 km^2; d=22 m	4	28×11
parallel 10×5 km^2; d=22 m	10	15×6
+45° rotated 10×10 km^2; d=30 m	15	18×15
parallel 10×10 km^2; d=30 m	14	12×12

Because the negatively orientated sandpits propagate not in the direct line of the sandpit but in the direction perpendicular to the pits' axis, the eastern slopes of these sandpits are significantly smaller than the slopes of the parallel and the positively rotated sandpits. One should ask oneself whether this method to determine the length of the slope results in a representative slope length. It does however give a good image of the development of the bottom levels in the original longitudinal section. Besides that, also the combination of the plots of the bottom levels and the bottom level changes and these values of the length of the slope give a rather well picture of the morphological development of the sandpit. Therefore, and in order to be consistent, this method is applied for all the pit configurations.

8.5.1 +45° rotated 25×5 km^2 sandpit

The plots of this sandpit and its development are presented in Figure 8.15. First of all the differences between the results obtained by the single tidal component and the combination of three harmonic components are highlighted. Figure 8.15d presents the results in case of the single harmonic component. The most striking difference is, again the direction of propagation of the sandpit. This different direction is caused by the lower tide velocities in the computations with the M2 component of the tide. This symmetrical tidal motion has a current velocity amplitude of 0.5 m/s. The velocities in the other case range from -0.52 m/s to +0.67 m/s.

This difference in propagation direction can also be seen from the plots of the sediment transports. The initial sediment transport in case of the more realistic boundary conditions

is directed from two sides into the sandpit. The initial sediment transport is on both lateral edges of the pit directed to the west. There is a lot of transport out of the pit over the northern short limit of the pit. In case of the simplified tidal motion a small transport into the sandpit over that same edge is noticeable. The sediment transport patterns after 1000 years differ as well. The 'final' sediment transport in the simplified case is a rather uniform pattern; a small transport in the pit itself and a somewhat larger transport rate outside the pit. In case of the tidal motion consisting of the three harmonic components, the transport after 1000 years is not uniform. The most remarkable aspect of that pattern is a strip of sediment transport in south-west direction, deflecting to the sandpit. Also the erosion at the eastern end due to the outflow of water during ebb and the inflow during flood can be discerned in the sediment transport pattern.

One should notice that, when interpreting the results, erosion and sedimentation are determined by the gradients of the sediment transport and not by the sediment transports themselves, see Equation (3.4). This makes the interpretation of the sediment transport patterns somewhat difficult. Therefore the emphasis of the discussing of the results of the morphological computations is on the bottom changes and not on the sediment transport rates. Only when the sediment transports clarify the interpretation of the results or when differences between two variants are to be indicated they are mentioned.

Before discussing the results with the help of the figures, a remark concerning these figures has to be made. As one can see from the plots of the cross-sections and the longitudinal sections, there are rather significant disturbances in the corners of the western boundary of the modelling area. The disturbances consist of sedimentation areas with a height up to 4 m above the undisturbed see bottom. Despite the height of these areas, the influence of these areas on the morphological development of the sandpit is limited. These areas are not only far upstream of the pits, but also far to the north or to the south of the pit. See also Section 8.7.

The features of the +45° 25×5 km^2 sandpit after 1000 years are summarized below:

- The propagation of the sandpit is in direct line of its longitudinal axis. The length of the eastern slope is about 15 km, as can be seen from Figure 8.15b and Table 8.5. The effect of the outwards orientated tide-averaged current velocity in the most northern corner of the pit, as it appears in Figure 7.7, can discerned. The outflow velocity is even stronger in case of these boundary conditions, resulting in the observed erosion north-eastwards of the sandpit.
- Sedimentation of the western end of the sandpit occurs, resulting in a propagation varying between 2 and 9 km. In this area of sedimentation, the influence of the acceleration of the current towards the pit during flood and the high outflow velocities during ebb can still be discerned. An area with a smaller sedimentation rate, thus a larger depth is present. This area can also be found in Figure 8.15b, where the line representing the situation after 1000 years shows an irregularity at a depth of 24 m, indicating that there is an area with an other, constant depth.
- Figure 8.15c shows that the slopes of the lateral limits of the pit become somewhat flatter, combined with a small deepening of the center longitudinal section of the sandpit, which is larger after 500 years than after 1000 years. Just besides the pit,

significant deposition takes place, which on its turn is larger after 1000 years than after 500 years. Something like a wave pattern has developed, as is also found in De Vriend (1987). The deepening of the pit is interesting with respect to a possible resemblance in behaviour between sandpits and tidal banks. The observed deepening indicates that such a resemblance is present.

- From Figure 8.15b appears that the horizontal position of the eastern end of the pit remains at the same place, despite some changes in the vertical position.

8.5.2 parallel 25×5 km^2 sandpit

Figure 8.16 shows the morphological development of a parallel 25×5 km^2 sandpit. Besides some small erosion at the boundaries no artificial effects of the boundary conditions can be discerned. The rather smooth bottom, shown in Figure 8.16c strengthens the confidence in the results of the simulations. Despite a small wiggle in the bottom in the very south of the model, a smooth bottom in the remainder of the cross-section is present even after 1000 years.

- Like the positively orientated sandpit, this pit has a propagation direction in the direct line of the longitudinal axis of the pit. The length of the slope of this pit after 1000 years is about 8 km. Also the area of erosion at the north-west corner of the pit is present. Again only the lower half of the sandpit fills up with sand at the western side of the pit. The slope of the upper half even retreats beyond the initial beginning of the sandpit.
- The rate of sedimentation and erosion is rather uniformly distributed over the width of the sandpit, except in the north-west corner where a larger amount of sedimentation takes place.
- The largest part of the bottom of the sandpit deepens slightly, while the most eastern part becomes shallower. This is probably caused by the increase of discharge in the sandpit and the decrease of the current velocity towards the end of the sandpit. Due to the asymmetrical tidal motion this results in a net sediment transport in the flood direction. The magnitude of the deepening as well as the magnitude of the shallowing is larger after 1000 years than after 500 years.
- Figure 8.16c shows, besides the smooth bottom, the uniformity of the changes in the cross-section. One can distinguish, like in the positively rotated variant, two rather larger sedimentation peaks just bordering the sandpit. The lateral slopes of the sandpit are hardly changed after 1000 years. Except near the ends of the sandpit, the current, and thus the sediment transport, through the sandpit itself is still mainly orientated in the longitudinal direction of the sandpit.
- The shape of the pit shifts from a rectangle into a parallelogram.
- The difference with the reference trench is the sedimentation area that occurs in the direct line of the sandpit. These areas are not present in the results of the reference trench. One can state that this is effect of the attraction of extra discharge into the sandpit. That extra water causes higher velocities, and thus a larger sediment transport. Outside the sandpit the current velocity drops and loses its transport capacity. Since the sediment transport is related to the current velocity to the fifth power, more sediment settles outside the sandpit compared to the rate of sedimentation in case of the reference trench.

8.5.3 -45° rotated 25×5 km^2 sandpit

The plots with the results concerning this pit are shown in Figure 8.17.

- The propagation direction of this pit is more parallel to the longitudinal axis.
- The effect of the acceleration areas at both sides of the sandpit are in this case also noticeable. The erosion at the eastern end is however spread over a larger area, compared to the parallel and positively rotated sandpits, which show a more concentrated erosion peak. The erosion in case of the negatively rotated sandpit might lead to a rotation in positive direction, which can also be seen as a resemblance in behaviour of sandpits and tidal sand banks.
- The bottom of the sandpit shows no deepening after 1000 years. It seams that this negatively rotated pit tends to fill up eventually, after a small deepening, that can be observed after 500 years in Figures 8.17b and c.
- Contrary to the parallel and the positively rotated sandpits, this pit shows no significant sedimentation along the lateral edges of the sandpit.

8.5.4 Influence of the length

The influence of the length is studied in order to find out whether a sandpit with a length-width ratio smaller than four shows a different behaviour than a pit with a length-width ratio larger than four. Chapters 6 and 7 showed that this ratio does have an influence on the tide-averaged current velocity pattern. Whether this also holds for the morphological development of sandpits depends not only on the averaged current pattern but also on the absolute magnitude of the velocities and on the influence of the waves on the current velocities near the bottom. Besides that, the different boundary conditions might also lead to another tide-averaged current pattern.

The influence of the length of the sandpit is studied by means of a parallel 10×5 km^2 sandpit. Before looking at the plots of the morphological results, the tide-averaged current patterns of the two length variants are compared with each other and with the tide-averaged current patterns of Chapter 7, where only a single component of the tidal motion was imposed. Figure 8.18 shows these tide-averaged current patterns. These plots show that the flood currents dominate the tide-averaged current pattern: no circulation areas are present. The tide-averaged current patterns of the two length-variants show no differences. Although there is no difference between these two patterns, the sediment transports might be different leading to different morphological results.

The morphological development that the 10×5 km^2 pit has gone through is plotted in Figure 8.19. One can see that the length of the pit hardly has an influence on the morphological development of the pit. Even the magnitude of the changes are in both length-variants the same. The shape of the pit also changes from a rectangle to a parallelogram. The outflow of water out of the north-east corner of the sandpit can be recognized in the bottom pattern after 1000 years.

Also this short sandpit shows the sedimentation areas along the lateral edges of the sandpit, as they were found in the previous parallel and positively rotated sandpits and in De Vriend (1987).
It might be possible that shallower pits do show an influence of the length of the sandpit, since the velocities in a shallow sandpit are lower than in a deeper pit and since the waves in shallow pits have a larger influence on the sediment transport.

8.5.5 Influence of the depth

This section discusses the influence of the depth on the morphological results. The depth of the sandpit is changed from 30 m to 22 m. Not only the standard sandpits are studied. In order to be able to determine whether the depth of the pit indeed suppresses the morphological consequences of the length-width ratio of the sandpit, the morphological development of a parallel, 22 m deep 10×5 km^2 sandpit is studied. The results of these computations are presented in Figures 8.20 (+45° rotated 25×5 km^2 sandpit), 8.21 (parallel 25×5 km^2 sandpit), 8.22 (-45° rotated 25×5 km^2 sandpit) and 8.23 (parallel 10×5 km^2 sandpit).

When comparing the two depth-variants of the 10×5 km^2 sandpit one can see that the erosion due to the outflow of water out of the north-east corner of the sandpit has disappeared. Since this erosion is still present in the 25×5 km^2 sandpits, one can state that this is an effect of the length-width ratio of the pit. The deep pits and the shallow, 25×5 km^2 sandpits still attract enough water to cause a jet-like outflow at the north-east corner. This is contrary to the shallow, 10×5 km^2 sandpit, which is both too short and too shallow to attract a sufficient amount of water to create such an erosion area.

These shallow sandpits show the same behaviour as the deeper ones. Also the parallel and the positively rotated sandpits show a deepening of the bottom of the sandpit. The plots of the bottom levels in the center longitudinal section show, however, that the shape of the slope differs from the shape of slopes of the deep pits. The slopes of the shallow pits are flat near the bottom of the pit and become steeper towards the water surface, resulting in a sedimentation area at the eastern end of the pits. These sedimentation areas are most pronounced in case of the parallel sandpits. From plots of the bottom-levels in the cross-section can be concluded that the slopes become much flatter than in case of the deeper pit. The eastern slopes are on their turn flatter than the western slopes. This is confirmed by the plots of the bottom levels and the bottom changes. The length of the slope can be read from Table 8.5.

Also the sediment transport patterns differ from the patterns in case of the deep sandpits. The transport rates are not as large as in case of the deeper pits. The direction of the initial transport near the eastern limit of the pit is eastwards, contrary to the deep sandpit. The sediment transport pattern after 1000 years does not show the area with the south-westerly directed transport. The sediment transport rates in the sandpit are somewhat larger in case of the shallower pits. This is explained as follows. After 1000 years one can state that the sandpit has reached a dynamic equilibrium -dynamic in the sense that the pit still changes, and equilibrium in the sense that no strong gradients are present anymore. The pit has adjusted itself to the asymmetry of the tide. This can be concluded from the rather smooth

sediment transport pattern. No large gradients in the transport rates are visible. Therefore only a small influence is left of the tidal asymmetry on the tide-averaged transports in the sandpit; the waves have a relatively large contribution to the sediment transport. Since the influence of the waves increases as the water depth decreases, the influence of the waves is larger in case of the shallow pit.

The parallel (long as well as short) and positively rotated depth variants show also the wave-like pattern along the lateral limits of the sandpit, though their amplitudes are smaller. Due to the smaller depth, the development of the negatively rotated sandpit, that can be described as a rotation in the positive direction, is more pronounced present.

At the eastern end of the sandpit the erosion due to the out- and inflow of water during flood and ebb, respectively, is less than in case of the deeper sandpit. The small depth reduces the current velocities in the sandpit, as it was found in Chapter 5.

Another remarkable aspect of these depth-variants is the fact that the area of erosion is now not present along both lateral edges of the sandpit like in the deep variants, but that only the eastern lateral limit erodes significantly. It is also noticeable that the dimensions of the area of influence of the positively rotated and parallel sandpits are hardly different from the initial area, when the erosion due to the out- and inflow in the north-east corner is not considered. The negatively rotated sandpit shows that the width of eastern part of the pit is considerably larger than the initial width. This is mainly due to the already mentioned in- and outflow at the north-east corner of the sandpit, although a rather smooth depth contour line is visible.

8.5.6 Influence of a larger M0 velocity caused by wind driven currents

The influence of a larger magnitude of the M0 component is studied on a 10×5 km^2 sandpit. The M0 velocity is increased from 0.035 m/s to 0.1 m/s. This stationary velocity is in the flood direction. The plots of Figure 8.24 show this sandpit, the bottom changes and the initial sediment transport and the sediment transport after 1000 years.

One can see that the initial pit is almost completely disappeared. The erosion due to the jet-like outflow has created a 'new' pit with an angle of about +45° between the x-axis and the longitudinal axis of the 'new' pit. The bottom levels in the original cross-section are hardly of importance anymore since the pit has propagated about its own length. A remarkable aspect of the sandpit after 1000 years is the fact that the southern limit of the sandpit, though it propagates a little to the north, remains a straight line.

Figure 8.25 shows the morphological development in time of this sandpit. It indeed shows that the sedimentation of the pit starts in the north-west corner. That sedimentation front propagates in the south-east direction. Again the erosion area due to the outflow in the south-east corner can still be recognized.

8.6 Morphological computations of square 10×10 km^2 sandpits

This section discusses the results of the morphological calculations of a parallel and a +45° rotated 10×10 km^2 sandpit. Figures 8.26 and 8.27 show the results of the parallel and the +45° rotated square sandpit, respectively.

The parallel sandpit has the same behaviour as the other parallel sandpits. The shape shifts from a rectangle to a parallelogram and a significant erosion near the north-east corner. Also in this pit a small deepening of (the first part of) the pit occurs. Like in the other cases, the area with south-westerly directed sediment transport is present. The overall dimensions of the sandpit increases with about 20%. Again the sedimentation areas along the lateral edges are found, but their shape is rather irregular.

The +45° rotated variant has, as far as the slopes are considered, the same behaviour. Sedimentation of the western part of the sandpit, in which the erosion due to inflow during tide and outflow during ebb can be recognized. Like the other positively orientated sandpits, a deepening can be observed. The initial shape of the pit hardly can be recognized anymore after 1000 years. The magnitude of the area that is influence by the sandpit is relatively large. Figure 8.27b shows that also this pit causes the sedimentation areas along the lateral limits of the sandpit.

8.7 Influence of the boundary conditions

The boundary conditions cause in the modelling area artificial erosion and sedimentation. In order to quantify the bottom changes purely caused by the boundary conditions a computation has been performed with a flat sea bottom, without a sandpit. Figure 8.28 shows the bottom changes of a flat bottom without a sandpit. The upper plot shows, besides the depth contours, the 20 m isoline. In the lower plot the contour of a parallel 25×5 km^2 sandpit is plotted to give an indication of the location of the sandpits. The bottom changes vary from -7 to +3.5 m. The magnitude of these areas are however very limited and the position of these areas are not in the vicinity of the sandpits. The area just around the sandpit shows changes varying from -1.0 to 0.5 m. Though that are considerable changes, it is only about 1 mm/year.

To study 'purely' the effect of the sandpit on the sea bottom the bottom levels and changes are corrected for the influence of the boundary conditions. The bottom levels and changes that are found with the simulation of the flat, undisturbed bottom are subtracted from the bottom levels and changes that are found in the computations with sandpits. The corrected bottom levels with respect to the undisturbed sea bottom are presented in Figure 8.29 and the corrected bottom changes are presented in Figure 8.30. These figures present the bottom topographies of the three 25×5 km^2 and the 10×5 km^2 sandpits. It is emphasized that this procedure does not diminish morphological effects of the sandpit that are caused by artificial aspects of the boundary conditions; the bottom changes are purely compensated for the bottom changes caused by the boundary conditions are compensated.

One can see that, when one compares this figure with the other results, that there is hardly any difference, certainly not in qualitative sense.

8.8 Conclusions

The comparison between the SUTRENCH-results of Walstra (1998) and the Delft3D-computations of the trench shows that the qualitative behaviour resembles reasonbly well, but the quantitative behaviour differs to some extend. In the Delft3D computations the morphological response appears to be slower (larger time scales), which are probably due to differences in the tide-averaged transport rates. The artificial effects of the boundary conditions are not very large but do influence the results of the morphological computations quantitatively. One should therefore use the results with a certain care.

Almost all slopes of the sandpit become much flatter. The shape (convex or concave) of the slope depends on the depth of the sandpit.

Positively rotated and parallel sandpits propagate in direct line of their longitudinal axis, with a shift of up to 5 km. Negatively rotated sandpits propagate about perpendicular to their longitudinal axis with a shift up to about 3 km. The depth variants show significantly larger propagations. The depth also influences the direction of propagation in case of the positively rotated sandpit.

The asymmetrical inflow of water into the sandpit, which causes the high-velocity jet out of the north-east corner of the sandpit in case of stationary boundary conditions including the influence of Coriolis, causes also erosion of the pit in that direction. The standard pit and the square sandpits show that the shape of the pit changes from a rectangle to a parallelogram, partly under influence of that erosion. This erosion in the variant with the influence of wind driven currents is so dominant that more or less a new pit has been formed with an orientation that is about similar to the positively rotated variants.

All the results indicate that the positively orientated and, to a less extent, the parallel sandpits tend to deepen themselves. So, with respect to the growing amplitude, a sandpit can show the same behaviour as tidal banks. The sandpits that show a deepening of the bottom also show a wave-like pattern parallel along the lateral limits of the sandpit. These phenomena were already analytically found in De Vriend (1987). The negatively rotated sandpits show phenomena that looks to correspond with the preferential direction of tidal banks.

One should keep in mind that adverse weather conditions might lead to relatively large morphological changes in a short time. The morphological consequences are such that erosion areas develop with a complete other orientation.

9 Conclusions and recommendations

This final chapter summarizes the conclusions of this study and states the recommendations for further research into the behaviour of large-scale sandpits.

9.1 Conclusions

The (stationary) current pattern around sandpits is determined by water level gradients, which are caused by the acceleration of the current towards the sandpit and the sudden increase of the water depth in the sandpit. The result of these gradients is that water flows over the lateral limits into the sandpit in the upstream part of the sandpit and water flows out of the sandpit, mainly over the short downstream edge, but also partly over the lateral edges of the pit. The Coriolis force disturbs this pattern significantly. This force causes an asymmetrical inflow, which on its turn causes concentration of high current velocities along the lateral limits towards which the Coriolis force is directed. This process finally leads, under influence of constant inflow into the sandpit and a longitudinal water level gradient in the downstream part of the sandpit, to an outflow over the short downstream edge opposite to the direction of the Coriolis force. An important parameter for the flow in the sandpit is the length-width ratio of the sandpit. A critical value for this parameter is three, above which the maximum current velocity in the sandpit is larger than the undisturbed current velocity that is imposed with the boundary conditions.

In case of tidal boundary conditions large tide-averaged circulation patterns develop. Due to deceleration effects of the instationary water motion the critical value for the length-width ratio is somewhat higher, viz. about four. Below this value local circulations around the corner of the sandpit in the tide-averaged current pattern are present. The influence of Coriolis on this tide-averaged current pattern is very limited. It has some influence on the magnitude of the tide-averaged velocities just outside the sandpit. In both situations, with and without Coriolis, the outflow of water at the north-east corner of the sandpit can be recognized.

The morphological results are obtained with boundary conditions that are based on representative weather conditions. The comparison of the two reference trenches showed that the quantitative results can be considered as rather reliable. But a factor two in the sediment transport might cause that changes that according to the numerical computations take place in 1000 years, in reality will occur after 500 years. On the other hand the order of magnitude of the propagation of the sandpits as they are observed in the computations (5-10 km in 1000 years or 10 m^2/m/year) do correspond with the rule of thumb for the annual sediment transport in front of the Dutch coast (also 10 m^2/m/year). Still one has to be careful with the quantitative results.

The influence of the boundary conditions on the morphological development of sandpits is limited. Artificial bottom changes ranging from -1.0 to +0.5 m are present in the vicinity of the sandpit.

The slopes of the sandpit become flatter. The largest area that is influenced by the boundary condition is approximately 50% larger than the original area in which the sandpit is present.

The positvely rotated and parallel sandpits propagate in the direction of their longitudinal axis. The amount of the propagation increases as the depth decreases.

The results concerning the deepening or shallowing of the pit, are qualitatively seen rather reliable. The parallel and positively rotated sandpits, that become deeper, show also sedimentation areas (a wave-like pattern) along the lateral limits of the sandpit. Analytical approaches already showed that these kind of patterns indeed might develop. The negatively rotates sandpit seems to rotate in positive direction, or the eastern end of the sandpit propagates faster to the north than the western end of the sandpit. This is also a characteristic of the behaviour of tidal banks.

The depth of the sandpit increases the magnitude of the area of influence, decreases the amplitude of the wave-like pattern along the lateral limits of the sandpit and increases the influence of the length-width ratio of the sandpit. In fact, the influence of the length-width ratio is only noticeable in case of the shallow sandpits.

The results as they are observed in case of the boundary conditions with an increased amplitude of the M0 component of the tide are to be kept in mind. Since such a velocity, in order to take the wind driven currents into account, is a rather realistic value, the observed behaviour of the pit might also be realistic. Extreme weather conditions might cause large morphological changes in a relatively short time. High current velocities not only occur in severe weather conditions, but might also be present locally in front of the Dutch coast, e.g. due to contraction around construction.

When interpreting the results of the (hydraulic and morphological) computations one should bear in mind that also physical assumptions have been made, like depth-averaged currents and the omission of turbulence.

9.2 Recommendations

In a possible continuation of this study it is advised to implement the model of the sandpit in a larger model of the North Sea with a so-called nesting procedure. Such a model of the North Sea is e.g. the PROMISE model. The reason for a nesting procedure is threefold:

- The boundary conditions that are obtained from a nesting-procedure hardly cause artificial effects near the boundaries of the modelling area, as they are observed in this study.
- When the proper boundary conditions are imposed on the boundaries of the large model, subsequently leading to realistic hydraulic conditions on the boundaries of the nested model, more realistic, quantitative results are obtained.
- Nesting in a model of the North Sea will probably also reduce the effects of the boundary conditions on the bottom outside the area of the influence of the sandpit. On the other hand, the autonomous developments that are present in such a model might

lead to even more additional erosion and sedimentation, so that the effect of the sandpit is even more covered by the autonomous bottom development.

One has seen that the tidal motion is very important for the development of sandpits. In this study three different tidal motions have been imposed:

- A symmetrical tide, due to which the sandpit propagates in the ebb direction
- An asymmetrical tide, due to which the sandpit propagates in the flood direction
- An asymmetrical tide with a stationary component with an increased M0 velocity component, which showed that the sandpit propagated significantly and rotated about +45°.

It is therefore recommended that even more realistic boundary conditions are applied. However it is impossible to determine weather conditions that are representative during 1000 years. In stead of putting effort in that kind of boundary conditions one migth use boundary conditions that represent large transport rates. Smaller time scales may be the result and still an upper level for the morphological development can be found.

In order to diminish the influence of the boundaries completely it is advised to use an even larger modelling area. The consequence is that the computational time will also increase.

A lot more combinations of sandpits and input parameters are conceivable. The applied sandpits in this study cover rather well the (practical) range of pit dimensions. Only the smaller sandpits (smaller than 100 million m^3) are not studied. Because of political, environmental and morphological reasons it might be desirable to use a number of smaller sandpit rather than one large one. But with decreasing dimension of the sandpit also the area of morphological influence decreases, which are already small. Therefore some computations of smaller sandpits are recommendable. This is also interesting with respect to the infuence of Coriolis; from which length scales on is the Coriolis an important aspect in the morphological development.

In this study the sensitivity of the results for parameters like the wave height and wave period are not studied. Although the influence of the wave height is rather trivial -the larger the wave height, the large the velocity near the bottom, the larger the sediment transport rate- the combination of e.g. a larger wave and wave period might lead to sediment transport rates that are much larger than one would expect.

References

De Vriend, H.J., 1983: Bodemliggingsontwikkeling bij quasi-stationaire tweedimensionale horizontale stroming, WL|Delft Hydraulics.

De Vriend, H.J., 1987: Analysis of horizontally two-dimensional morphological evolutions in shallow water. Journal of Geophysical Research, volume 92 (C4).

De Vriend, H.J., 1996: River Dynamics (f10). Lecture notes, Delft University of Technology, Subfaculty of Civil Engineering.

Hoitink, T, 1997: Morphological impact of large scale marine sand extraction. M.Sc. thesis. University of Twente, Faculty of Technology and management and WL|Delft Hydraulics.

Hoornstra, D.R. and van der Hout, G., 1998: Berekeningen stroomverlammingskuil.

Hulscher, S., 1996: Formation and migration of large-scale, rhythmic sea-bed patterns: a stability approach. Doctoral dissertation. University of Utrecht, RIKZ and WL|Delft Hydraulics.

Labeur, R.J., 1998: Waterbeweging in zandwingebieden t.b.v. product K2000*z.w.

Németh, A.A., 1998: Modelling of the dynamic behaviour of sand extraction pits and tidal sandbanks. M.Sc. thesis. University of Twente, Faculty of Technology and management and WL|Delft Hydraulics.

Ribberink, J.S., 1986: Introduction to a depth-integrated model for suspended transport (Galappatti, 1983). Report no. 6-86, Delft University of Technology, Faculty of Civil Engineering.

Ribberink, J.S., 1989: Zeezandwinning; onderbouwend rapport MER/RON en discussienota kustverdediging. Technisch Rapport 10, Delft Hydraulics.

Roelvink, J.A., 1998: Training Delft3D-MOR.

Stive, M.J.F., 1998: Expert judgment morfologische ontwikkeling grootschalige zandwinning

Van Rijn, L.C., Reniers, A.J.H.M., Zitman, T. and Ribberink, J.S., 1995: Yearly-averaged sand transport at the -20 m and -8 m NAP depth contours of the Jarkus-profiles 14, 40, 76 and 103. WL|Delft Hydraulics report H1887, project Kustgenese.

Walstra, D.J.R., Reniers, A.J.H.M., Roelvink, J.A., Wang, Z.B., Steetzel, H.J., Aarninkhof, S.G.J., van Holland, G. and Stive, M.J.F., 1997: Grootschalige lange-termijn effecten van Maasvlakte-2 en gerelateerde zandwinningsvarianten; morfologische effecten op de Nederlandse kust van Zeeuws-Vlaanderen tot Den Helder over een periode van 300 jaar, WL|Delft Hydraulics/Alkyon report Z2255.

Walstra, D.J.R., Rijn, L.C. van en Aarninkhof, S.G.J., 1998: Sand transport at the middle and lower shoreface of the Dutch coast; simulations of SUTRENCH-model and proposal for large-scale laboratory tests, WL|Delft Hydraulics.

WL|Delft Hydraulics, 1996: Delft3D-FLOW manual

WL|Delft Hydraulics, 1996: Delft3D-MOR manual

WL|Delft Hydraulics, 1997: Delft3D-WAVE manual

A Bijker sediment transport formula

$$S = S_b + S_s$$

in which:

S_b = bottom sediment transport [$m^3/s/m$]
S_s = suspended sediment transport [$m^3/s/m$]

$$S_b = bd_{50}\frac{q}{C}\sqrt{g}\cdot e^{(A_r)}(1-\varepsilon)$$

A_r = A_{ra} if $-50<A_{ra}<100$
= -50 if $A_{ra}<-50$
= 100 if $A_{ra}>100$

$$A_{ra} = \frac{-0.27\Delta d_{50}C^2}{r_\mu q^2\left(1-0.5\xi\left(\frac{u_b}{v}\right)^2\right)}$$

$$r_\mu = \left(\frac{C}{18\log(10\frac{12h}{d_{90}}}\right)^{1.5}$$

$$I_1 = 0.216\frac{\left(\frac{r_c}{h}\right)^{z_*-1}}{\left(1-\frac{r_c}{h}\right)^{z_*}}\int_{r_c/h}^{1}\left(\frac{1-y}{y}\right)^{z_*}dy$$

$$I_2 = 0.216\frac{\left(\frac{r_c}{h}\right)^{z_*-1}}{\left(1-\frac{r_c}{h}\right)^{z_*}}\int_{r_c/h}^{1}\ln y\left(\frac{1-y}{y}\right)^{z_*}dy$$

$$z_* = \frac{w}{\frac{\kappa q\sqrt{g}}{C}\sqrt{1+0.5\left(\xi\frac{u_b}{q}\right)^2}}$$

$$u_b = \frac{\omega h_w}{2\sinh(k_w h)}$$

$$\omega = \frac{2\pi}{T}$$

$$f_w = e^{(-5.977+\frac{5.123}{a_0^{0.194}})}$$

$$a_0 = \max(2.0, \frac{u_b}{\omega r_c})$$

$$\xi = C\sqrt{\frac{f_w}{2g}} \qquad \text{if } T>1.0*10^{-6}$$

$$\xi = 0 \qquad \text{if } T\leq 1.0*10^{-6}$$

in which:

k_w	=	wave number	[m^{-1}]
h_w	=	wave heigth (h_{rms})	[m]
h	=	water depth	[m]
q	=	magnitude of flow velocity	[m/s]
Δ	=	relative density of the sediment	[-]
u_b	=	wave velocity	[m/s]
ξ	=	correction coefficient	[-]

B Physical input parameters

FLOW

g	gravity acceleration	9.81	[m/s^2]
ρ_w	water density	1000	[kg/m^3]
T	water temperature	15	[°C]
S	salinity	31	[ppt]
C	Chézy coefficient	65	[m$^{1/2}$/s]
n	Manning coefficient	0.025	[m$^{1/3}$/s]
ν	horizontal eddy viscosity	1	[m^2/s]
D_v	horizontal eddy diffusity	10	[m^2/s]

WAVES

H_s	significant wave height	1.5	[m]
T_p	spectral peak period	6	[s]
χ_0	spectral peak enhancement factor	3.30	[-]
M_s	width energy distribution	4	[-]
C_{fw}	friction coefficient induced by waves	0	[-]
C_{fc}	friction coefficient induced by current	0	[-]

TRAN

ρ_s	density of sediment	2650	[kg/m^3]
d_{50}	characteristic of grain size distribution	0.2	[mm]
d_{90}	characteristic of grain size distribution	0.3	[mm]
ε	porosity of sediment	0.4	[-]
r_μ	kinematic viscosity of water	$1*10^{-6}$	[m^2/s]

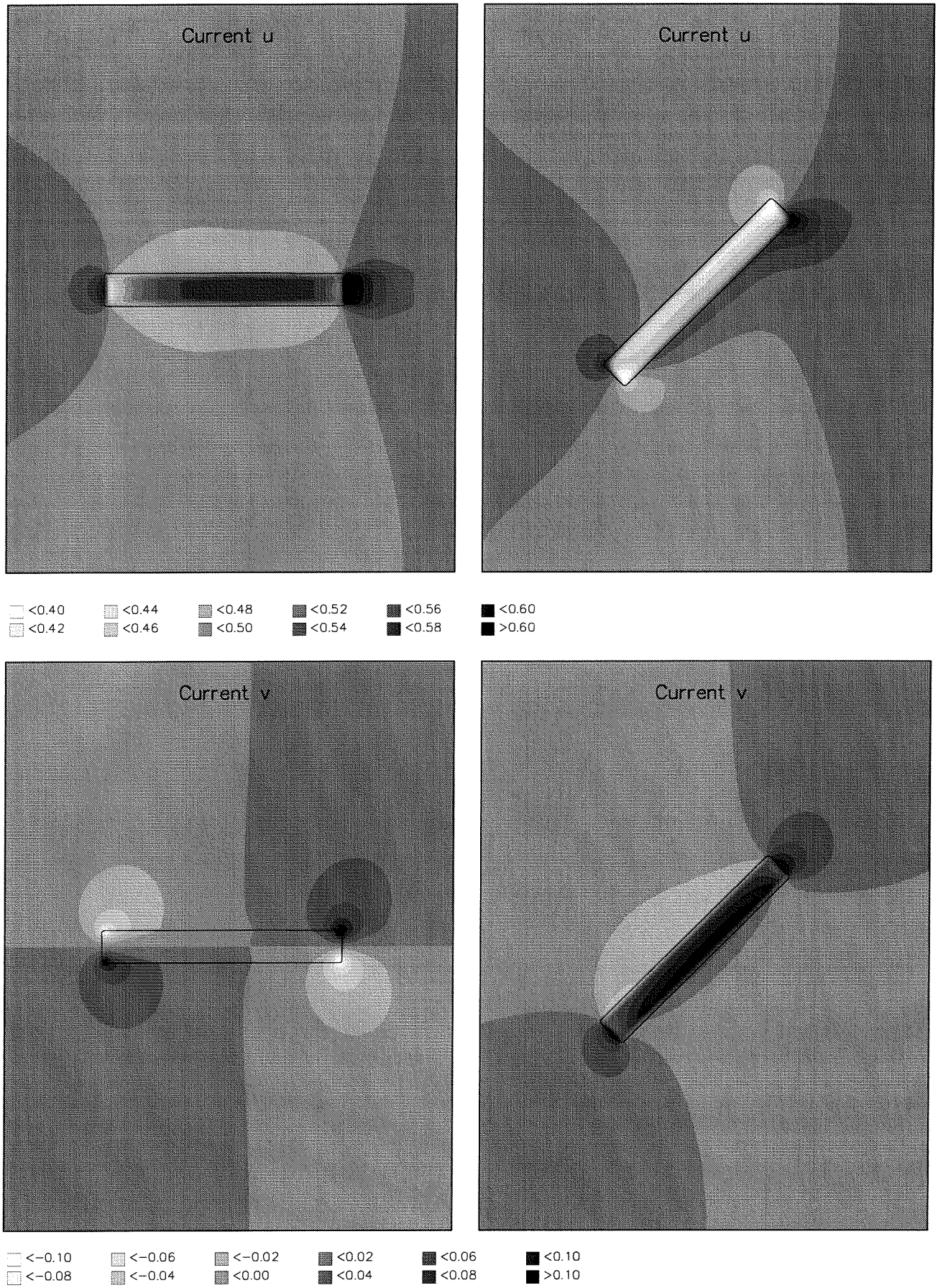

Current velocity components u and v [m/s]

Influence of obliquity of a 40x5 km^2 sandpit

Stationary boundary conditions

WL | DELFT HYDRAULICS

z2615

Figure 5.1

Figure 5.2: Current velocities in the center longitudinal section of a 40x5 km ^ 2 sandpit

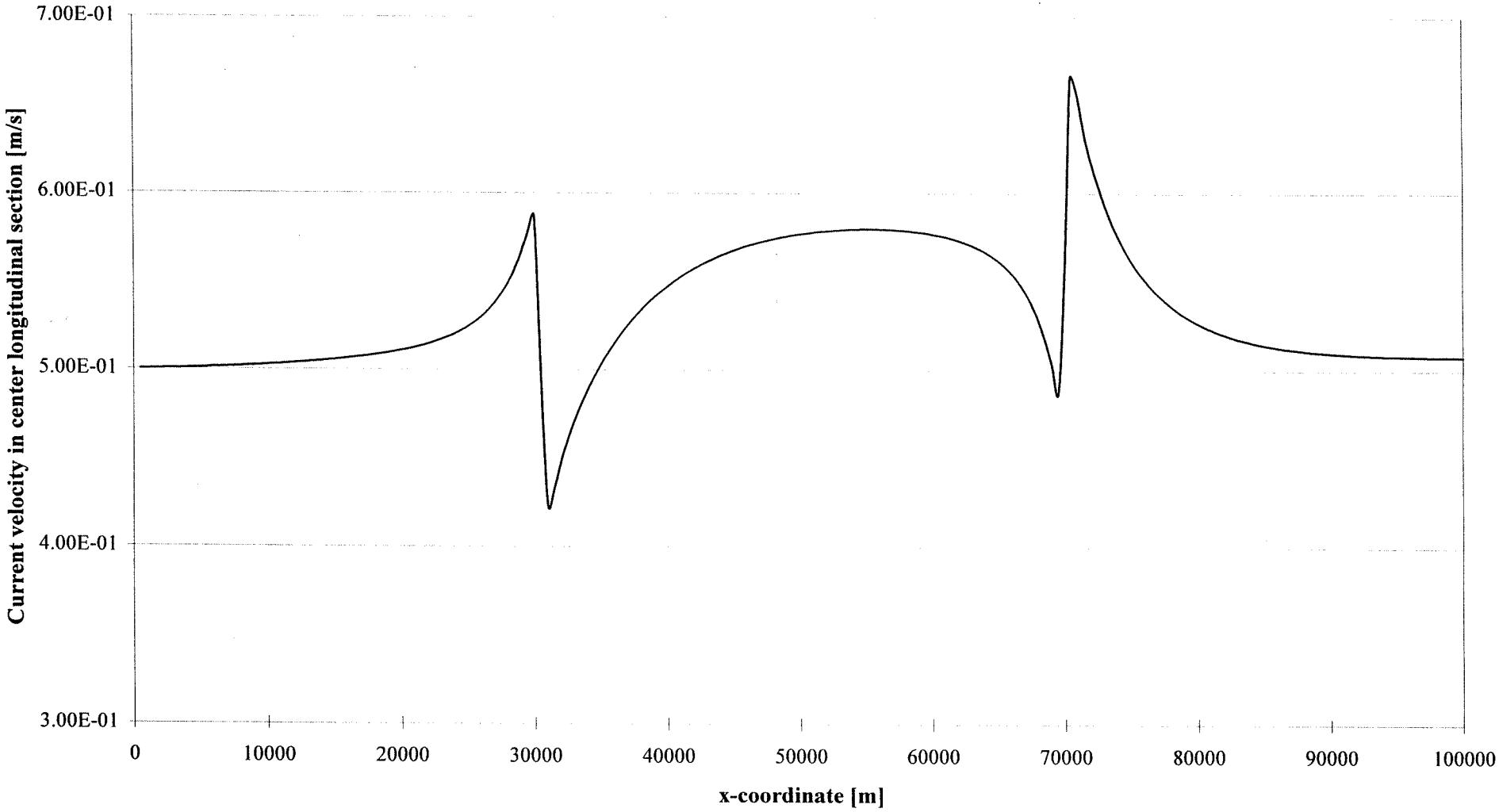

Figure 5.3: Relation between water level difference and discharge into the sandpit

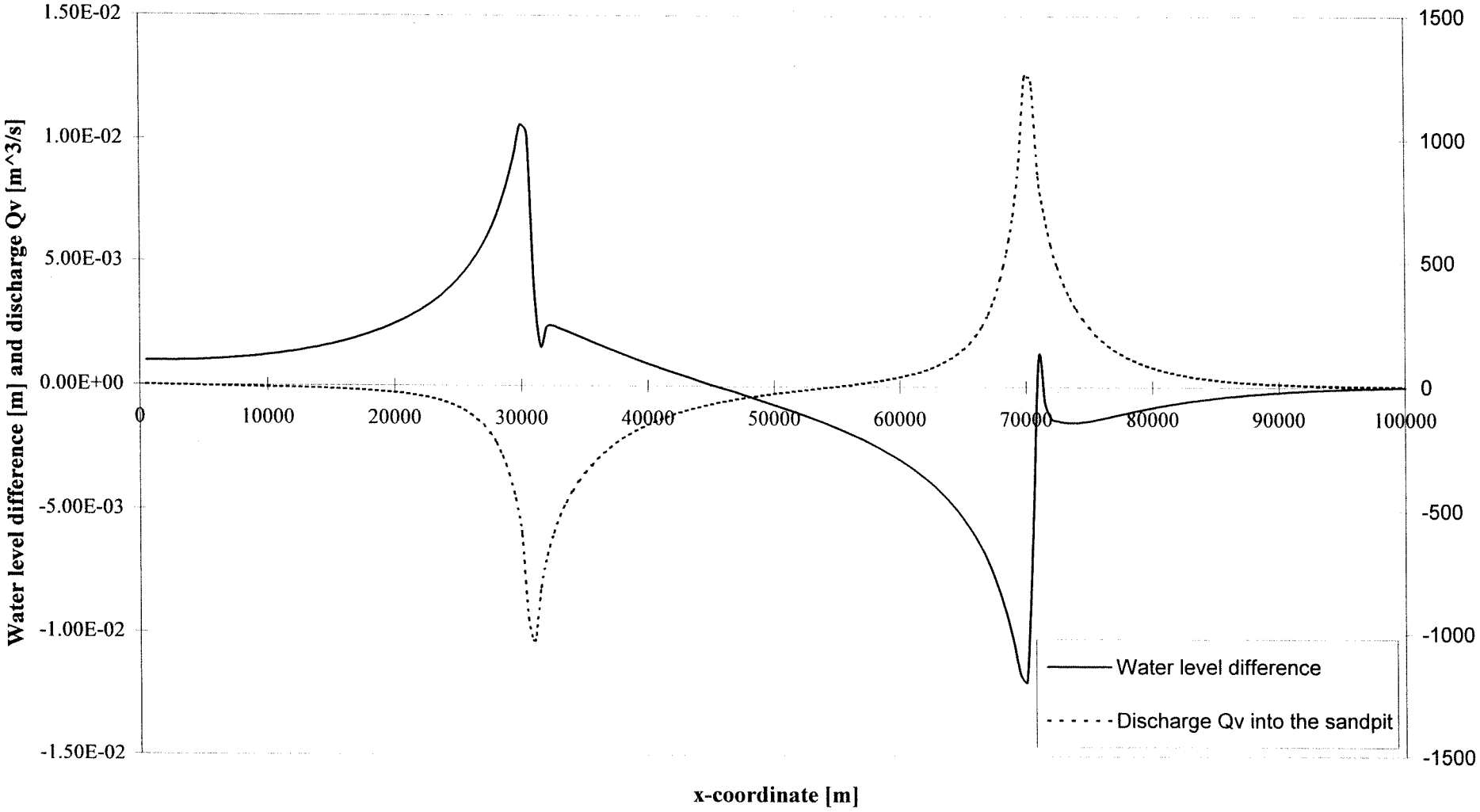

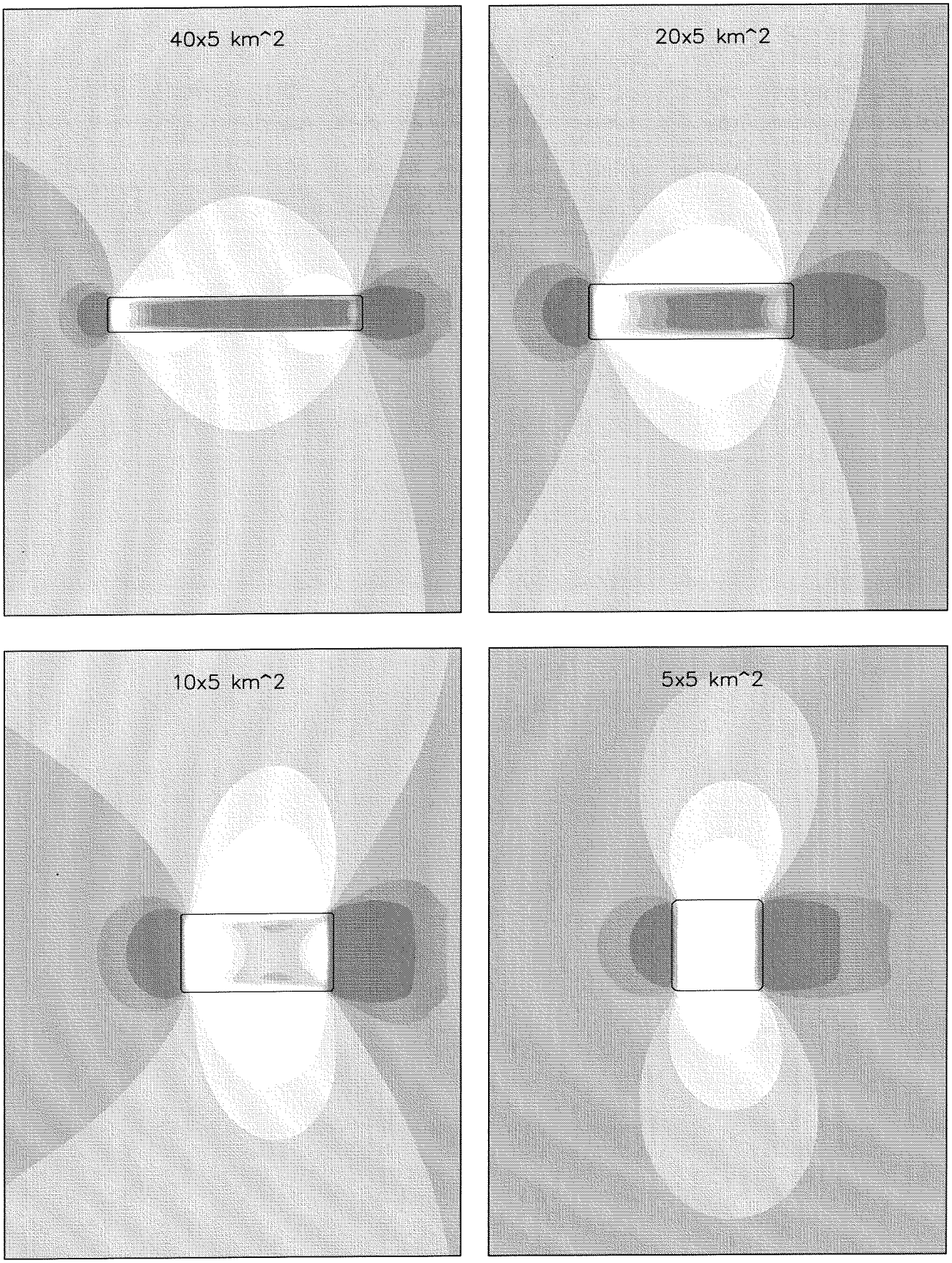

Current magnitude [m/s]

Area of influence around 30 m deep sandpits, varying in length

Stationary boundary conditions

WL | DELFT HYDRAULICS

z2615

Figure 5.6

Figure 5.7: Current velocities in an infinitely wide and a 5 km wide sandpit

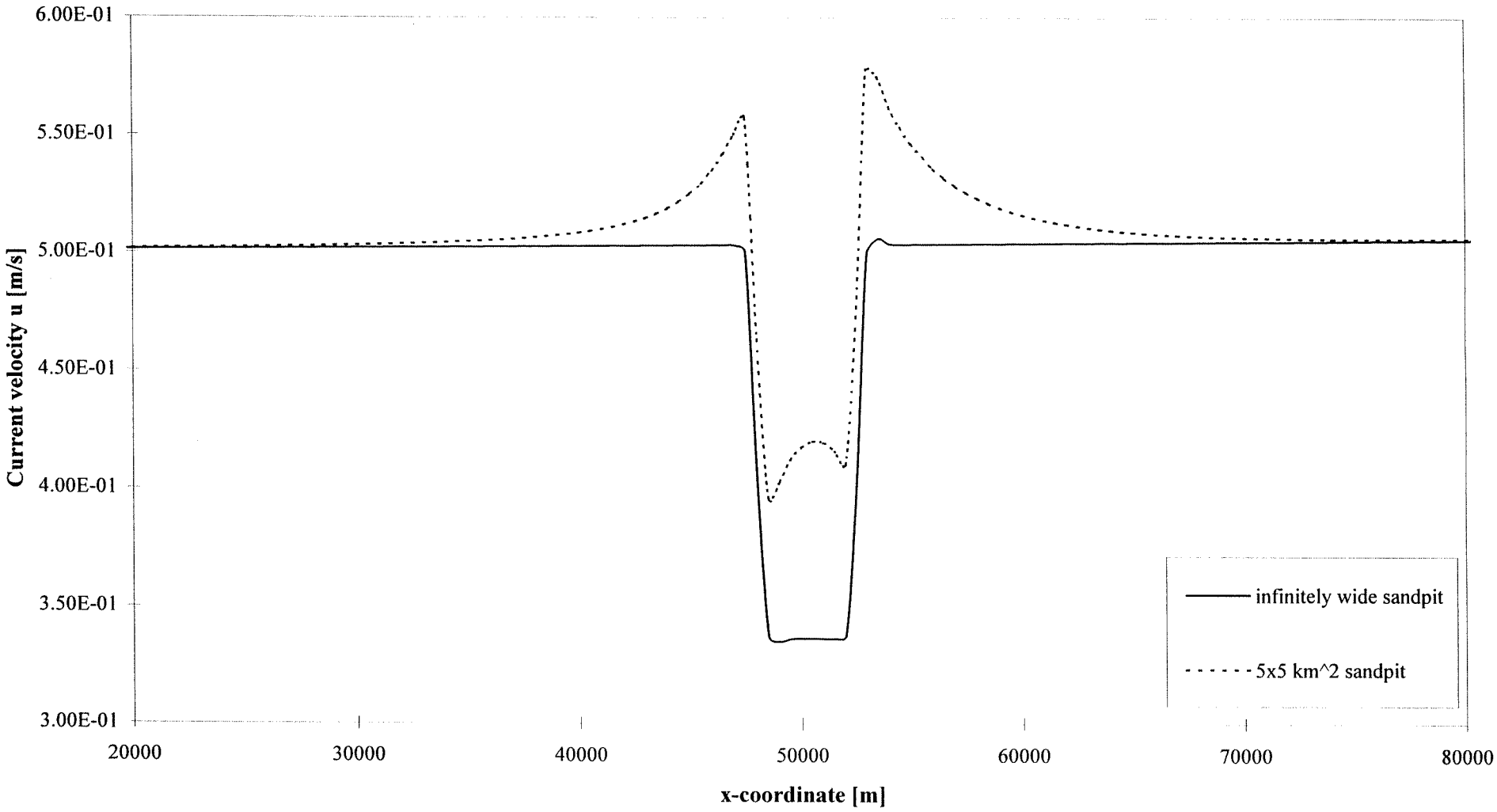

Figure 5.8: Distribution of u-velocity in three cross-sections

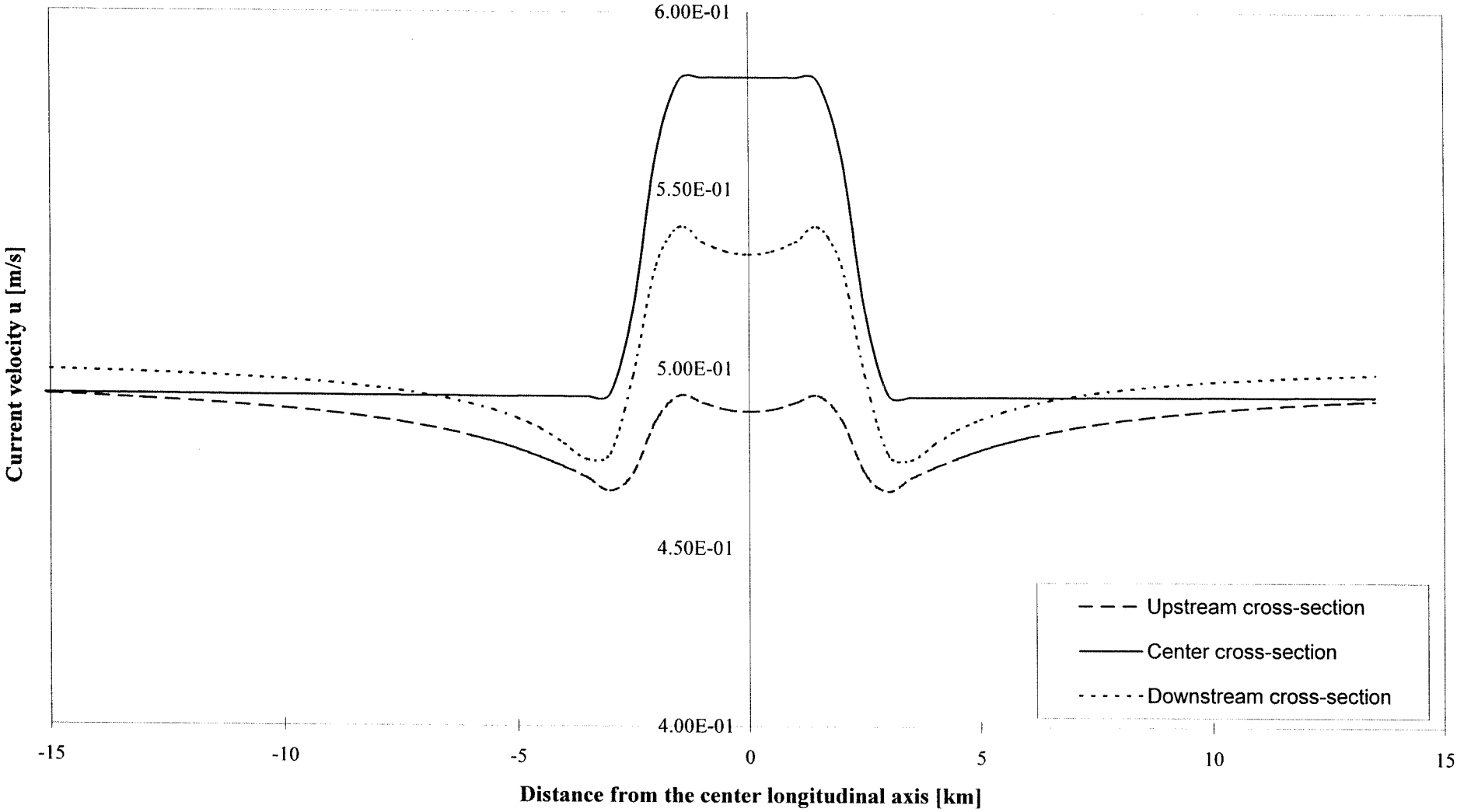

Figuur 5.9: Maximum current velocity vs. length of the sandpit

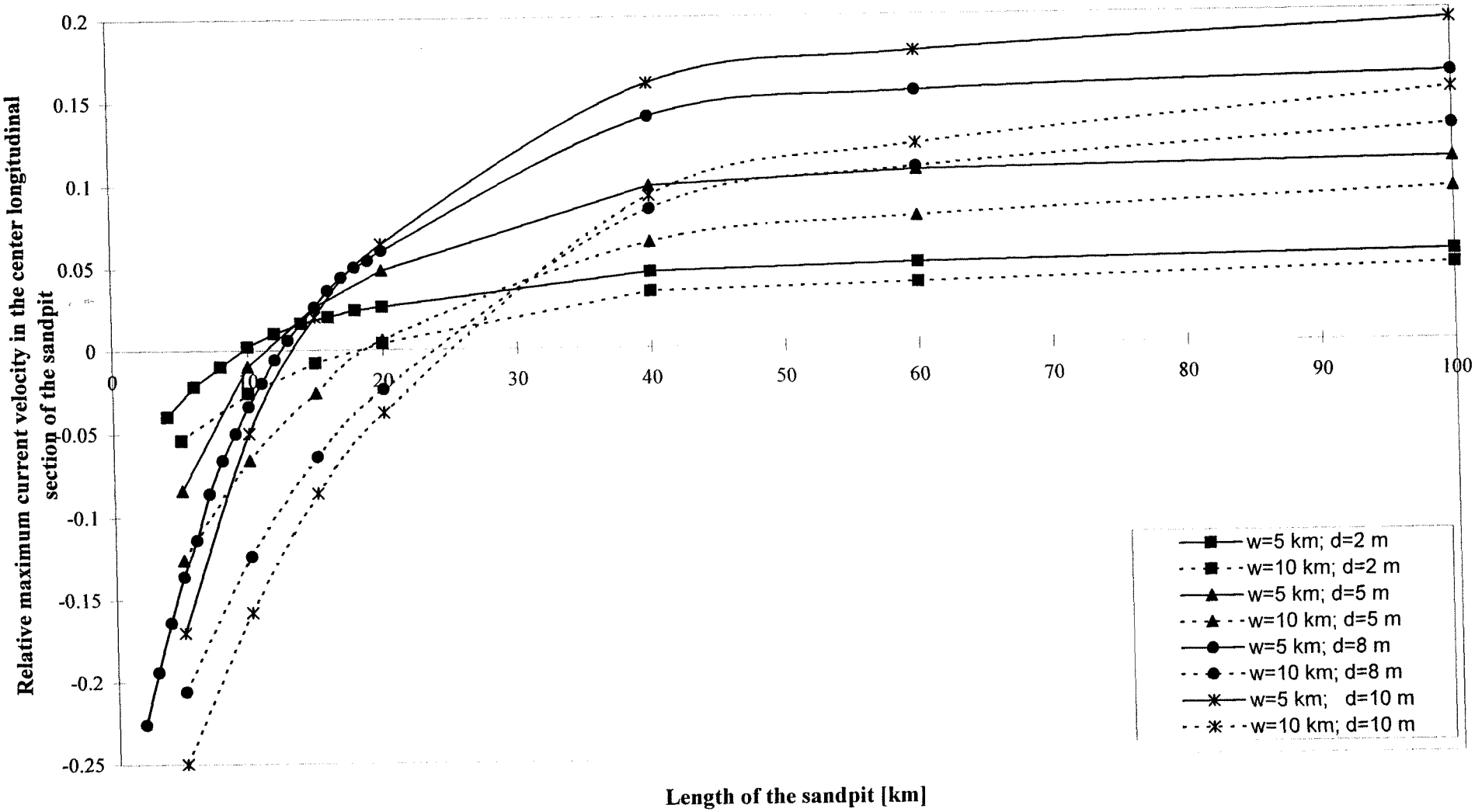

Figuur 5.10: Maximum current velocity vs. length-width ratio of the sandpit

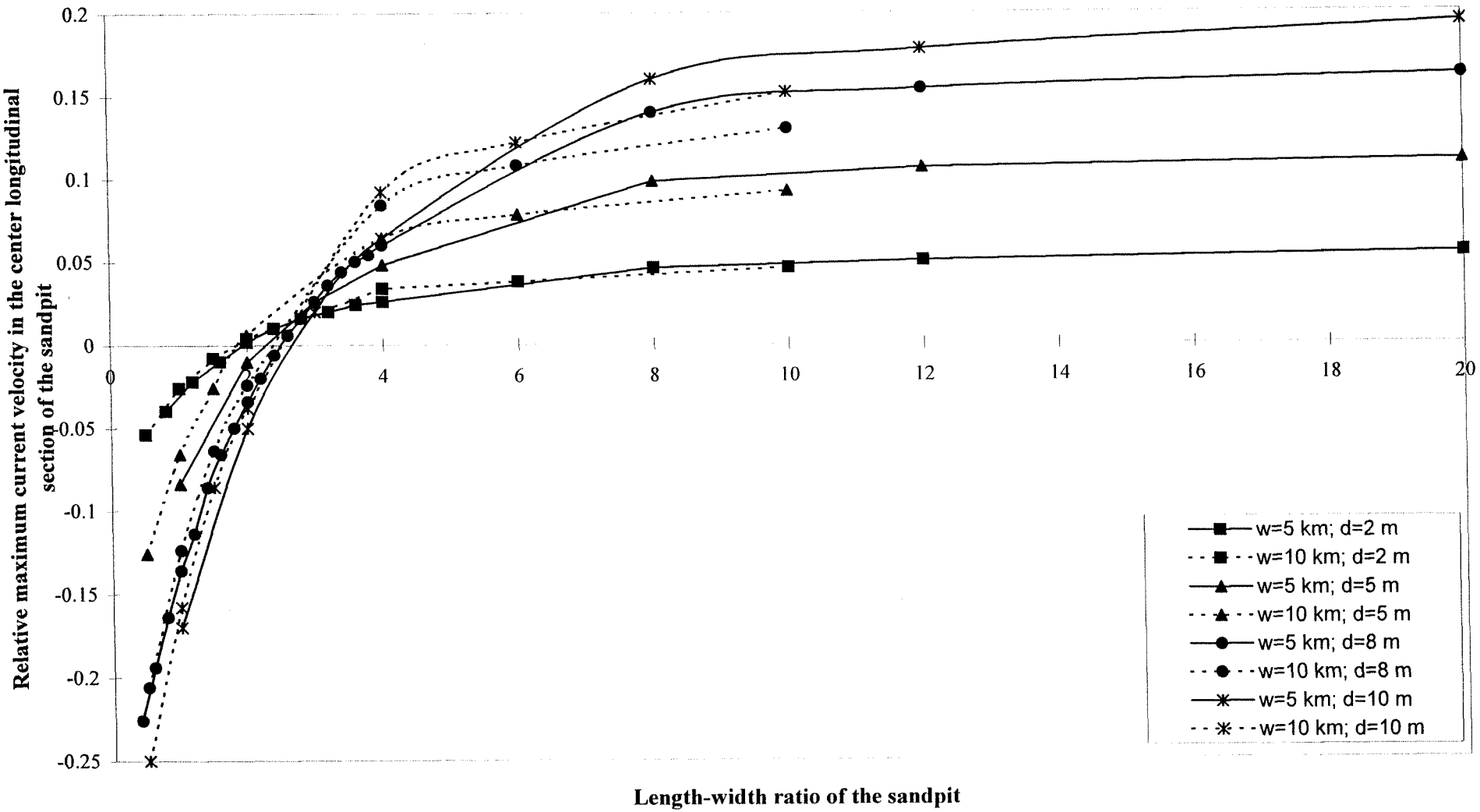

Figuur 5.11: Maximum current velocity vs. length-depth ratio of the sandpit

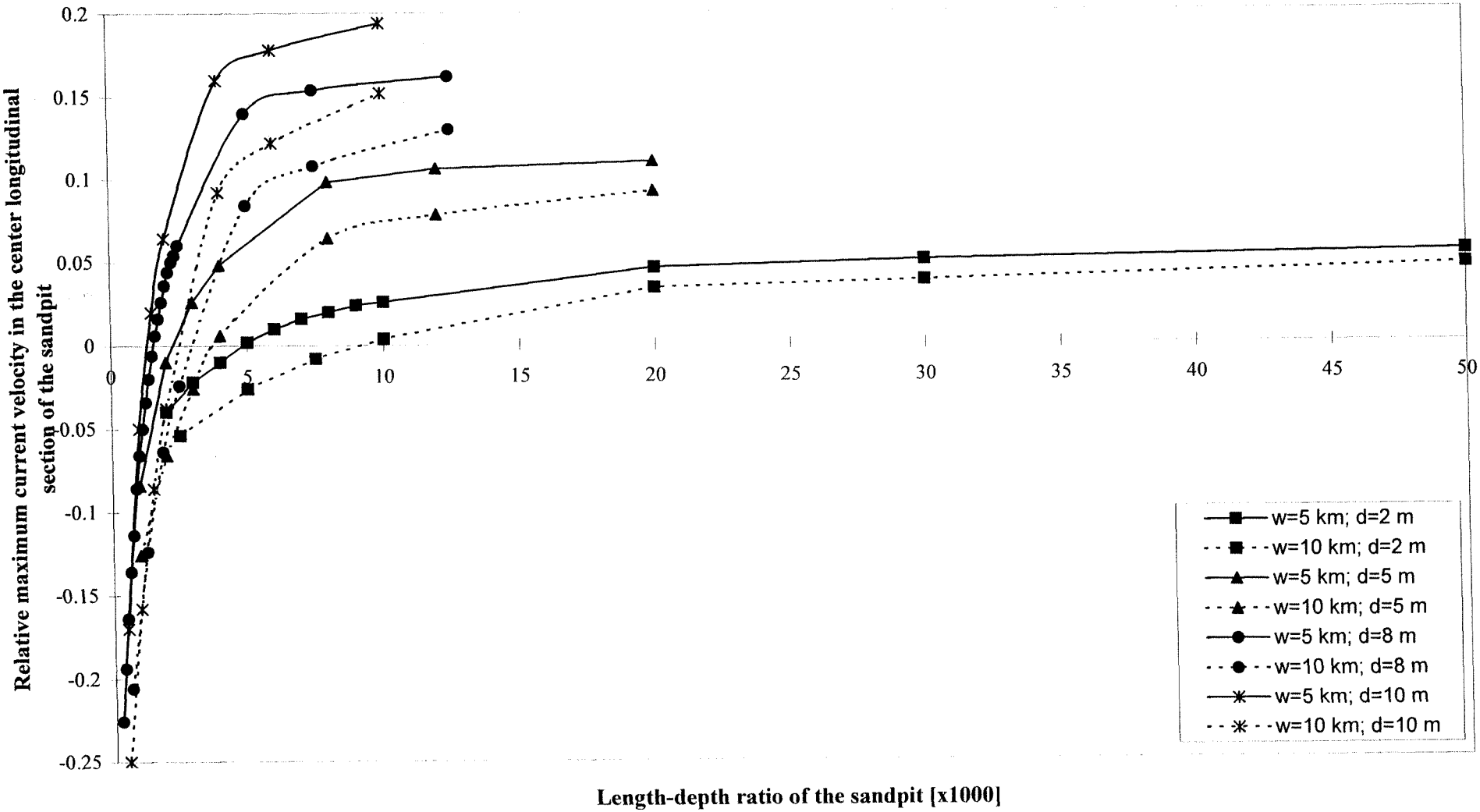

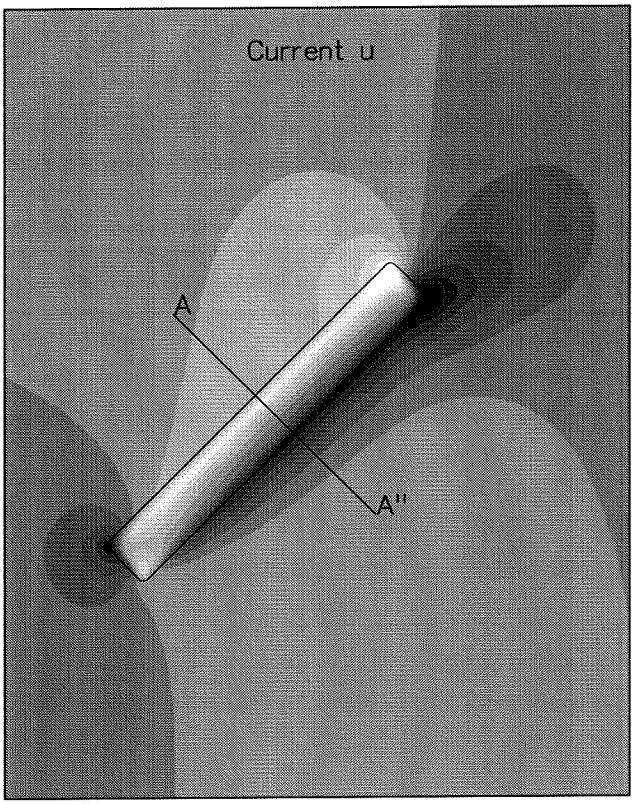

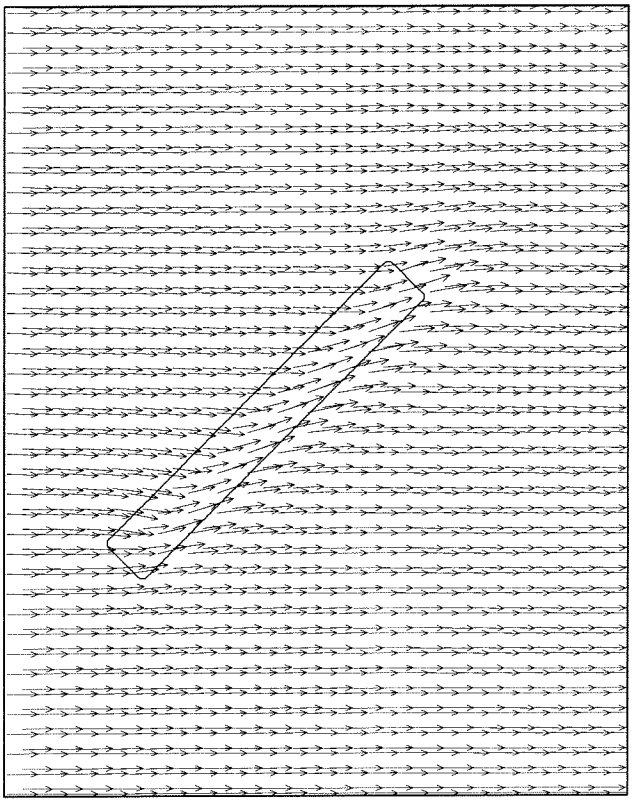

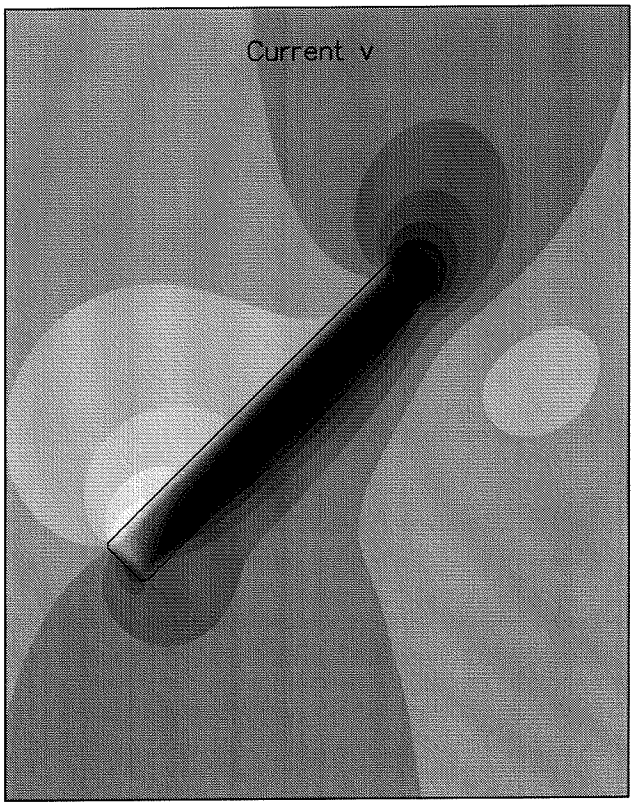

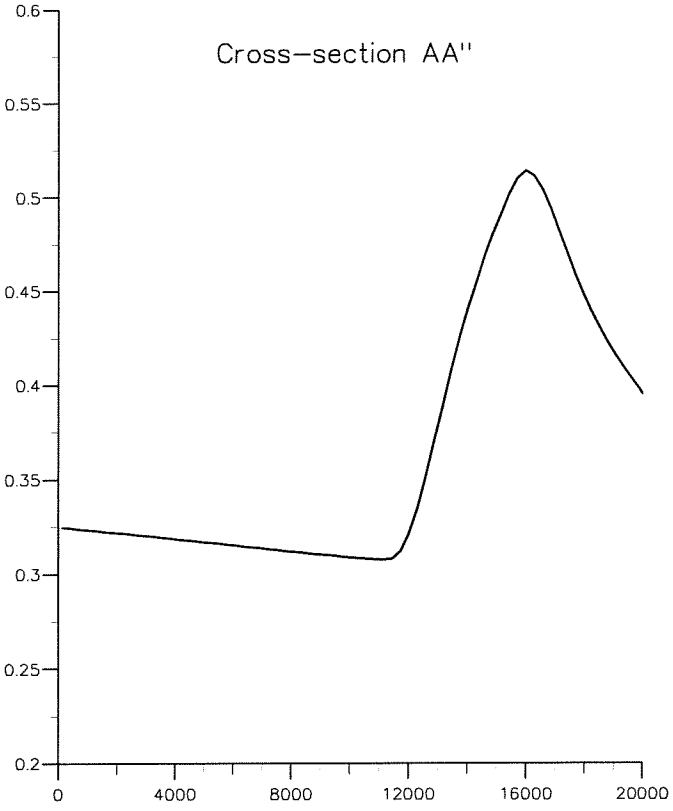

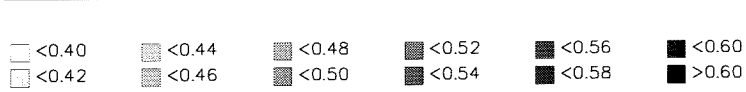

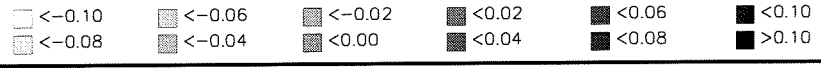

Current velocities u and v [m/s]

Stationary current pattern and current velocities in cross–section AA''

Stationary boundary conditions including Coriolis

WL | DELFT HYDRAULICS

z2615

Figure 6.2

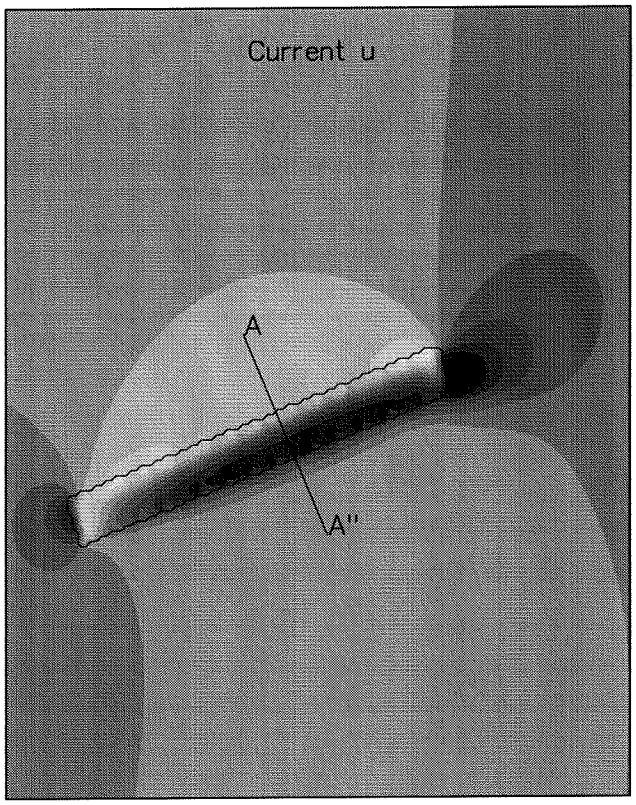

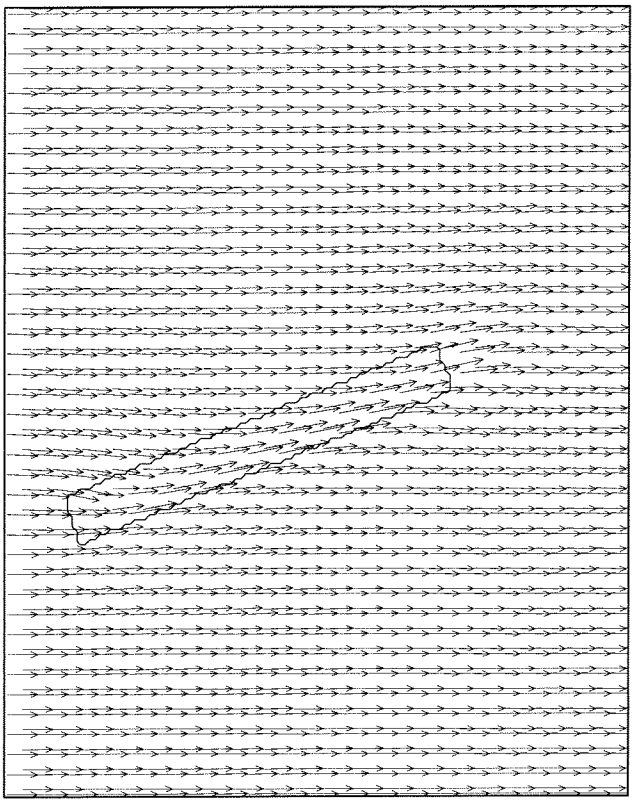

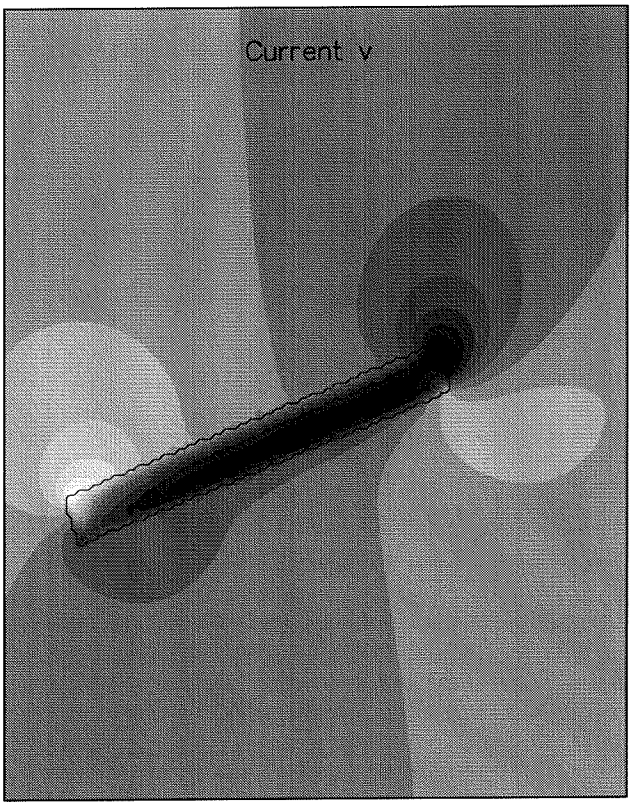

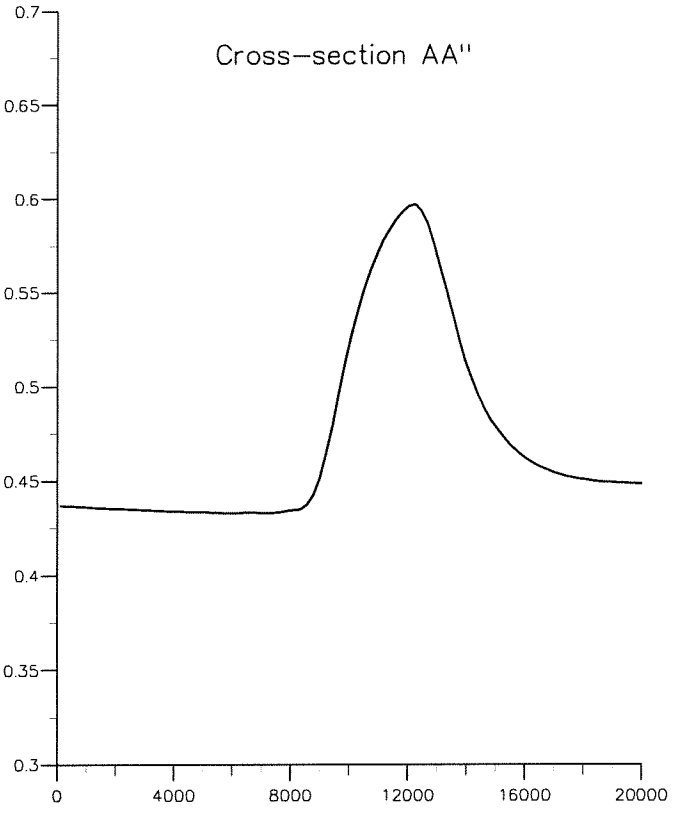

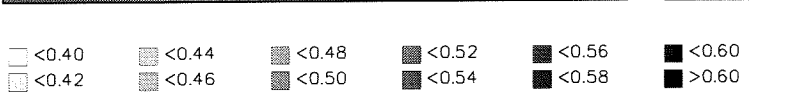

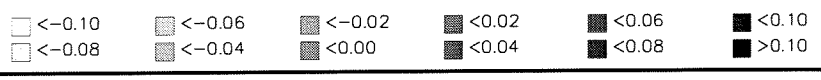

Current velocities u and v [m/s]

Stationary current pattern and current velocities in cross–section AA''

Stationary boundary conditions including Coriolis

WL | DELFT HYDRAULICS

z2615

Figure 6.3

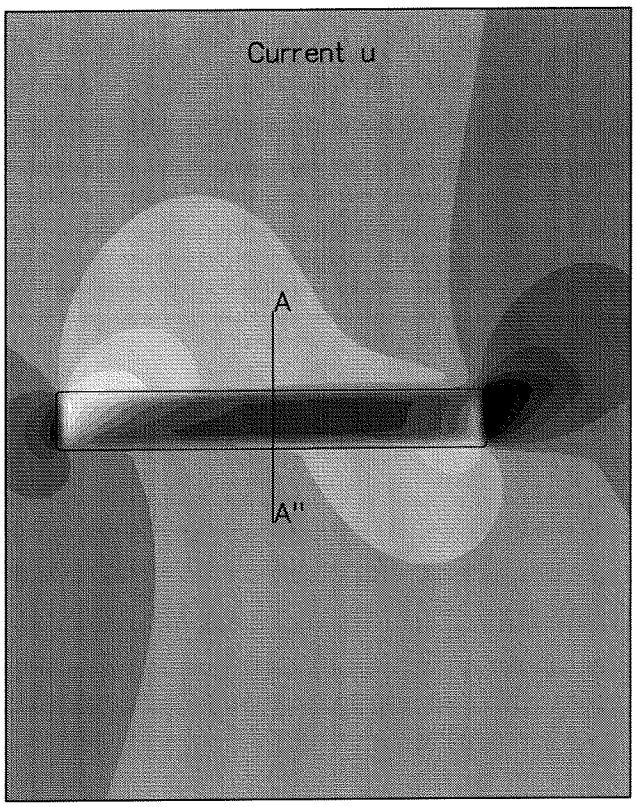

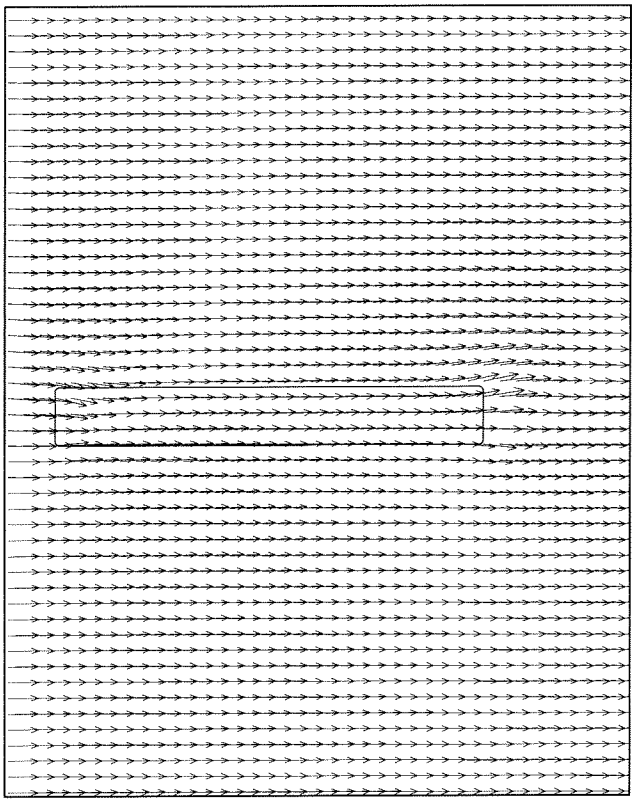

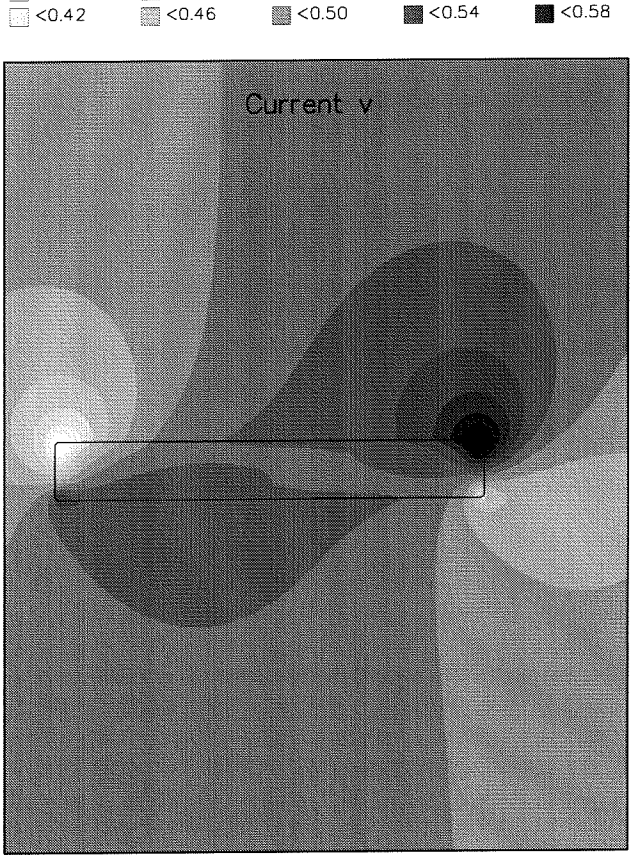

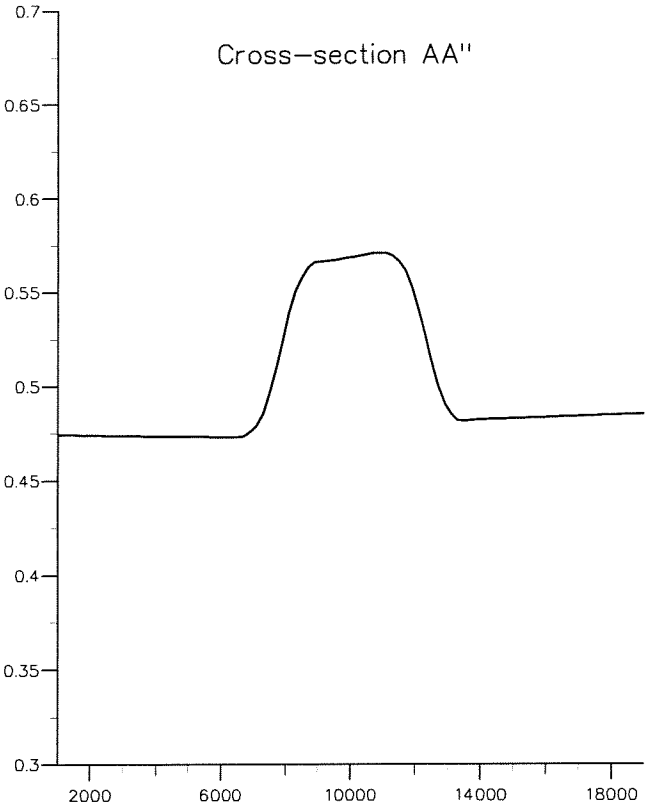

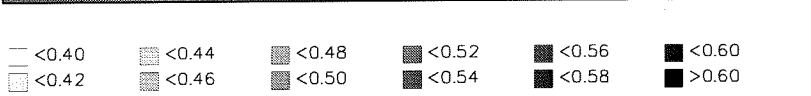

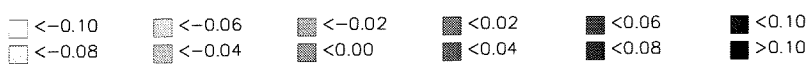

Current velocities u and v [m/s]

Stationary current pattern and current velocities in cross–section AA''

Stationary boundary conditions including Coriolis

WL | DELFT HYDRAULICS

z2615

Figure 6.4

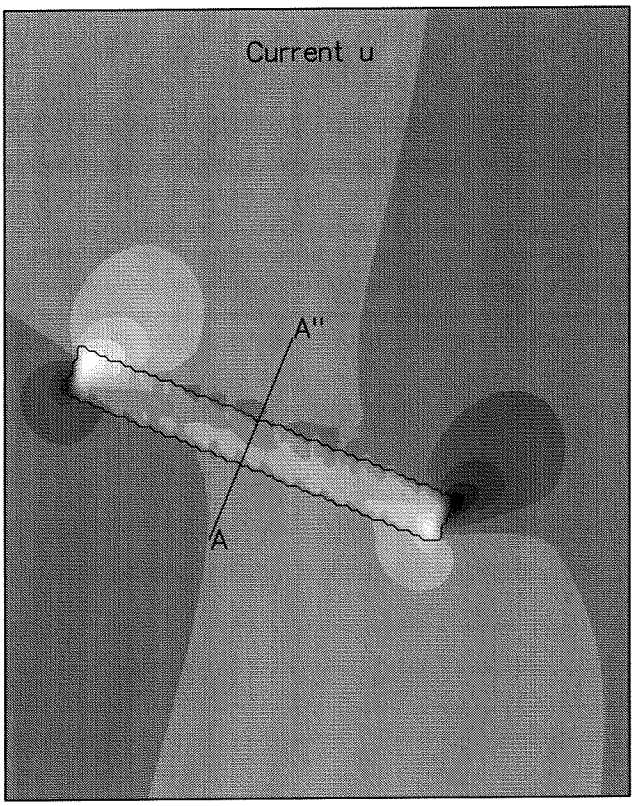

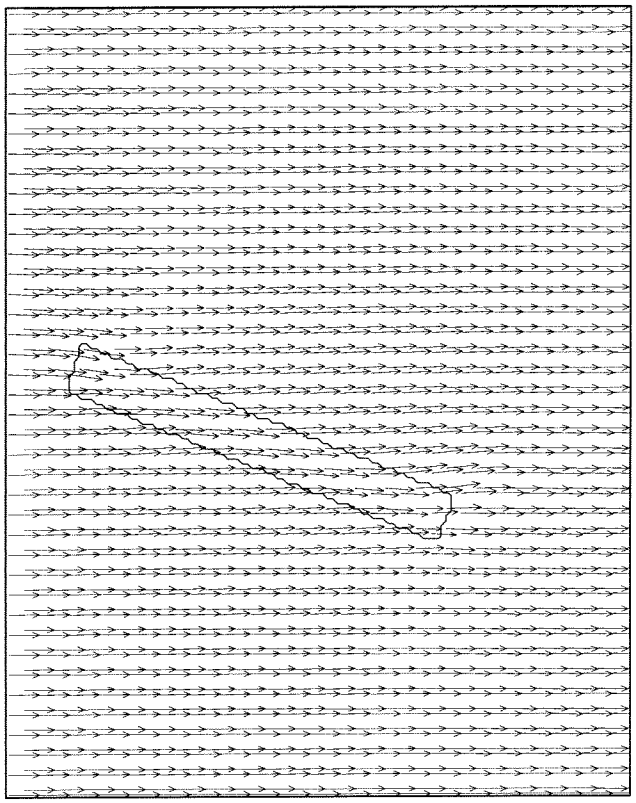

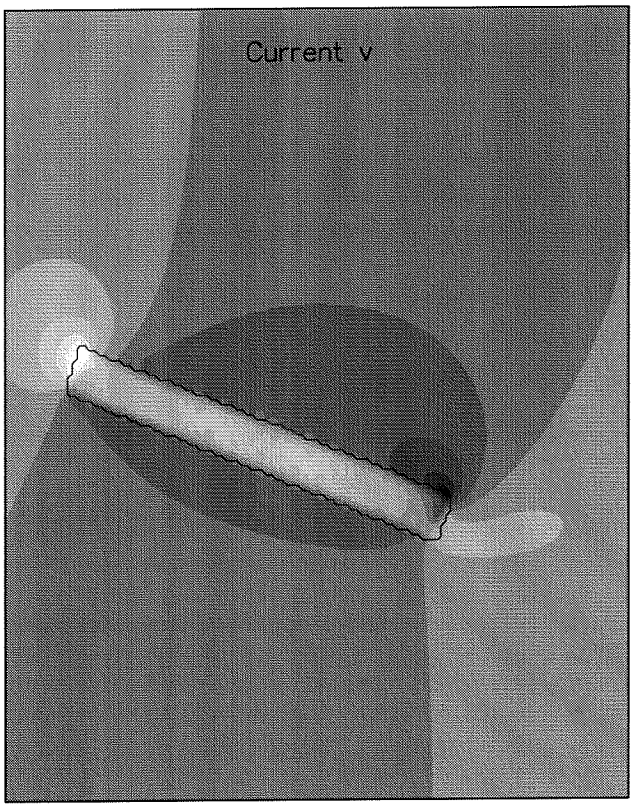

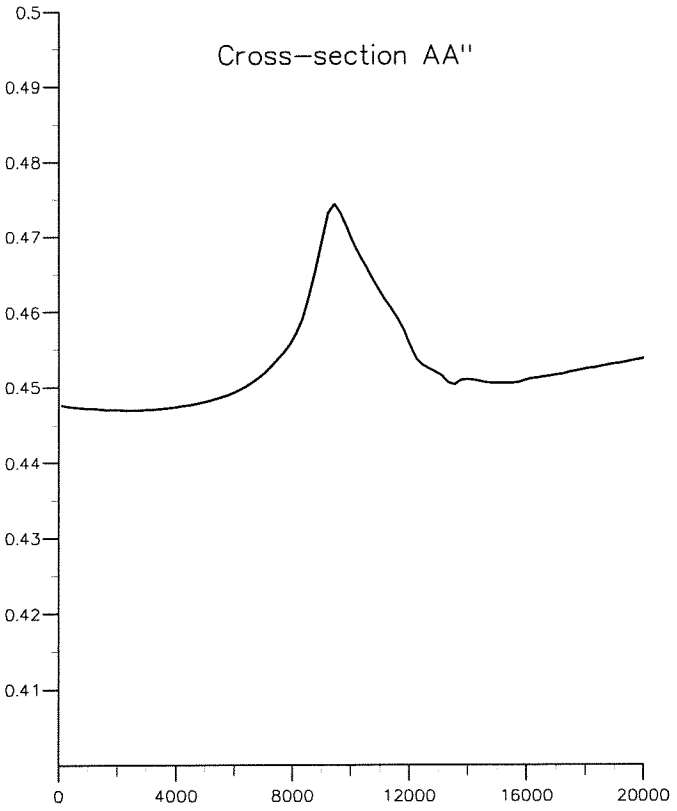

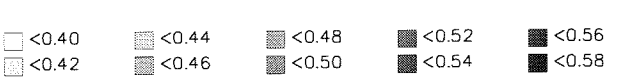

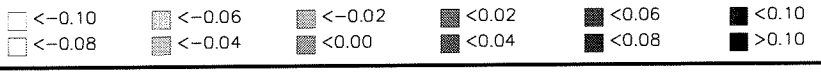

Current velocities u and v [m/s]

Stationary current pattern and current velocities in cross-section AA''

Stationary boundary conditions including Coriolis

WL | DELFT HYDRAULICS

z2615

Figure 6.5

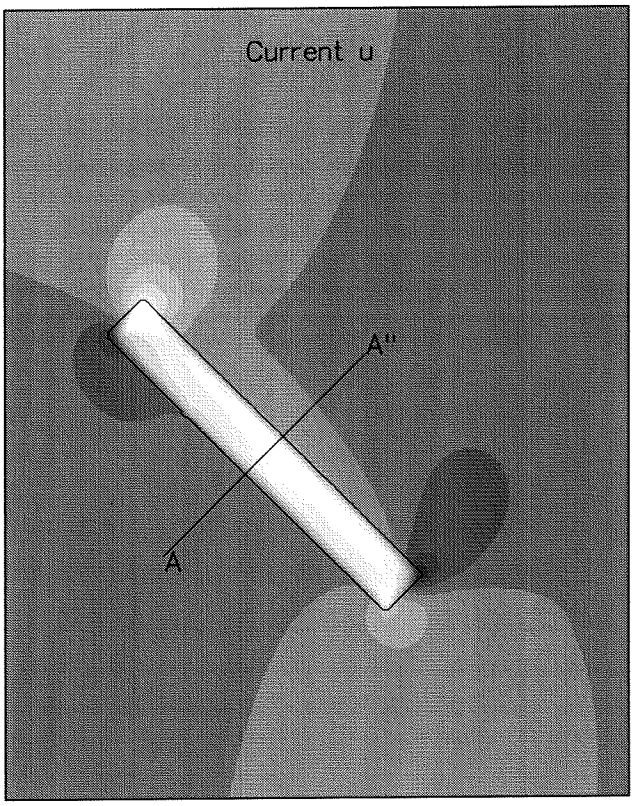

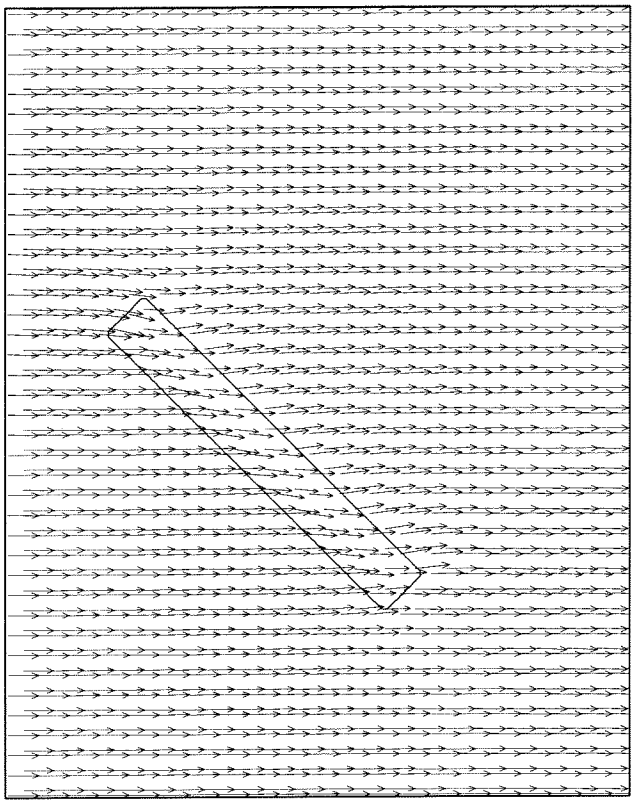

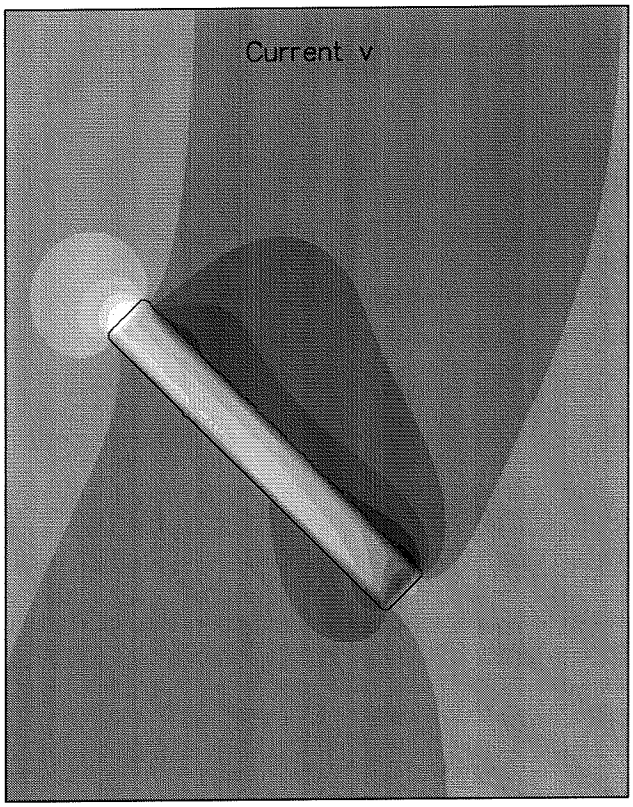

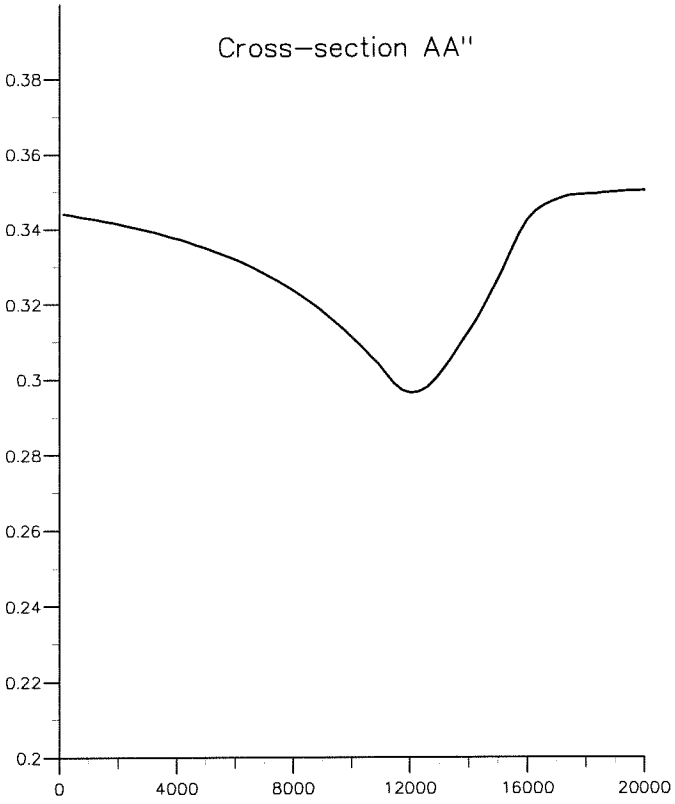

Current velocities u and v [m/s]

Stationary current pattern and current velocities in cross–section AA''

Stationary boundary conditions including Coriolis

WL | DELFT HYDRAULICS

z2615

Figure 6.6

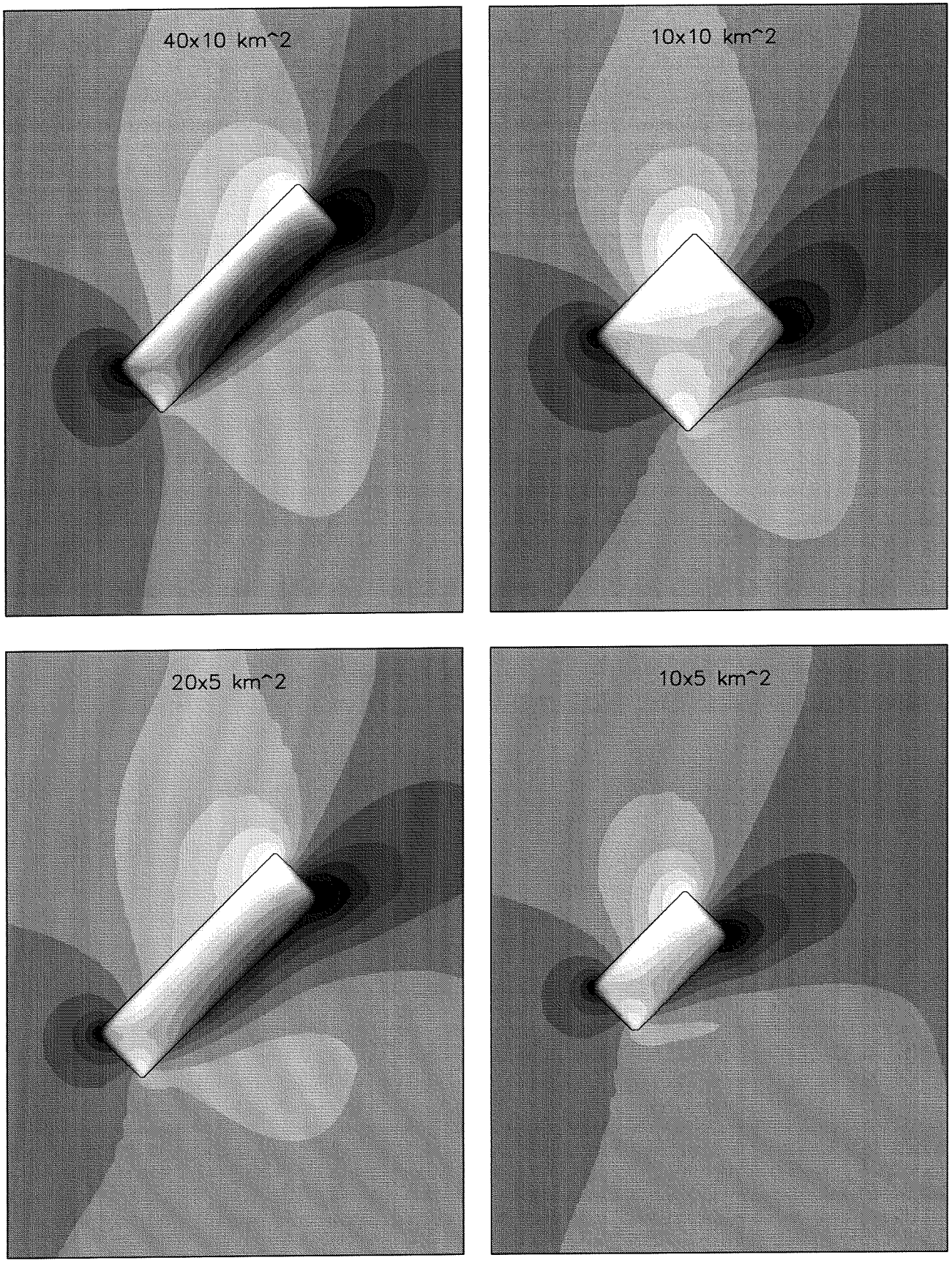

Current magnitude [m/s]

Influence of the length and the width on the current pattern

Stationary boundary conditions including Coriolis

WL | DELFT HYDRAULICS

z2615

Figure 6.7

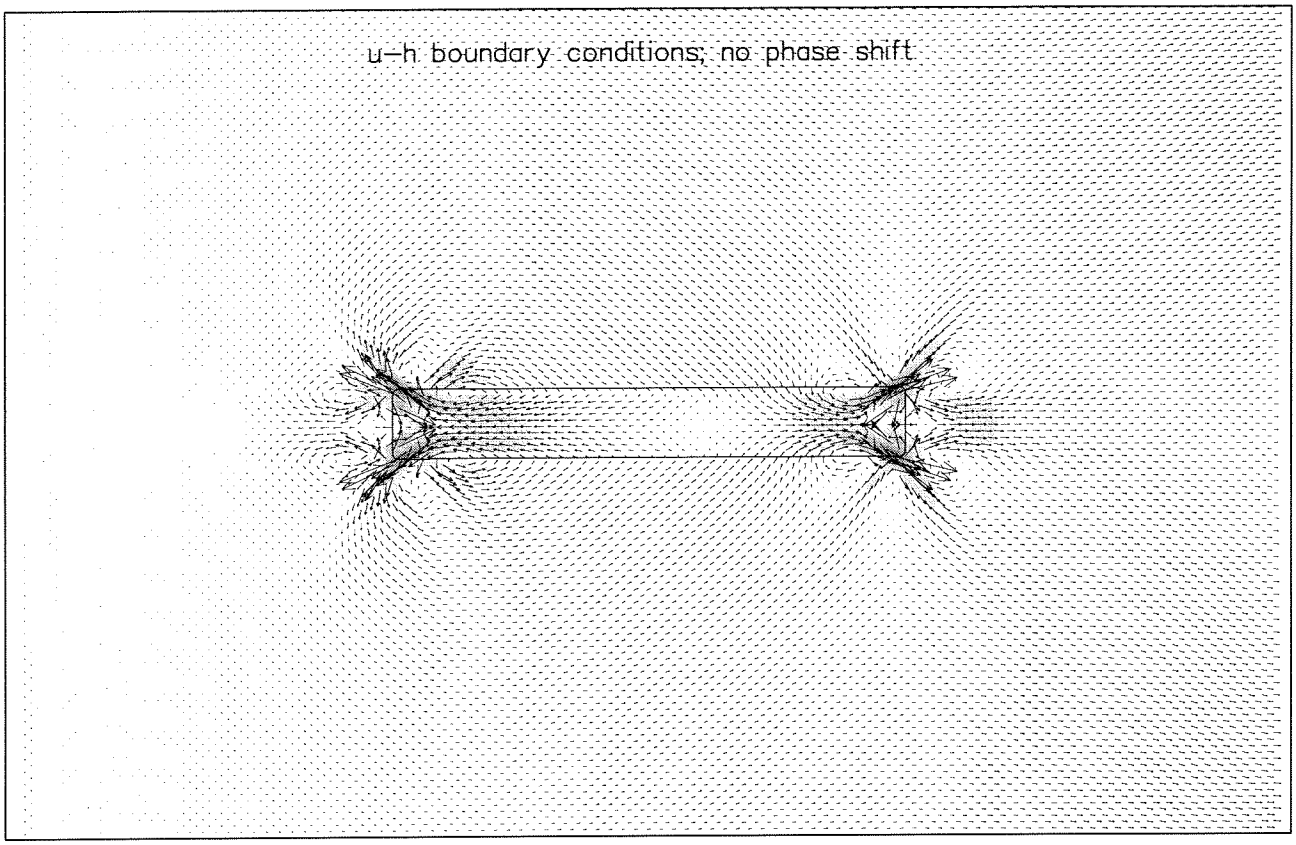

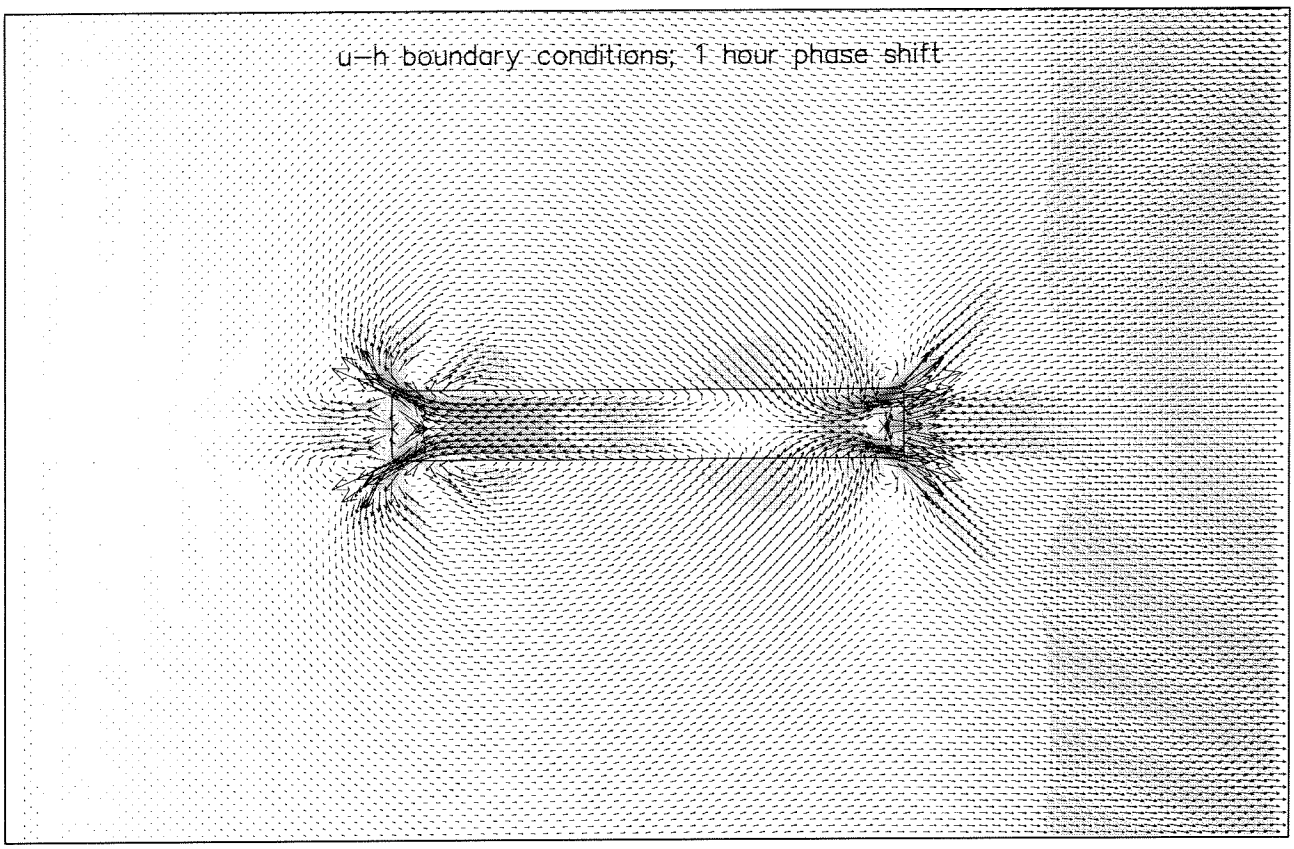

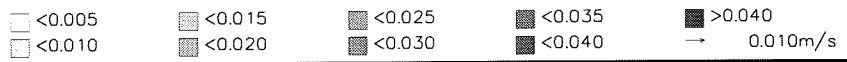

Tide–averaged current velocities [m/s]

Influence of the boundary conditions on the tide–averaged current pattern

Tidal boundary conditions

WL | DELFT HYDRAULICS

z2615

Figure 7.1

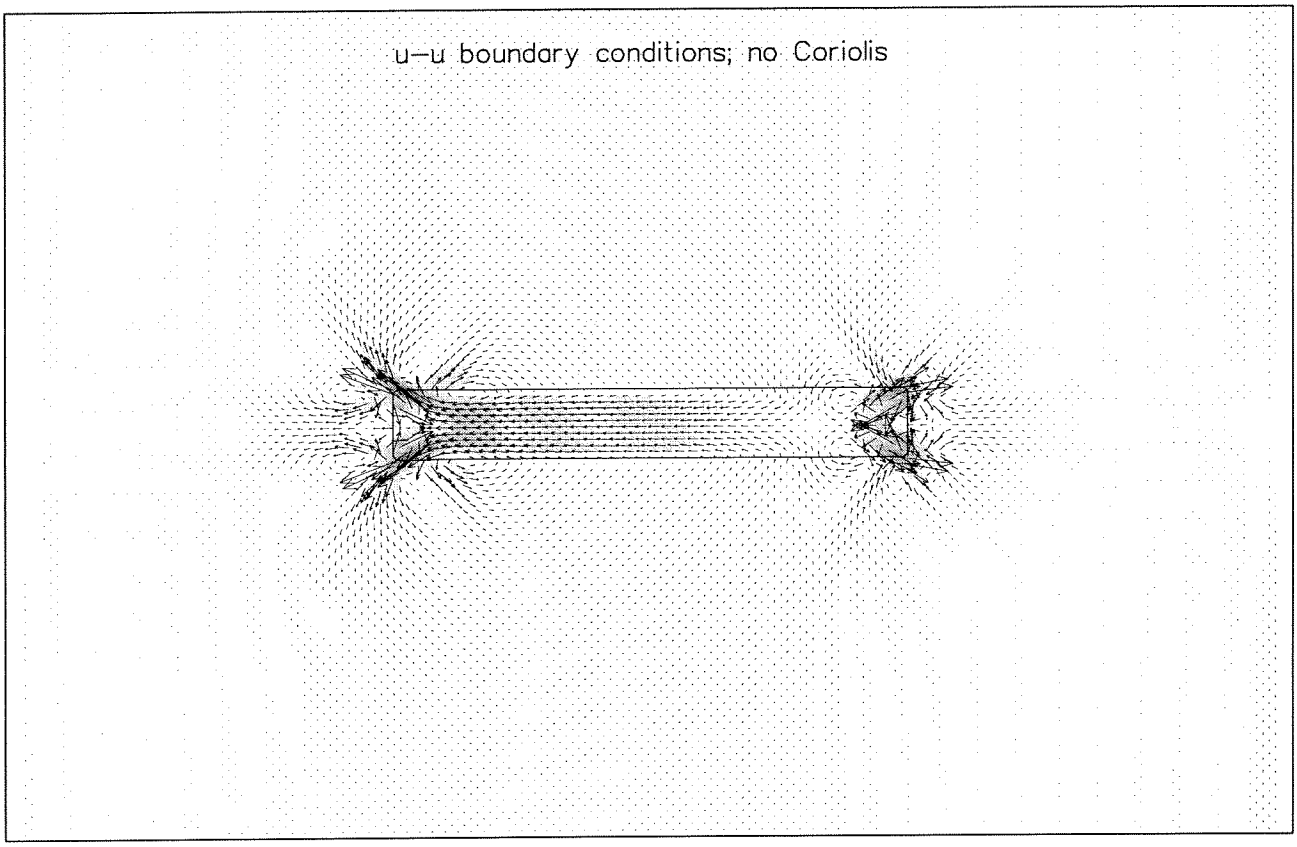

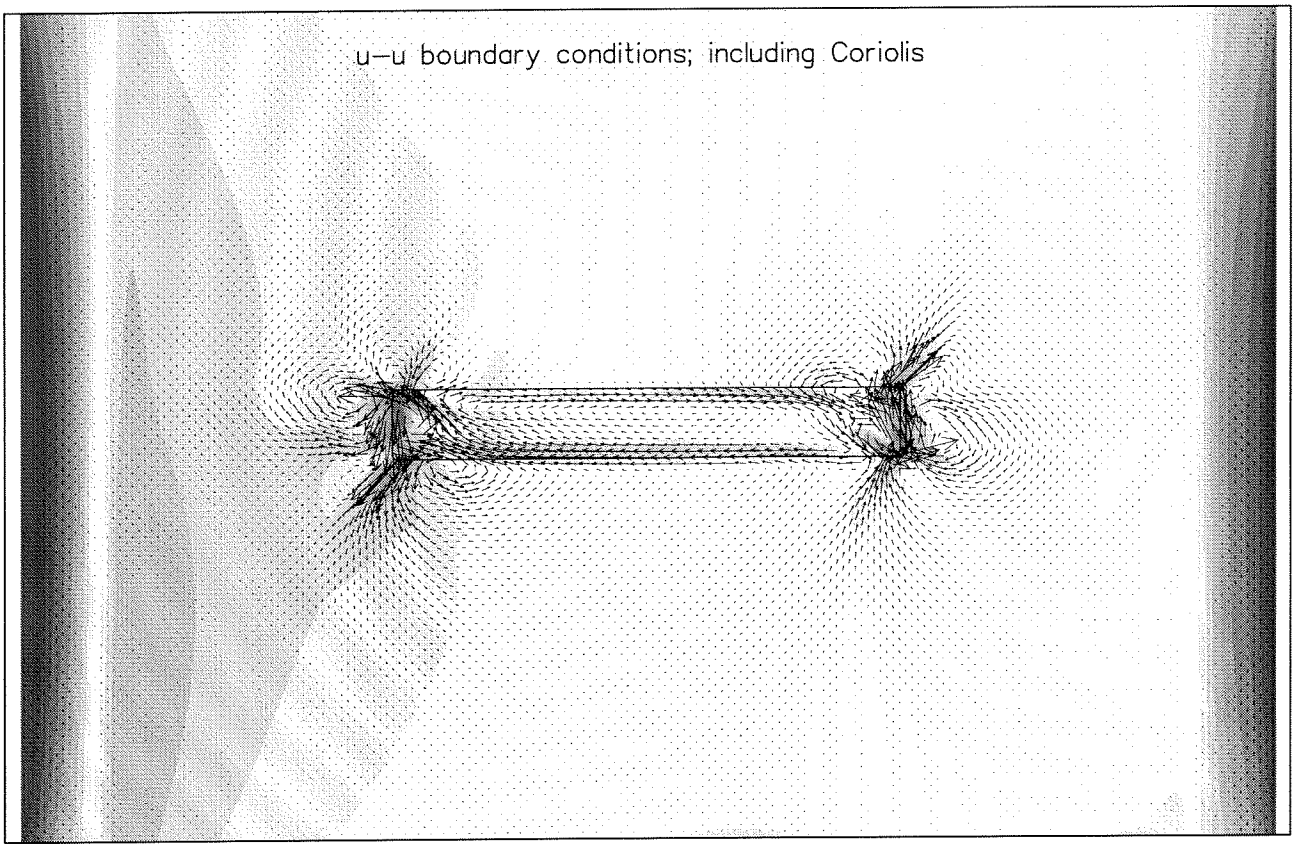

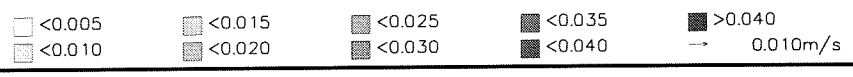

Tide–averaged current velocities [m/s]

Influence of Coriolis on the tide–averaged current pattern

Tidal boundary conditions with and without Coriolis

WL | DELFT HYDRAULICS

z2615

Figure 7.2

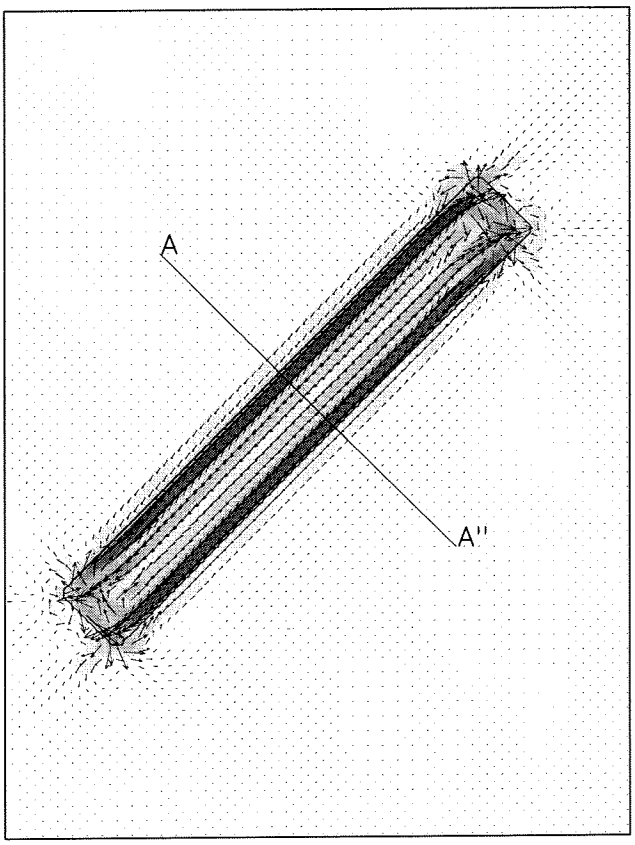

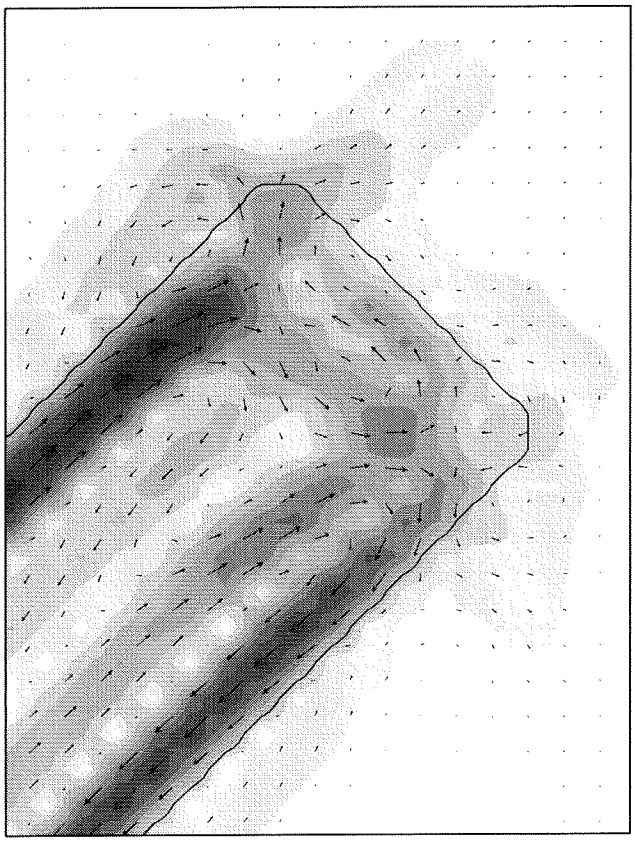

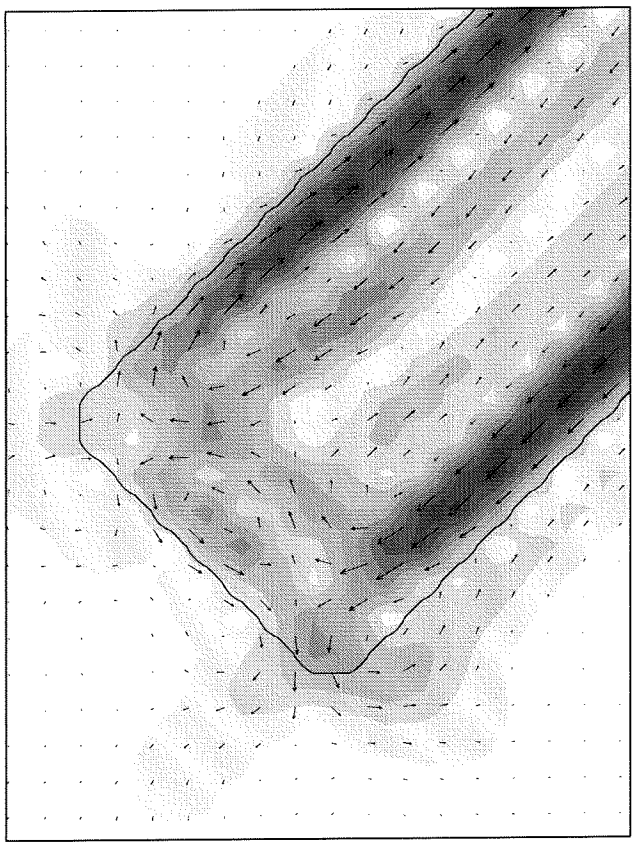

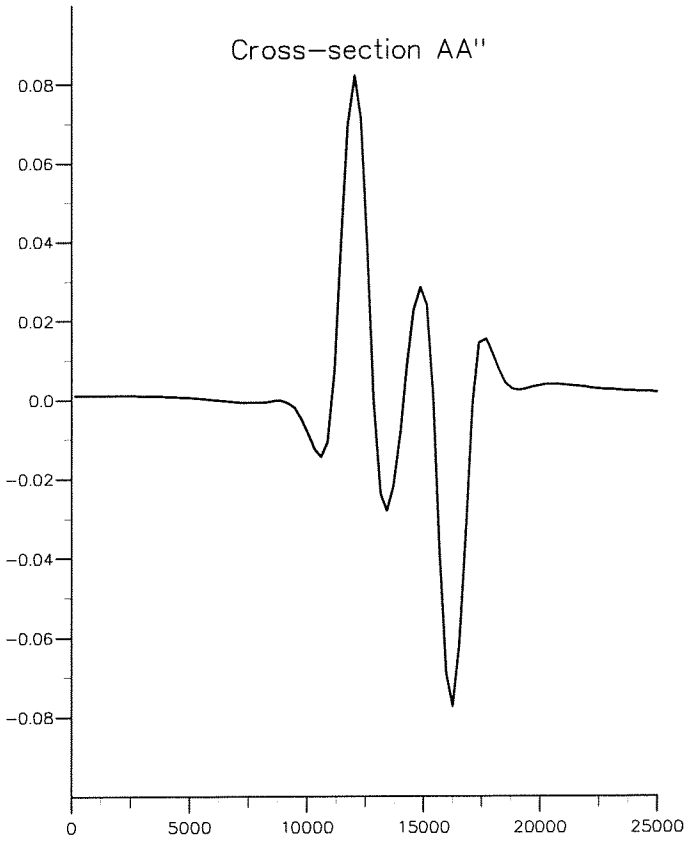

Tide–averaged current velocities [m/s]

Tide–averaged current pattern and tide–averaged velocities in cross–section AA''

Tidal boundary conditions

WL | DELFT HYDRAULICS

z2615

Figure 7.3

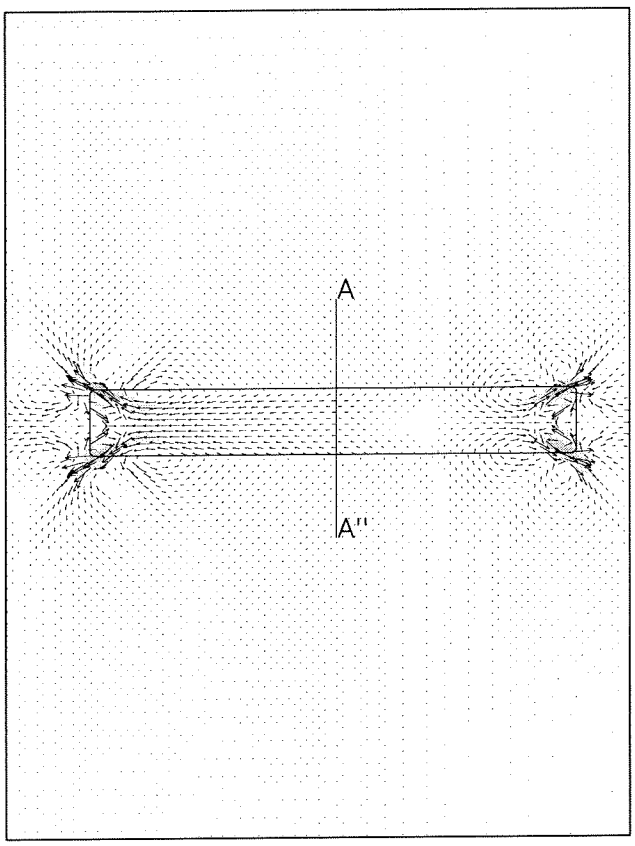

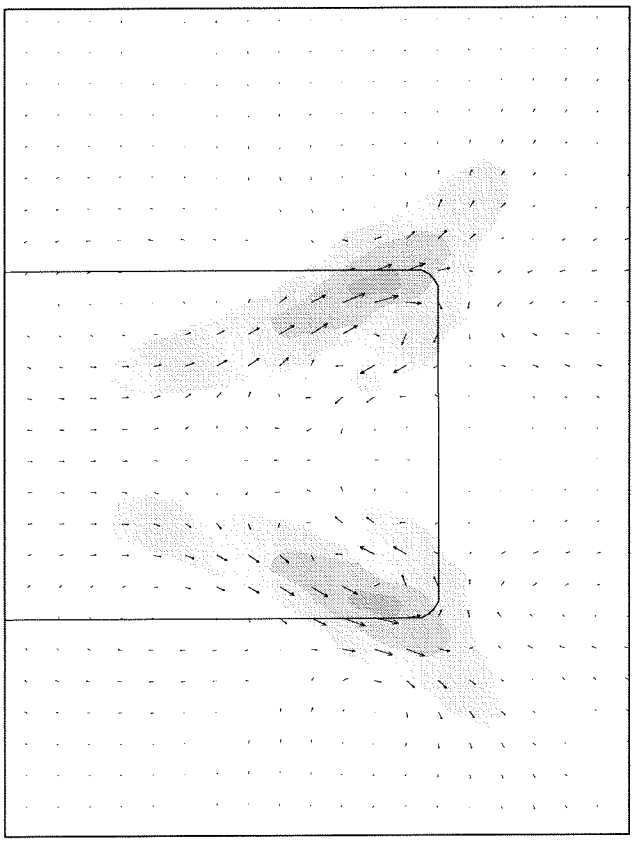

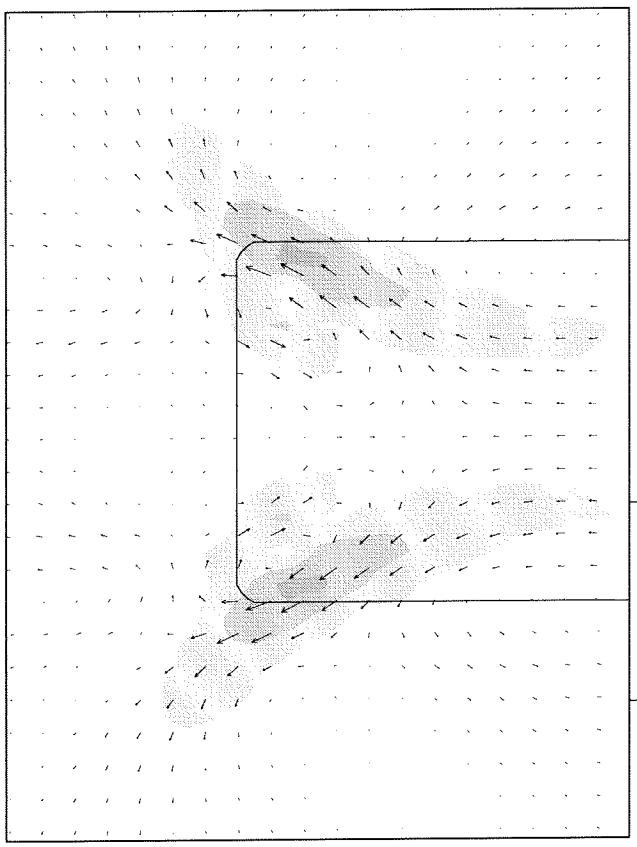

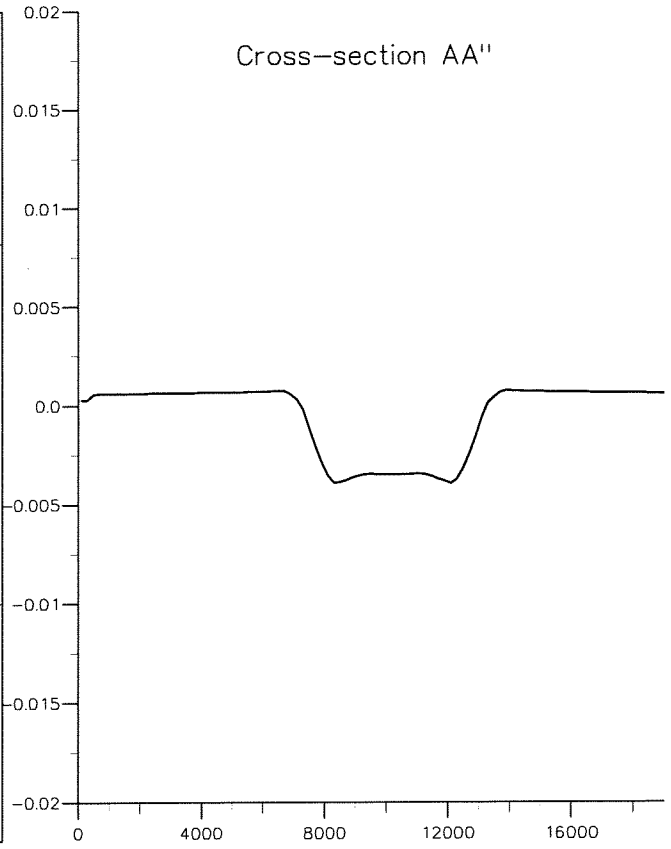

Tide–averaged current velocities

Tide–averaged current pattern and tide–averaged velocities in cross–section AA''

Tidal boundary conditions

WL | DELFT HYDRAULICS

z2615

Figure 7.4

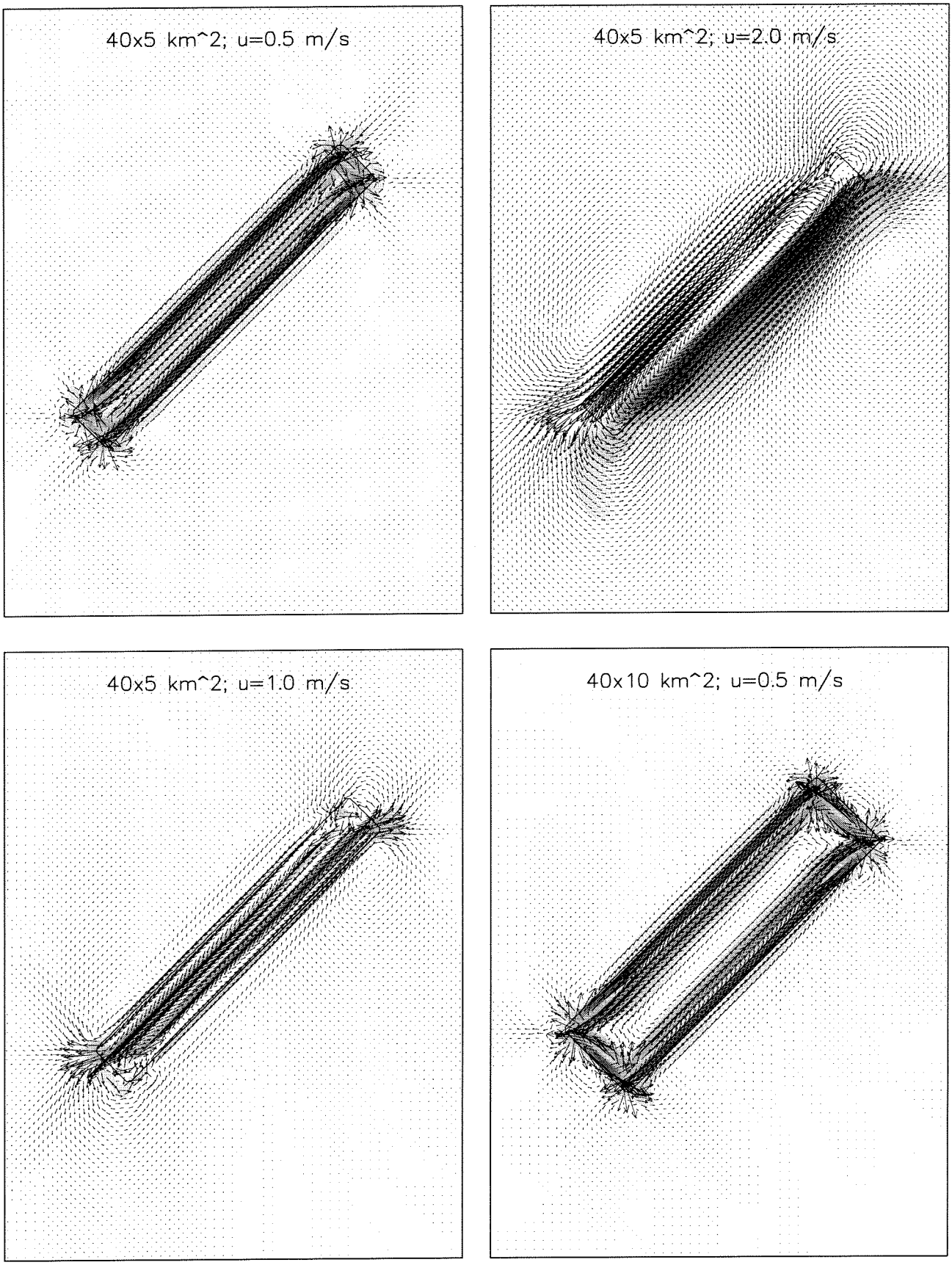

Tide-averaged current velocities [m/s]

Influence of the tidal amplitude and the width on the tide-averaged current pattern

Tidal boundary conditions

WL | DELFT HYDRAULICS

z2615

Figure 7.5

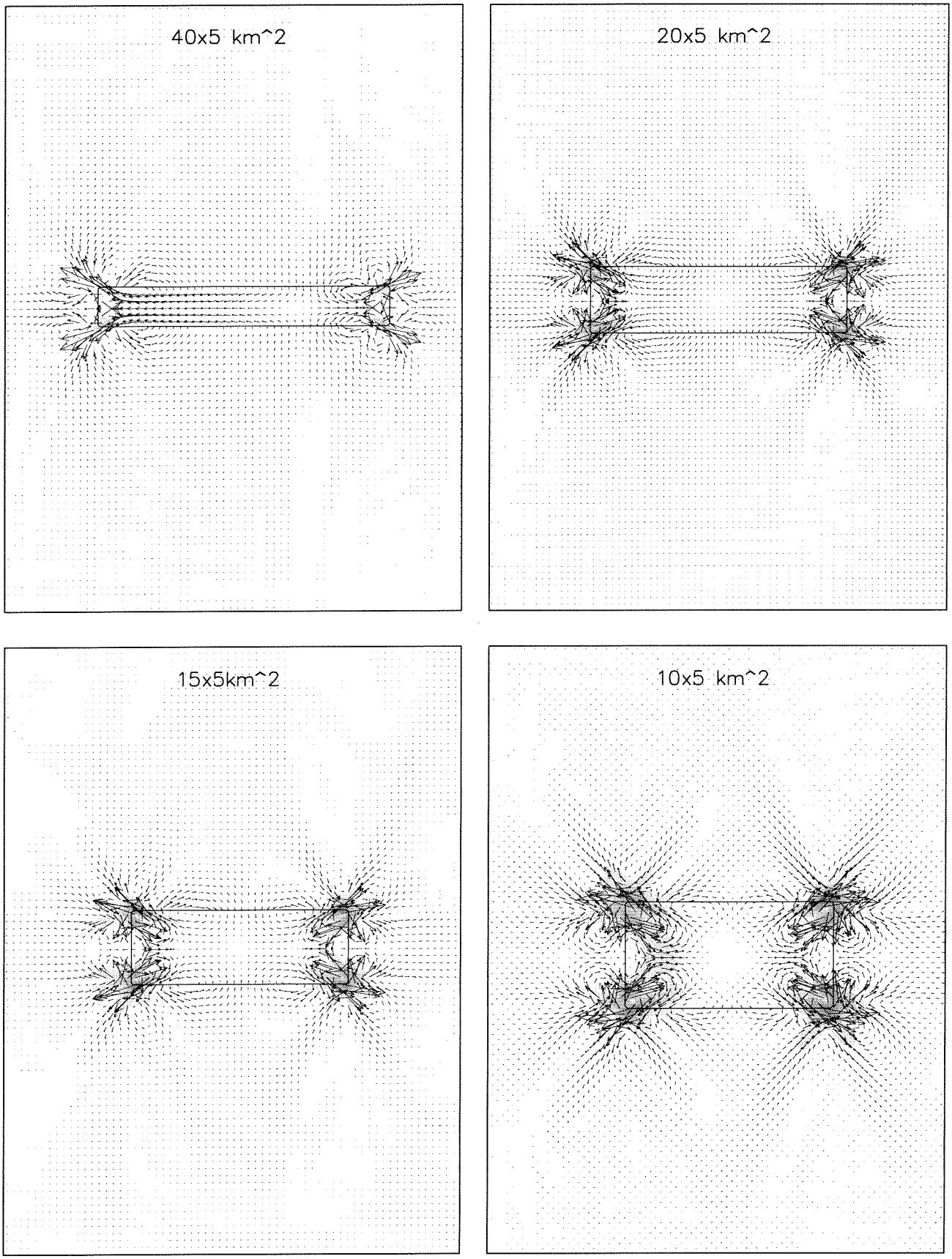

Tide-averaged current velocities [m/s]

Influence of the length on the tide-averaged current pattern

Tidal boundary conditions

WL | DELFT HYDRAULICS

z2615

Figure 7.6

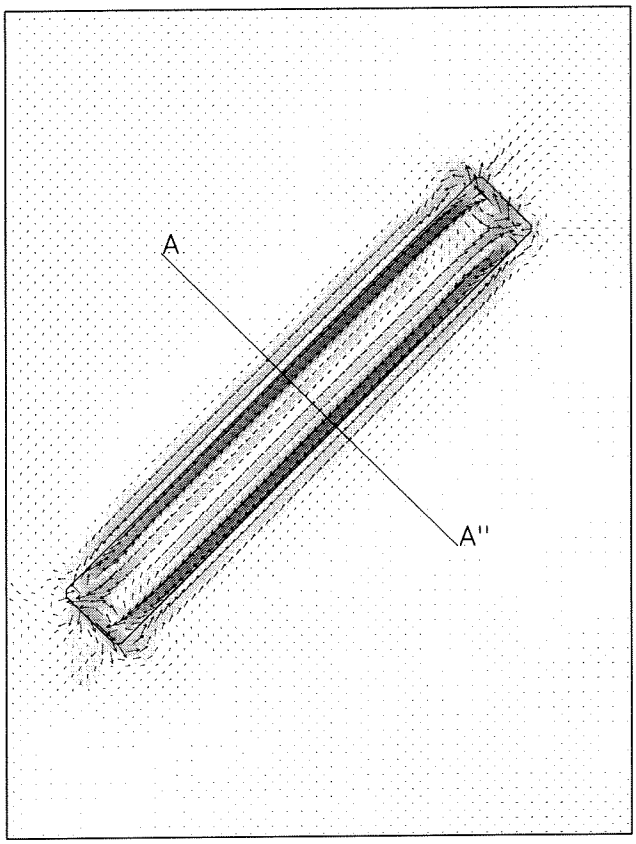

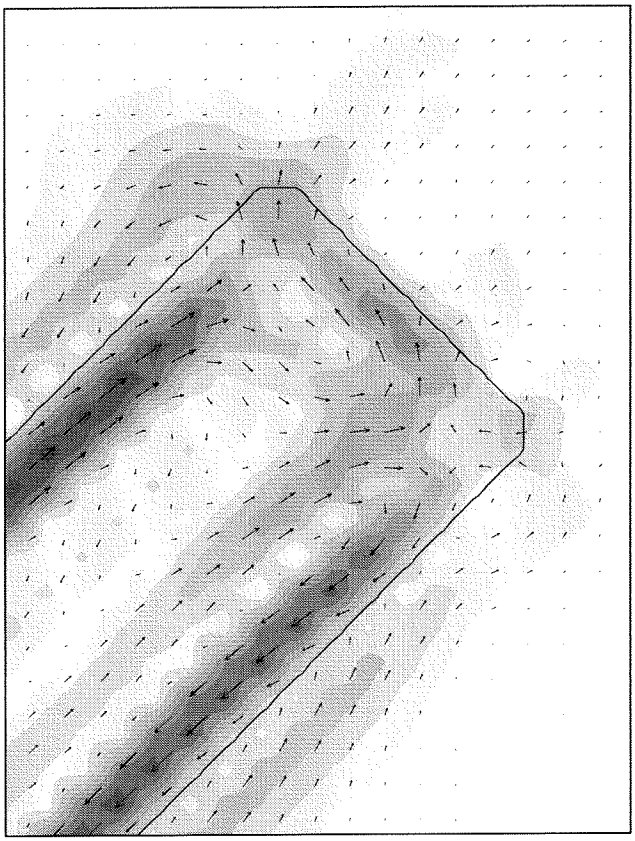

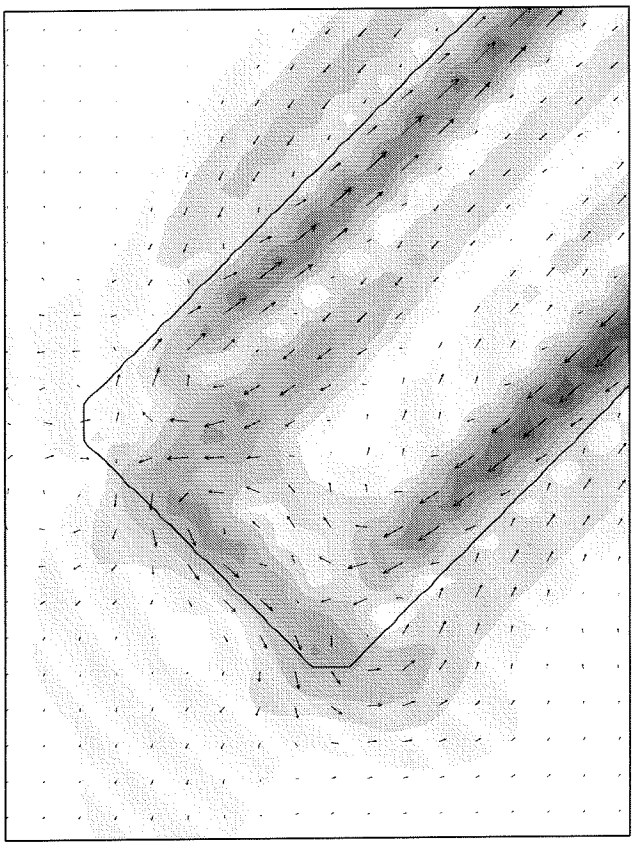

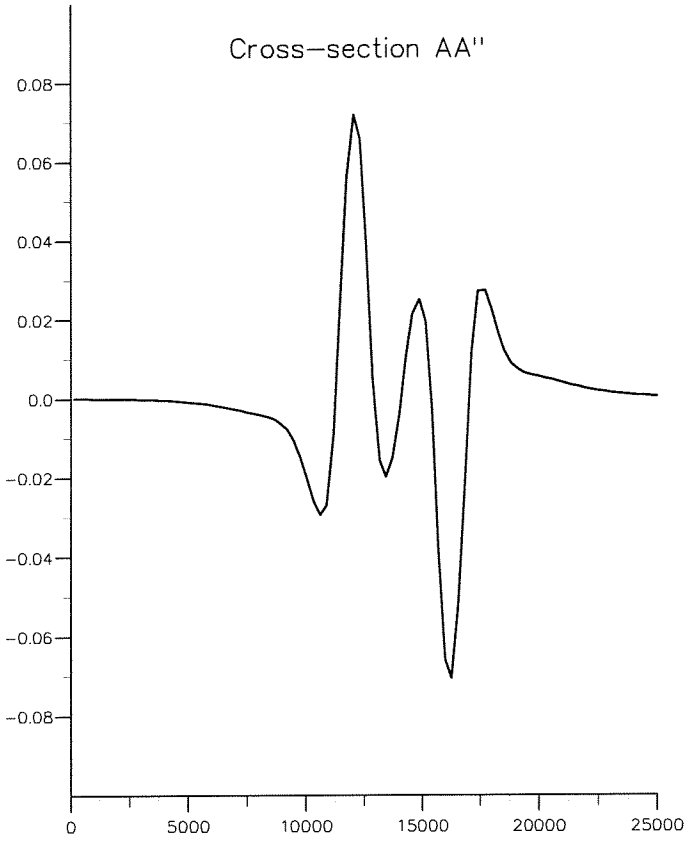

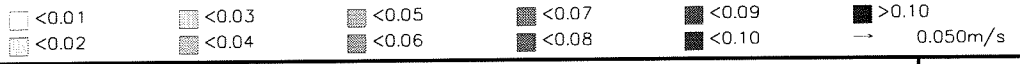

Tide–averaged current velocities [m/s]

Tide–averaged current pattern and tide–averaged velocities in cross–section AA''

Tidal boundary conditions including Coriolis

WL | DELFT HYDRAULICS

z2615

Figure 7.7

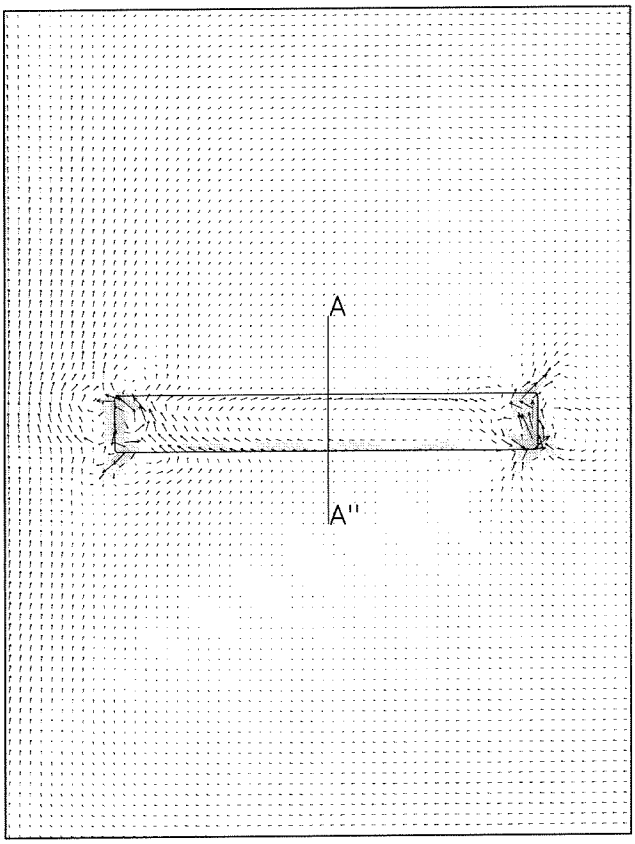

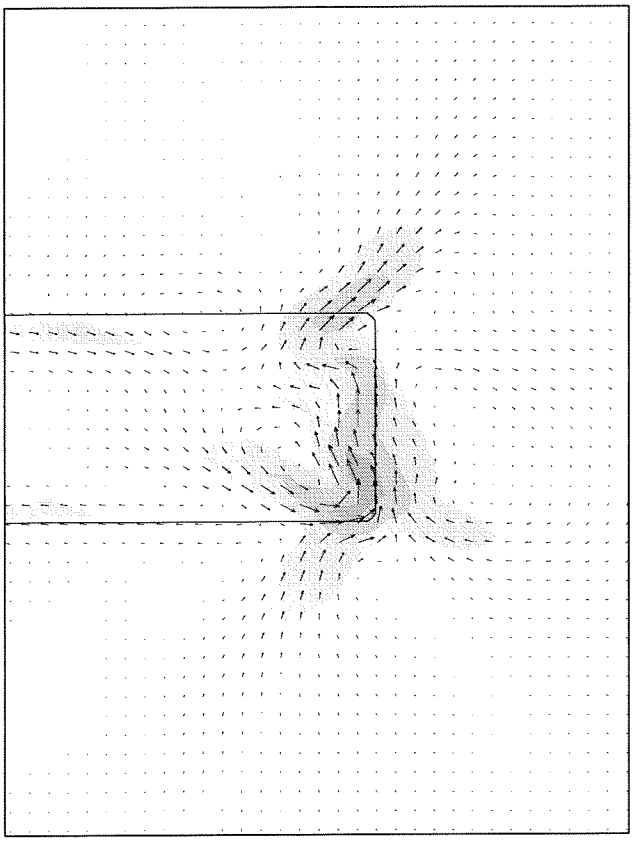

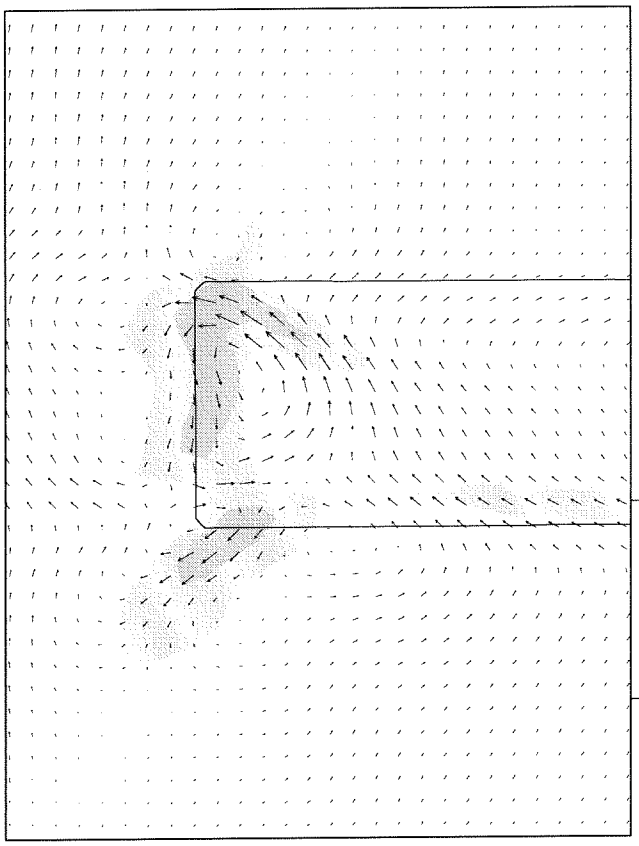

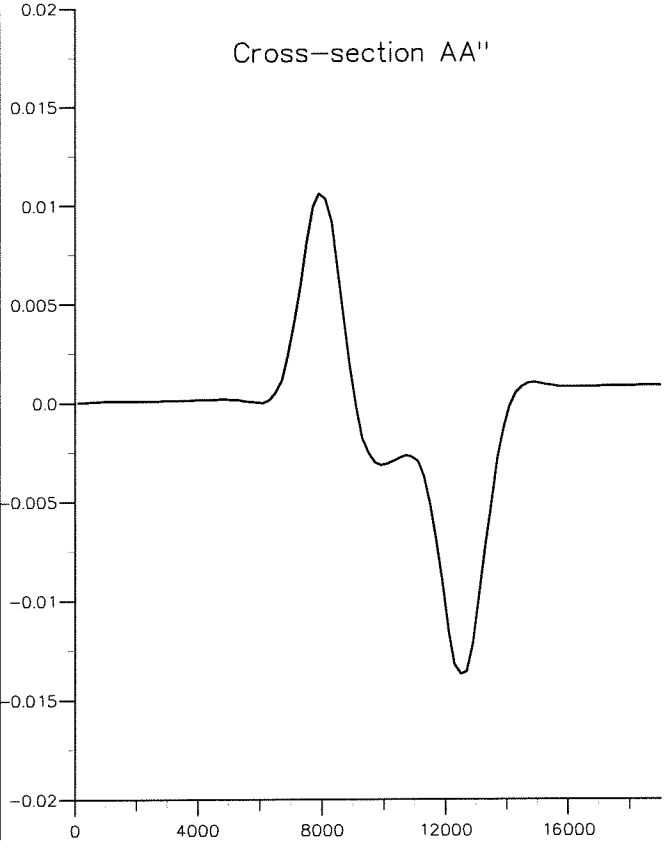

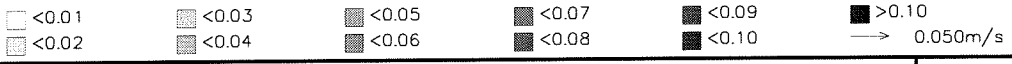

Tide-averaged current velocities [m/s]

Tide-averaged current pattern and tide-averaged velocities in cross-section AA''

Tidal boundary conditions including Coriolis

WL | DELFT HYDRAULICS

z2615

Figure 7.8

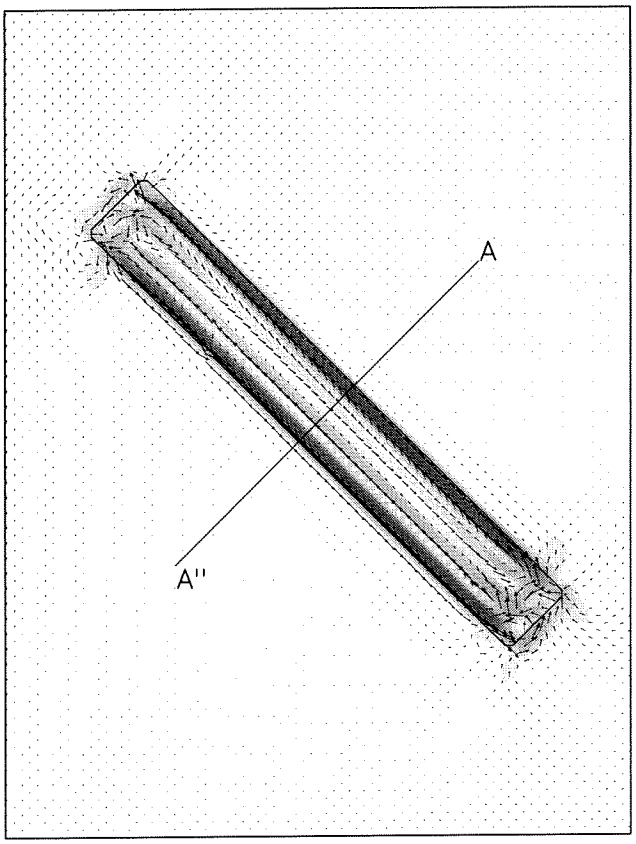

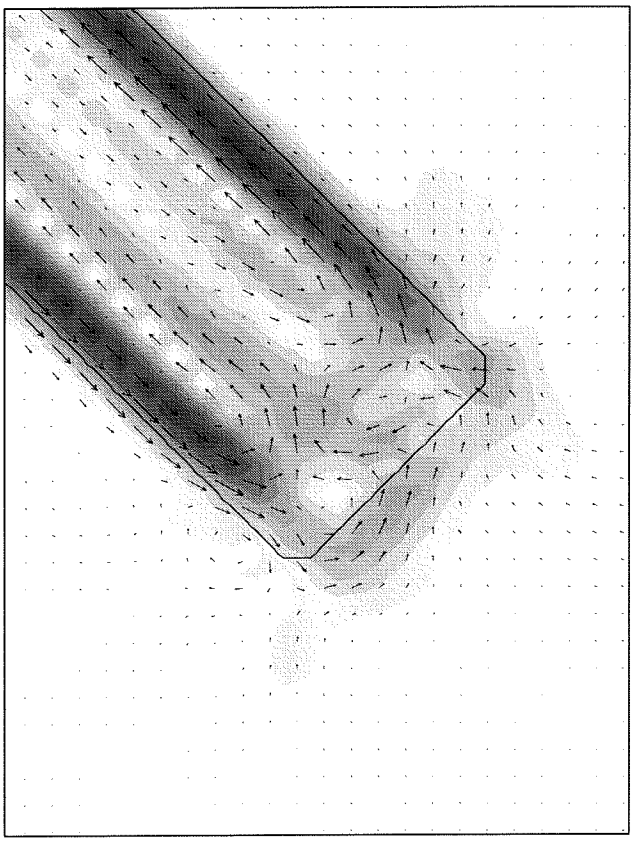

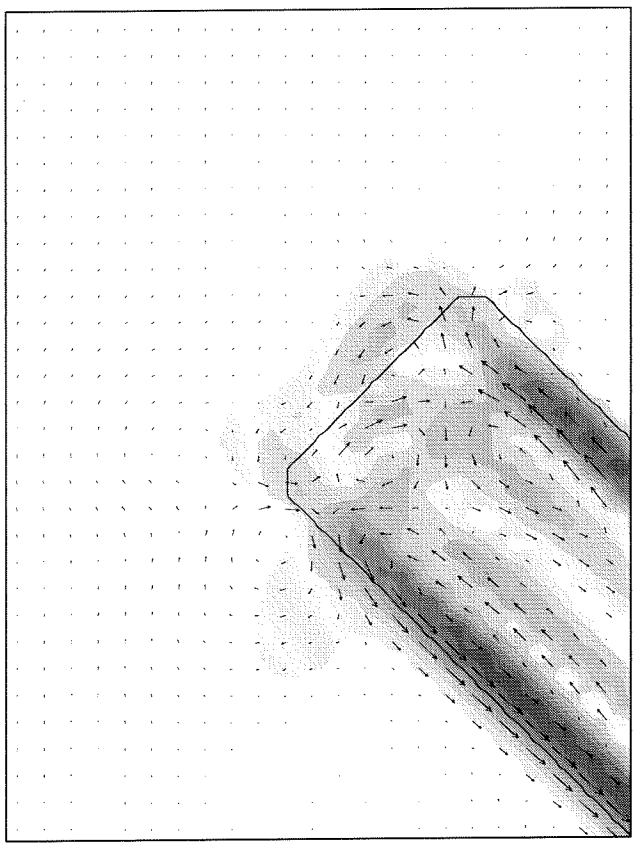

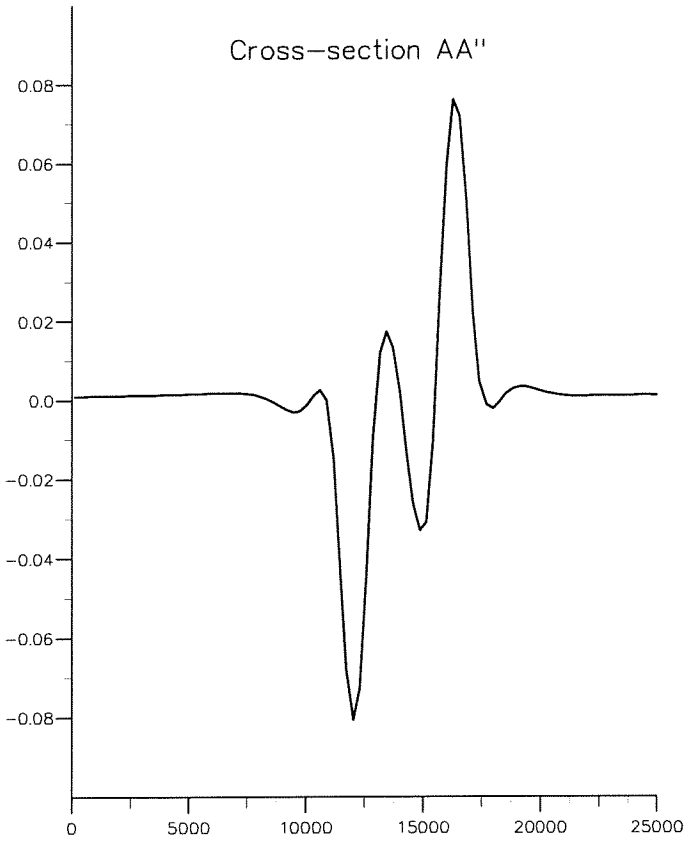

Tide–averaged current velocities [m/s]

Tide–averaged current pattern and tide–averaged velocities in cross–section AA''

Tidal boundary conditions including Coriolis

WL | DELFT HYDRAULICS

z2615

Figure 7.9

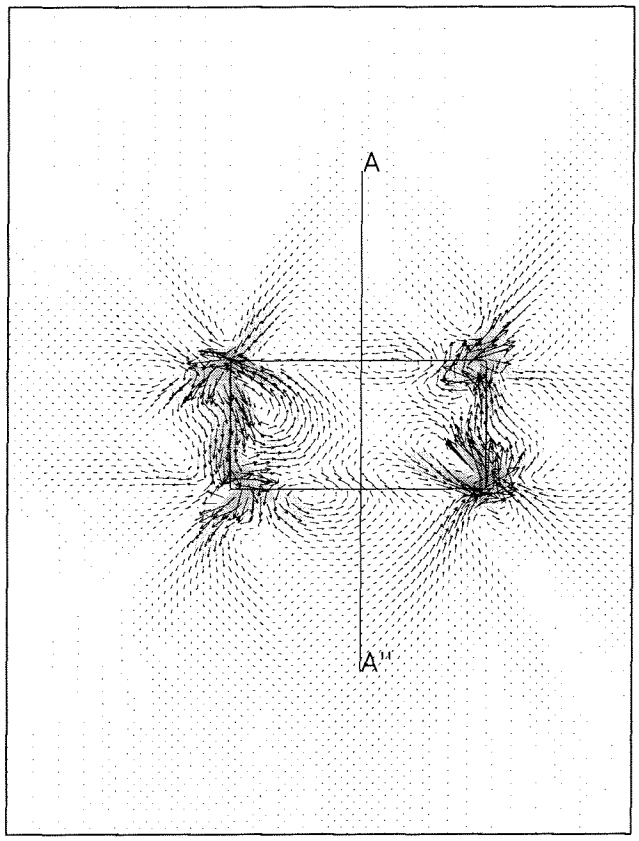

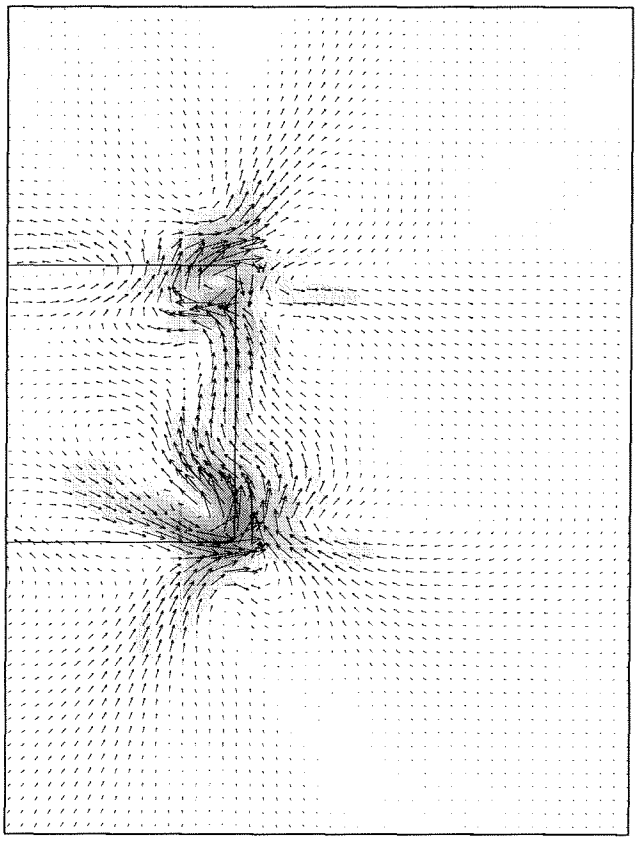

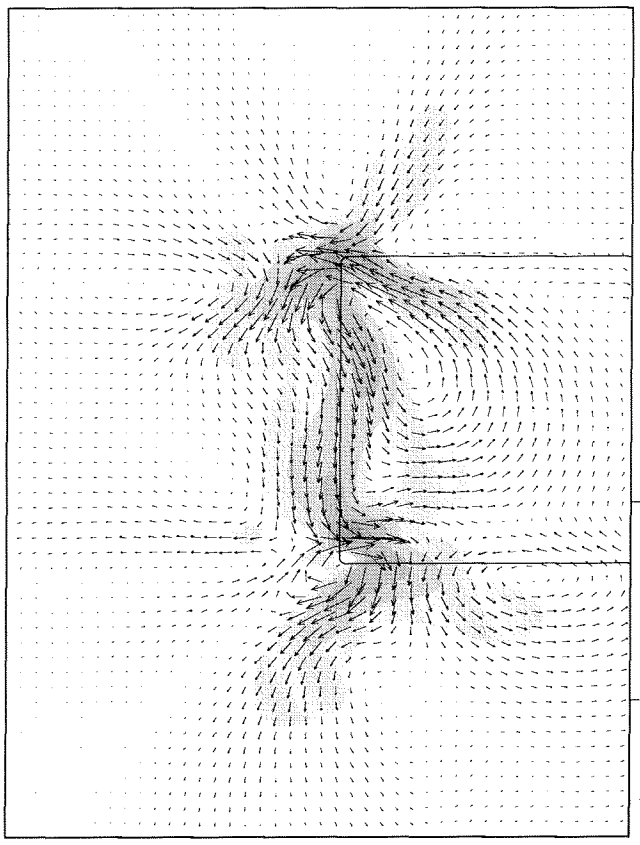

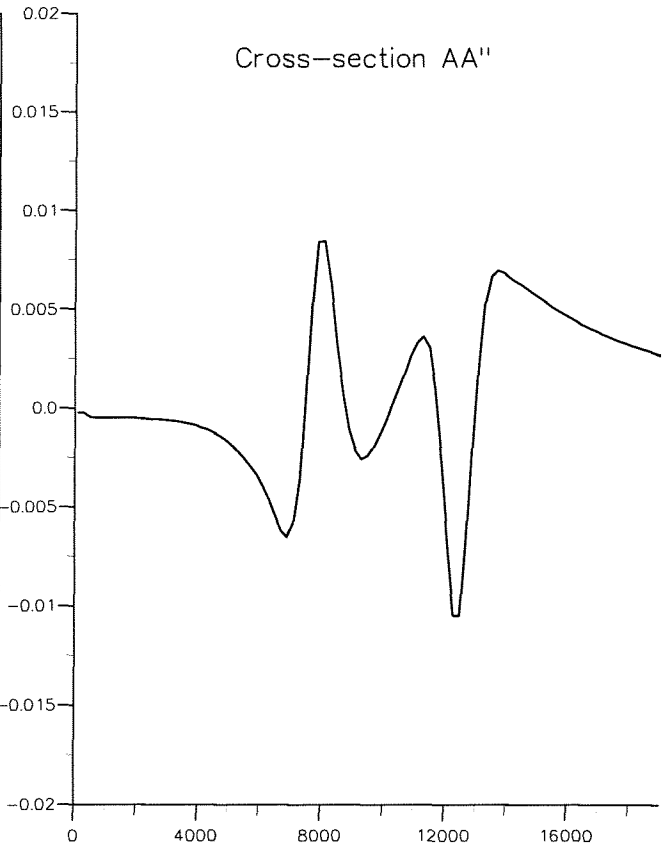

Tide–averaged current velocities [m/s]

Tide–averaged current pattern and tide–averaged velocities in cross–section AA''

Tidal boundary conditions including Coriolis

WL | DELFT HYDRAULICS

z2615

Figure 7.10

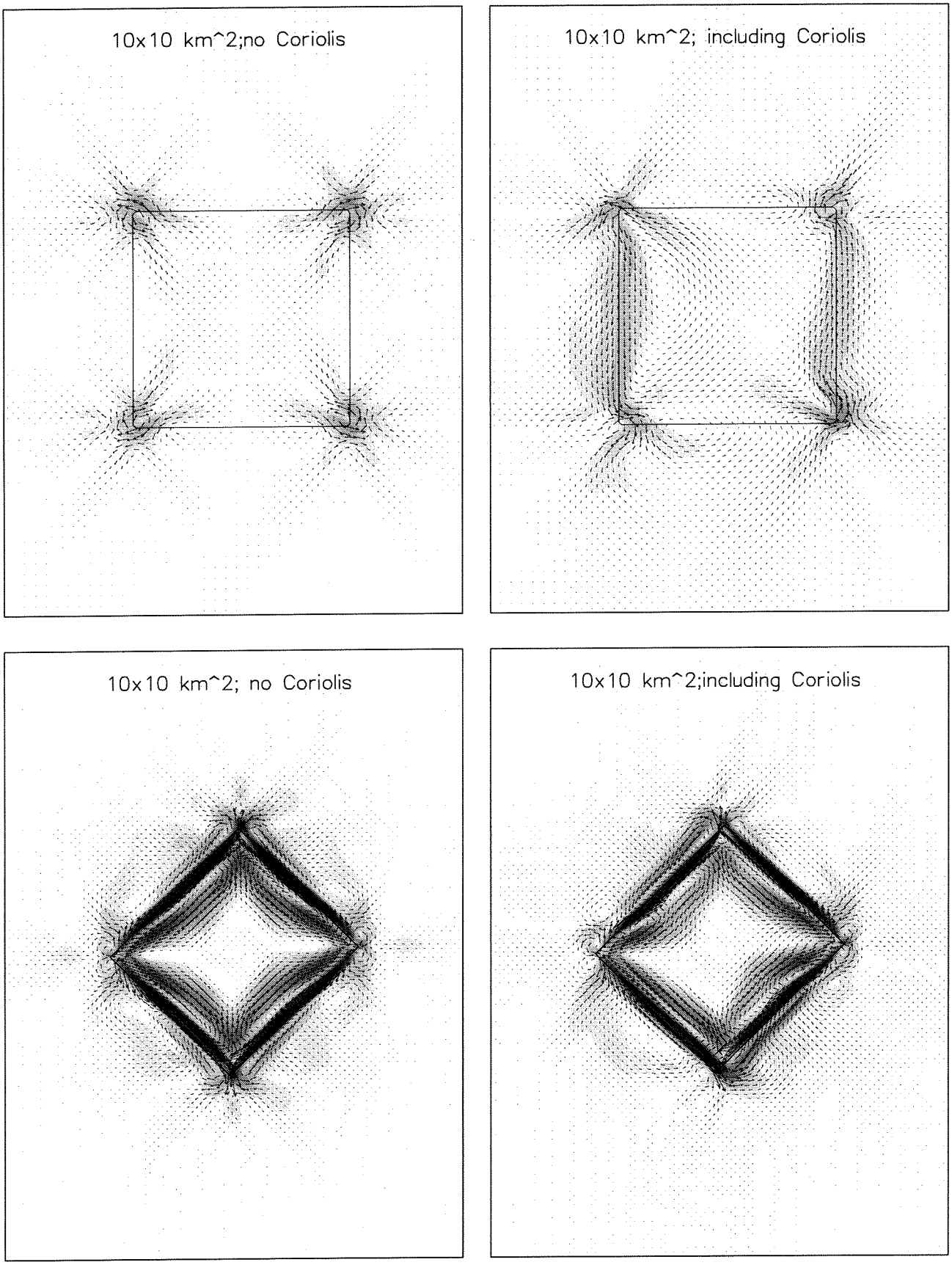

Tide-averaged current velocities [m/s]

Tide-averaged current pattern

Tidal boundary conditions with and without Coriolis

WL | DELFT HYDRAULICS

z2615

Figure 7.11

Figuur 8.2: Influence of the transport mode, while ALFABD is 1

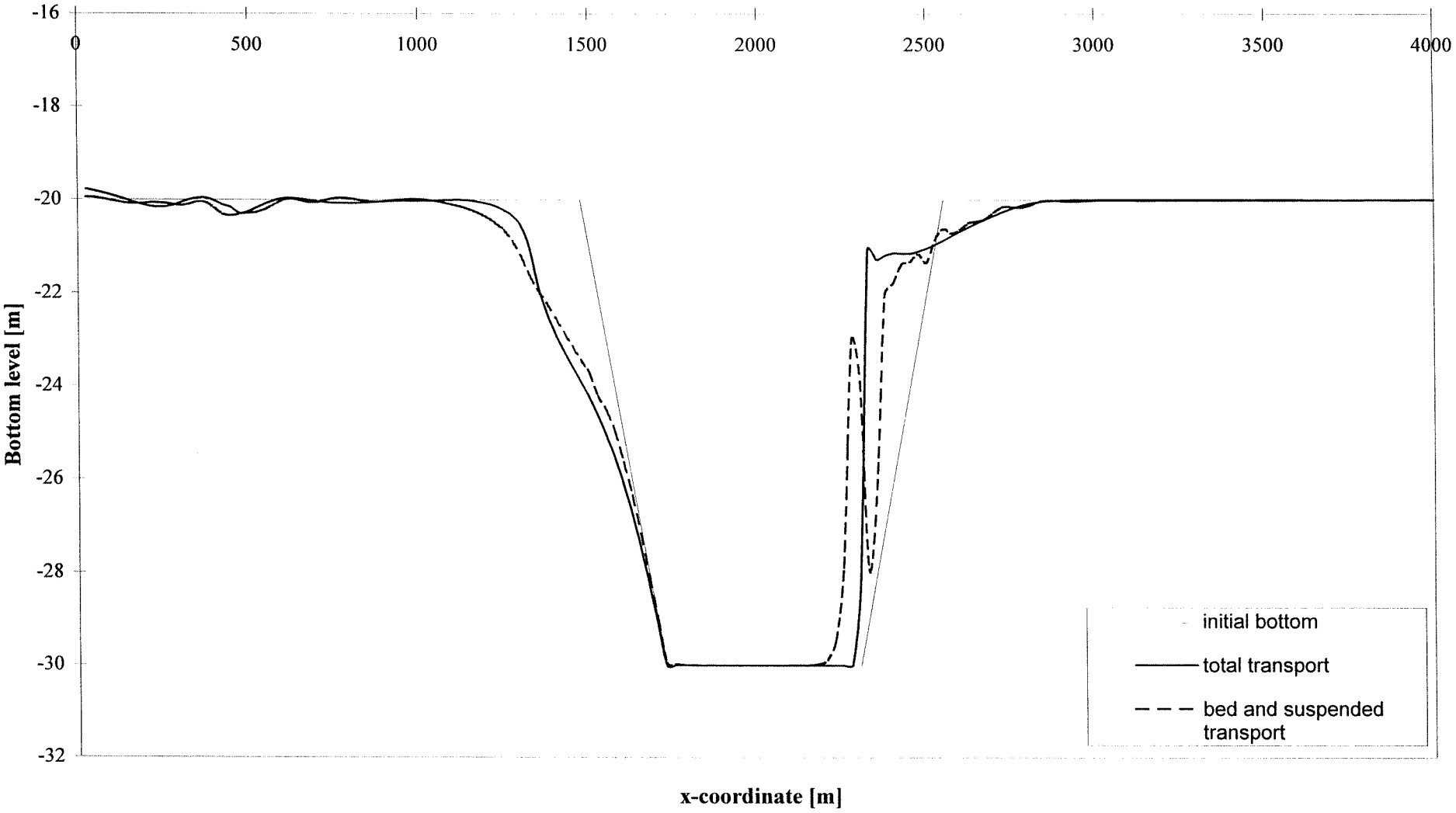

Figuur 8.3: Influence of the transport mode, while ALFABD is 5

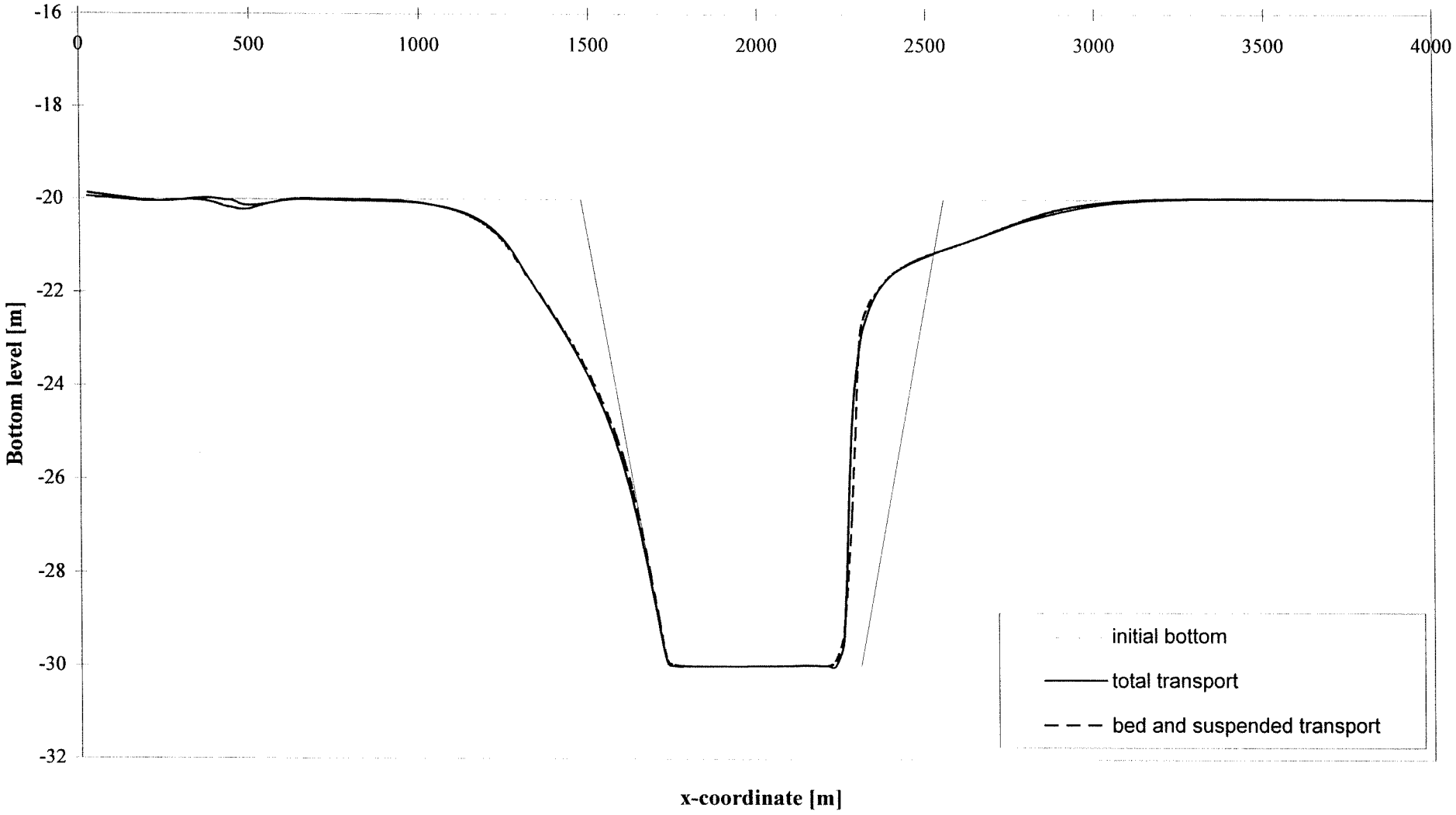

Figuur 8.4: Influence of the transport mode, while ALFABD is 10

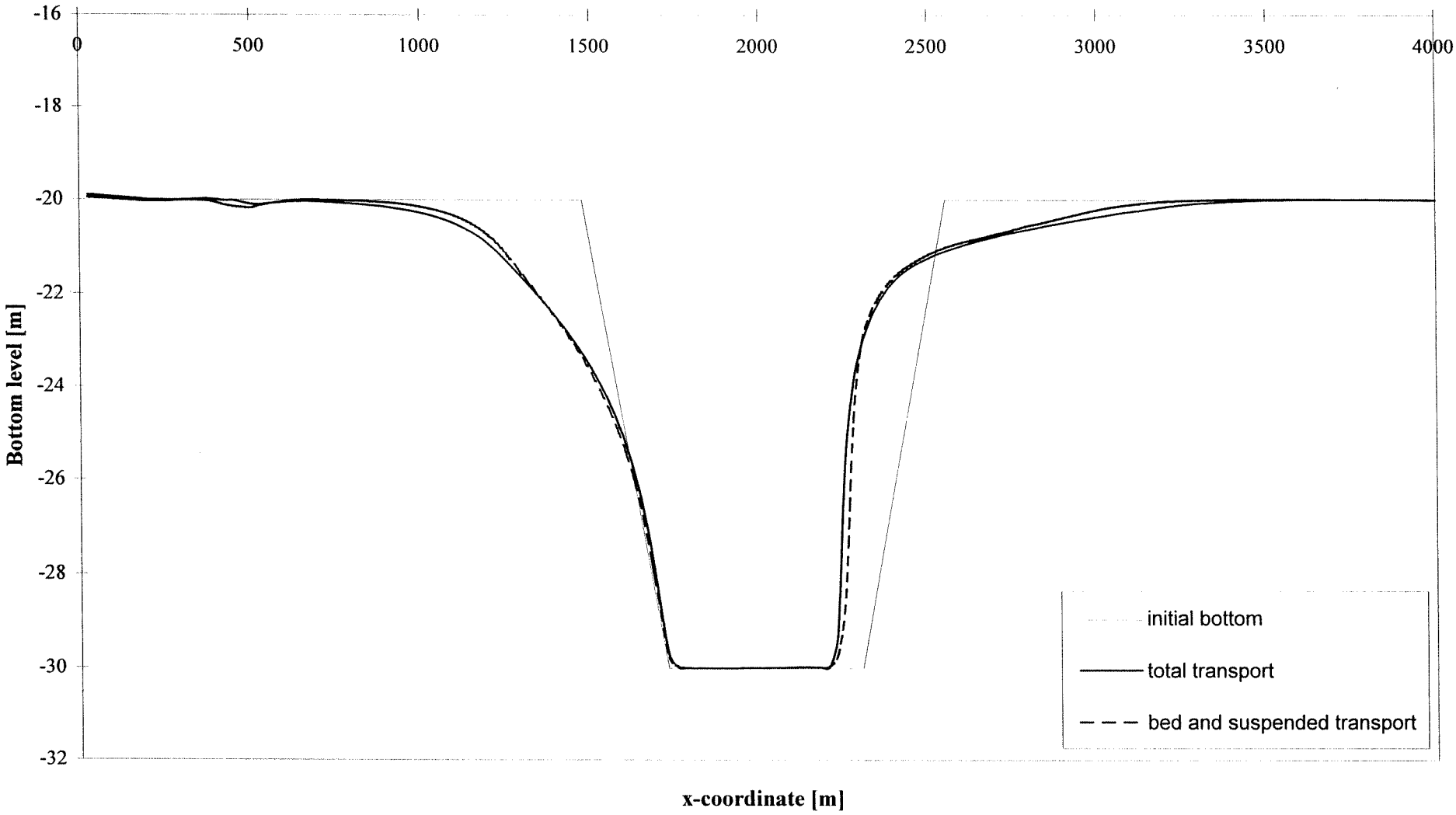

Figuur 8.5: Influence of ALFABD on the results of the total transport mode

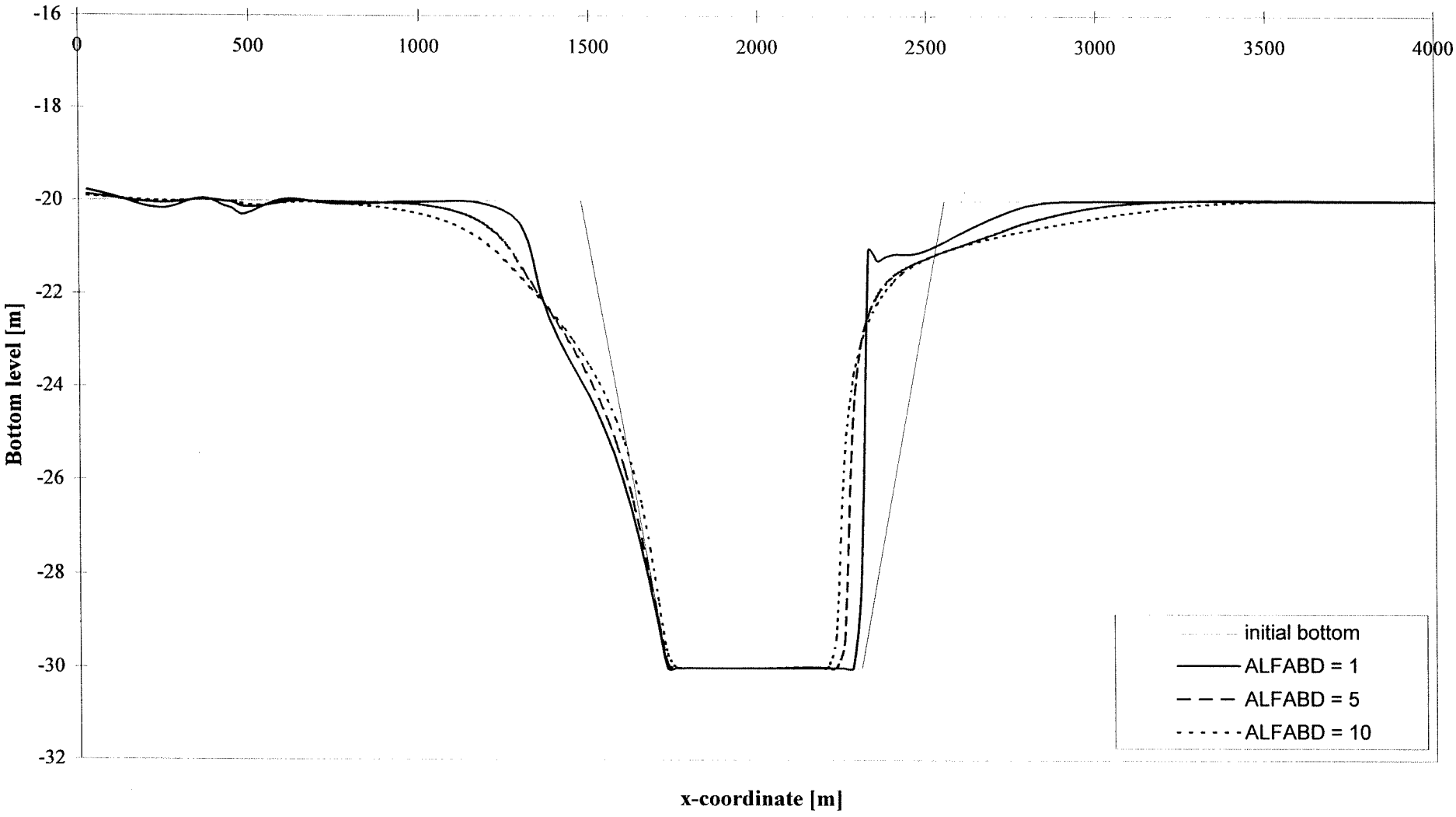

Figuur 8.6: Influence of ALFABD on the results of the bed and suspended transport mode

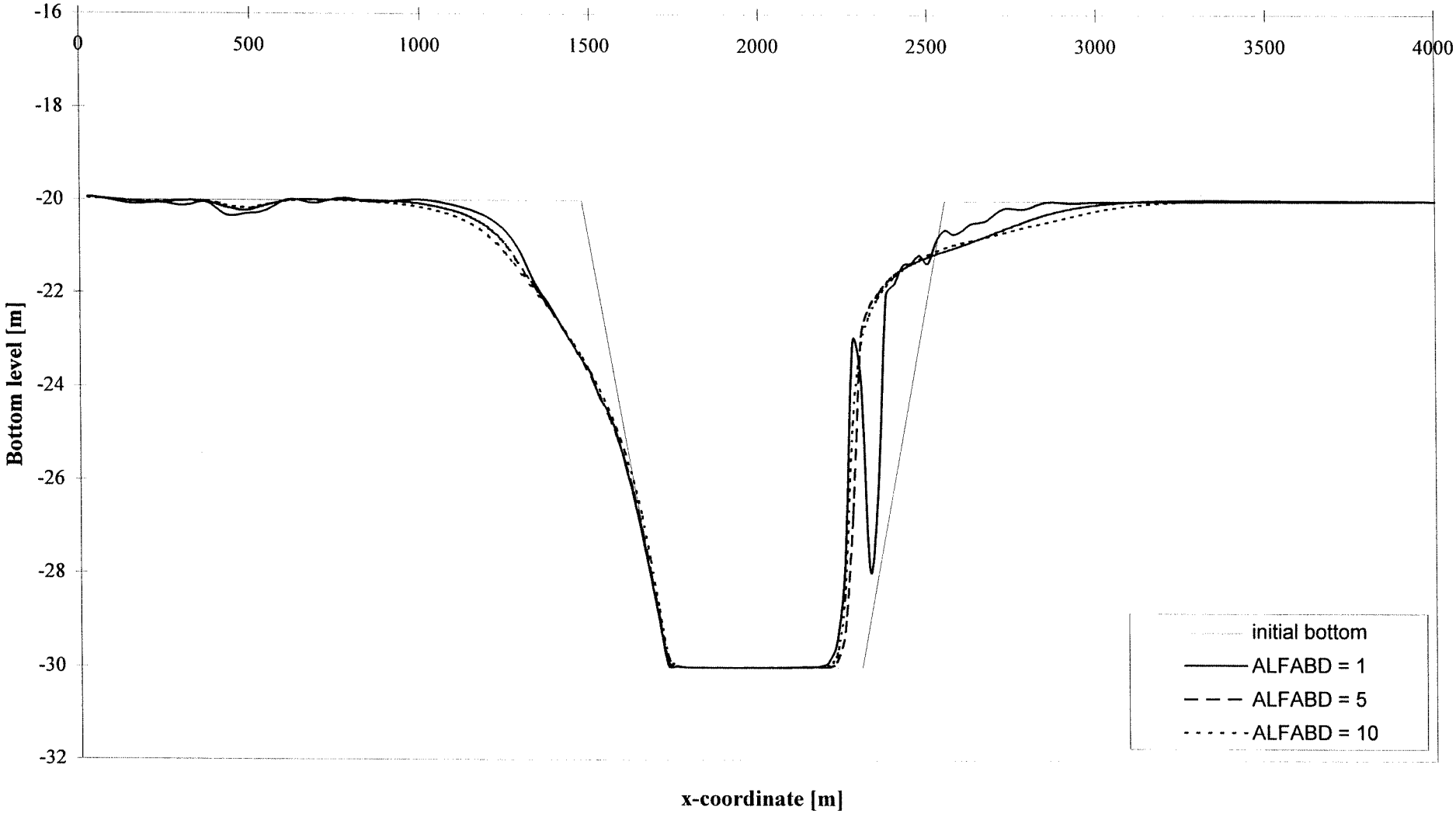

Figuur 8.7: Influence of ALFABD on a 10x10 km ^ 2 sandpit with total transport

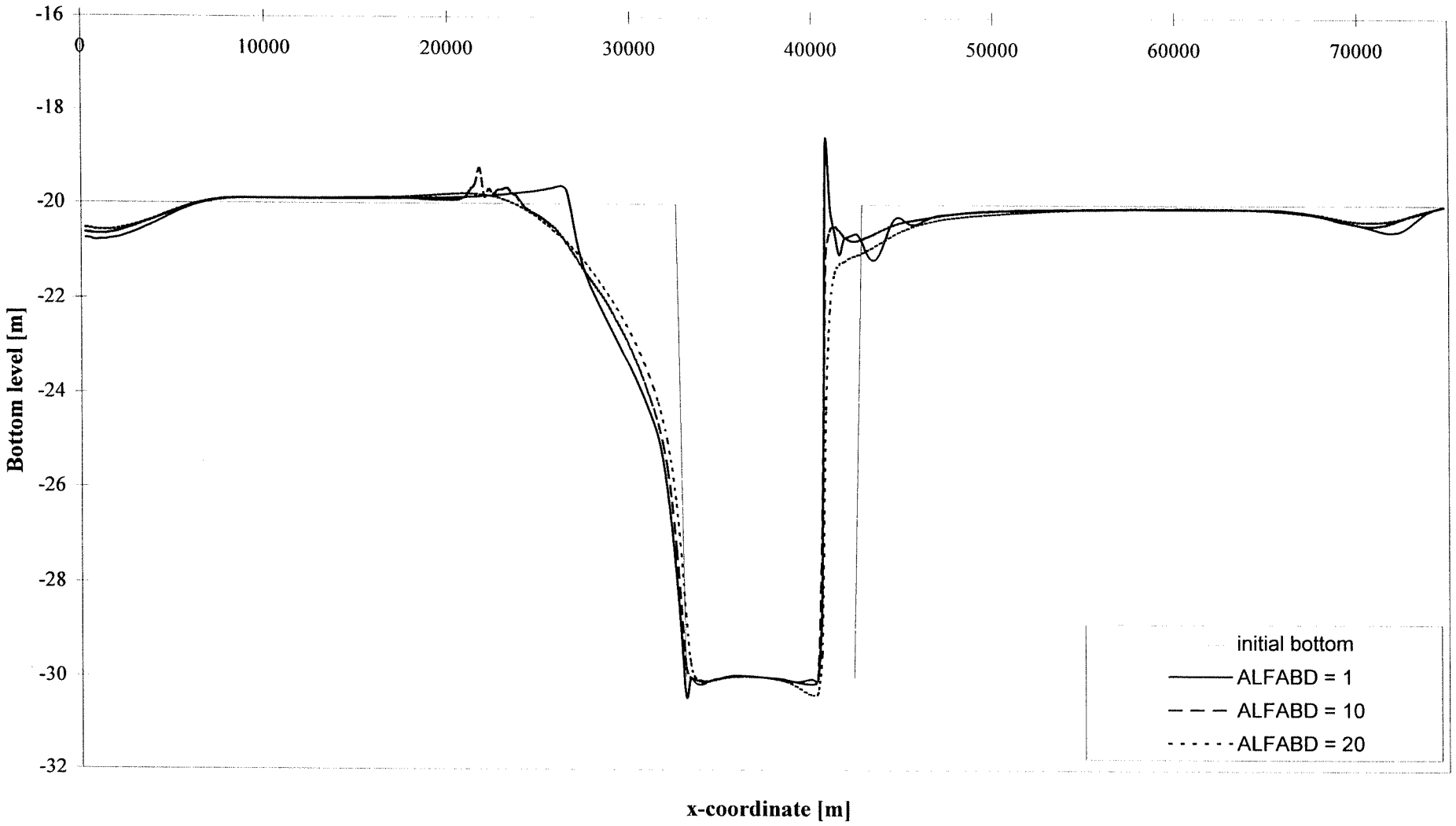

Figuur 8.8: Influence of the grid cell size on the morphological results

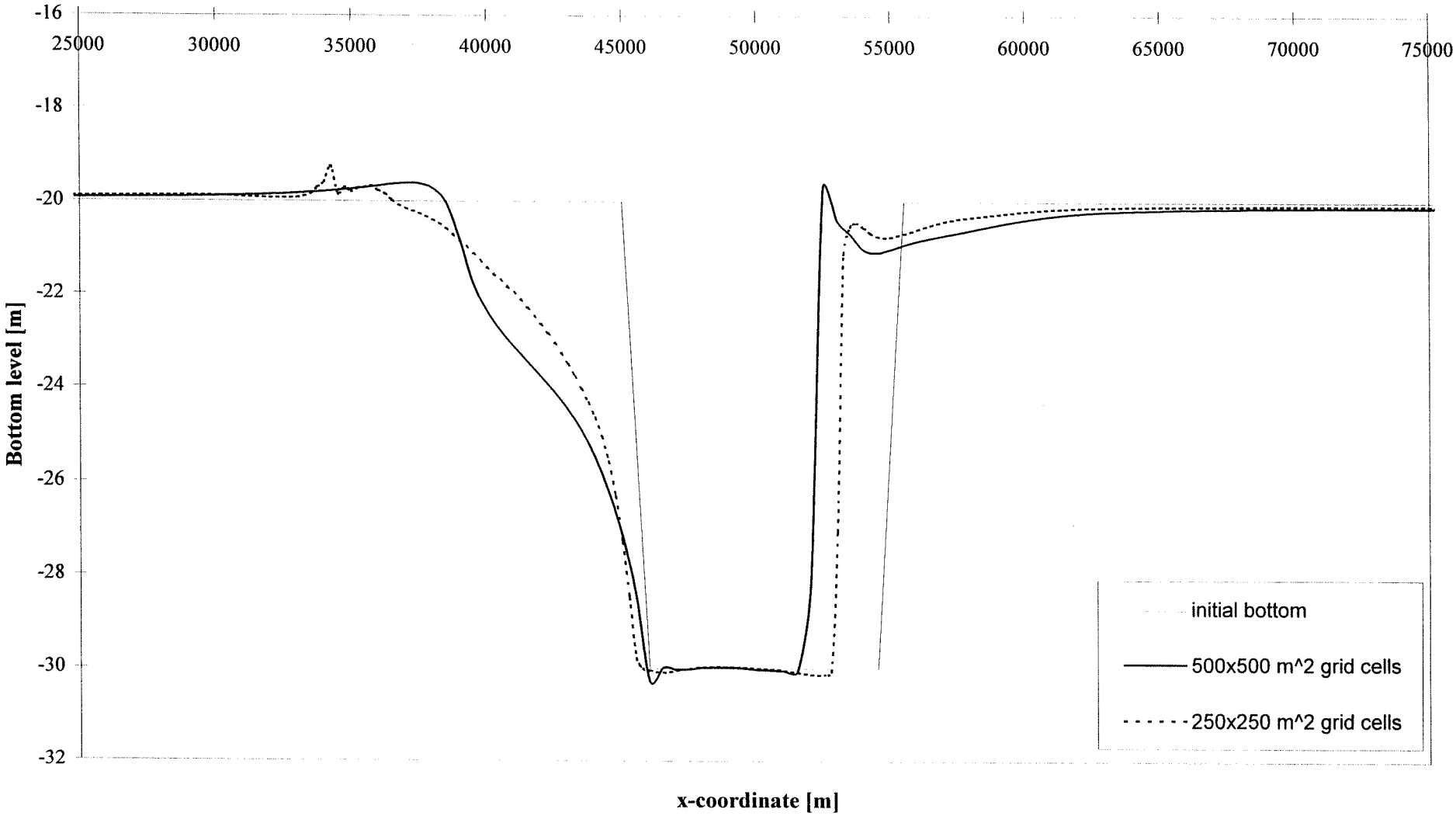

Figuur 8.9: Influence of the slope of the sandpit on the morphological results

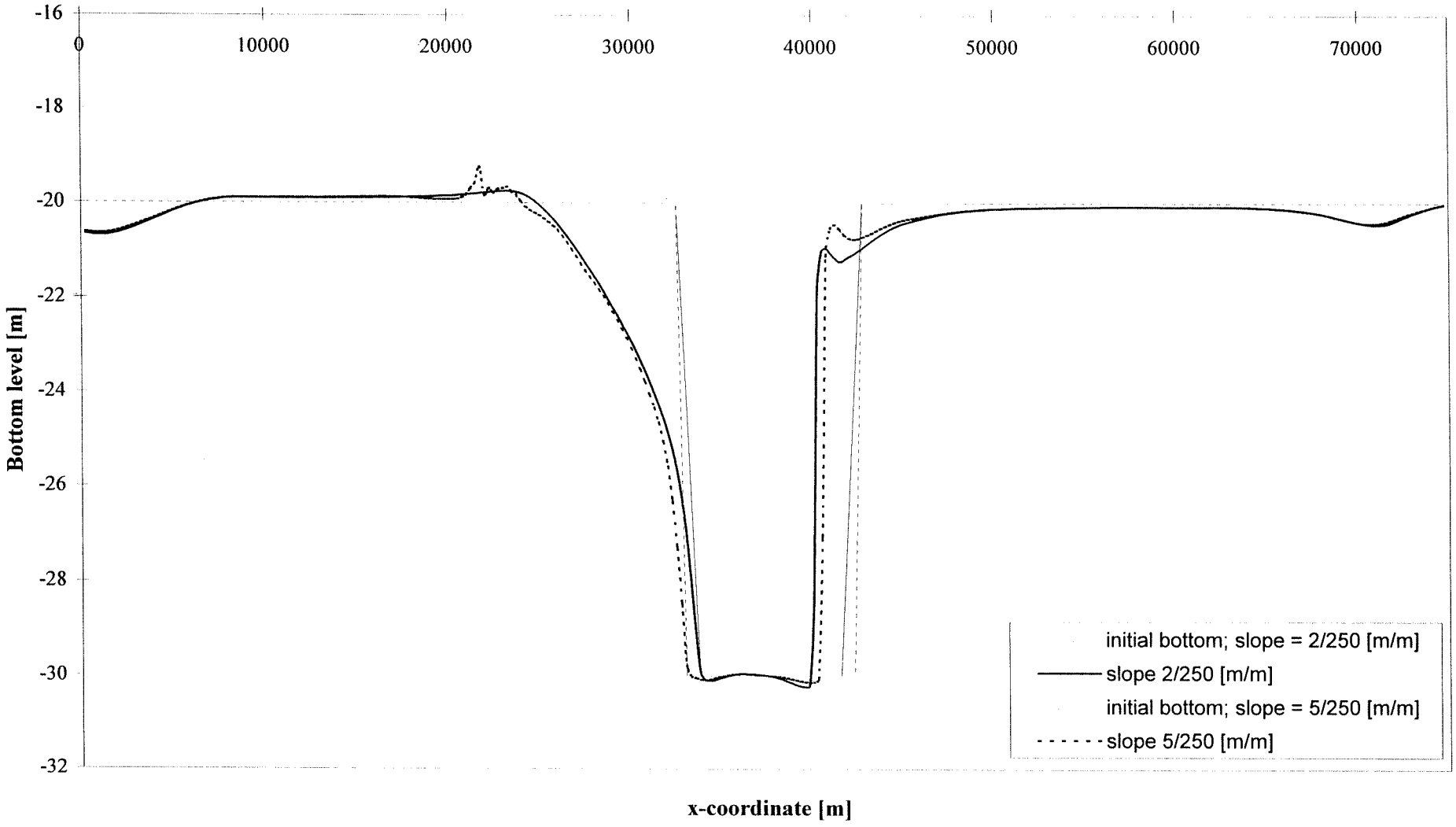

Figuur 8.10: Influence of the number of bottom computations per flow computation

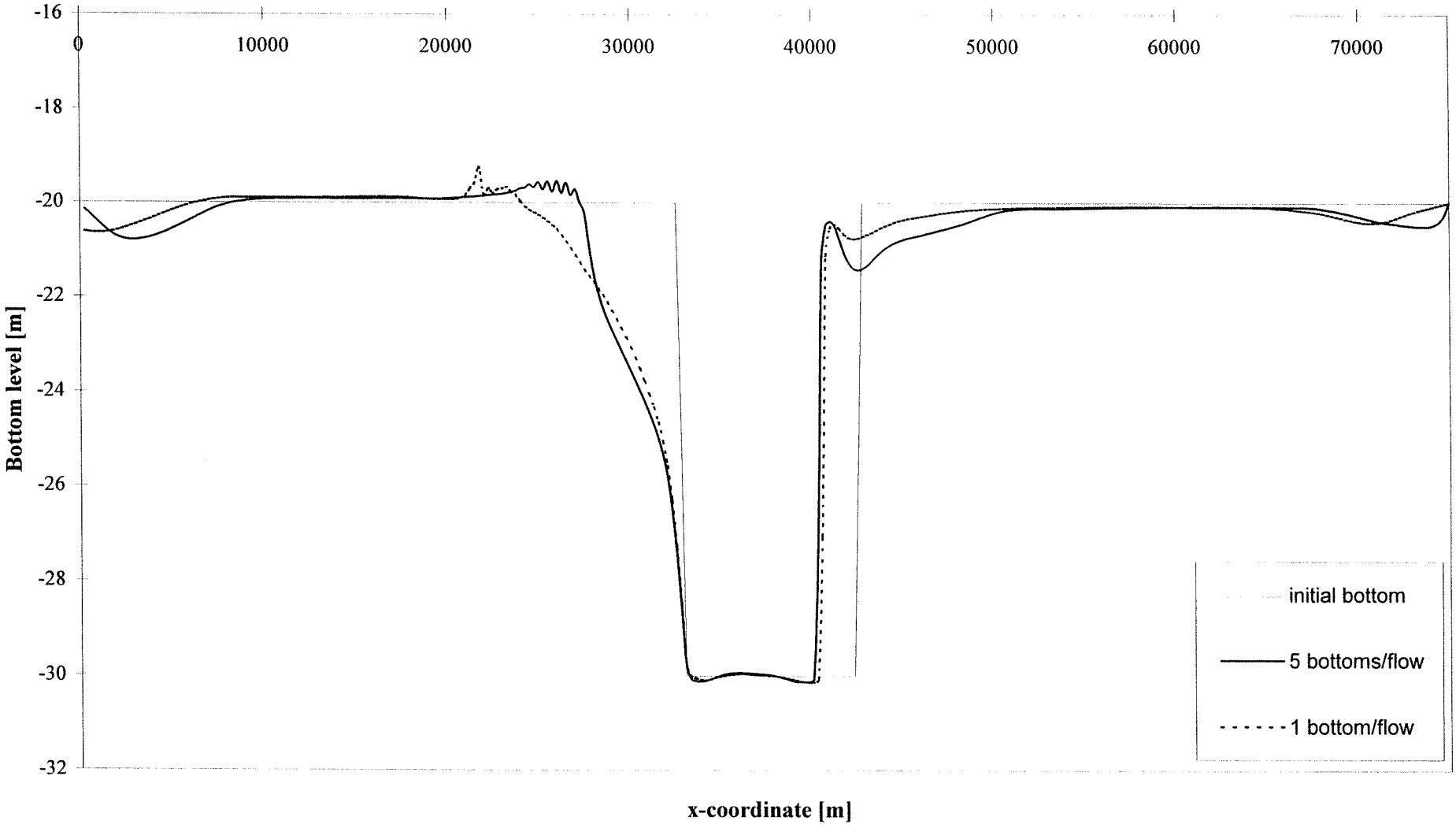

Figure 8.11: Data points for tide analysis

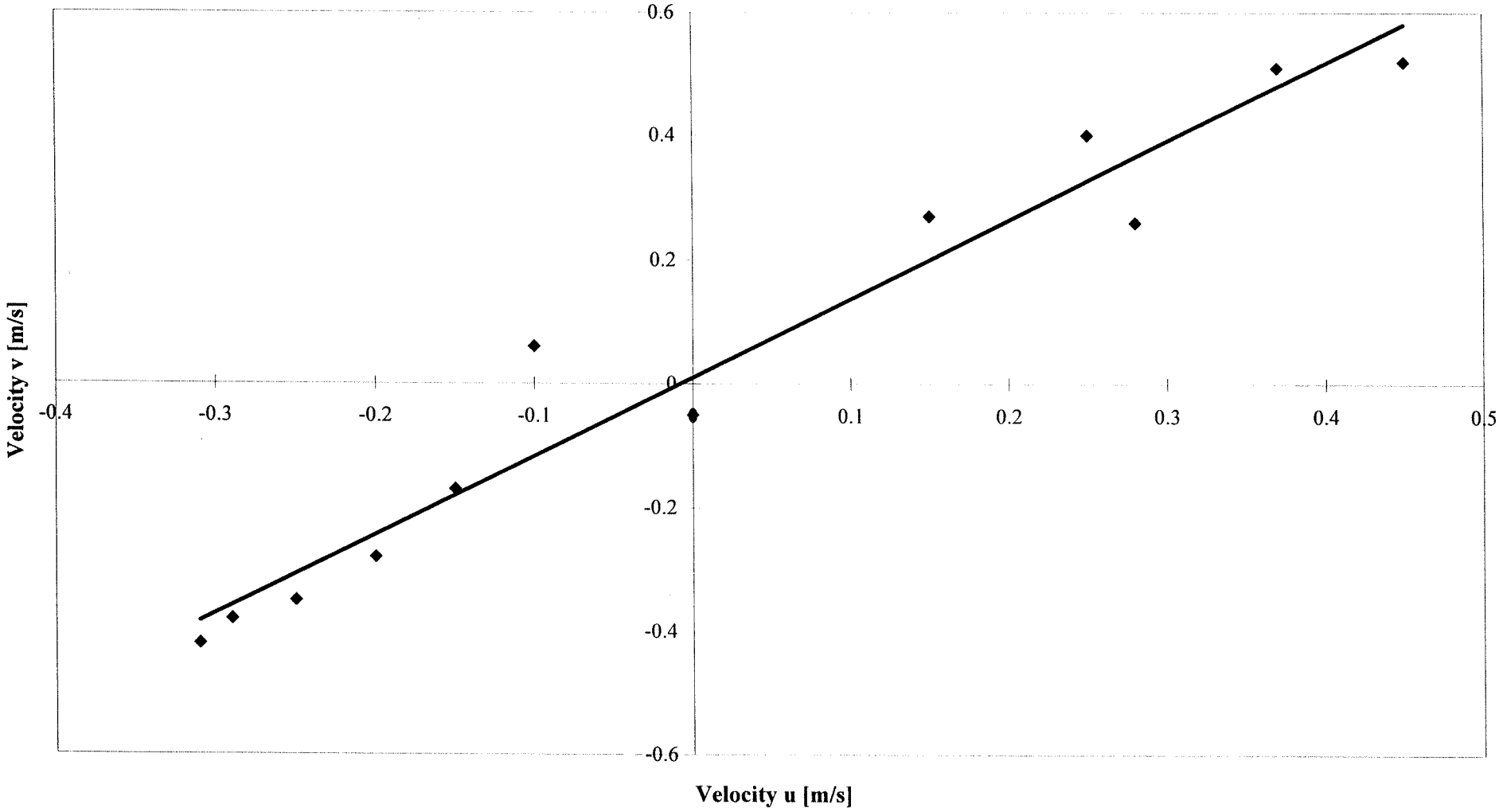

Figure 8.12: Results of the tide analysis

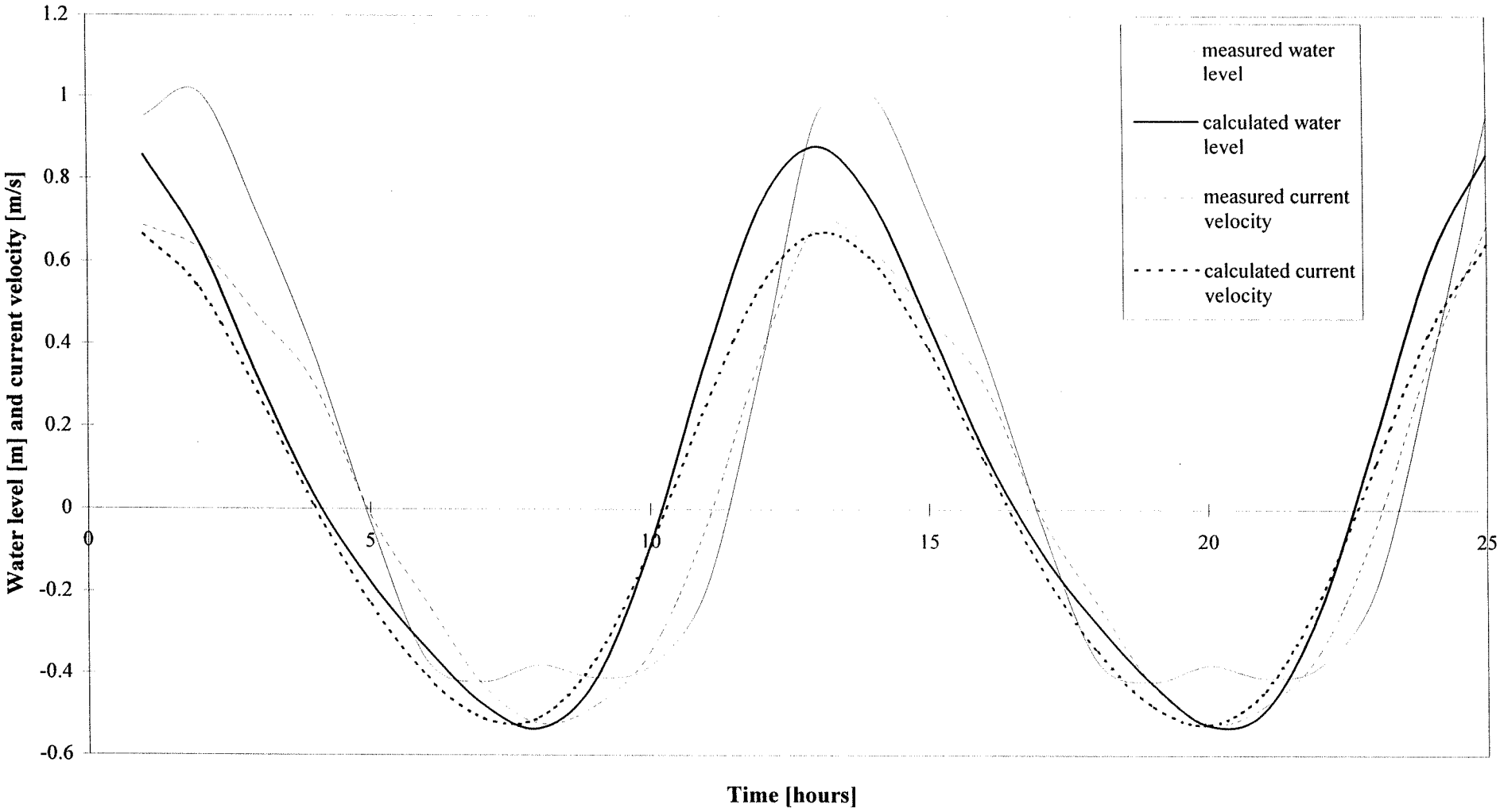

Figuur 8.13: SUTRENCH and Delft3D results of a reference trench

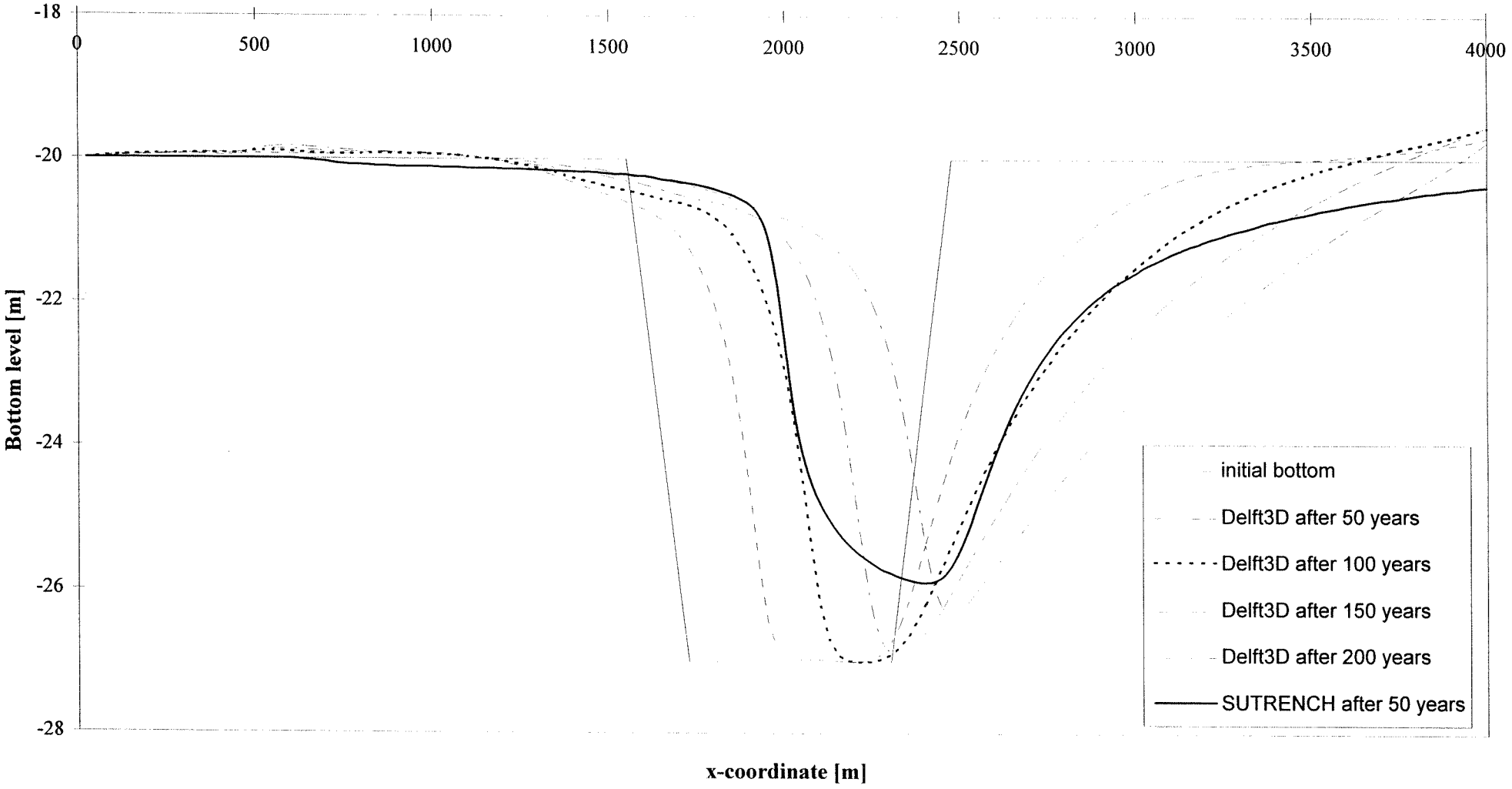

Figuur 8.14: SUTRENCH results of Walstra (1998)

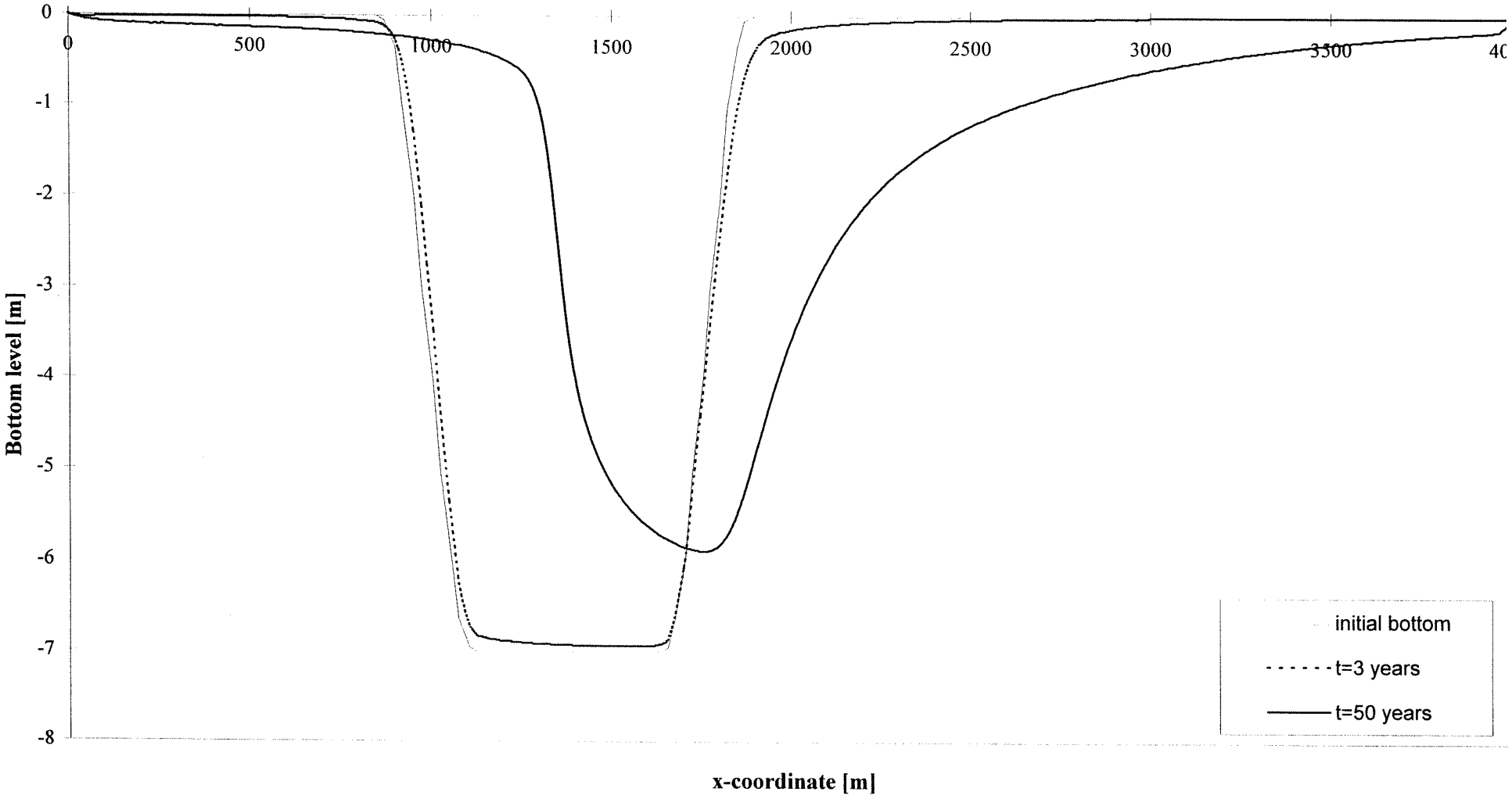

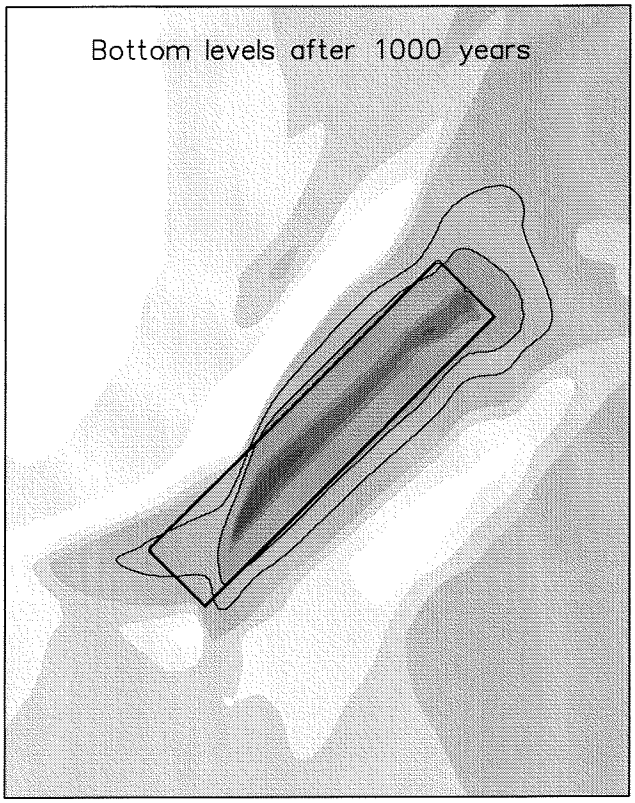

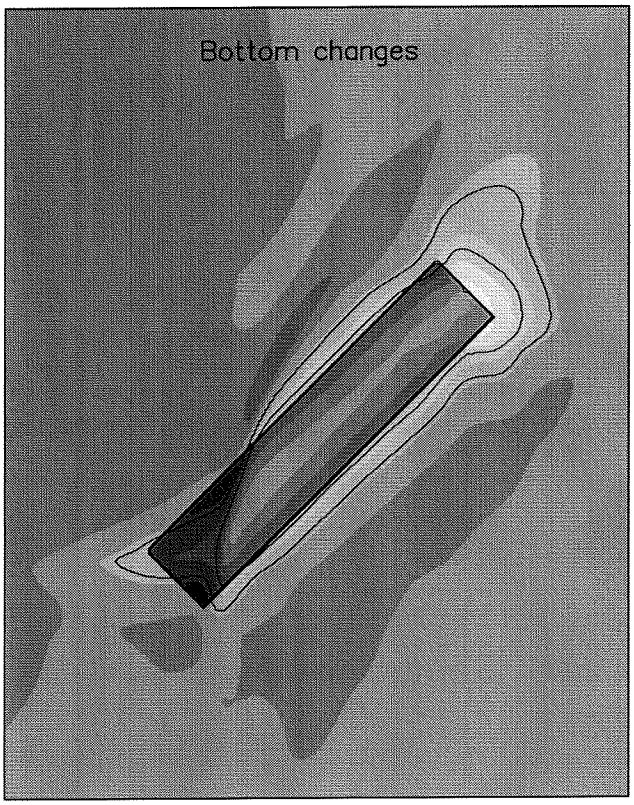

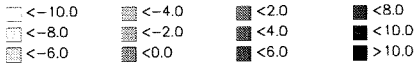

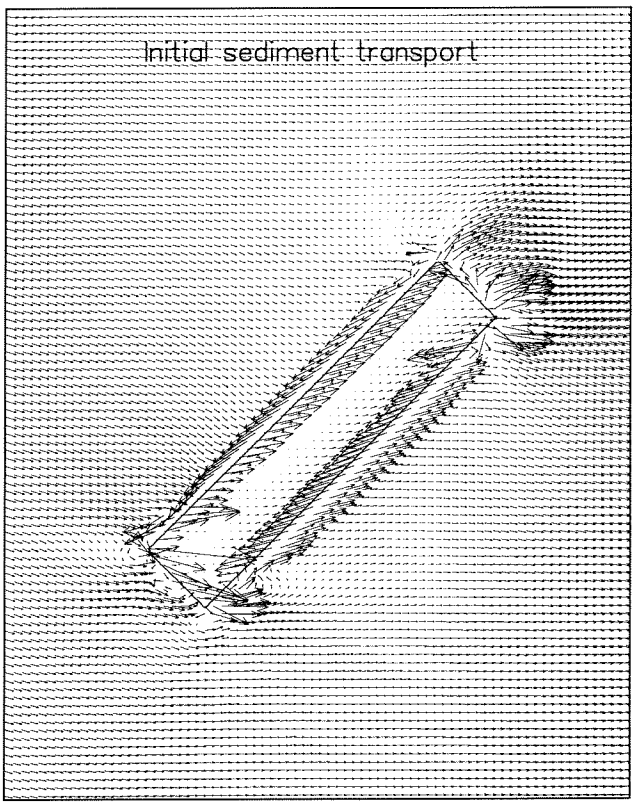

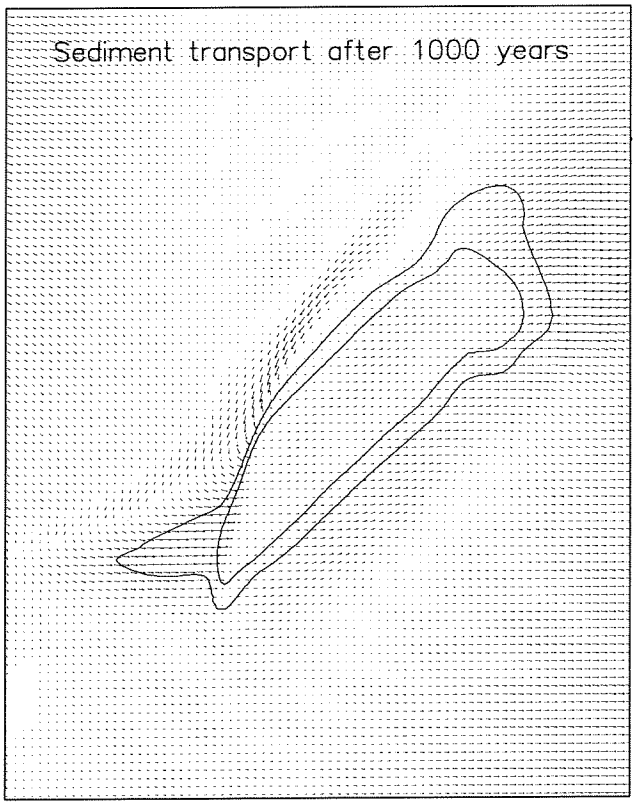

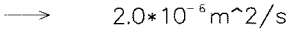

Bottom levels and changes [m]; sediment transport [m^2/s]

+45 degrees rotated 25x5 km^2 sandpit

Morphological results after 1000 years

WL | DELFT HYDRAULICS

z2615

Figure 8.15a

Figure 8.15b: Bottom levels in the longitudinal section of a +45° rotated 25x5 km ^ 2 sandpit

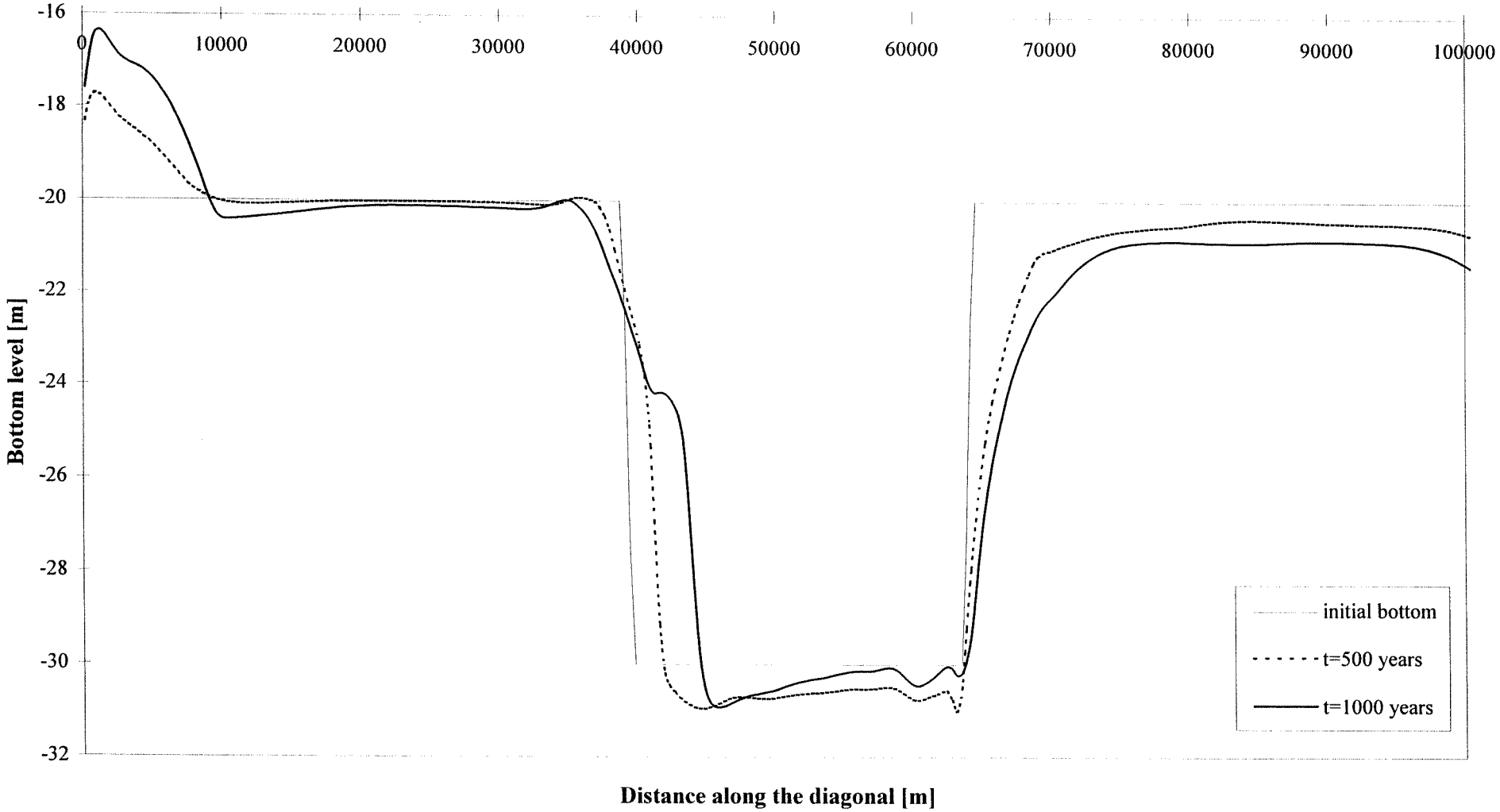

Figure 8.15c: Bottom levels in the center cross-section of a +45° rotated 25x5 km2 sandpit

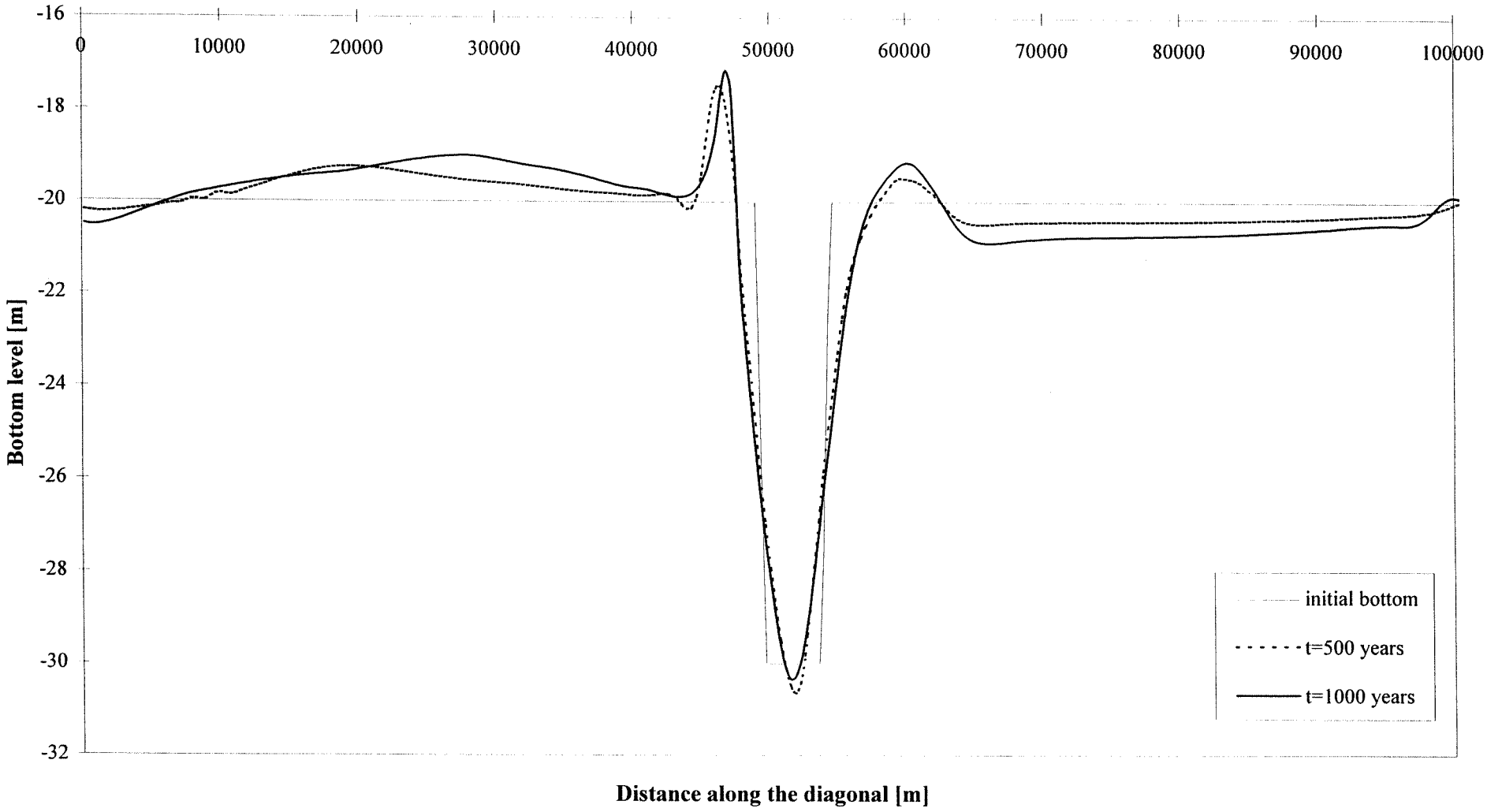

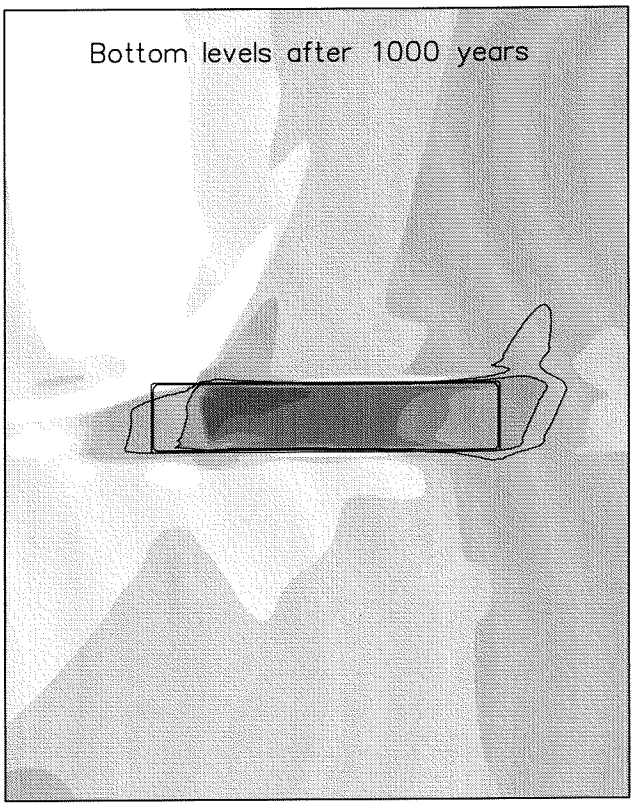

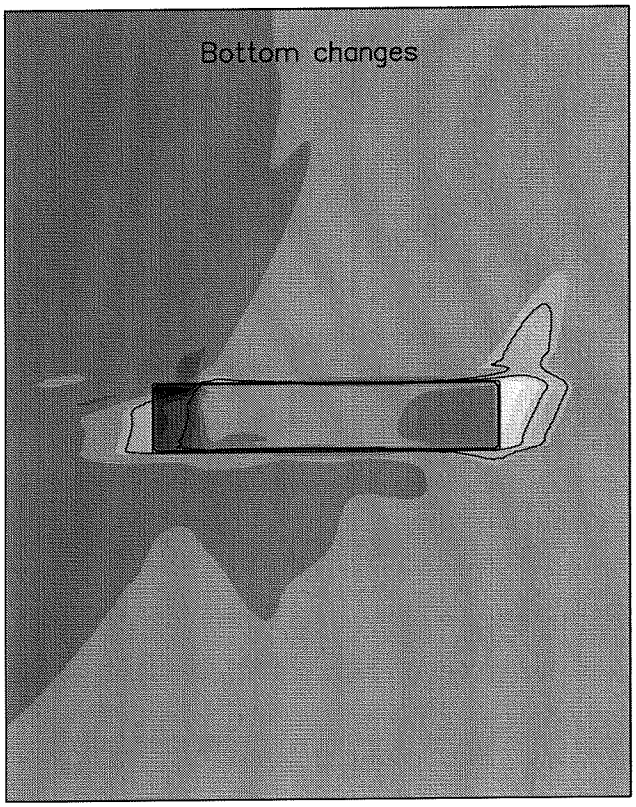

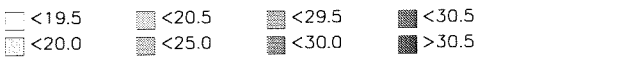

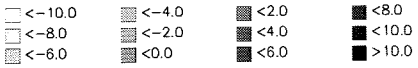

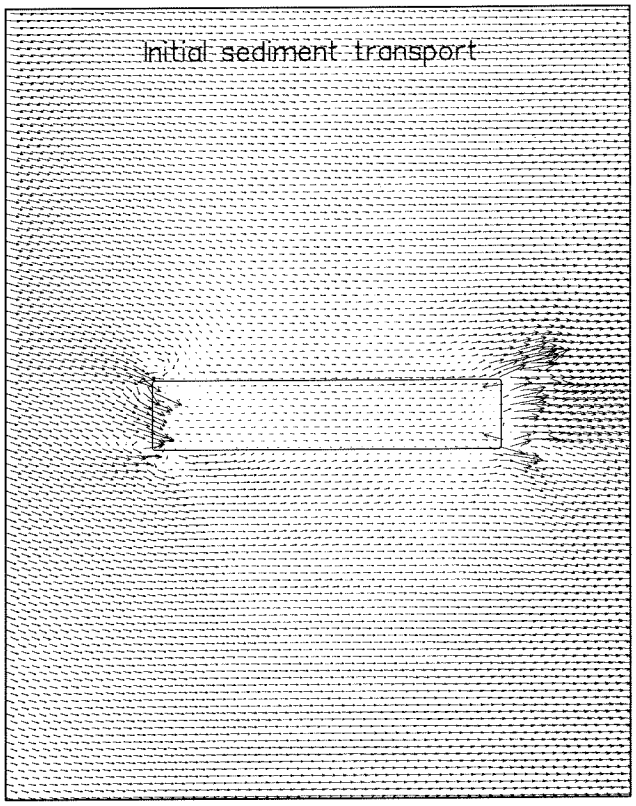

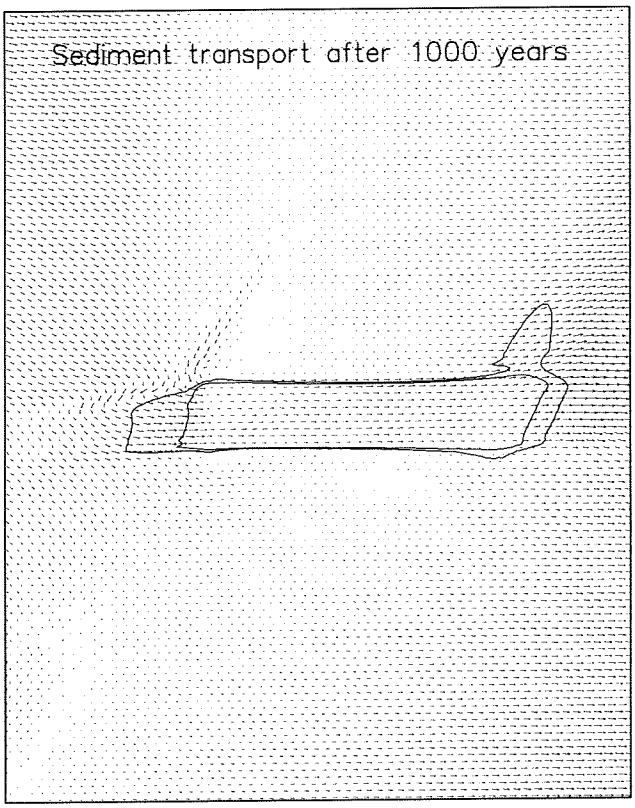

⟶ $2.0*10^{-6}$ m^2/s

Bottom levels and changes [m]; sediment transport [m^2/s] Parallel 25x5 km^2 sandpit Morphological results after 1000 years		
WL | DELFT HYDRAULICS	z2615	Figure 8.16a

Figuur 8.16b: Bottom levels in the center longitudinal section of a parallel 25x5 km ^ 2 sandpit

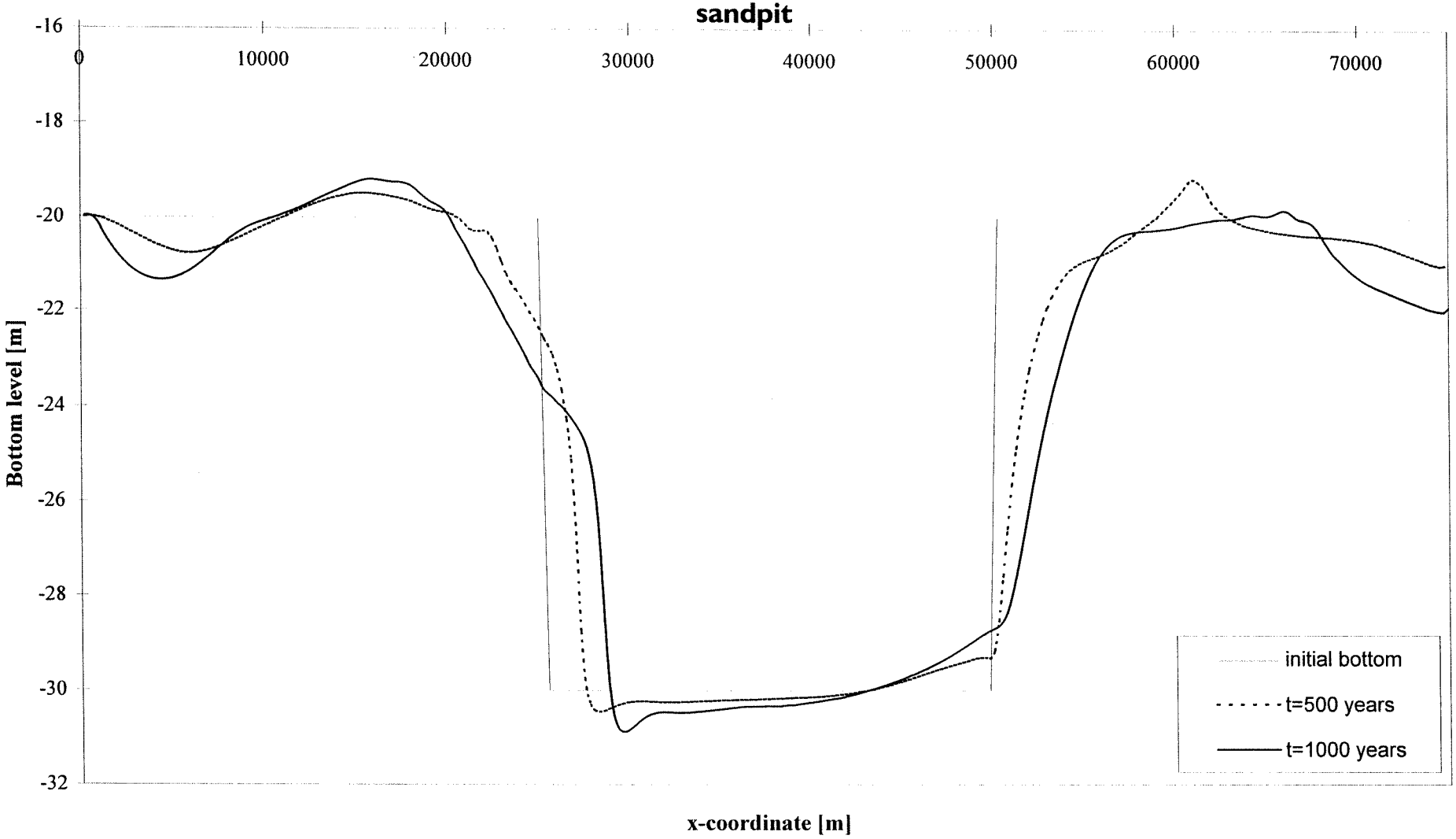

Figure 8.16c: Bottom levels in the center cross-section of a parallel 25x5 km ^ 2 sandpit

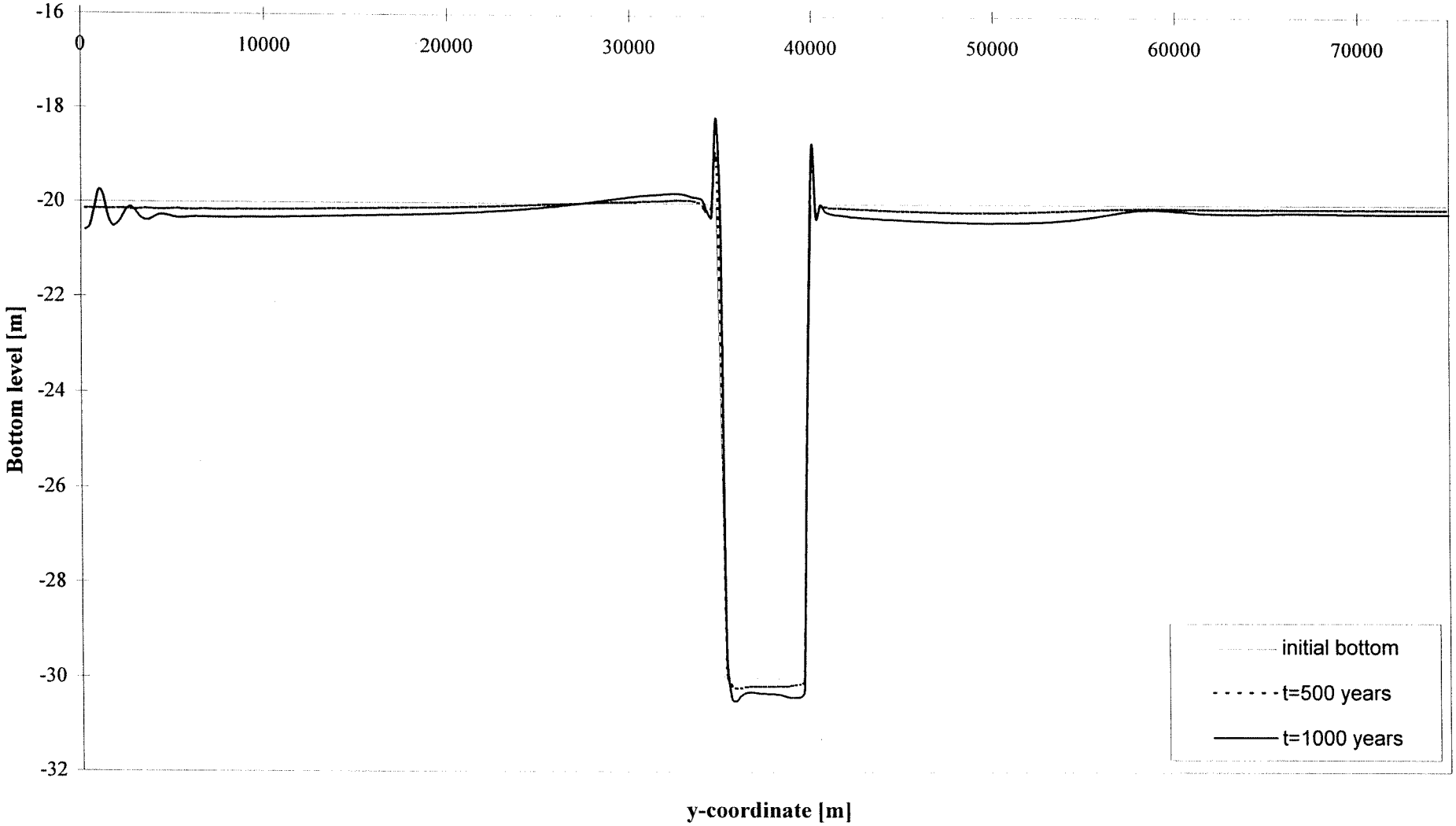

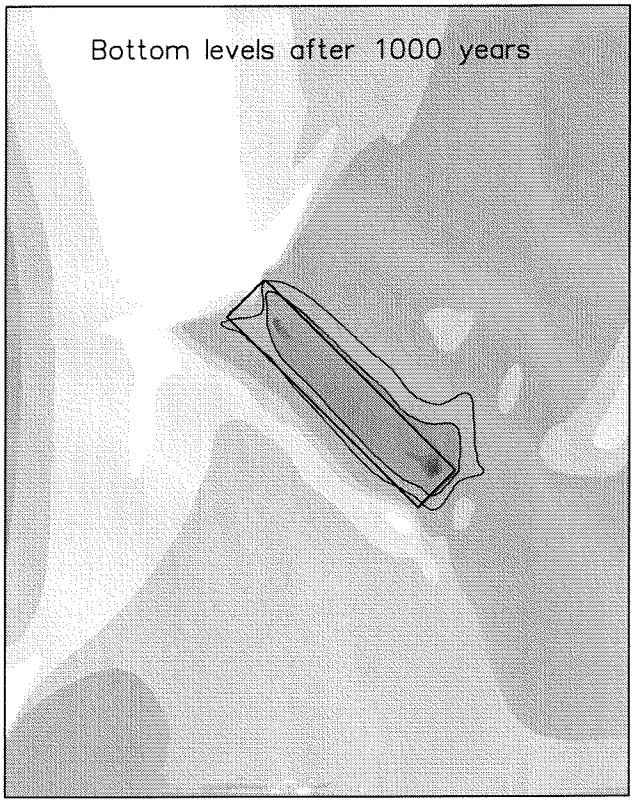

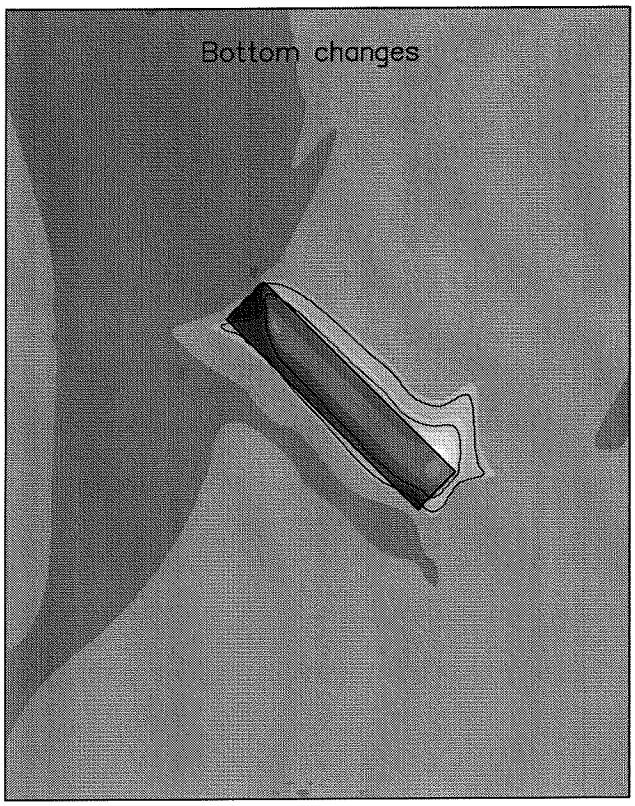

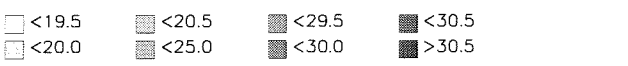

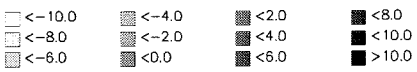

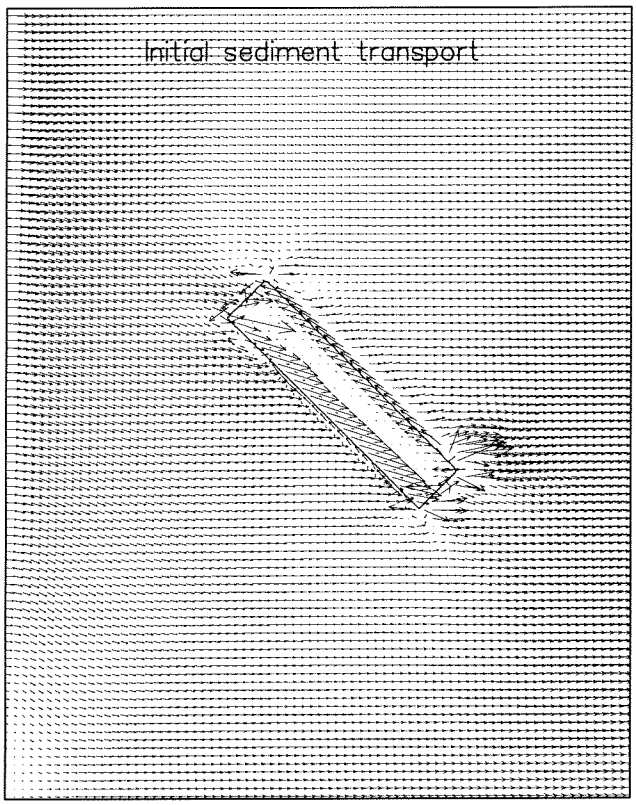

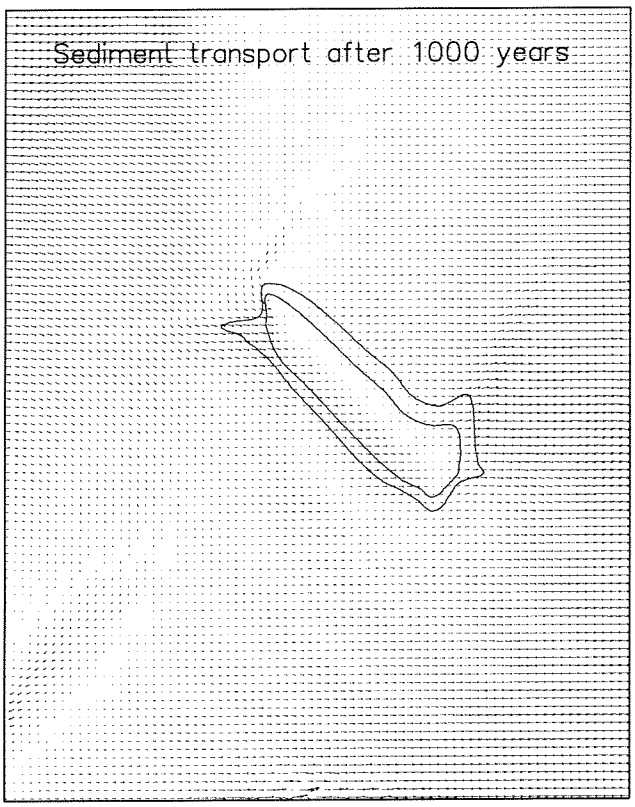

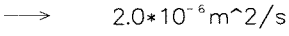

Bottom levels and changes [m];sediment transport [m^2/s]

-45 degrees rotated 25x5 km^2 sandpit

Morphological results after 1000 years

WL | DELFT HYDRAULICS

z2615

Figure 8.17a

Figure 8.17b: Bottom levels in the center longitudinal section of a -45° rotated 25x5 km ^ 2 sandpit

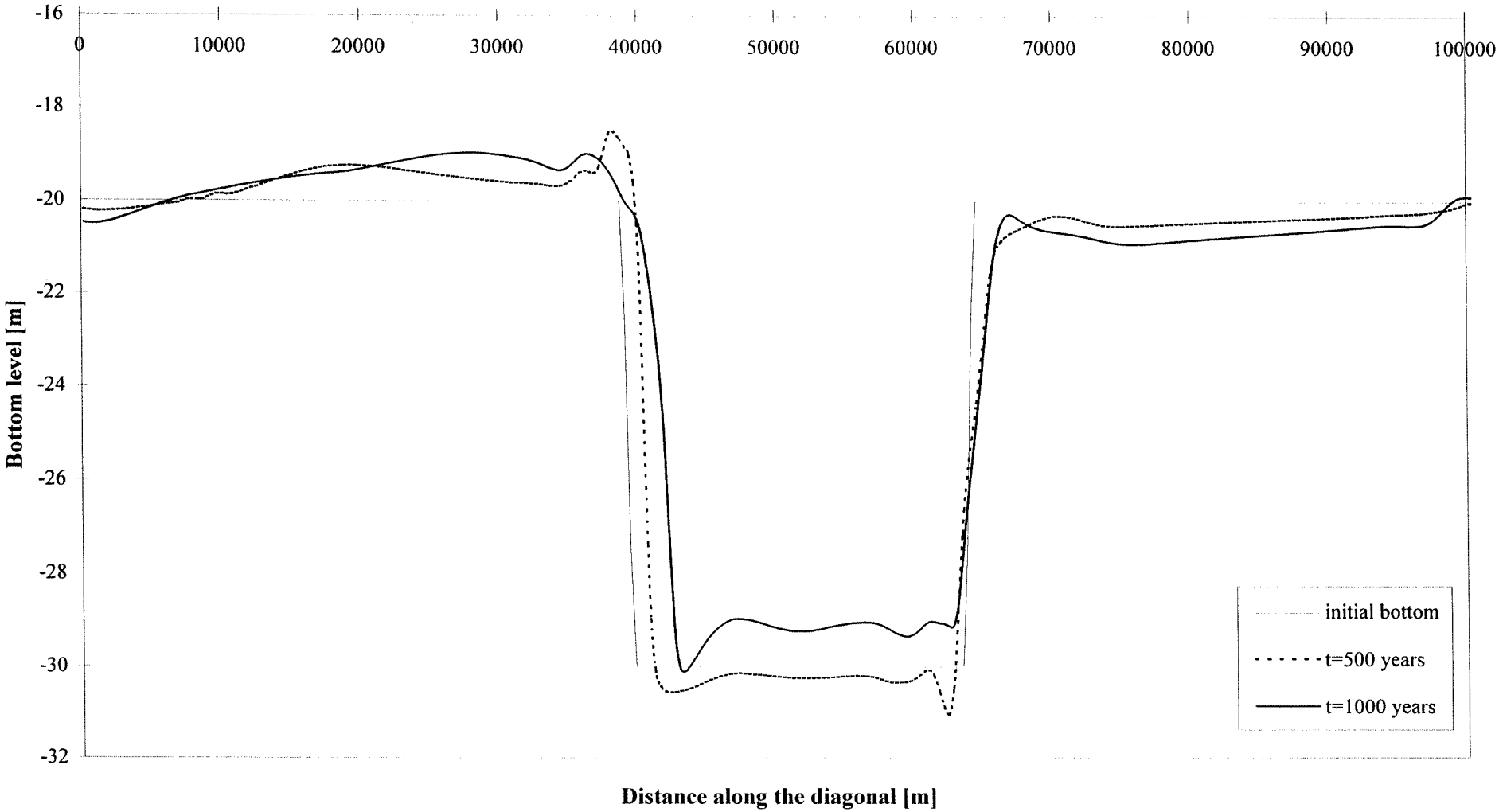

Figure 8.17c: Bottom levels in the center cross-section of a -45° rotated 25x5 km2 sandpit

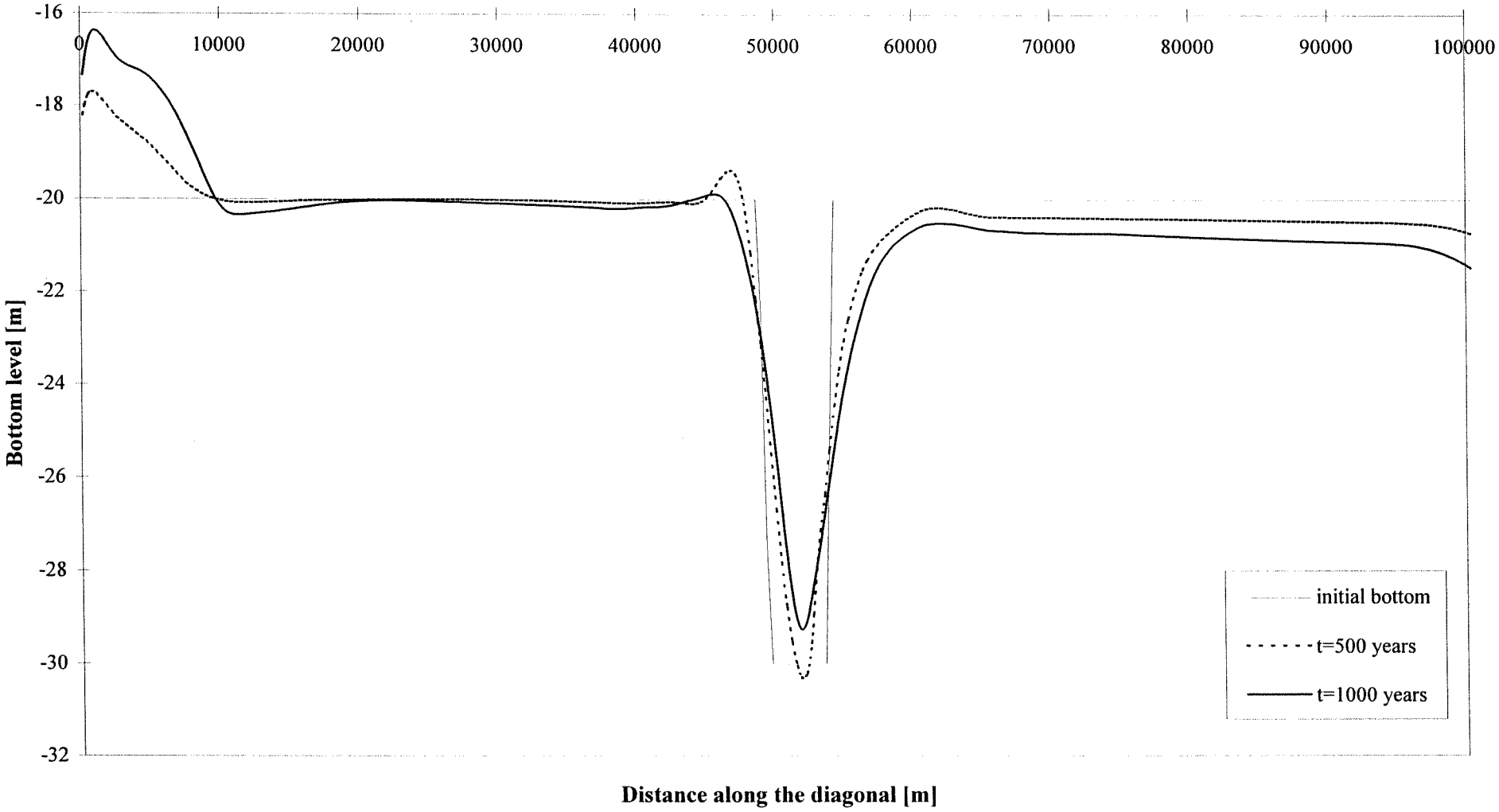

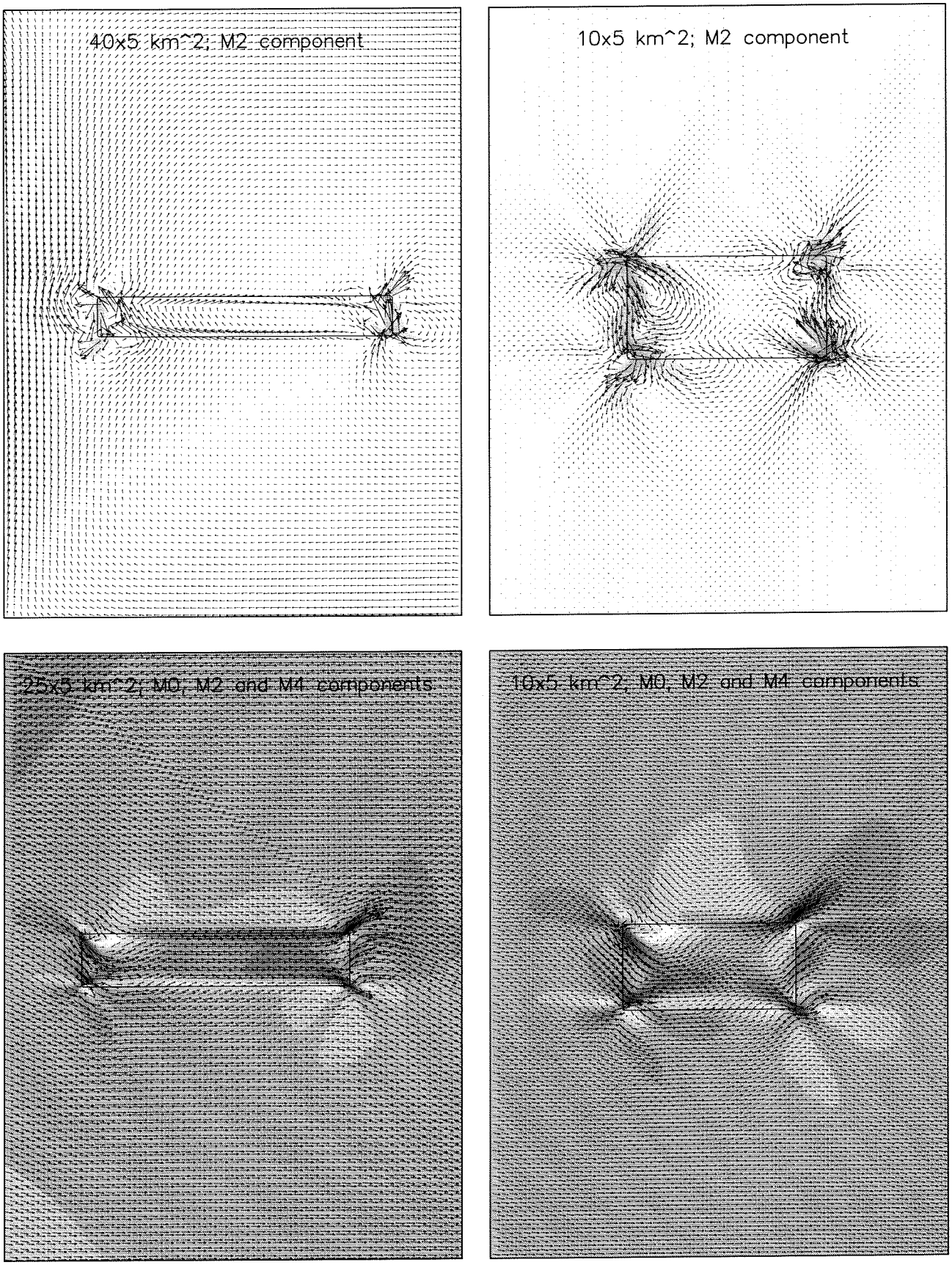

Tide-averaged current velocities [m/s]

Influence of the tidal motion and the length on the averaged current pattern

Tidal boundary conditions including

WL | DELFT HYDRAULICS

z2615

Figure 8.18

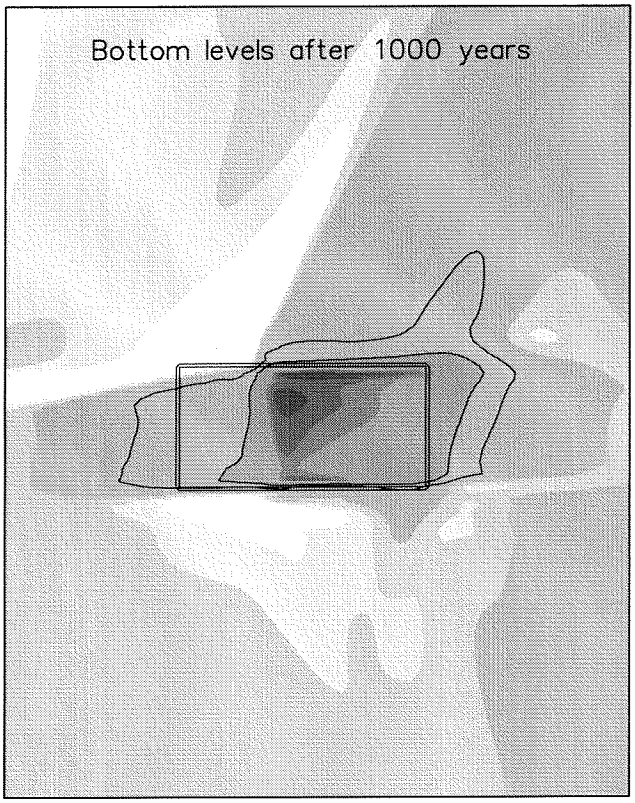

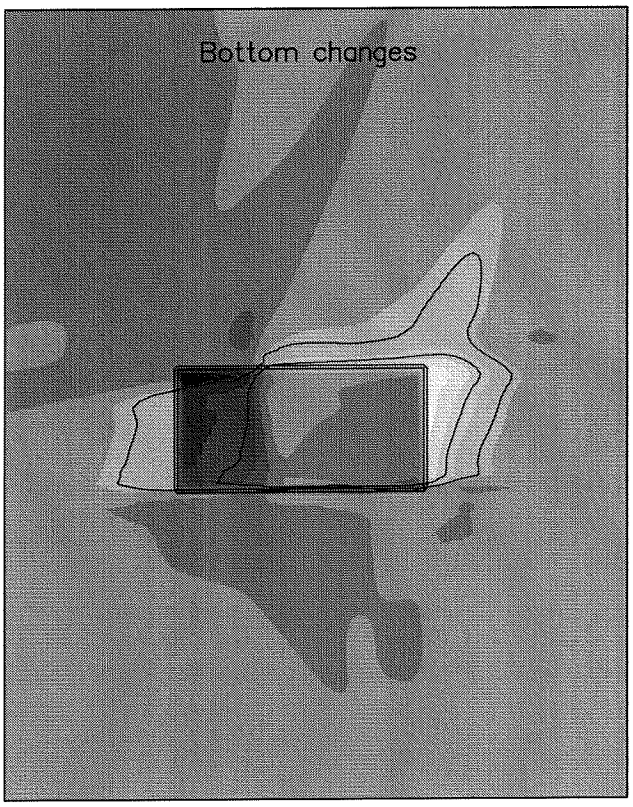

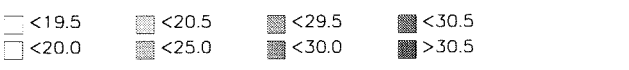

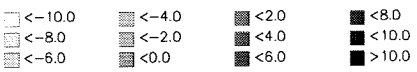

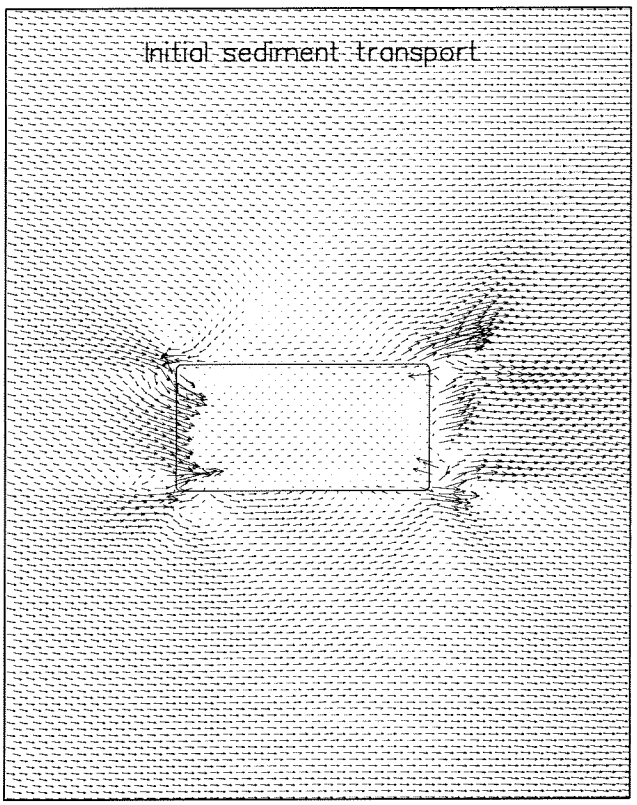

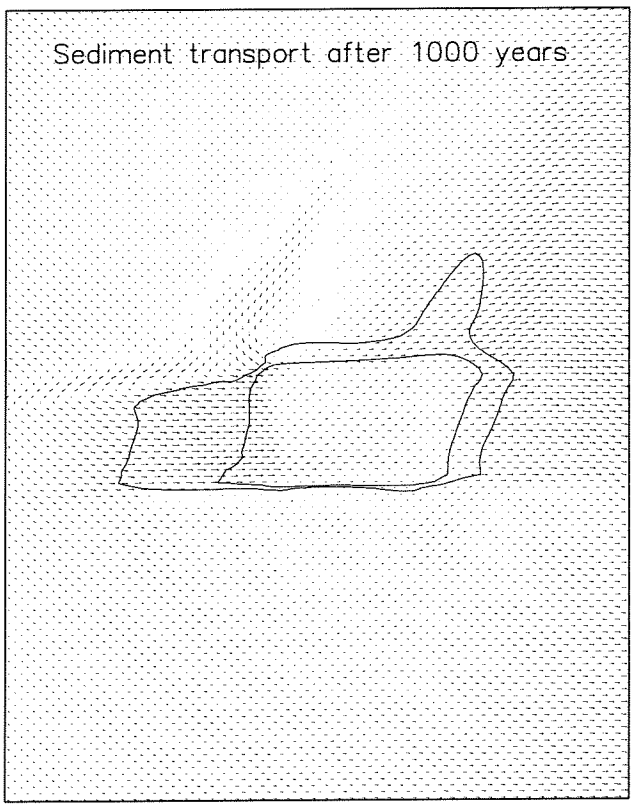

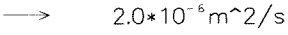

Bottom levels and changes [m]; sediment transport [m^2/s]

Parallel 10x5 km^2 sandpit

Morphological results after 1000 years

WL | DELFT HYDRAULICS

z2615

Figure 8.19a

Figure 8.19b: Bottom levels in the longitudinal section of a parallel 10x5 km ^ 2 sandpit

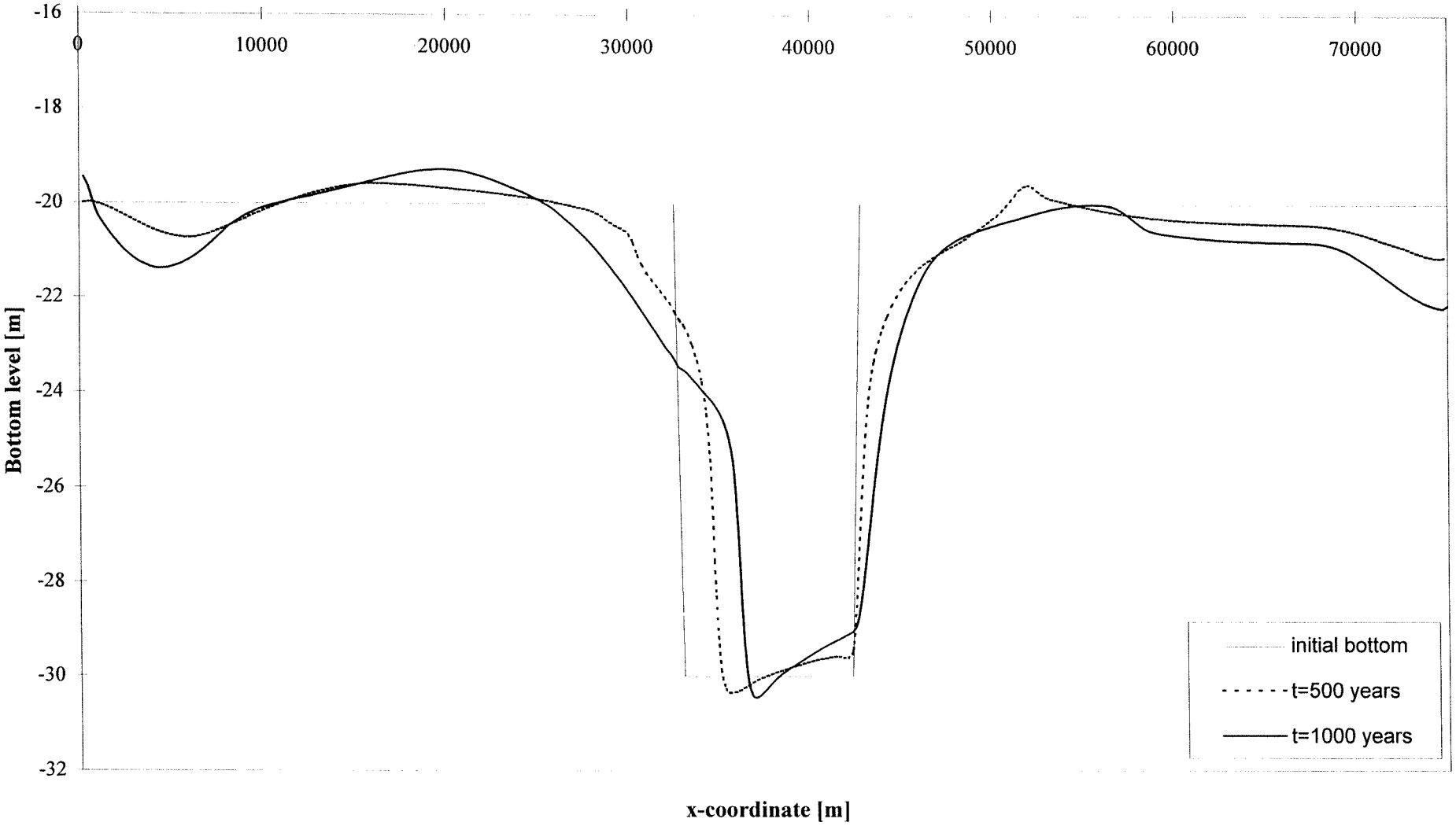

Figure 8.19c: Bottom levels in the center cross-section of a parallel 10x5 km ^ 2 sandpit

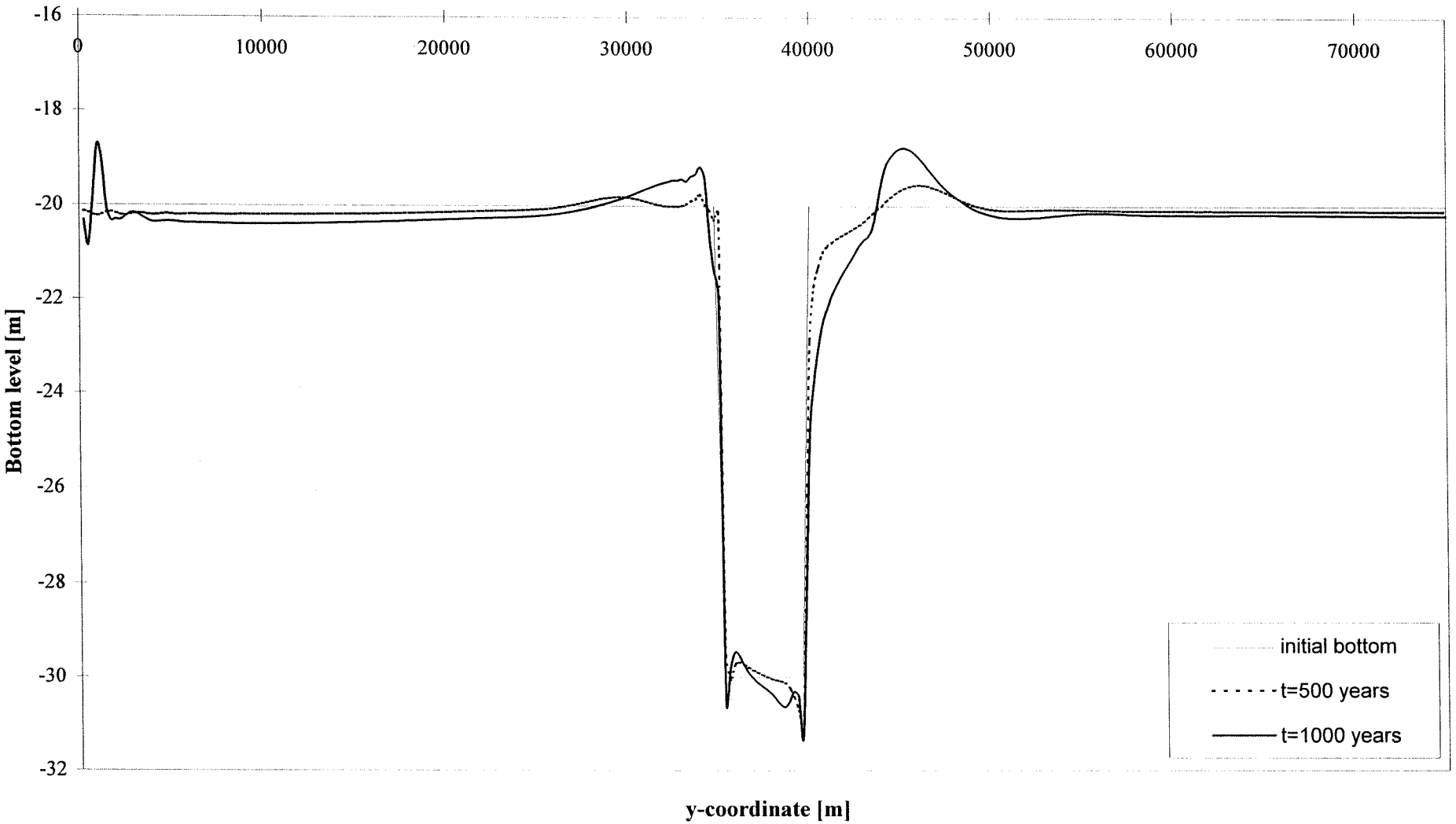

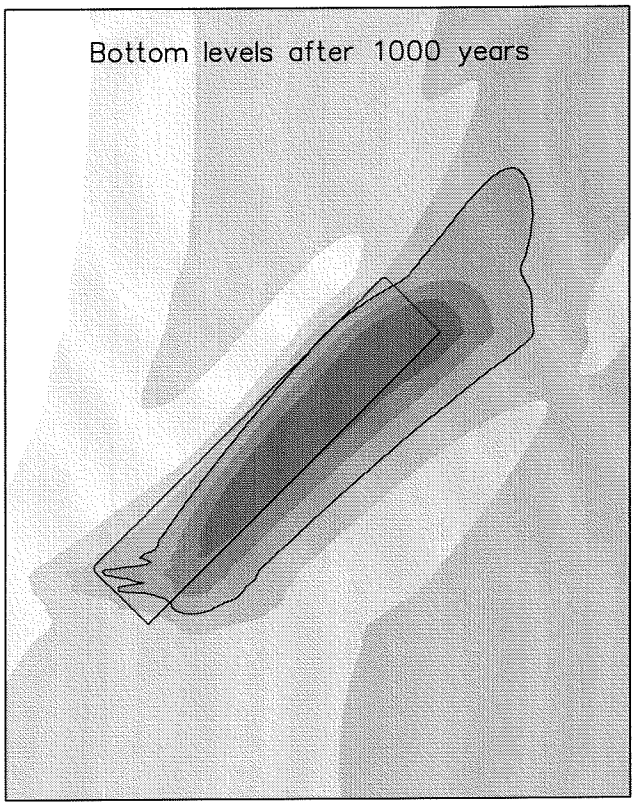

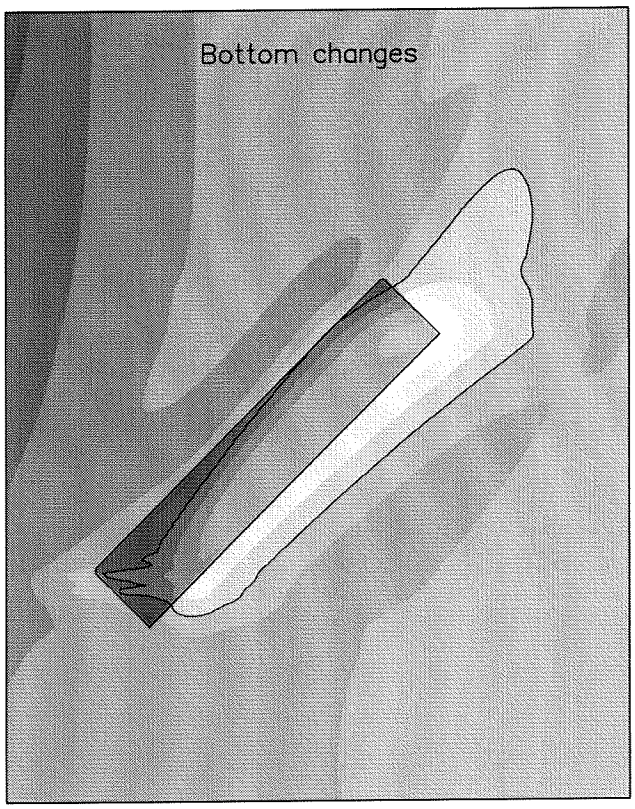

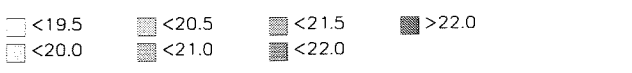

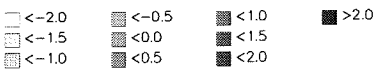

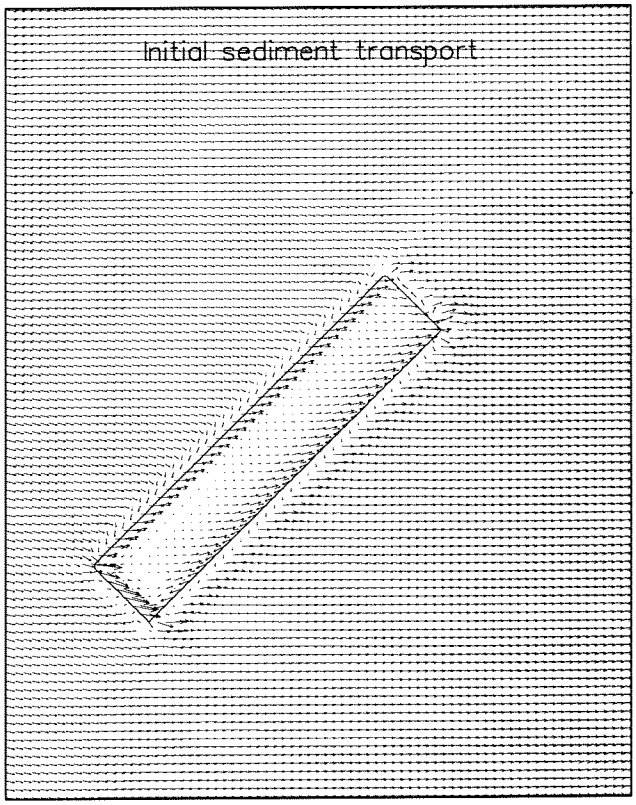

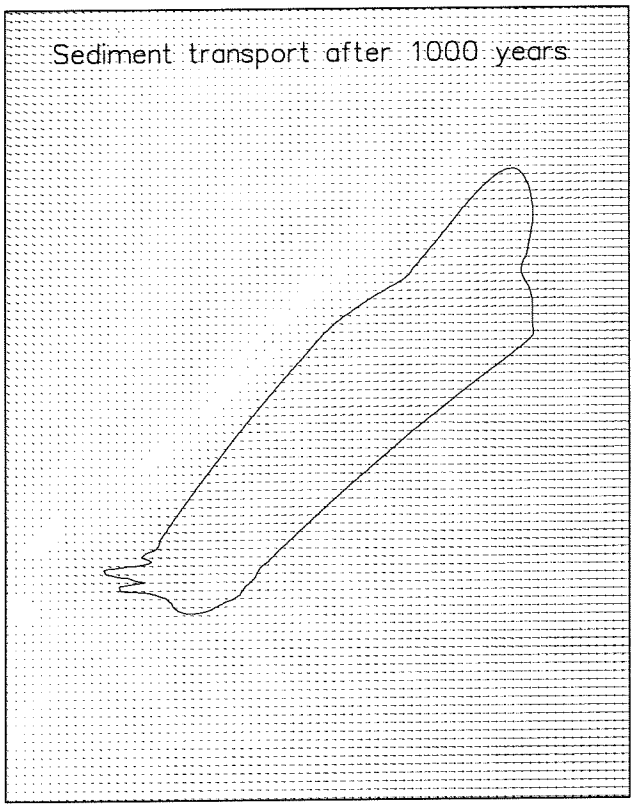

⟶ $2.0*10^{-6}$ m^2/s

Bottom levels and changes [m]; sediment transport m^2/s

+45 degrees rotated, 22m deep 25x5 km^2 sandpit

Morphological results after 1000 years

WL | DELFT HYDRAULICS

z2615

Figure 8.20a

Figure 8.20b: Bottom levels in the center longitudinal section of a +45° rotated 25x5 km ^ 2, 22m deep sandpit

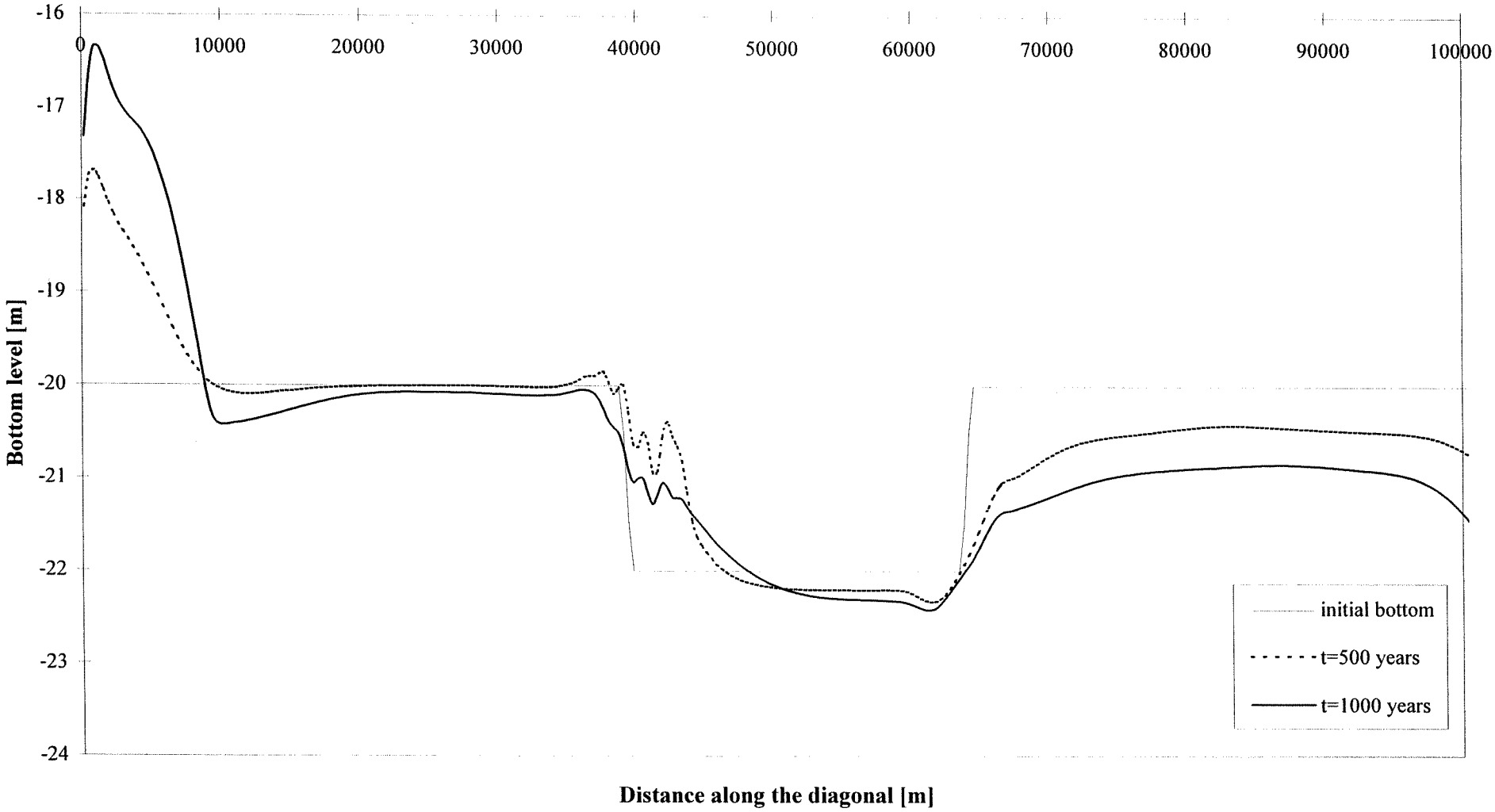

Figure 8.20c: Bottom levels in the center cross-section of a +45° rotated, 22 m deep 25x5 km^2 sandpit

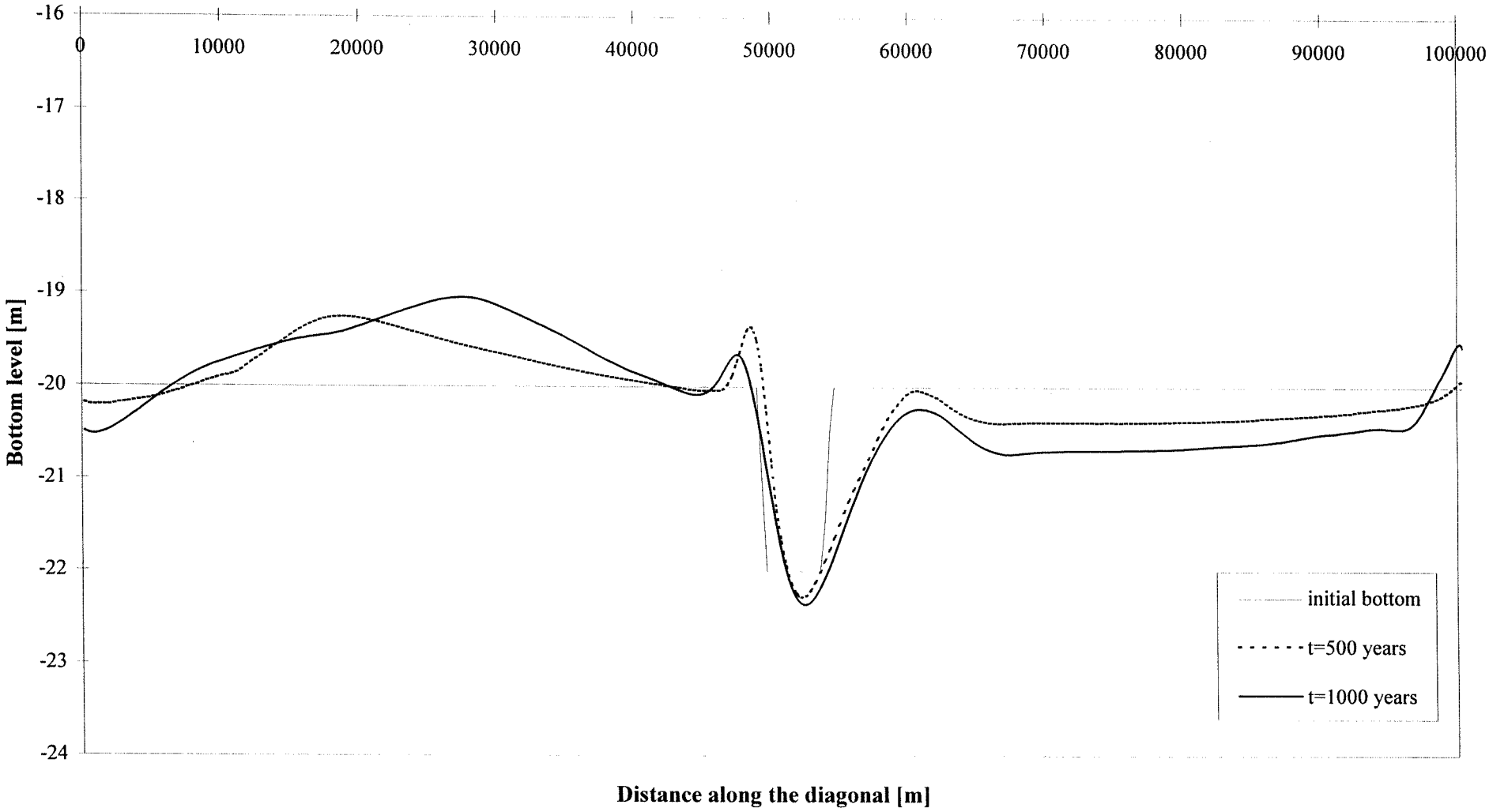

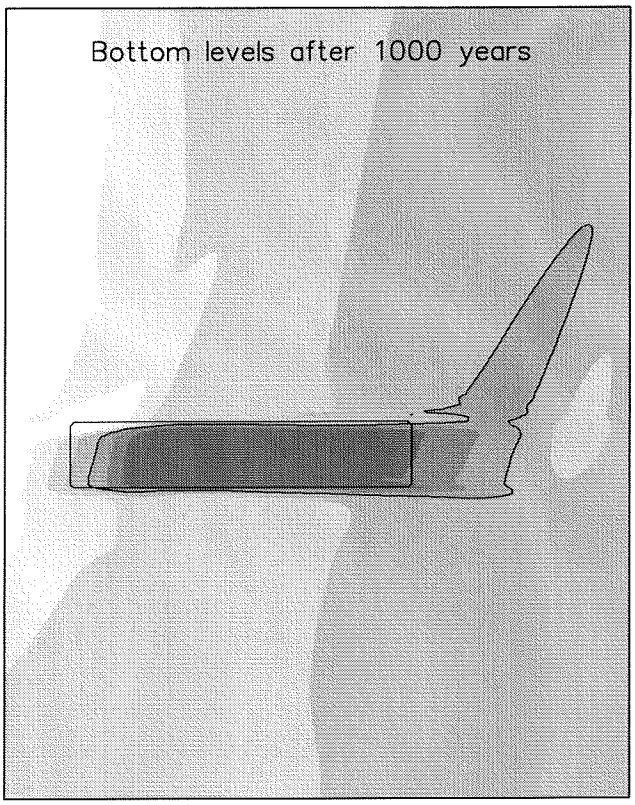

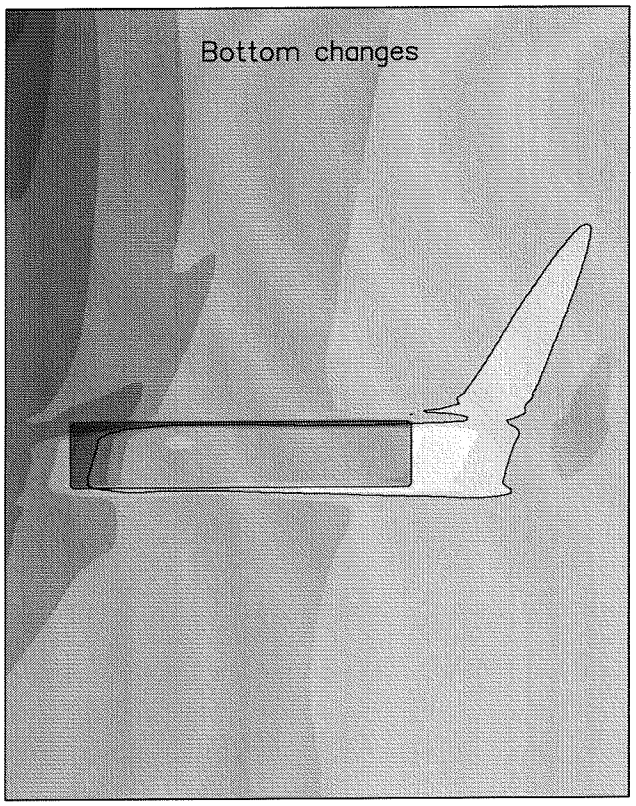

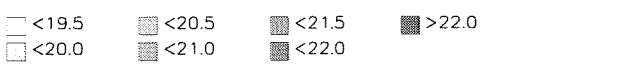

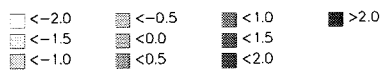

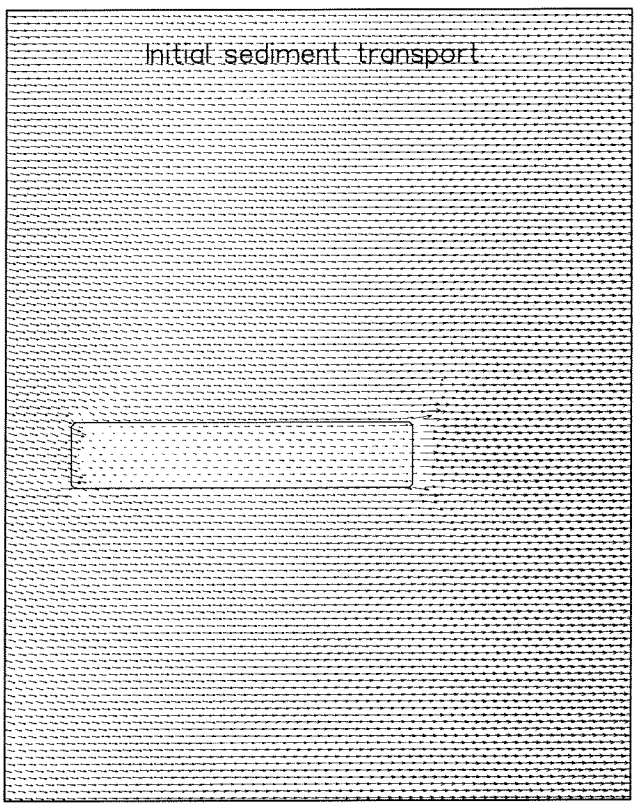

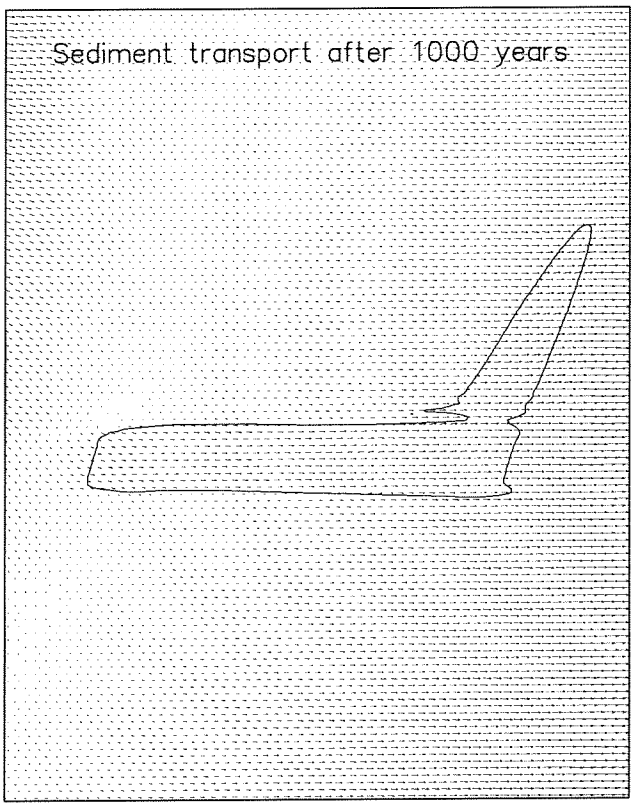

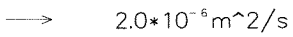

Bottom levels and changes [m]; sediment transport [m^2/s]

Parallel, 22 m deep 25x5 km^2

Morphological results

WL | DELFT HYDRAULICS

z2615

Figure 8.21a

Figure 8.21b: Bottom levels in the center longitudinal section of a parallel, 22 m deep, 25x5 km ^ 2 sandpit

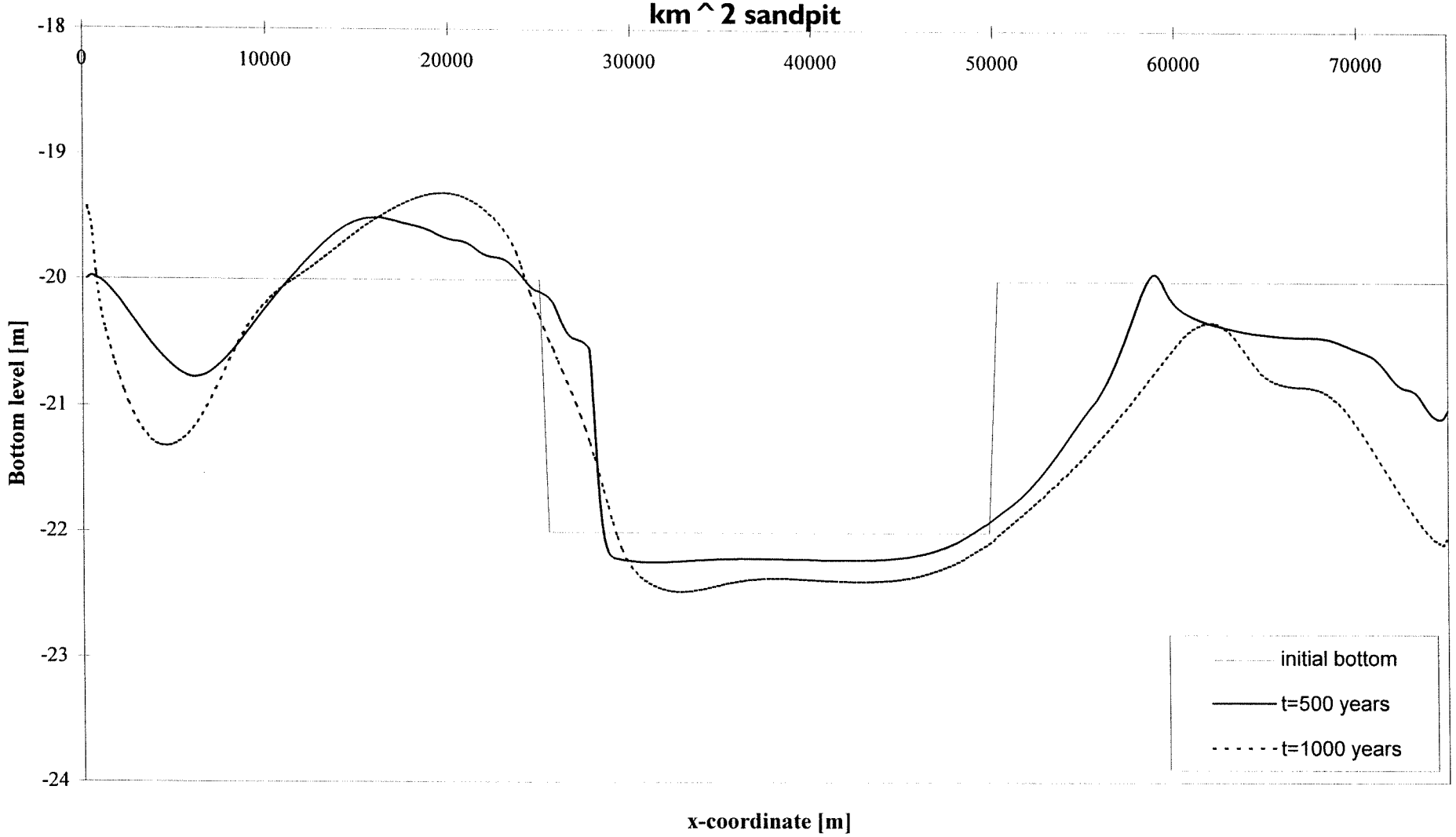

Figure 8.21c: Bottom levels in the center cross-section of a parallel, 22 m deep, 25x5 km ^ 2 sandpit

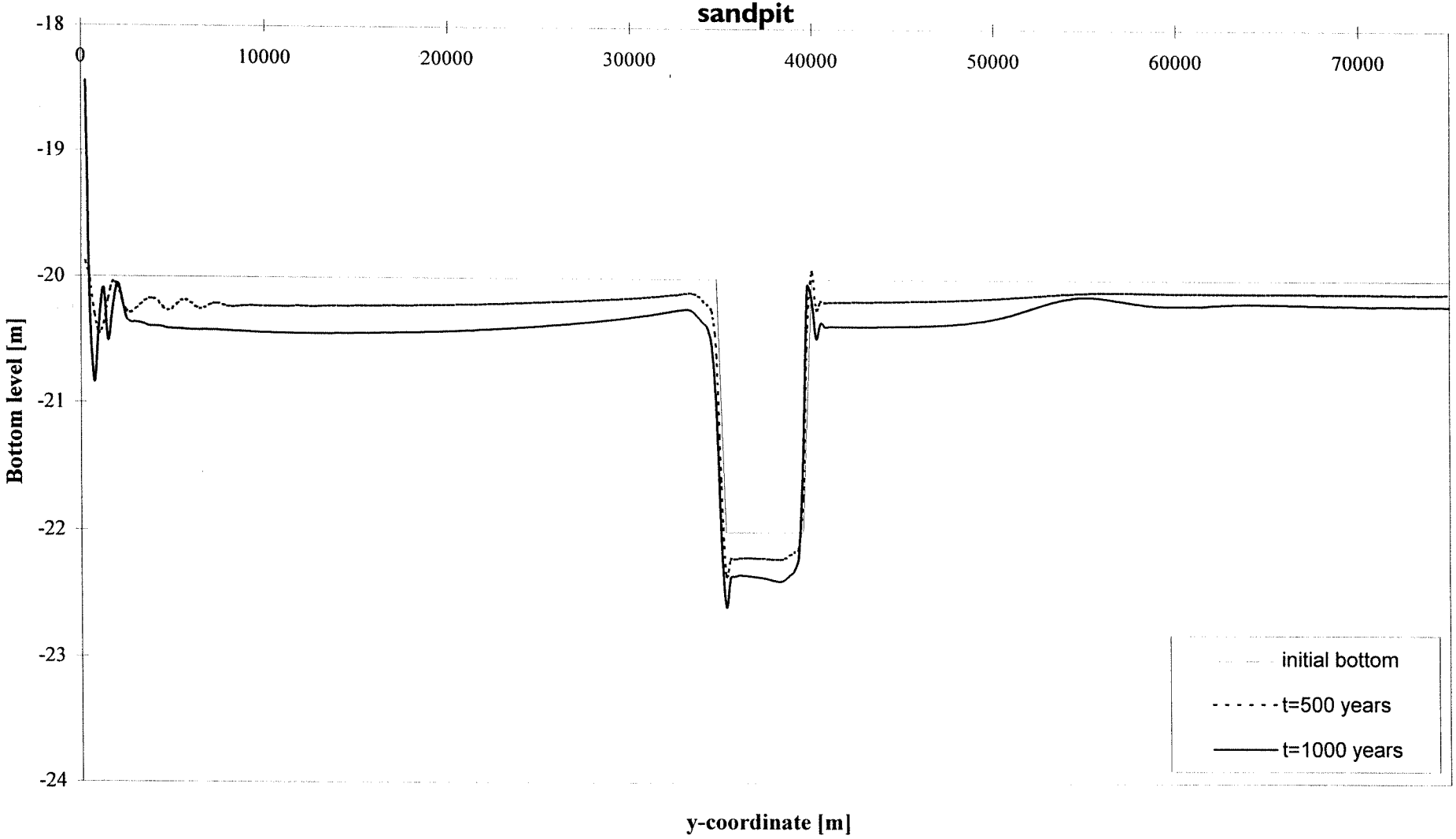

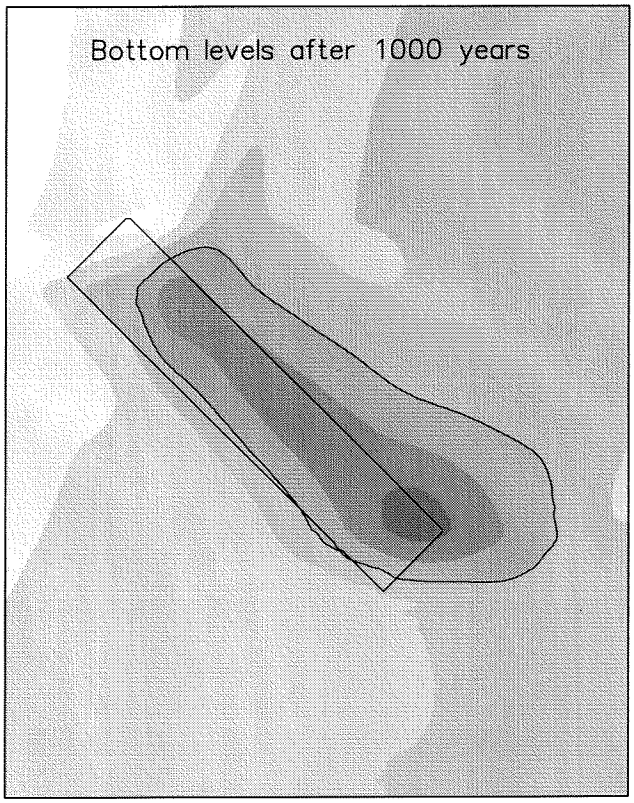

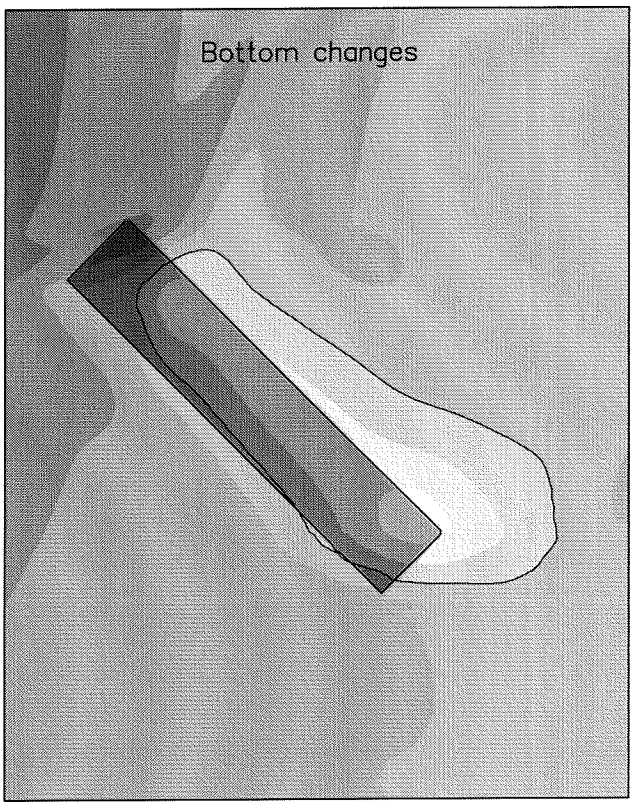

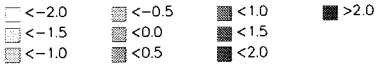

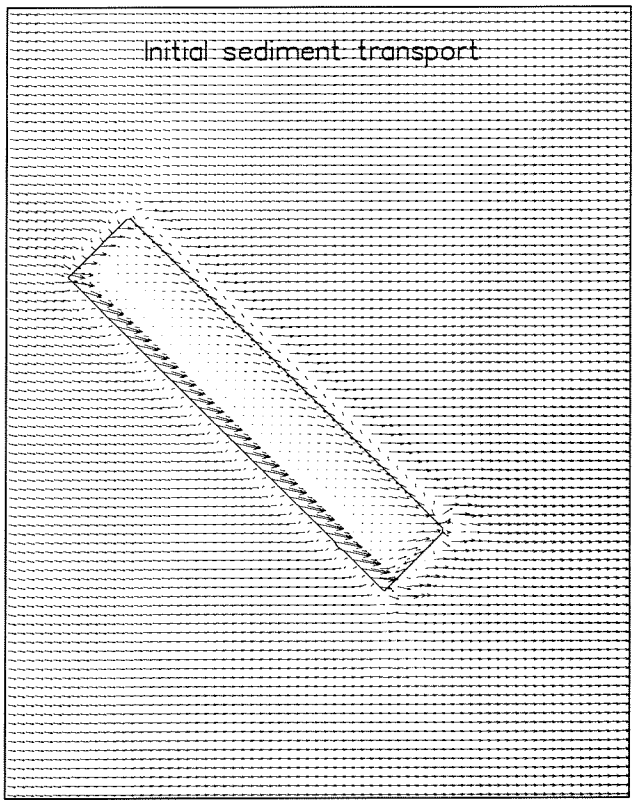

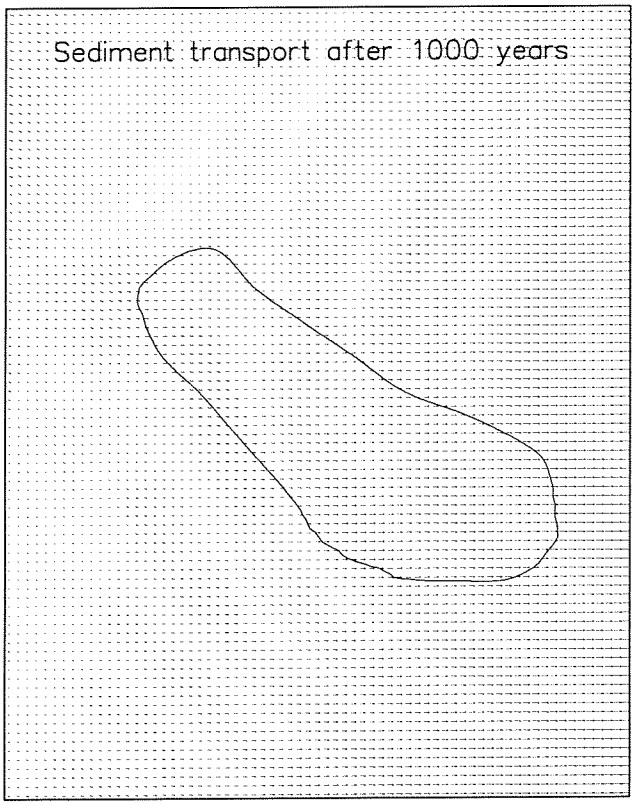

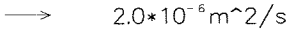

Bottom levels and changes [m]; sediment transport [m^2/s]

-45 degrees rotated, 22m deep 25x5 km^2 sandpit

Morphological results after 1000 years

WL | DELFT HYDRAULICS

z2615

Figure 8.22a

Figure 8.22b: Bottom levels in the longitudinal section of a +45° rotated, 22 m deep 25x5 km ^ 2 sandpit

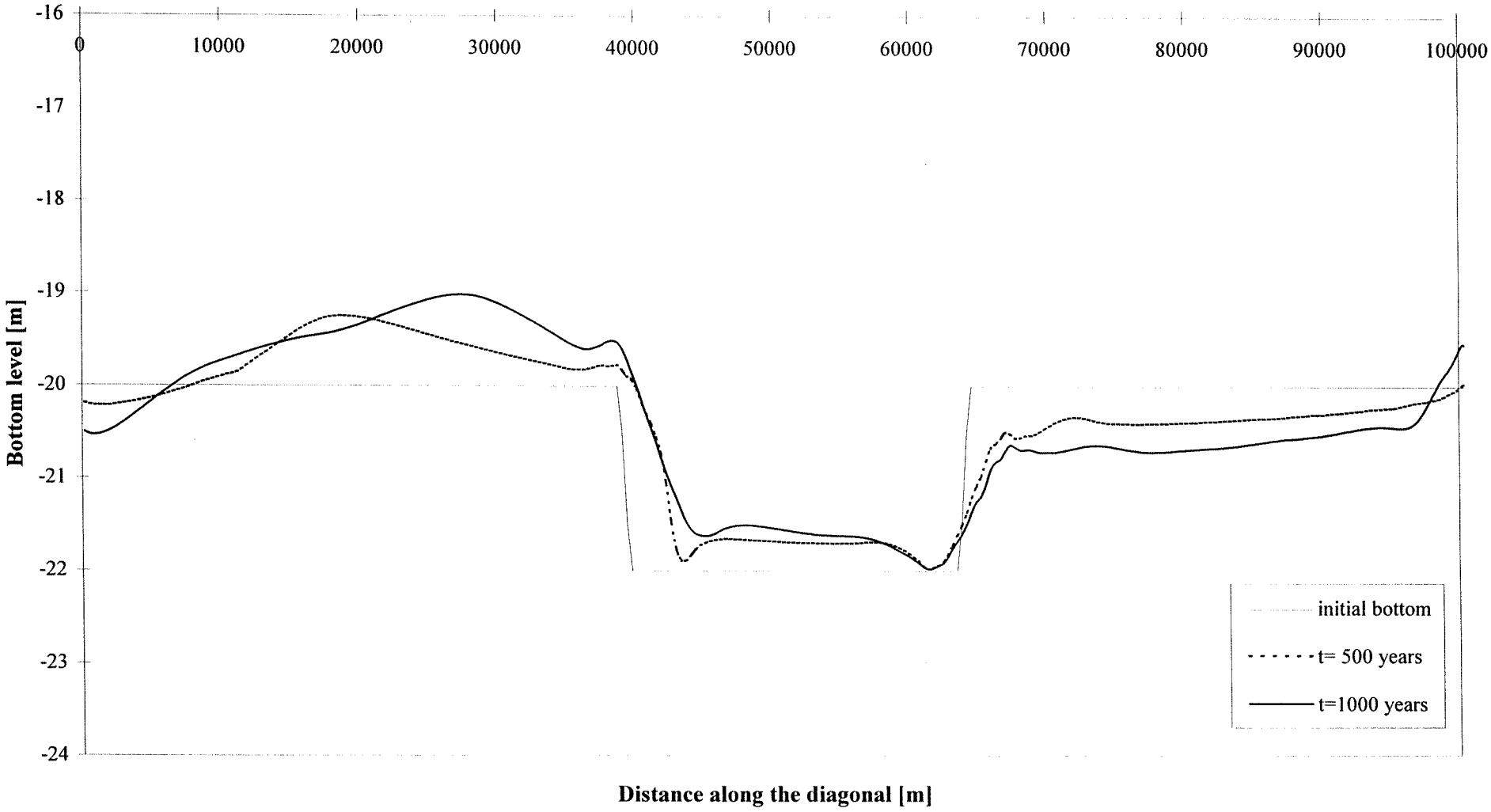

Figure 8.22c: Bottom levels in the center cross-section of a -45° rotated, 22m deep 25x5 km2 sandpit

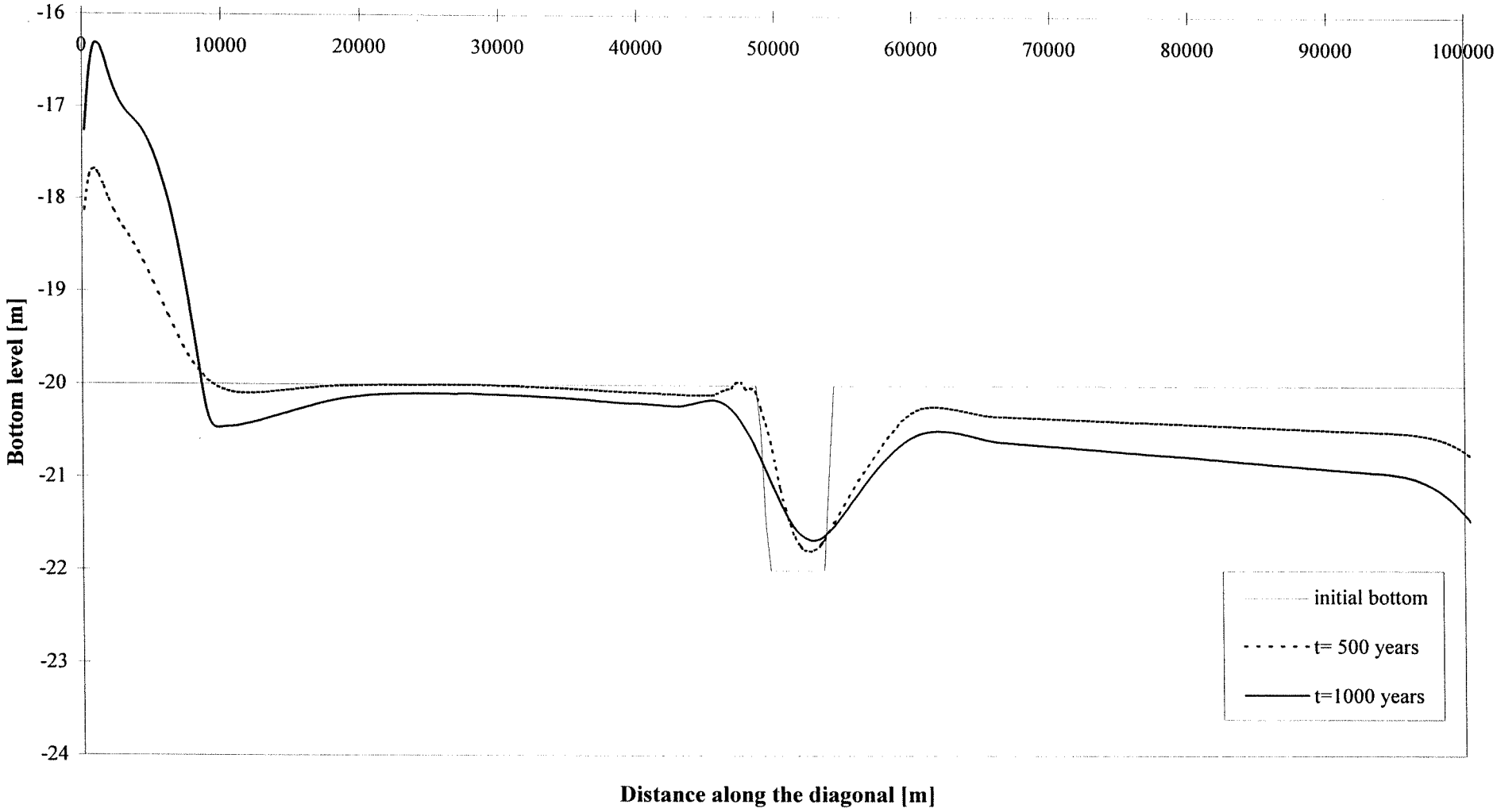

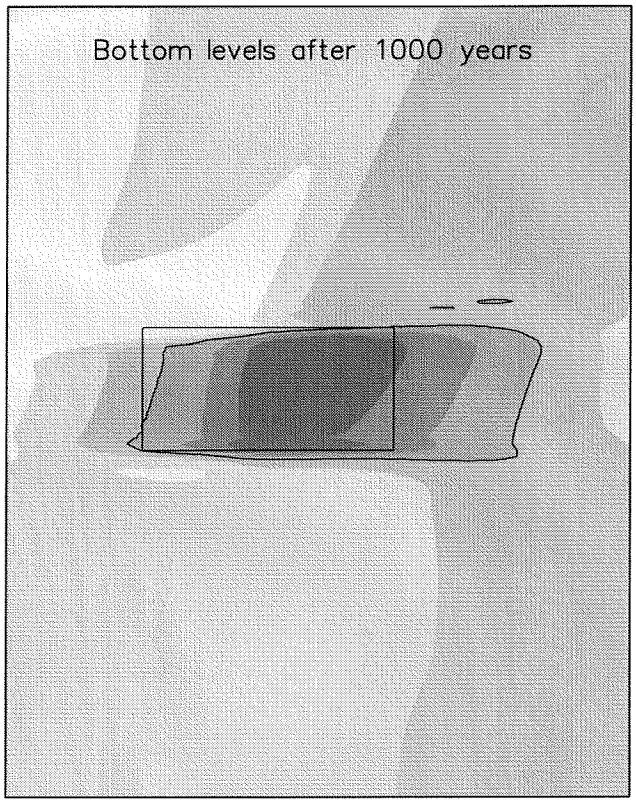

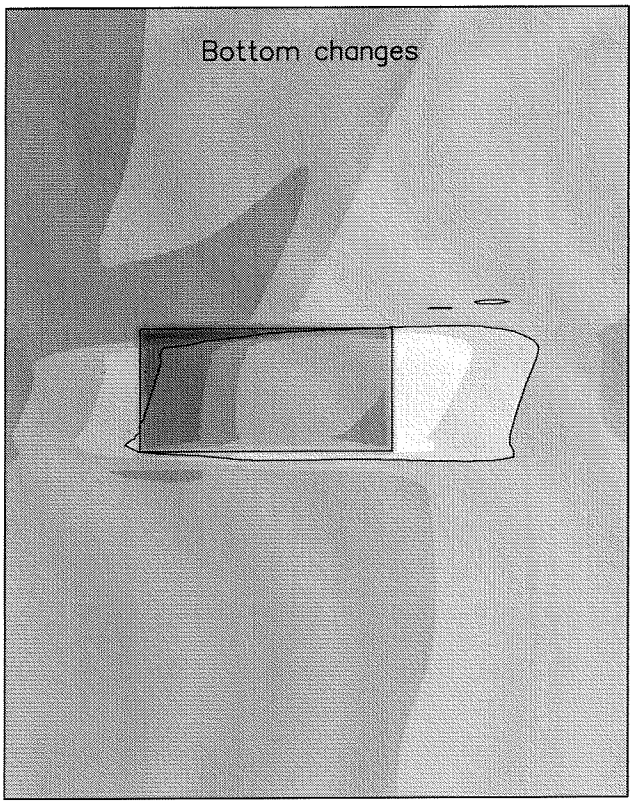

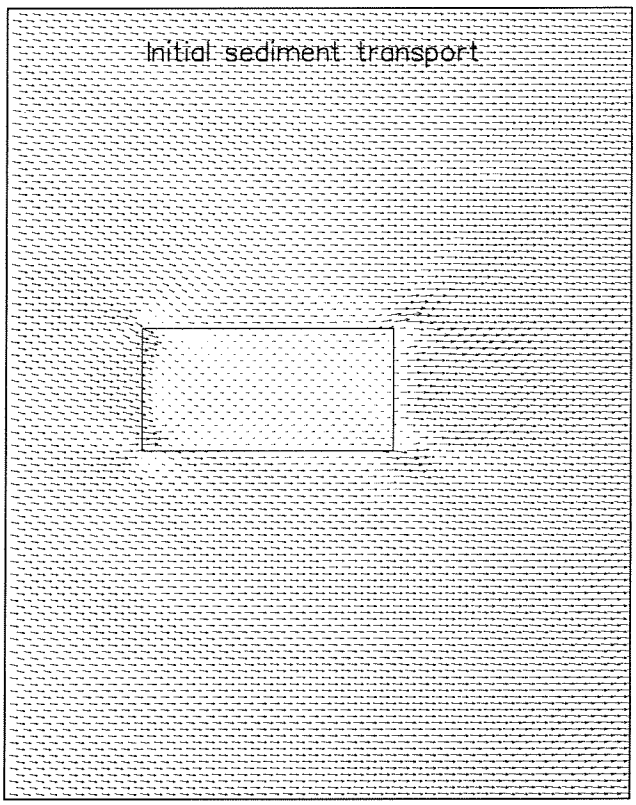

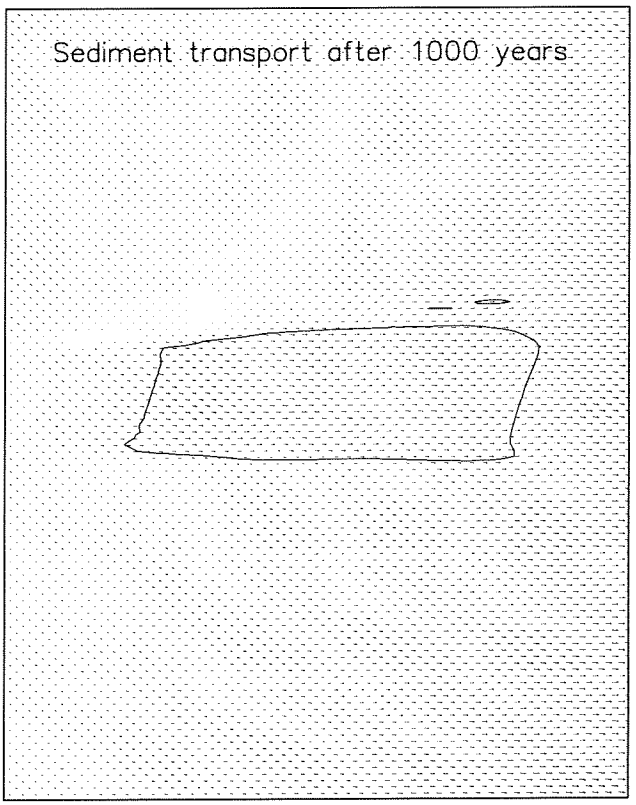

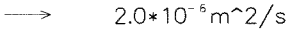

Bottom levels and changes [m]; sediment transport [m^2/s]

Parallel, 22 m deep 10x5 km^2 sandpit

Morphological results after 1000 years

WL | DELFT HYDRAULICS

z2615

Figure 8.23a

Figuur 8.23b: Bottom levels in the center longitudinal section of parallel, 22 m deep 10x5 km ^ 2 sandpit

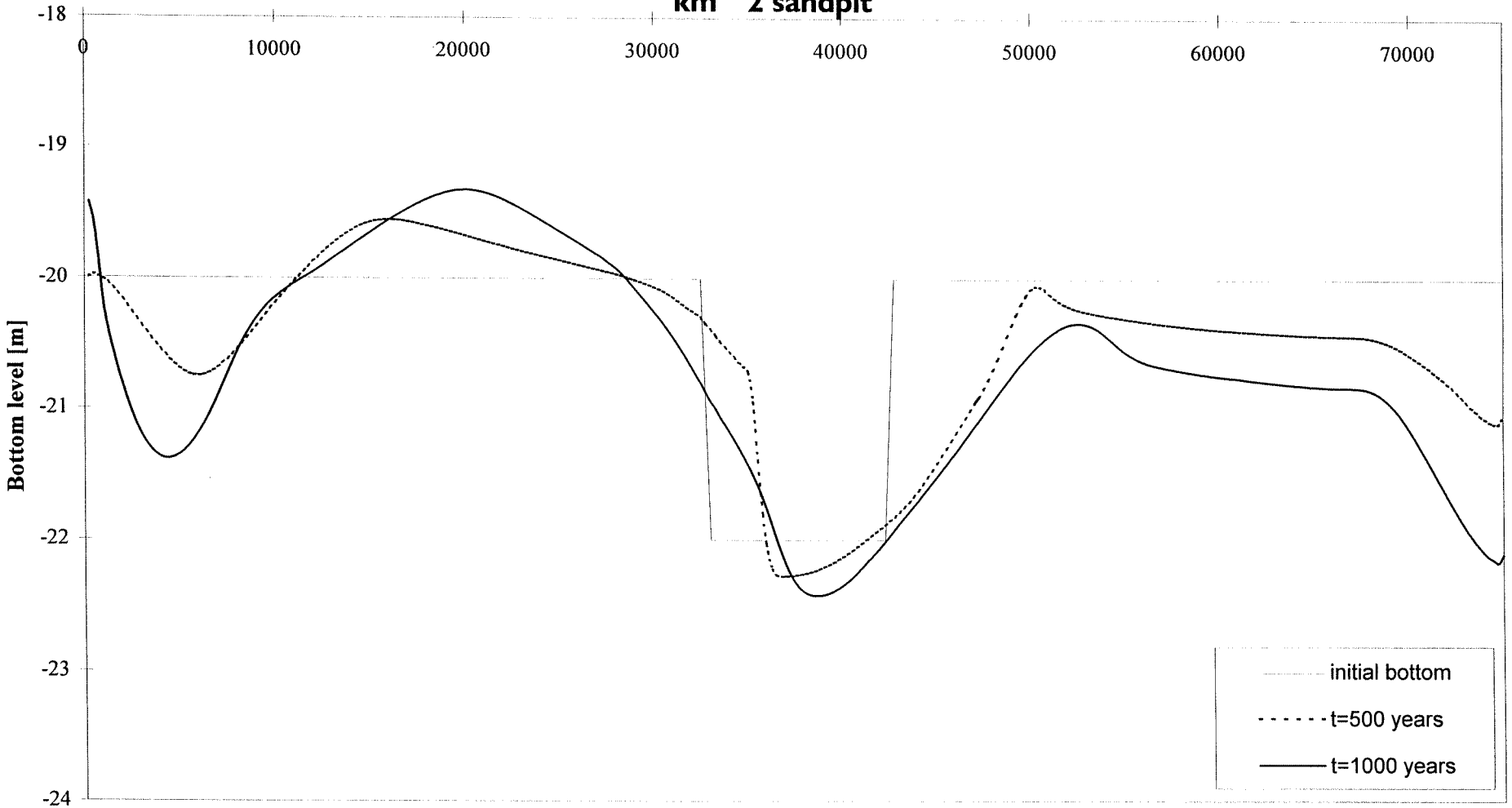

Figuur 8.23c: Bottom levels in the center cross-section of parallel, 22 m deep 10x5 km ^ 2 sandpit

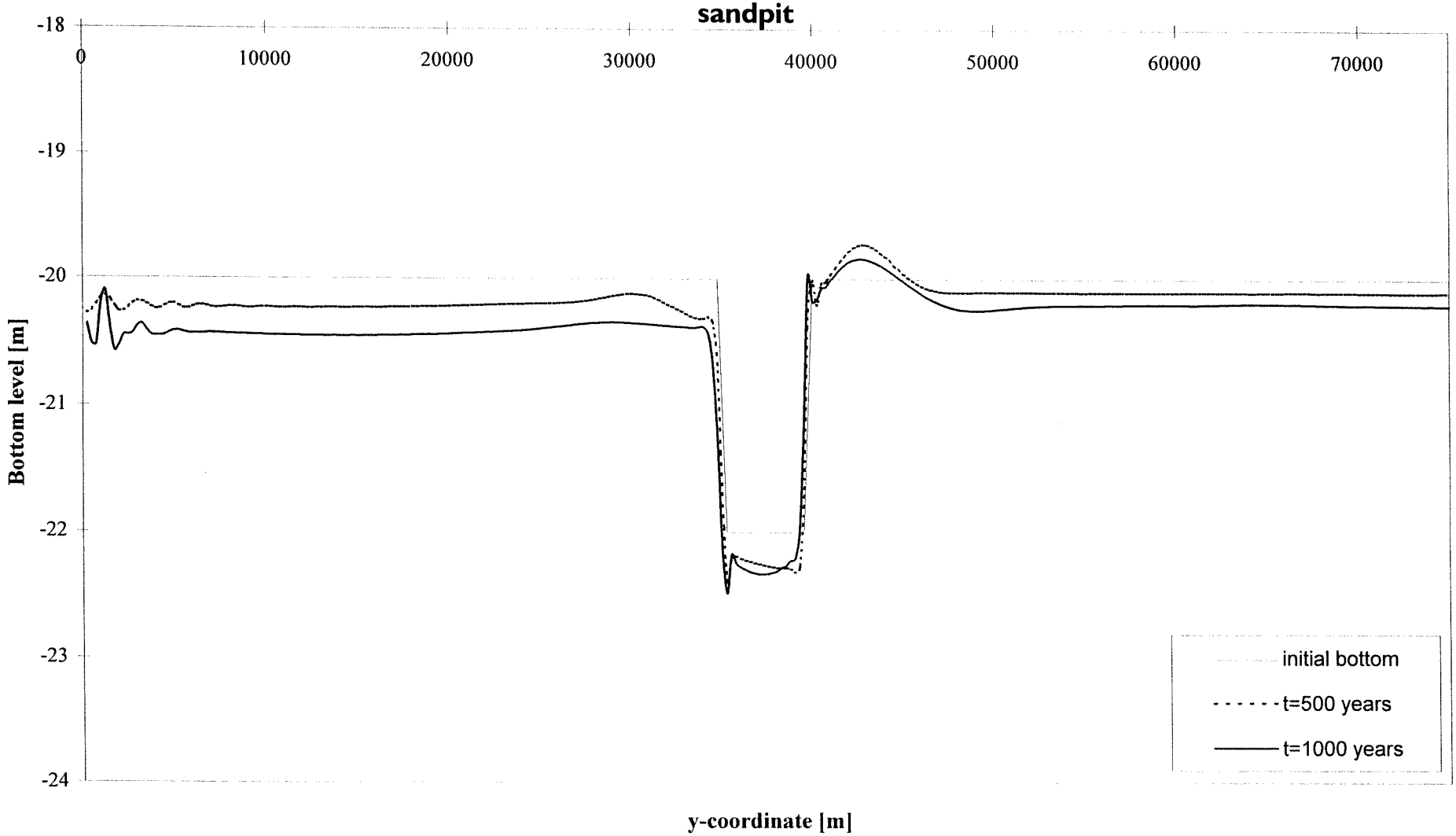

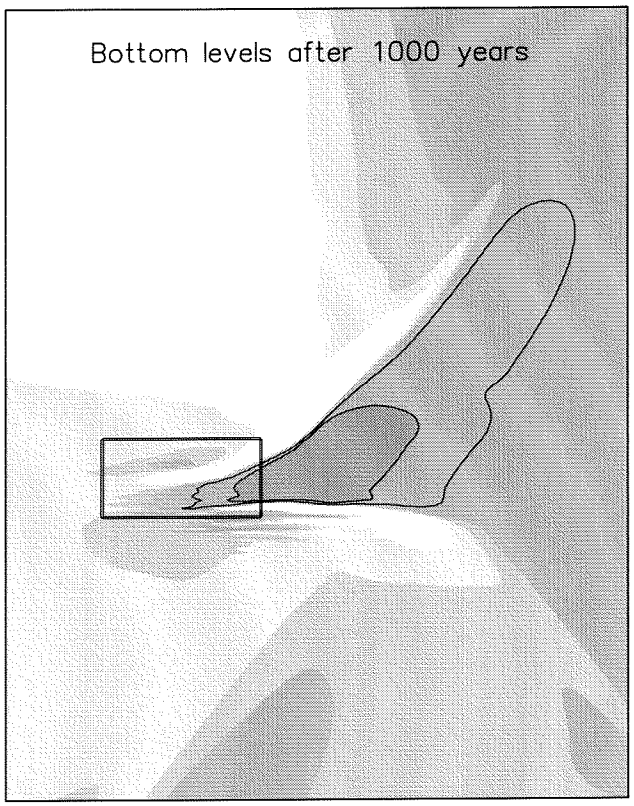

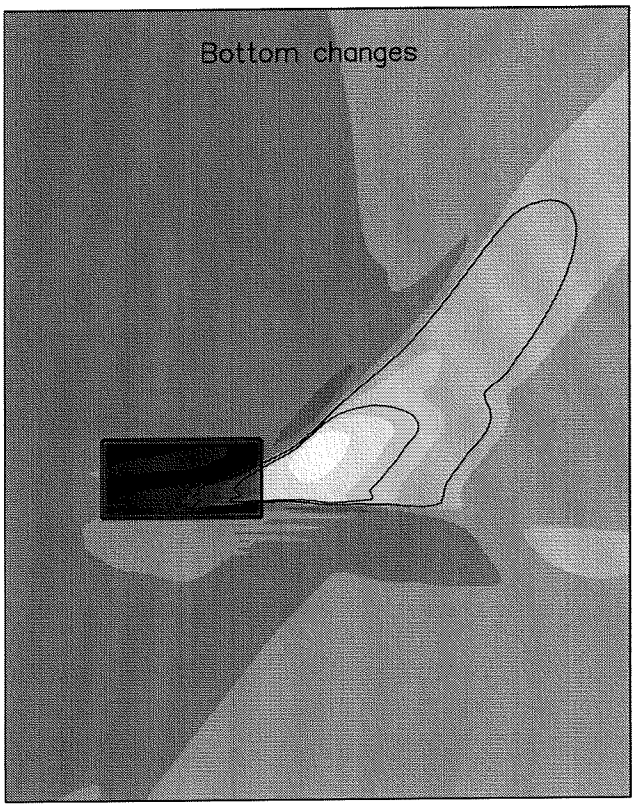

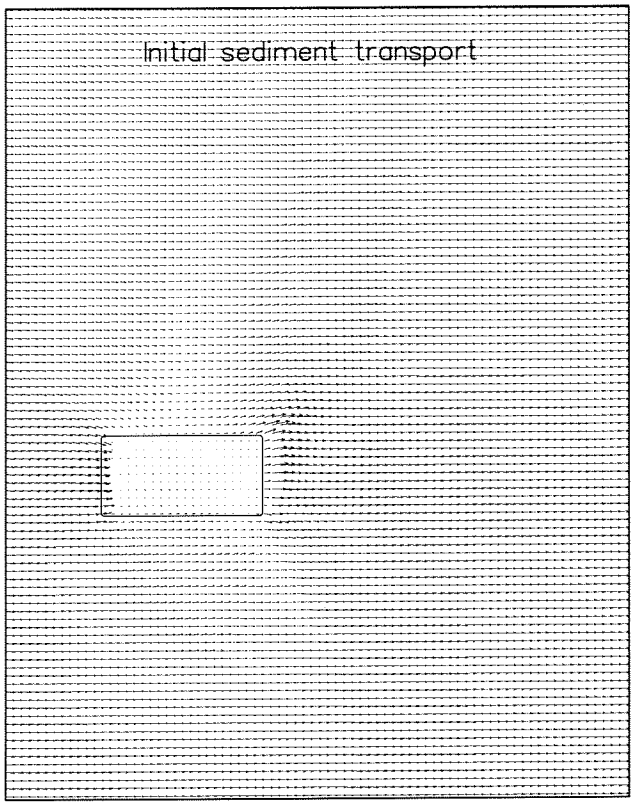

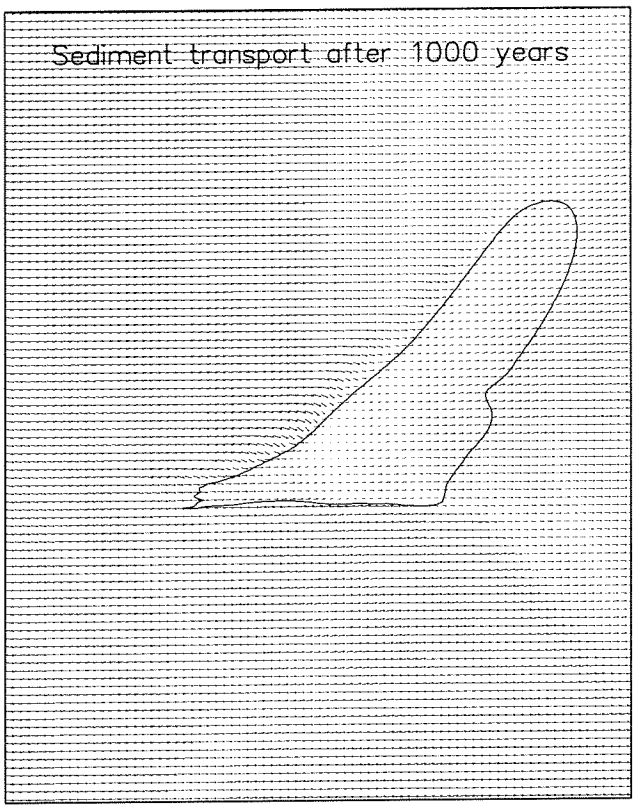

$\longrightarrow$ $1.0*10^{-5}$ m^2/s

Bottom levels and changes [m]; sediment transport [m^2/s]

Parallel 10x5 km^2 sandpit; variant with increased M0 velocity

Morphological results after 1000 years

WL | DELFT HYDRAULICS

z2615

Figure 8.24a

Figuur 8.24b: Bottom levels in the center longitudinal section of a parallel 24x5 km ^ 2 sandpit, in case of increased velocity of M0 component

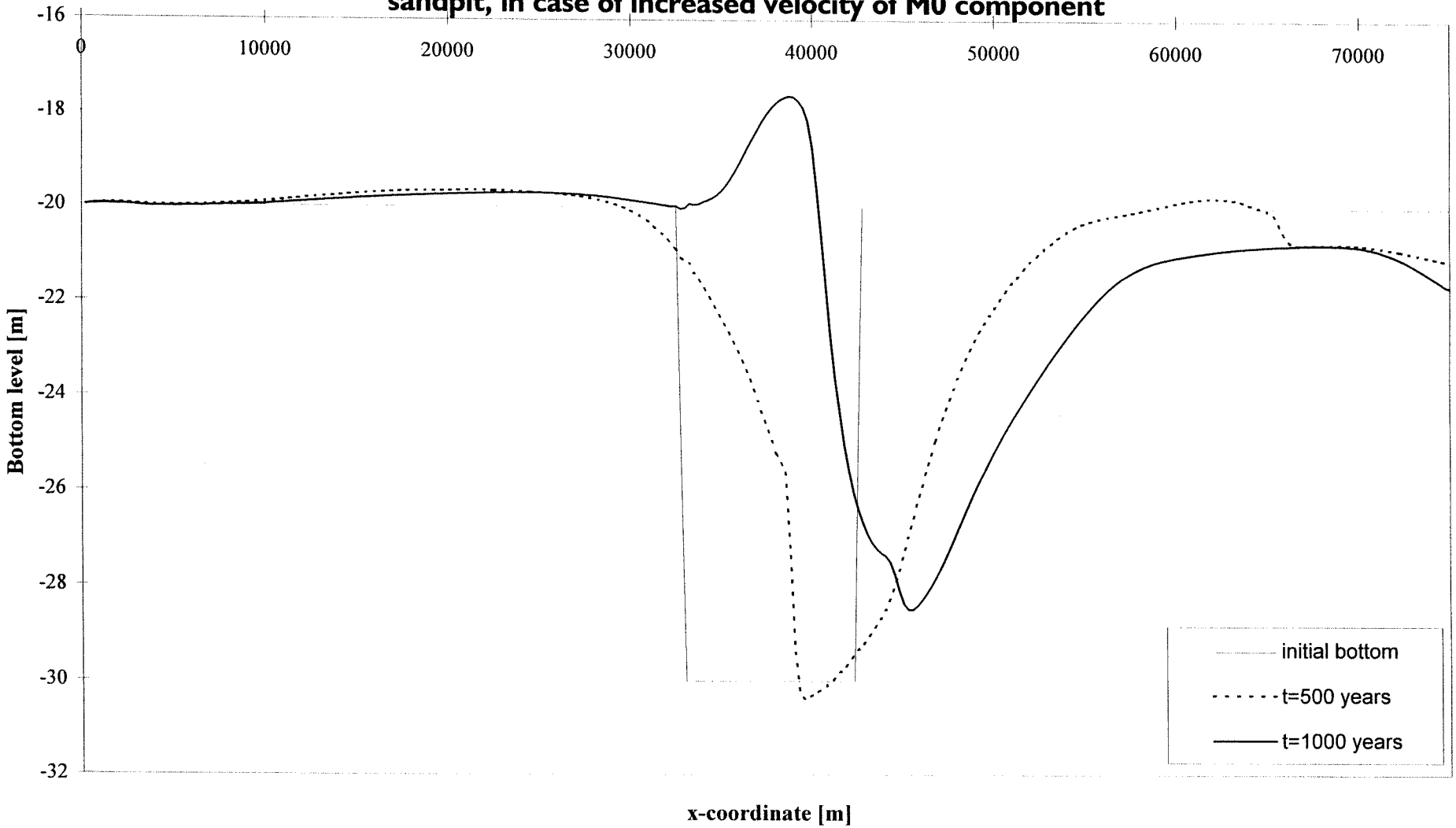

Figuur 8.24c: Bottom levels in the center cross-section of a parallel 10x5 km ^ 2 sandpit, in case of increased velocity of the M0 component

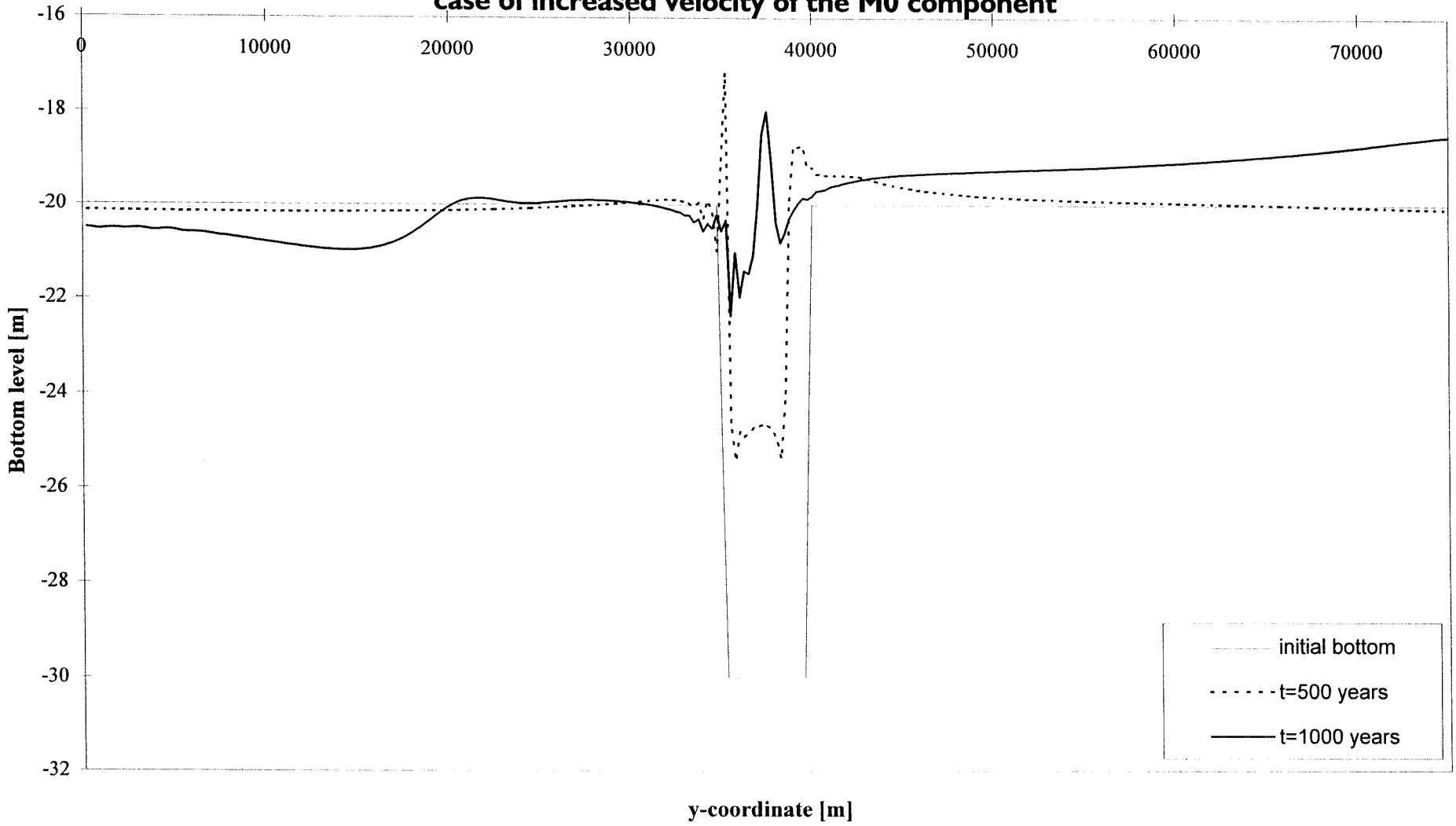

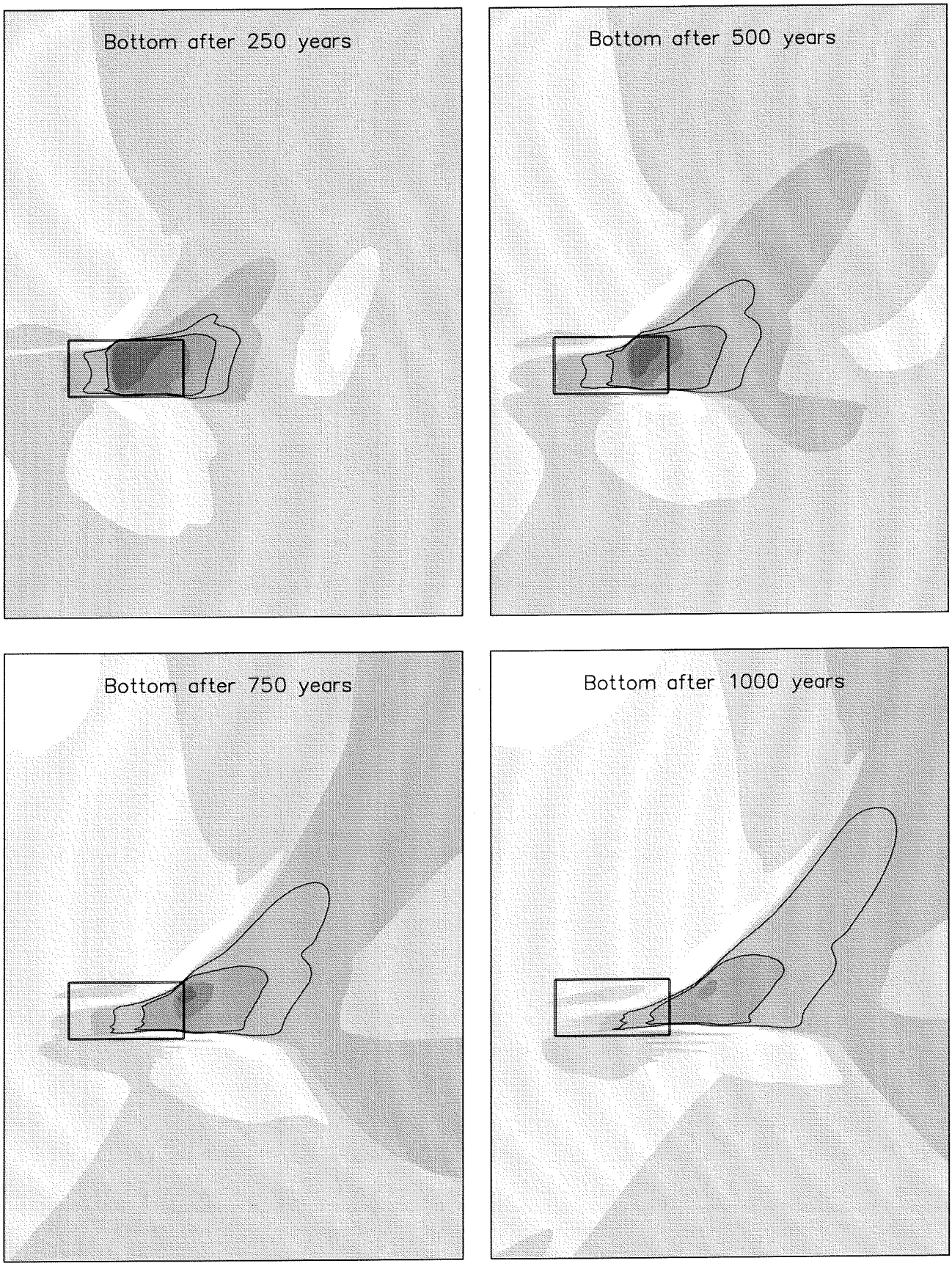

Bottom levels [m]

Parallel 10x5 km^2 sandpit; velocity variant

Morphological development in time

WL | DELFT HYDRAULICS

z2615

Figure 8.25

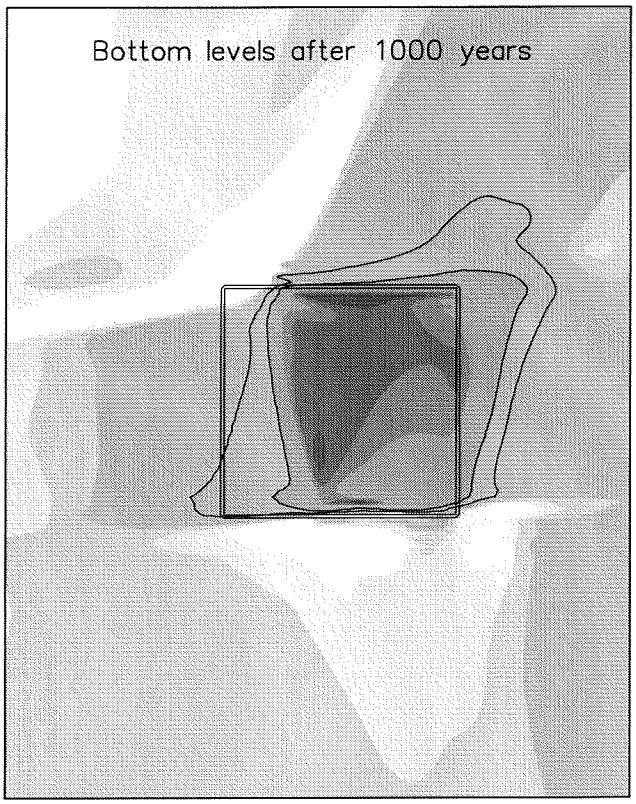

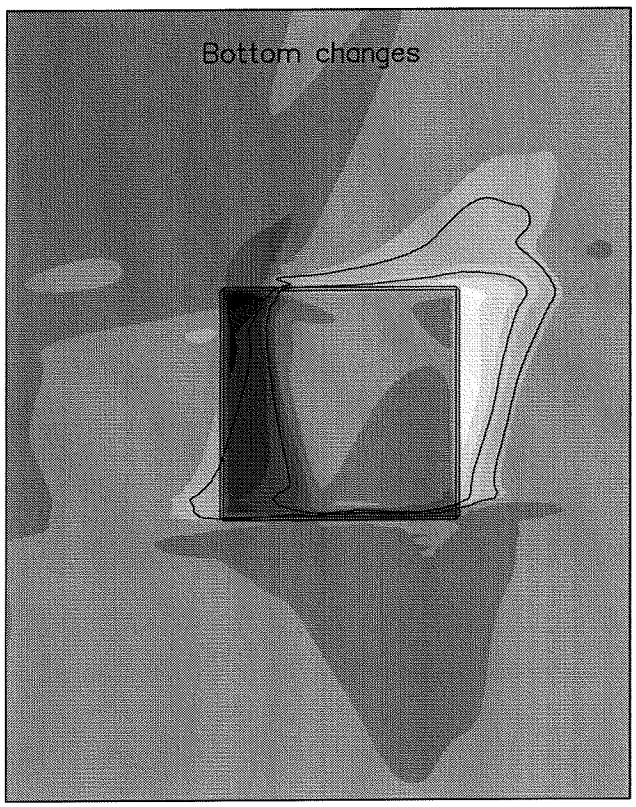

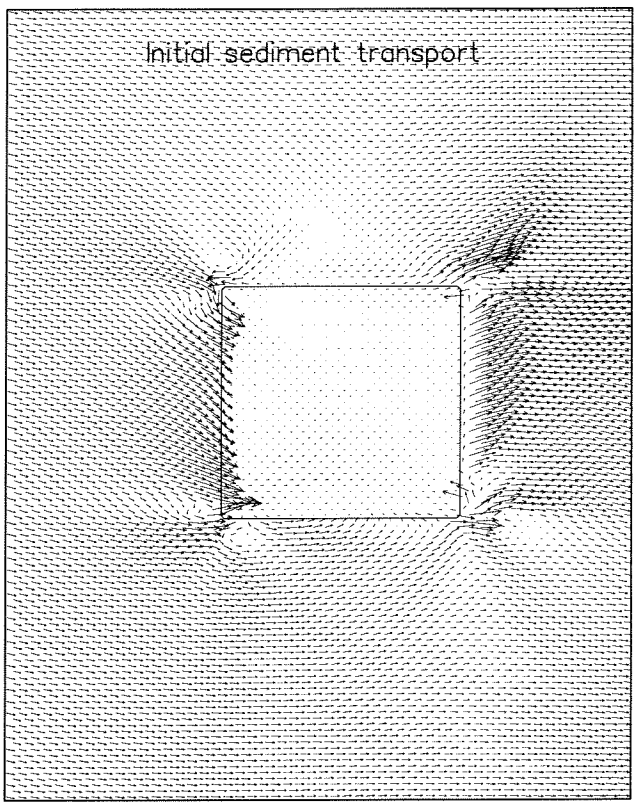

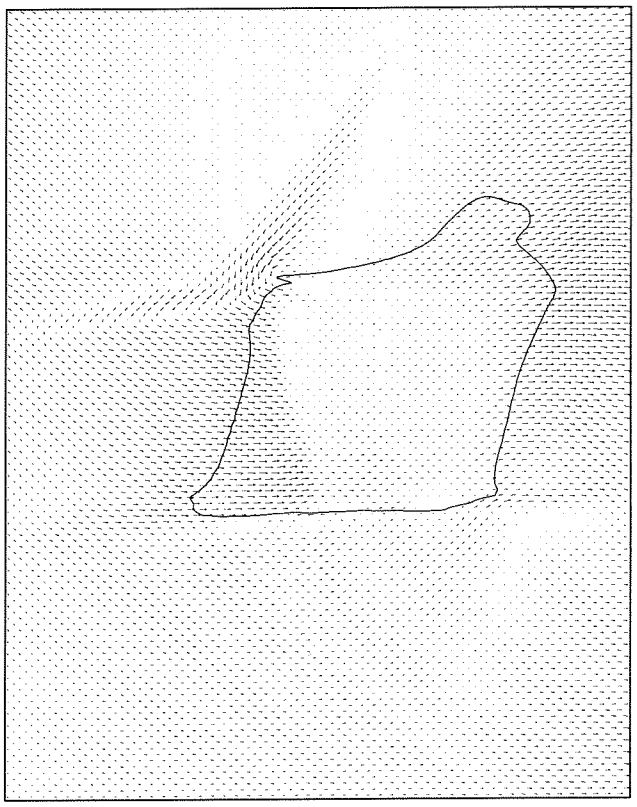

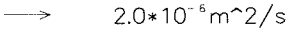

Bottom levels and changes [m]; sediment transport [m^2/s]

+45 degrees rotated 10x10 km^2 sandpit

Morphological results after 1000 years

WL | DELFT HYDRAULICS

z2615

Figure 8.26a

Figure 8.26b: Bottom levels in the center longitudinal section of a parallel 10x10 km ^ 2 sandpit

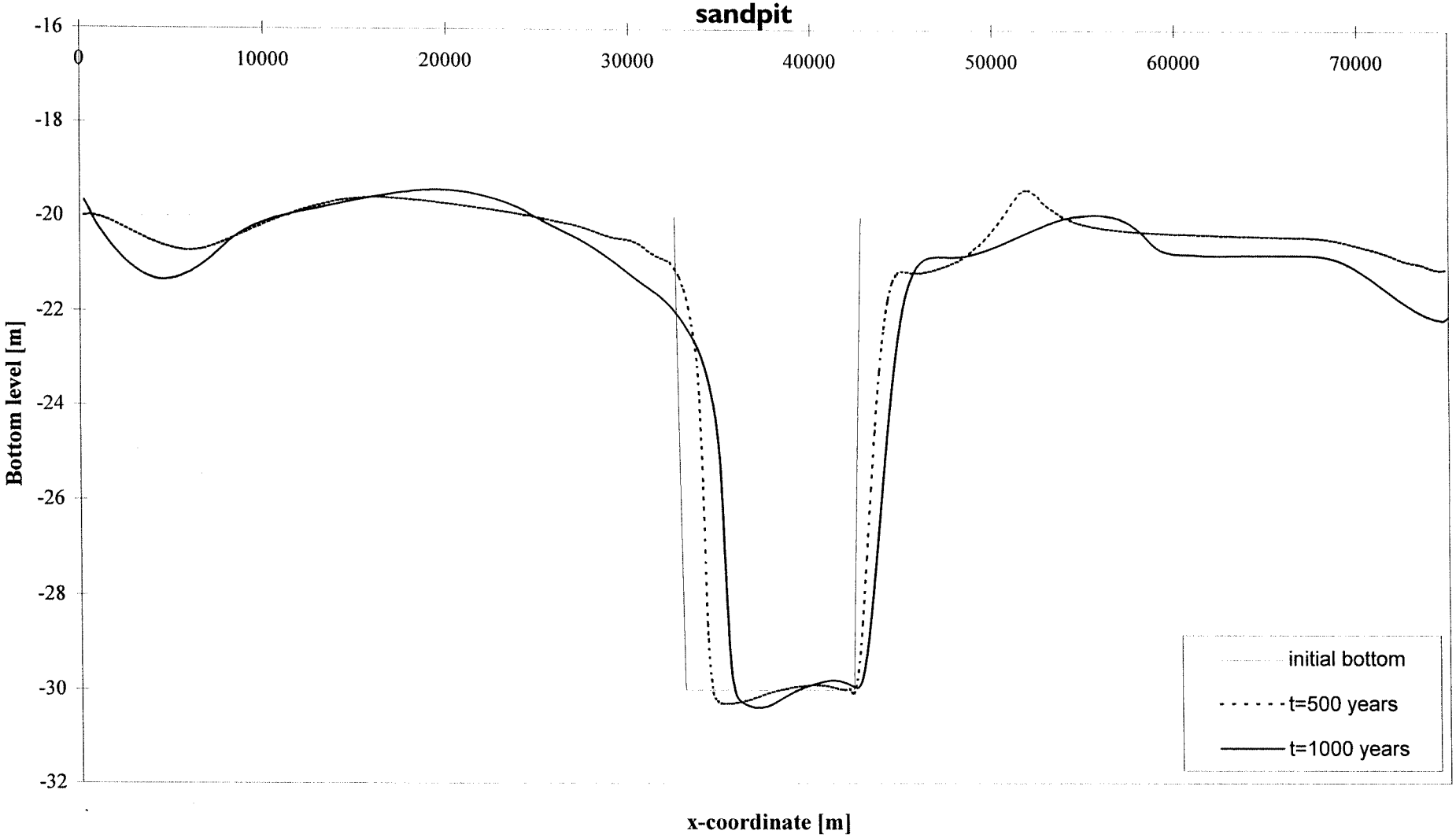

Figure 8.26c: Bottom levels in the center cross-section of a parallel 10x10 km ^ 2 sandpit

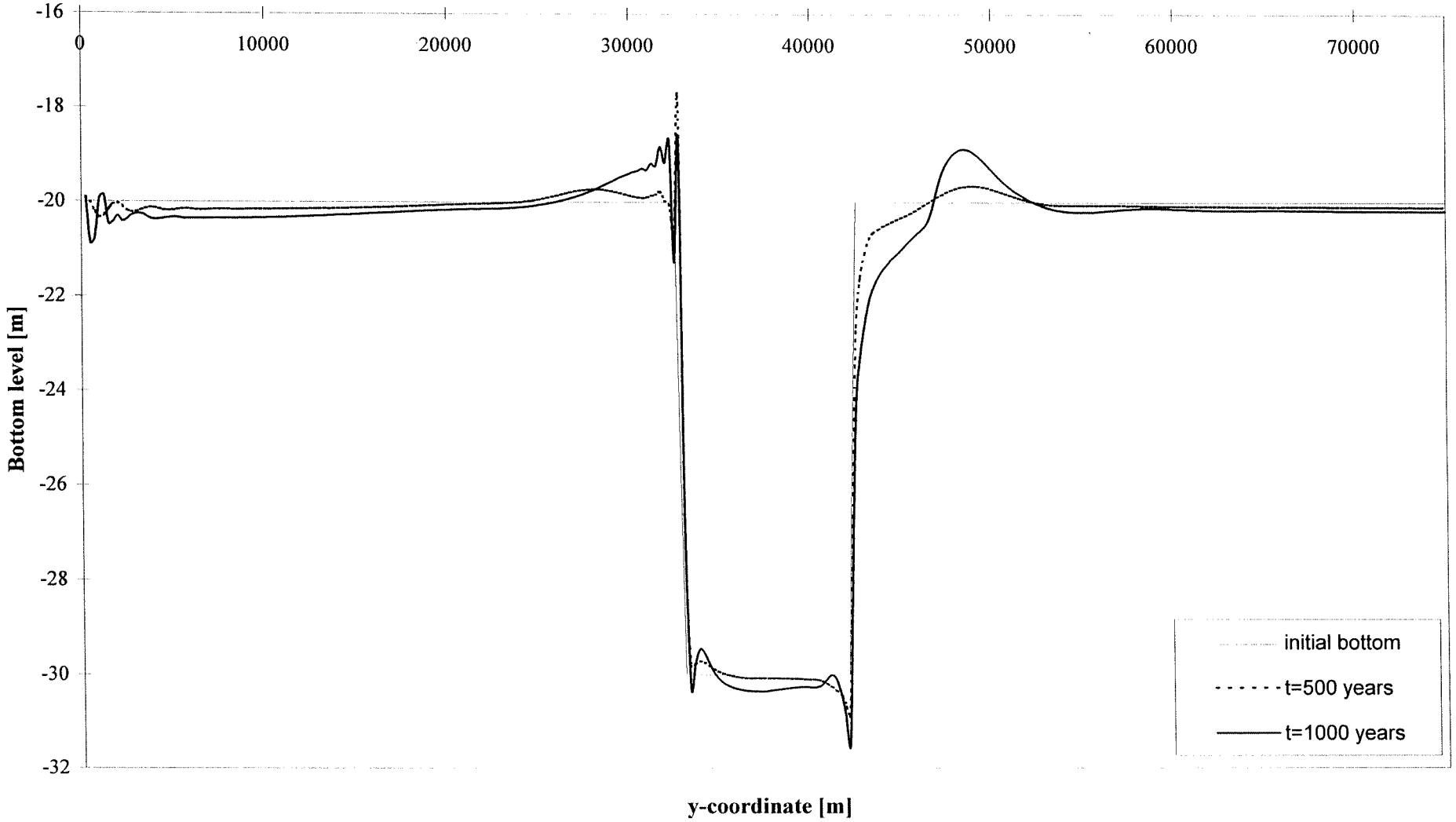

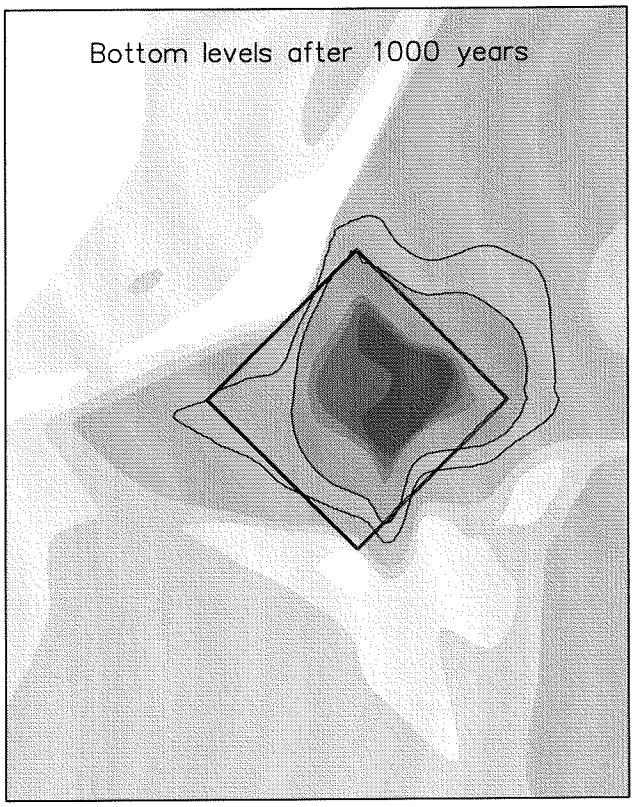

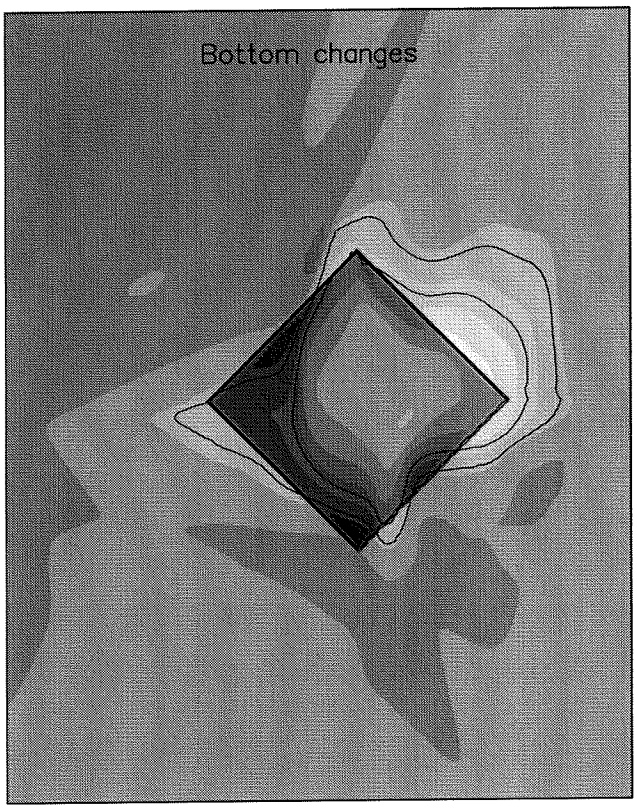

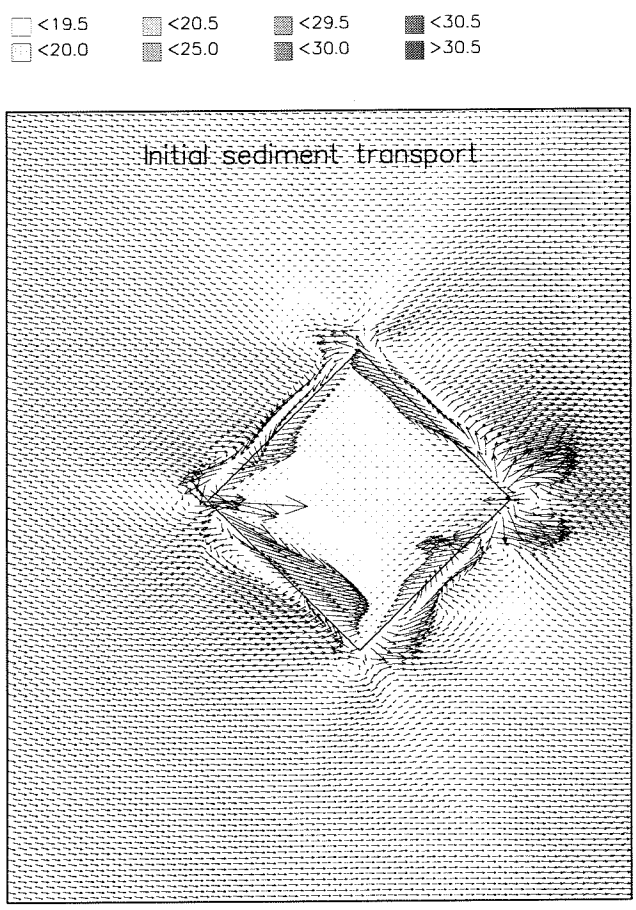

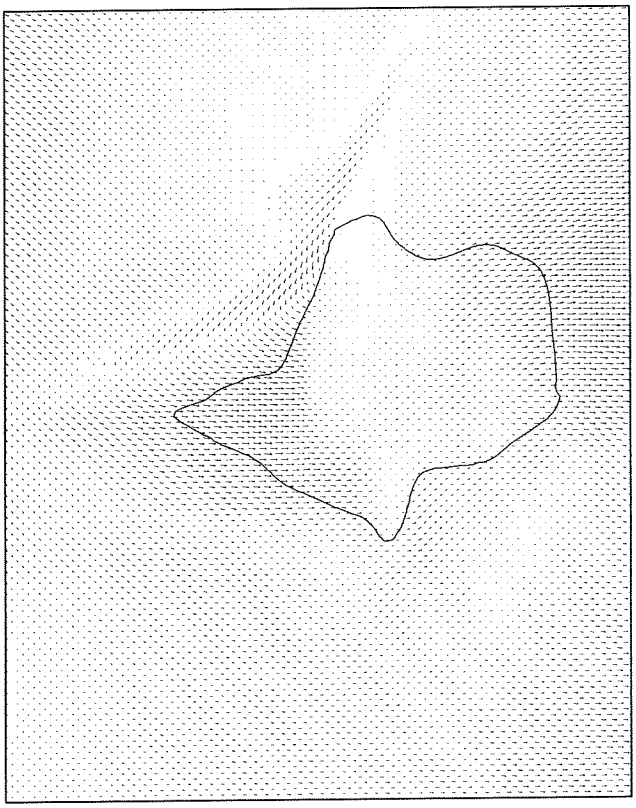

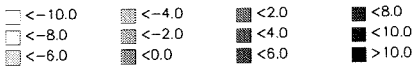

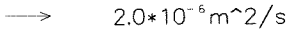

Bottom levels and changes [m]; sediment transport [m^2/s]

+45 degrees rotated 10x10 km^2 sandpit

Morphological results after 1000 years

WL | DELFT HYDRAULICS

z2615

Figure 8.27a

Figure 8.27b: Bottom levels in the longitudinal section of a +45° rotated 10x10 km ^ 2 sandpit

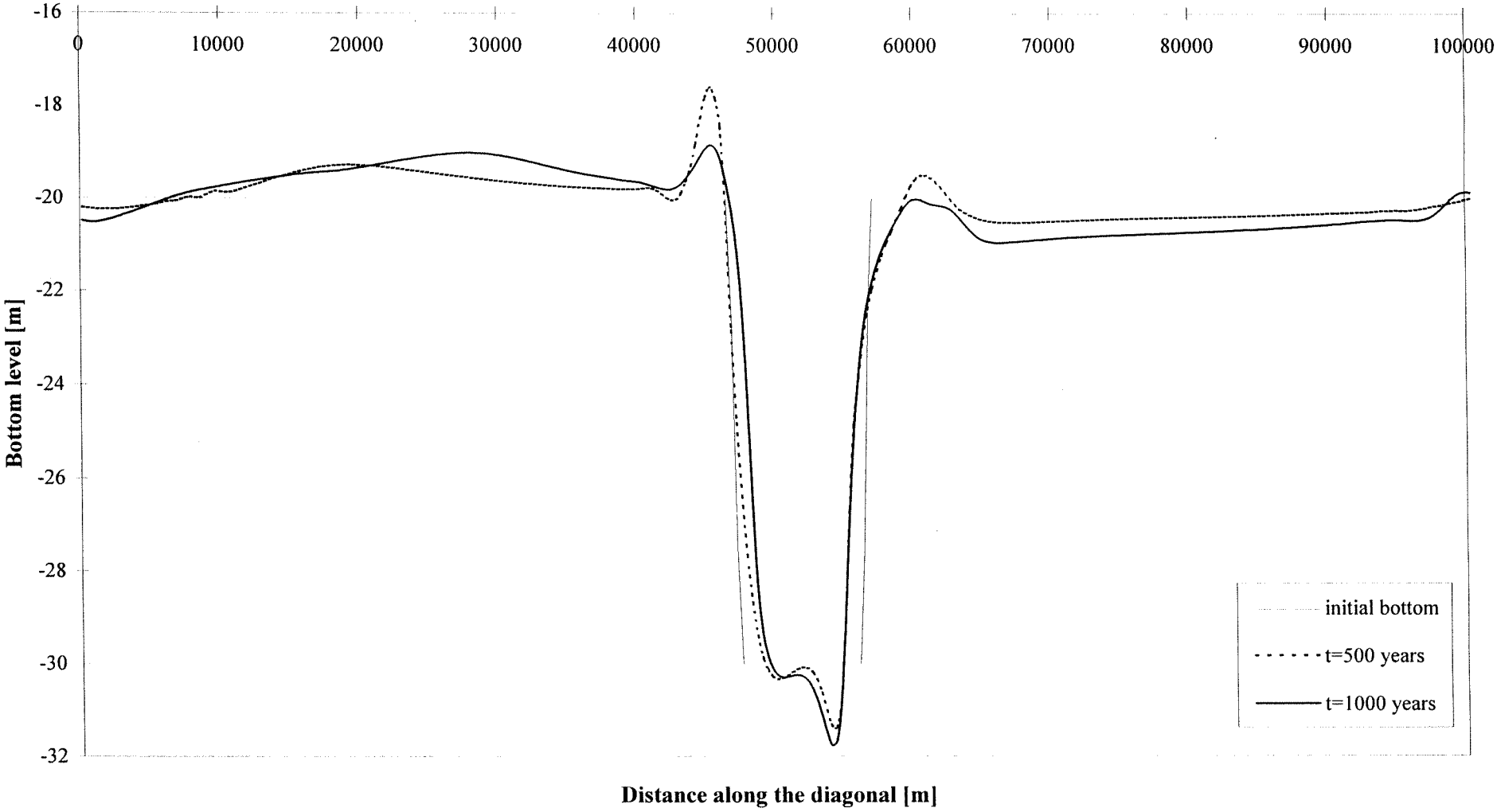

Figure 8.27c: Bottom levels in the center cross-section of a +45° rotated 10x10 km2 sandpit

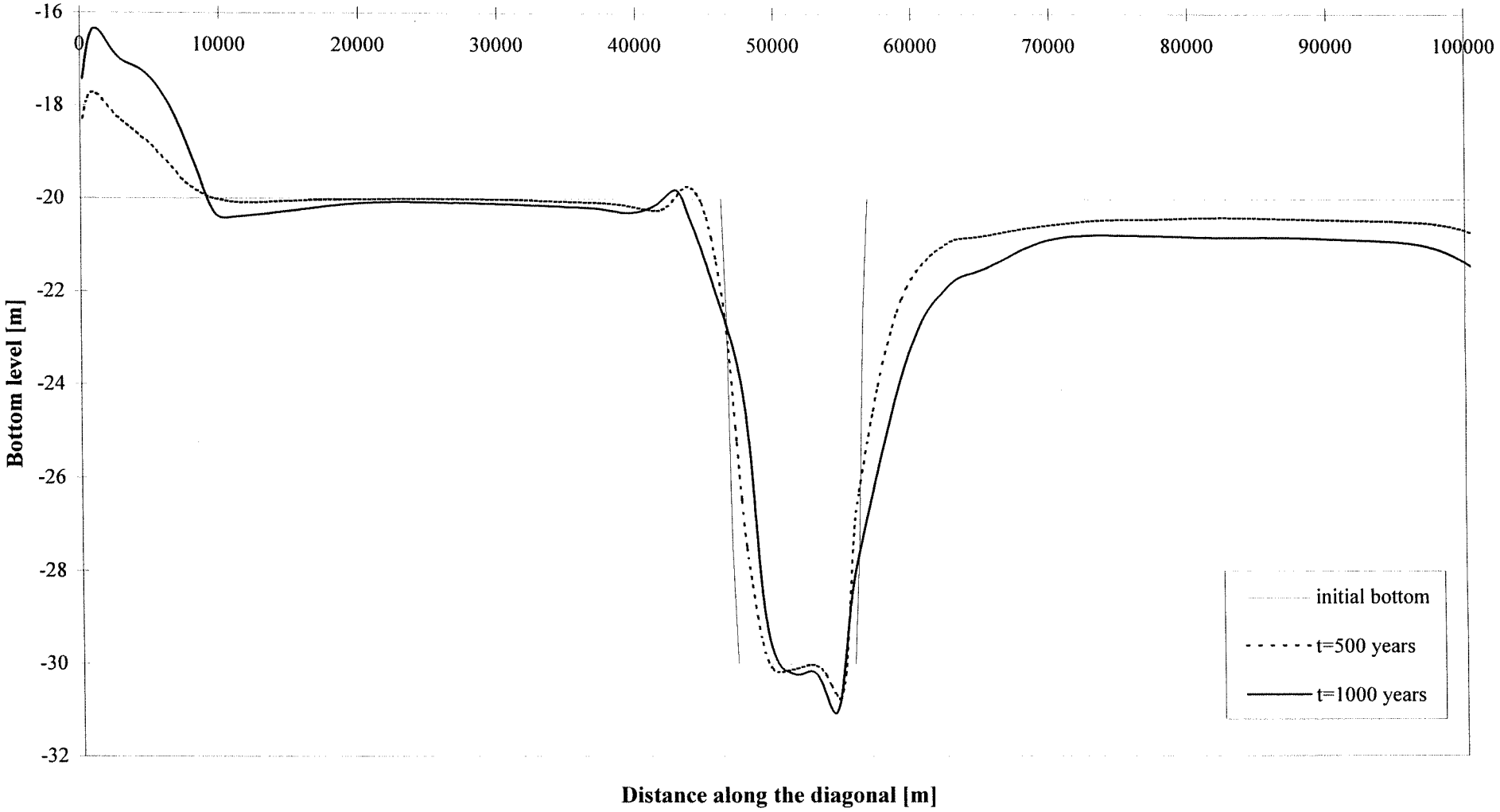

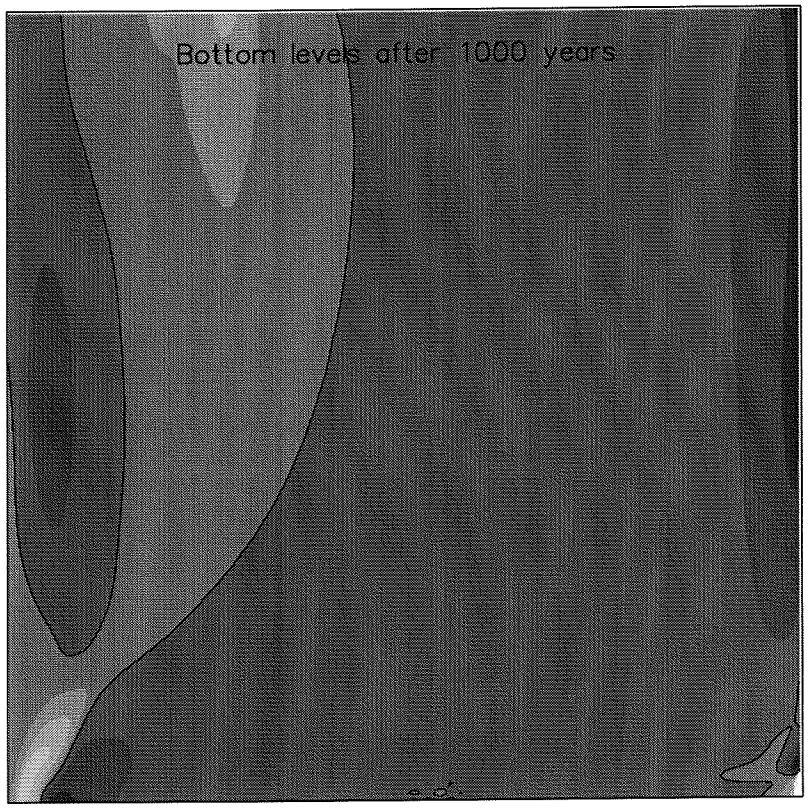

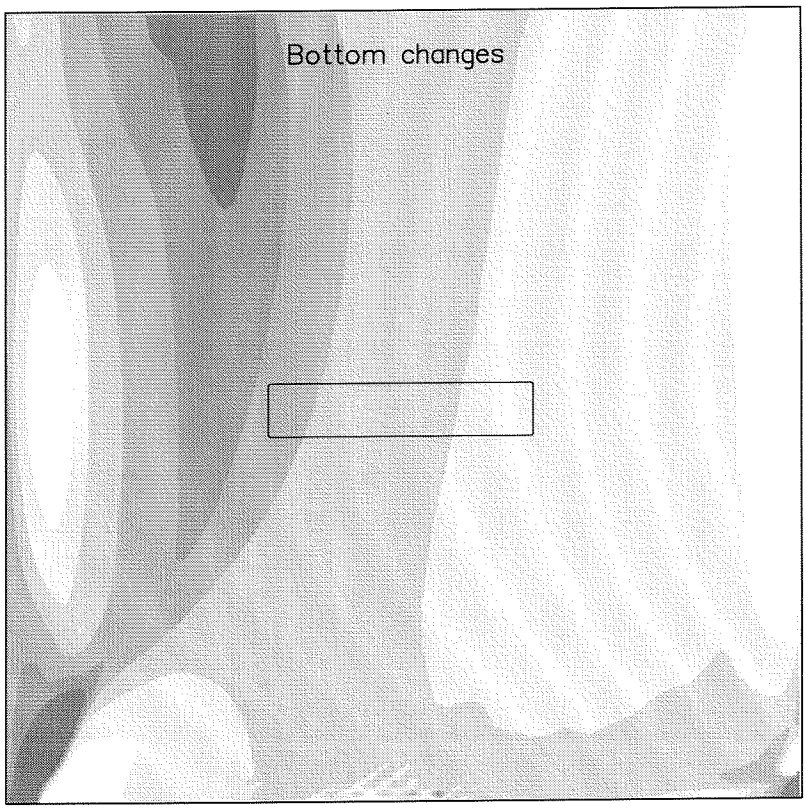

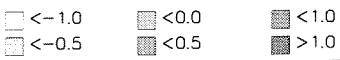

Bottom levels and changes [m]

Flat bottom without a sandpit

Morphological results after 1000 years

WL | DELFT HYDRAULICS

z2615

Figure 8.28

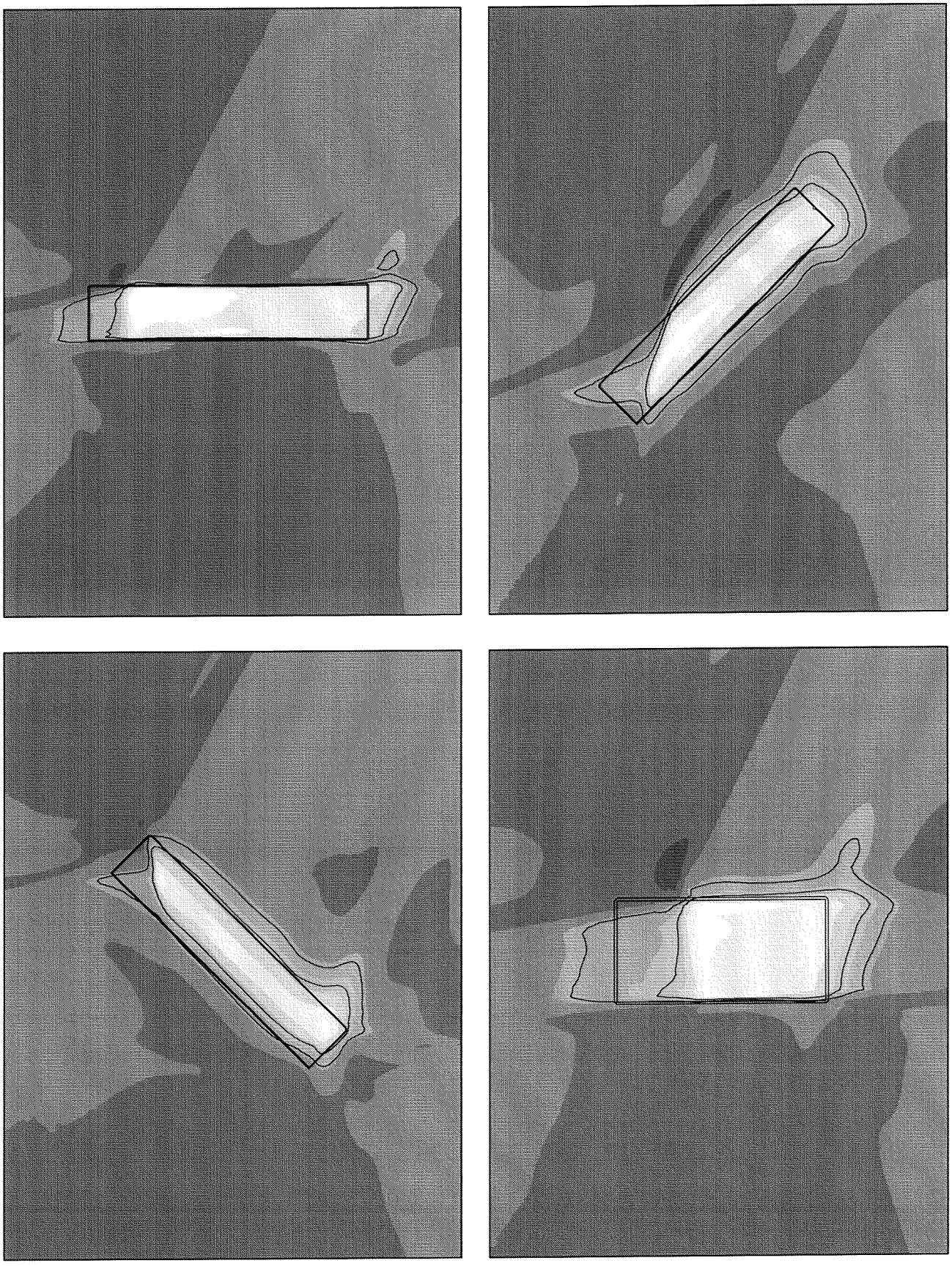

Bottom levels [m] with respect to undisturbed sea bottom

Correction for the influence of the boundary conditions

Morphological results after 1000 years

WL | DELFT HYDRAULICS

z2615

Figure 8.29

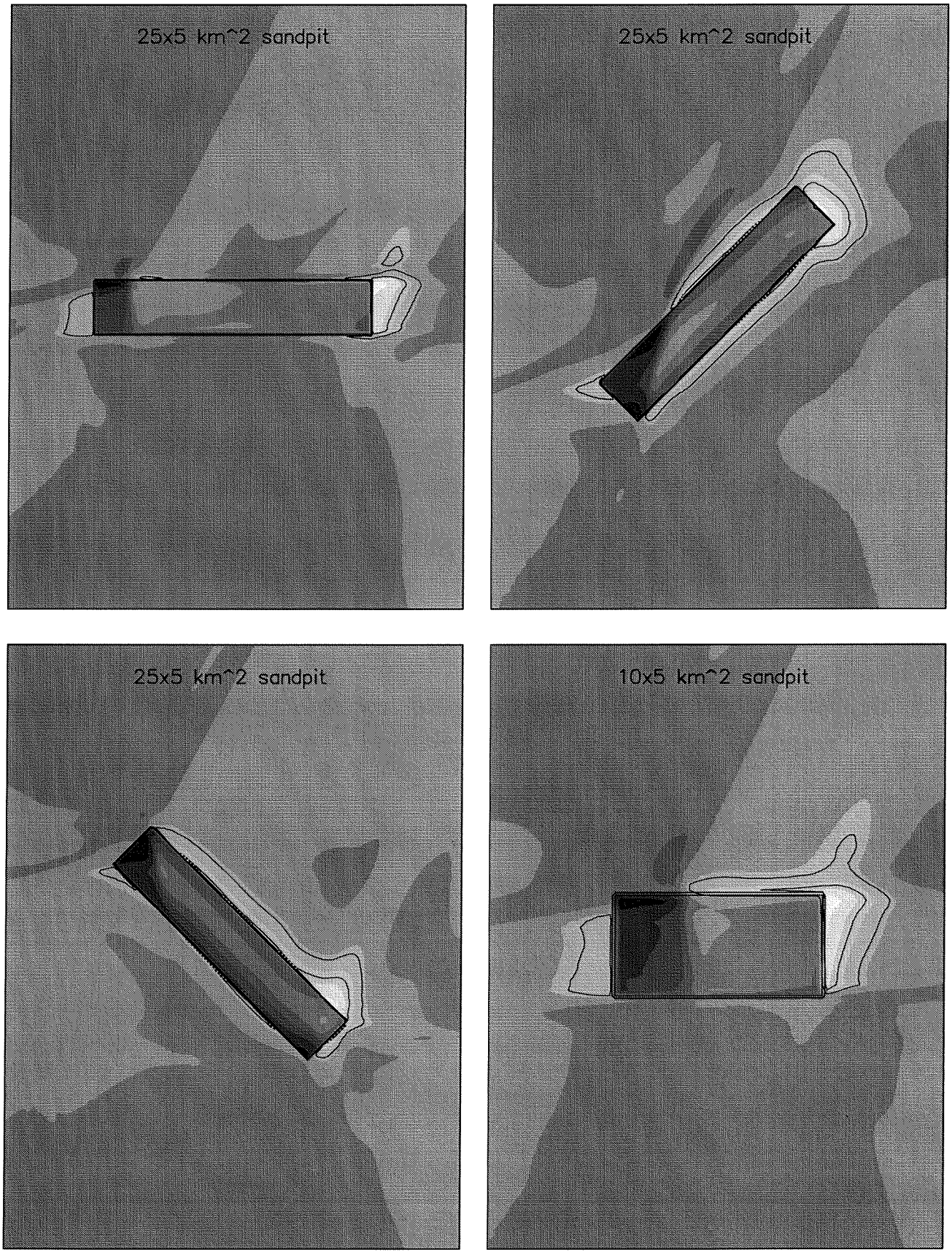

Bottom changes [m]

Correction for the influence of the boundary conditions

Morphological results after 1000 years

WL | DELFT HYDRAULICS

z2615

Figure 8.30